3-26-2015

Evaluation of the Military Utility of Employing an Angle of Arrival Payload Hosted on a CubeSat as an Augmentation to Existing Geolocation Systems

Nicholas S. Schmidt

EVALUATION OF THE MILITARY UTILITY OF EMPLOYING AN ANGLE OF ARRIVAL PAYLOAD HOSTED ON A CUBESAT AS AN AUGMENTATION TO EXISTING GEOLOCATION SYSTEMS

THESIS

Nicholas S. Schmidt, Capt, USAF

AFIT-ENY-MS-15-M-213

DEPARTMENT OF THE AIR FORCE
AIR UNIVERSITY

AIR FORCE INSTITUTE OF TECHNOLOGY

Wright-Patterson Air Force Base, Ohio

AFIT-ENY-MS-15-M-213

EVALUATION OF THE MILITARY UTILITY OF EMPLOYING AN ANGLE OF ARRIVAL PAYLOAD HOSTED ON A CUBESAT AS AN AUGMENTATION TO EXISTING GEOLOCATION SYSTEMS

THESIS

Presented to the Faculty

Department of Aeronautics and Astronautics

Graduate School of Engineering and Management

Air Force Institute of Technology

Air University

Air Education and Training Command

in Partial Fulfillment of the Requirements for the

Degree of Master of Science in Aeronautical Engineering

Nicholas S. Schmidt, B.S.M.E.

Capt, USAF

March 2015

AFIT-ENY-MS-15-M-213

EVALUATION OF THE MILITARY UTILITY OF EMPLOYING AN ANGLE OF ARRIVAL PAYLOAD HOSTED ON A CUBESAT AS AN AUGMENTATION TO EXISTING GEOLOCATION SYSTEMS

Nicholas S. Schmidt, B.S.M.E.
Capt, USAF

Committee Membership:

Dr. R. G. Cobb
Chair

Col M. D. Sambora, PhD
Member

LtCol R. J. Simmons, PhD
Member

Abstract

Geolocation of adversary RF emitters has long been a military priority and is becoming even more critical in an increasingly information driven battlespace. During the Afghanistan and Iraq conflicts many new geolocation systems were fielded, however, most of those systems are regional in nature and hosted on either ground based or air breathing platforms. While these platforms have strengths, they have limited range and are limited to permissive airspace. This research proposes utilizing an angle of arrival geolocation payload hosted on a CubeSat as an inexpensive and simple augmentation to existing geolocation systems and seeks to evaluate the military utility of such a system.

This research models the performance of the proposed augmentation system as well as three and four-ball TDOA satellite systems and AOA and three-ball TDOA airborne systems individually, and performs geolocation estimate fusion via a variety of techniques to determine the resulting increase in performance in operationally representative scenarios. This research also introduces a high fidelity surface of the earth constraint based upon a digital elevation model across all geolocation algorithms and evaluates its merit.

The results from this research show that the proposed augmentation system does have military utility. Across all scenarios, fusing geolocation estimates resulted in an average 51% reduction in SMA and 47% reduction in average miss distance using a Kalman filter fusion technique. The addition of the surface of earth constraint alone, without fusing multiple estimates, resulted in a 38% average reduction in SMA size, with the greatest improvement occurring in mountainous terrain.

Acknowledgements

I would like to extend my sincerest thanks to Dr. Richard Cobb, my research adviser and committee chair, for his stalwart guidance and insightful recommendations. His help enabled me to adapt and overcome challenges while still focusing on the end goal. I'd also like to extend thanks to Col Matthew Sambora and Lt Col Ronald Simmons. I truly appreciate their interest, suggestions, and feedback throughout my research process.

Nicholas S. Schmidt

Table of Contents

Page

Page

List of Figures

List of Tables

Table Page

Table Page

Table Page

Table Page

Table Page

Acronyms

1D one dimensional.

2D two dimensional.

3D three dimensional.

6U Six Unit.

ACS Attitude Control Subsystem.

ADCS Attitude Determination and Control Subsystem.

AFIT Air Force Institute of Technology.

AOA Angle of Arrival.

ARSR-4 Air Route Surveillance Radar-4.

ASIC Application Specific Integrated Circuit.

AV Aerial Vehicle.

C3 Command, Control, and Communications.

C&C Command and Control.

CAF Complex Ambiguity Function.

CCF Cross Correlation Function.

CI Covariance Intersection.

COTS Commercial Off The Shelf.

CRLB Cramer-Rao Lower Bound.

dB Decibel.

dBi Decibel-isotropic.

dBW Decibel-Watts.

DEM Digital Elevation Model.

DF Direction Finding.

DFO Differential Frequency Offset.

DOD Department of Defense.

DPD Direct Position Determination.

DSM Digital Surface Model.

DTED Digital Terrain Elevation Data.

DTM Digital Terrain Model.

DTO Differential Time Offset.

ECEF Earth Centered Earth Fixed.

EGM 96 Earth Gravitational Model 1996.

EI Ellipsoid Intersection.

EIRP Equivalent Isotropic Radiated Power.

ELINT Electronic Intelligence.

ENU East-North-Up.

F/TDOA Frequency/Time Difference of Arrival.

FAA Federal Aviation Administration.

FDOA Frequency Difference of Arrival.

FIM Fisher Information Matrix.

FOM Figure of Merit.

FPGA Field Programmable Gate Array.

FSPL Free Space Path Loss.

GDOP Geometric Dilution of Precision.

GPS Global Positioning System.

HRTe High Resolution Terrain elevation.

LE Largest Ellipsoid.

LEO Low Earth Orbit.

LHCP Left Hand Circular Polarized.

LIDAR Light Detection and Ranging.

LOB Line of Bearing.

MOP Measure of Performance.

MPTPS Maximum Post-to-Post Separation.

MSL Mean Sea Level.

MUSIC Multiple Signal Classification.

NGA National Geospatial-Intelligence Agency.

NLO Nonlinear Optimization.

NTM National Technical Means.

PRF Pulse Repetition Frequency.

QFH Quadfillar Helix.

RAAN Right Ascension of the Ascending Node.

RF Radio Frequency.

RHCP Right Hand Circular Polarized.

RMS Root Mean Square.

RMSE Root Mean Square Error.

SAMSON Satellite Mission for Swarming and Geolocation.

SAR Synthetic Aperture Radar.

SDR Software Defined Radio.

SEU Single Event Upset.

SMA Semi-Major Axis.

SNR Signal to Noise Ratio.

SOI Signal of Interest.

SRAM Static Random Access Memory.

SRFT Shuttle Radar Finished Topography.

SRTM Shuttle Radar Topography Mission.

STK Systems Tool Kit.

SV Space Vehicle.

TDOA Time Difference of Arrival.

TNG Theater Netcentric Geolocation.

TUI Tethers Unlimited Incorporated.

UAV Unmanned Aerial Vehicle.

UCA Uniform Circular Array.

WGS 84 World Geodetic System 1984.

EVALUATION OF THE MILITARY UTILITY OF EMPLOYING AN ANGLE OF ARRIVAL PAYLOAD HOSTED ON A CUBESAT AS AN AUGMENTATION TO EXISTING GEOLOCATION SYSTEMS

I. Introduction

Military users have been interested in geolocating, determining the position of, Radio Frequency (RF) sources for as long as radio transmissions have been an important part of warfare. Initially, efforts were focused on the location of communication signals, but as electronic devices proliferated and exploded in complexity and capability, the focus and capability expanded to match [13; 14]. Today, geolocation missions encompass the entire range of emitter types and operational frequencies. Military uses include locating the emergency locator beacons of downed pilots, fixing the position of adversary headquarters and Command, Control, and Communications (C3) nodes via geolocation of their transmissions, and determining the locations of hostile radars [14; 2; 15]. In an increasingly information driven battlespace, this intelligence is critical at both the tactical and strategic levels.

During the Afghanistan and Iraq conflicts, an influx of spending enabled the acquisition of many new geolocation systems [16; 17; 18]. However, most of those systems are regional or tactical in nature and are therefore unable to provide wide area, persistent coverage. Additionally, the systems were designed to operate in the prevailing environment of the time. Namely, uncontested airspace with an adversary with few effective anti-air weapons [17; 16]. As a consequence, the resulting systems are predominantly ground based or air breathing systems that operate at low altitudes. This class of systems has many advantages. They are operationally flexible and responsive,

benefit from very low signal attenuation losses due to their close proximity, and can easily collect a signal from many different directions via course changes. However, they are severely limited in access capability, particular in denied areas [18], in some cases are not capable of suitable persistence, and may require a sizable in-theater logistics train to operate.

These access, persistence, and logistics issues can be ameliorated by an orbital platform, however, satellites come with their own unique set of weaknesses. Foremost among these weaknesses are cost and development time, which are in direct conflict with the realities of increasing fiscal constraints. The optimal solution may be an inexpensive, simple, orbital system that is capable of augmenting existing systems by filling coverage gaps, improving geolocation accuracy via cross-platform collects, and collecting lower profile and/or easier to collect targets to allow more capable systems to focus elsewhere.

1.1 Problem Statement

Although the Department of Defense (DOD) already operates an array of different geolocation systems, there is assessed to be a need for an inexpensive augmentation to baseline systems. The goals of this augmentation are to fill coverage gaps, collect less challenging or lower priority signals to allow mainline systems to focus on hard to collect, high priority signals, and to improve geolocation accuracy through cross-platform collects. To this end, this research is focused on determining the military utility of a geolocation payload on a CubeSat/NanoSat-scale satellite, hereafter referred to as a CubeSat for brevity, operating in either a tipping-and-cueing or a cross-platform collection capacity. Tipping-and-cueing refers to the process of using one collector to determine a coarse identification and location of an emitter for subsequent, more precise, geolocation by another collector. It is analogous to a scouting

function. Cross-platform geolocation refers to the ability and process by which data from multiple collectors is combined to yield a superior geolocation than either collector can produce independently. Specifically, cross-platform geolocation is commonly used to refer to multiple dissimilar collectors acting in unison. For example, a collect utilizing one aircraft and a satellite, or two satellites in different orbits would represent two possible configurations of cross-platform geolocation.

1.2 Current Research

Geolocation is a topic of significant interest and research. However, the nature and uses of geolocation are somewhat esoteric, and hence published materials are less common than might otherwise be expected. That being said, the most popular areas in the study of geolocation are the development and analysis of geolocation algorithms [19; 20; 21], geolocation from a UAV platform [22], and using swarms and/or optimal trajectories to improve geolocation from airborne UAV platforms [23]. There is also significant research in regards to performing a geolocation mission from a small CubeSat/NanoSat-scale vehicle [24; 25]. The Air Force Institute of Technology (AFIT)'s own satellite design sequence has studied the problem on several occasions [26; 27; 28; 29; 30], and numerous theses have also been dedicated to the topic [31; 32; 33]. The topic of cross-platform geolocation, particular to utilizing dissimilar collection platforms, is much less well developed. However, cross-platform geolocation can be considered to be a specific form of general sensor fusion, which is a popular area of research [34; 35; 33].

In particular, this research builds off of previous efforts at AFIT to examine the feasibility of using "off the shelf" Commercial Off The Shelf (COTS) hardware in a Six Unit (6U) CubeSat to perform a geolocation mission. DiGiacomo used the systems engineering process to propose a two-ball Frequency/Time Difference of Arrival

(F/TDOA) geolocation system which he showed to be accurate and feasible. Additionally, two design teams, as part of the AFIT Satellite Design Sequence, focused development efforts on COTS based geolocation solutions. This research will leverage those results.

1.3 Scope

The scope of this research is an assessment of the ability of a geolocation payload on a CubeSat sized satellite to provide a militarily useful capability. While there are many potential civil applications of geolocation technology, particularly in the realm of cooperative emitters, this research will focus on the geolocation of militarily representative signals of interest in a non-cooperative environment. In particular, the system's utility will be evaluated in the cross-platform geolocation use case. Metrics will be developed to quantify performance. The result will be an assessment as to whether or not the proposed system has utility, as well as recommendations on the most promising use cases.

1.4 Assumptions

In order to make this effort tractable, a number of assumptions will be put into place. First, it will be assumed that there is a suitable ground system for satellite Command and Control (C&C), data processing, and dissemination. Additionally, it will be assumed that communication paths to the ground are available in near real-time. This research will also assume that the satellite in question is small (CubeSat or NanoSat scale), operates in a Low Earth Orbit (LEO) and is always operationally available while the target of interest is within its field of view. The target emitter is assumed to be stationary, on the surface of the earth with a clear line-of-sight to the collector, and operating at a frequency known *a priori*. Finally, the processes of

signal detection, correlation and association, as described in section 2.2, are assumed to occur perfectly.

1.5 Limitations

In addition to the simplifying assumptions, there are a number of limitations to this research. First, this effort will not take into consideration the launch and orbital placement of the satellite(s). This limitation includes not considering constellation phasing or required orbital maintenance. It is expected that an operational system would require a source of propulsion to perform those functions, but the manner of such will not be considered in this research. Additionally, all external collectors included in the cross-platform performance analysis will be modeled with arbitrary reasonable values for geolocation performance. These values may not be an accurate representation of the true capabilities of similar operational systems.

1.6 Organization

This thesis is organized in five chapters. The first chapter provides a brief introduction, and explains the impetus behind the research as well as the objectives. Chapter II covers necessary background information and literature review. Chapter III covers the methodology employed, significant variables, and the metrics used to evaluate military utility. The results for each use case are presented in Chapter IV, and conclusions and recommendations are located in Chapter V.

1.7 Approach

The overall approach of this research effort will be simulation and analysis focused. Representative use cases will be developed and modeled in Systems Tool Kit (STK) from which to draw time-dependent geometries, range, and range-rate information.

These physical parameters will be imported into MATLAB ® where the applicable geolocation and sensor fusion algorithms will be implemented on simulated signals.

In order to evaluate the benefit of the inclusion of the additional geolocation system in the cross-platform use case, baseline geolocation accuracy will first be measured without inclusion of the new system, and then the simulation will be re-run to determine the improvement in geolocation accuracy with the inclusion of the additional collector(s). The primary performance metric will be the reduction in the 95 percent confidence ellipsoid size. Variables will include emitter characteristics such as power and Pulse Repetition Frequency (PRF) as well as the collection geometry.

It is expected that the results of this study will identify the magnitude of the improvement in geolocation accuracy due to augmentation, if any, as well as the most promising use cases for augmentation.

II. Background

As mentioned in Chapter I, geolocation is a topic of significant interest and research. It is also an incredibly broad subject with many applications and techniques that are specific to the point of obfuscation. This chapter will cover the background research required and current state-of-the-art as applicable to the goal of determining the military utility of an Angle of Arrival (AOA) payload hosted on a small CubeSat/NanoSat-scale Space Vehicle (SV). The discussion will start with the SV to include bus and payload considerations, followed by geolocation, including signal measurement and algorithms, continue to surface of the earth constraints focusing on Digital Elevation Model (DEM)s, and finally discuss geolocation fusion techniques.

2.1 Space Vehicle

The term SV refers to the totality of a satellite including the bus and payload. A complete SV design is outside of the scope of this research, but a brief discussion of the unique aspects of a CubeSat including the mission specific payload components is a necessary starting point when trying to consider the military utility of such a system. This section will discuss the current state of research on CubeSats, software defined radios, and collection specific antennas.

2.1.1 CubeSat Characteristics.

The subject of this thesis is a CubeSat, chosen due to the advantages of rapid development and low construction and launch costs when compared to traditional large satellites. These very reasons have made small satellites, to include micro, nano, and pico sized subtypes, a very popular area of research. The CubeSat standard was codified in 1999 by Puig-Suari and Twiggs at Cal Ploy and Stanford University in order to

"accelerate opportunities with small, low construction cost, low launch cost space experiment platforms" [36]. The basic building block, or "unit" is a $10\text{cm} \times 10\text{cm} \times 10\text{cm}$ cube with a mass of no greater than 1.33 kg [36]. Multiple "units" can be combined to create larger SVs. Since the standard was codified, CubeSat and other small satellite research has grown exponentially, taking place in universities, government labs, and private industry [36; 26; 37; 29; 38]. Progress in the fields of electronics miniaturization, energy storage, and computational efficiency has reached a point where there is potential for a CubeSat to have an actual military mission utility. Several examples of operationally focused CubeSats, as well as a brief discussion of some of the limiting factors associated with CubeSats, are useful as a base of knowledge.

The Satellite Mission for Swarming and Geolocation (SAMSON) project, led by the Distributed Space Systems Lab and the Asher Space Research Institute at the Technion-Israel Institute of Technology, is an operationally focused CubeSat mission that is scheduled to launch in 2016. The goals of the SAMSON project are to demonstrate long-term autonomous cluster flight as well as RF geolocation. It consists of a formation of three 6U CubeSats employing cold gas thrusters and differential drag for formation keeping [25; 38]. SAMSON employs two foundational technologies for effective CubeSat-based Time Difference of Arrival (TDOA) geolocation; chip-scale Rubidium atomic clocks and inter-satellite comms. The SAMSON project is very similar, albeit much further along, to previous AFIT efforts including the BLACKJACK, GeoLoco, and Anubis geolocation missions described below.

AFIT has been considering CubeSats for operational missions for several years as part of the "Satellite Design" course sequence. Several iterations of RF geolocation missions have been examined, including cluster TDOA and single-ball AOA based solutions. The BLACKJACK project was the first AFIT project to examine the use of a Software Defined Radio (SDR) to perform an Electronic Intelligence (ELINT)

mission from a single satellite [28]. GeoLoco was a follow-on project that sought to perform primarily TDOA geolocation via a cluster of three 6U CubeSats [27]. In 2014, the Anubis project built off the progress of prior years, focusing on a single ball AOA geolocation capability utilizing an SDR. All three efforts reached the conclusion that their respective mission goals were feasible, albeit with limitations and a significant amount of development risk [27; 28; 7]. It is worth noting that all three geolocation focused efforts at AFIT identified many of the same limitations. These limitations will be addressed shortly.

While the CubeSat platform is flexible and well suited to rapid development efforts, the very nature of a small satellite leads to some common limitations, many of which are interrelated. First and foremost, a 6U CubeSat is, by definition and intent, a small volume. While miniaturization has in many cases allowed for a reduction in size of electronic components, the nature of some subsystems does not lend themselves well to small volumes. In particular, the Attitude Control Subsystem (ACS), star trackers, and batteries take up a large portion of the volume in a 6U CubeSat [29; 27; 28]. The limited volume available for batteries is one of the most impactful limitations of the CubeSat paradigm. Even with state-of-the-art lithium-ion and lithium-polymer batteries, total energy storage capacity typically limits geolocation missions to a regional nature [39; 27]. That is; the system cannot operate continuously and must periodically pause mission operations to recharge system batteries. Star trackers are another component that are difficult to implement in the volume constrained confines of a CubeSat. Star trackers are required to meet the attitude knowledge requirements of an AOA geolocation payload [7; 26]. Currently, CubeSat star tracker options are limited, and those available consume at least 1U of volume [7]. Finally, the ACS system is another component that requires a significant volume. Despite the fact that CubeSats are low mass satellites, it is still necessary to have an

ACS capable of controlling the SV attitude and performing momentum dumping. As the angular momentum of a spinning object (e.g. a reaction wheel) is proportional to its radius, there is a lower bound on how small an ACS can be miniaturized while still providing the required angular momentum.

The preceding CubeSat attributes and limitations, including attitude knowledge and control agility as well as the power constrained nature of CubeSat operations, serve to provide general background information. The focus of this thesis is determining the military utility of a AOA geolocation payload hosted on a CubeSat, but it is still useful to consider the limitations of the CubeSat platform and how those limitations may impact geolocation performance. In this way, system models may be designed to more accurately reflect expected real-world performance.

2.1.2 Software Defined Radio.

SDRs are an important enabling technology towards the goal of performing geolocation missions on a CubeSat. An SDR is basically a very flexible radio in which "components that are traditionally pieces of hardware are instead handled as software code" [27]. This is accomplished via means of Field Programmable Gate Array (FPGA)s, consisting of millions of logic cells, the actions of which are controlled by software logic. By changing the programming on the FPGAs, it is possible to change how the hardware circuit functions and reacts. The primary advantage of an SDR is flexibility. A single set of hardware, SDR and antenna, can be reprogrammed to collect a variety of different Signal of Interest (SOI)s and process them in different ways [7]. The ability to reprogram is also useful for changing how collected data is processed. For instance, an SDR can be reprogrammed if the emitter-of-interest is updated with additional or modified operational modes, or if changing priorities dictate collection of a different signal [40; 41].

While SDRs are a relatively recent development, the application of such in CubeSats is already widely studied. In fact, SDRs have played a central role in much of the AFIT CubeSat research. The BLACKJACK, GeoLoco, and Anubis geolocation projects [28; 27; 7; 26] all employed SDRs as central components. Additionally, DiGiacomo studied the application of a COTS SDR to the problem of geolocation from a CubeSat in his thesis [31]. That work included a market survey of SDRs that may be suitable for use in a CubeSat and compatible with Theater Netcentric Geolocation (TNG). Twelve different vendors were identified as offering potentially suitable options, one of which, the Ticom Geomatatics FireFlyII, had been previously fielded on an Unmanned Aerial Vehicle (UAV) platform [31] and was the chosen receiver for DiGiacomo's design. The Anubis project made use of an even more flexible SDR from Tethers Unlimited Incorporated (TUI), the Swift WRX, capable of a wide frequency range and wide bandwidth [42].

The flexibility of an SDR is its greatest strength. However, the flexibility does not come without cost. The SDRs examined in previous research all had significant power draws, which tended to be correlated to the flexibility of the receiver [26; 7]. In general, an FPGA-based SDR will consume more power than a similar radio implemented via Application Specific Integrated Circuit (ASIC)s [43], and the more flexible a receiver, the higher the power draw. Another drawback of FPGA-based SDRs is a vulnerability to radiation. Radiation in the space environment can cause Single Event Upset (SEU)s in the Static Random Access Memory (SRAM) that stores the FPGA configuration [44; 40; 41]. This vulnerability can be mitigated in a variety of ways [44; 40], which are outside of the scope of this discussion, but nonetheless remains a drawback to highly re-configurable SDRs.

Although the exact details and implementation of an SDR is outside the scope of this effort, this research will make use of some of the previously researched and doc-

umented radio parameters. For details, please see the limited distribution addendum to this research.

2.1.3 Antenna.

Collection antennas are, unsurprisingly, a critical part of the overall geolocation payload. The most important antenna considerations are gain, gain pattern, and polarization. Although antenna design and application was not a goal of this research, the above topics are briefly described for completeness.

Antenna gain refers to the ability of an antenna to receive or transmit RF power, as well as the directionality of the antenna, and is defined as the ratio between the power input of the antenna in question and an isotropic radiator [45]. In the absence of losses due to dissipation or impedance mismatch, the antenna gain is equal to the directive gain, given by equation (1). A higher gain antenna results in more received power, and thus a correspondingly higher Signal to Noise Ratio (SNR) and better geolocation performance.

$$G = \frac{\text{maximum power intensity}}{\text{average power intensity over } 4\pi \text{ steradians}} \tag{1}$$

However, increased gain comes at the cost of a more directional antenna pattern, which in-turn requires more accurate SV pointing accuracy [7]. Common types of low directivity antennas include monopole, dipole, and patch antennas. The optimal antenna for geolocation is dependent upon the targeted emitter characteristics. For instance, an isotropic transmitter can be collected whenever there is a line-of-sight between the transmitter and receiver, so a collection antenna with a wide, or hemispherical, beam pattern such as a dipole or patch antenna is desirable [7]. In contrast, a highly directional transmitter may motivate the use of a collection antenna with a different gain pattern. For example, collecting an air surveillance radar from LEO

results in collections near the horizon rather than from nadir. To accommodate this collection geometry, an antenna design with a gain pattern pushed out to the sides, rather than directed down, is beneficial. One such antenna design is the Quadfillar Helix (QFH).

Inherent to the treatment of antenna gain is the consideration of source and antenna polarization. It must be noted that an antenna/transmitter pair reaches the highest possible gain only when the signal and receive antenna are well matched in polarization, linear (horizontal or vertical), or circular (Right Hand Circular Polarized (RHCP), Left Hand Circular Polarized (LHCP)), and orientation. A linearly polarized transmission antenna results in a signal that propagates wholly in one plane, which can have any arbitrary orientation but is often oriented vertically, with the electric field perpendicular to the surface of the earth, or horizontally, with the field parallel. A circularly polarized signal has a plane of radiation that makes one rotation about the boresight of the antenna per signal period. If the rotation is clockwise, per the right hand rule about the vector along the path of transmission with origin at the transmitting antenna, the signal is a RHCP signal, and if the rotation is counterclockwise, then the signal is LHCP [46]. Properly matching the polarization of the receive antenna to the polarization of the signal is important because a mismatch will dramatically reduce the received power levels. A linear polarized antenna will suffer a three Decibel (dB) loss with a misalignment of 45° and a 20 dB loss at 90°. Similarly, a circular antenna with the incorrect "handedness" will suffer a 20 dB loss [46]. Fortunately, circular antennas can be used to collect linearly polarized signals, albeit with a maximum 3 dB loss, so in practice a circular polarized antenna is a good choice to collect a range of different emitters.

In the preceding section, antennas and their primary characteristics of interest were introduced. This research does not specify a precise antenna type to be utilized

by the geolocation payloads. Rather, it assumes a realistically achievable gain for use in calculations.

2.1.4 Vehicle Conclusion.

The preceding three subsections have highlighted some of the basic CubeSat, SDR, and antenna capabilities and limitations. Taken as a whole, they illustrate the significant challenges, and potential rewards, of developing CubeSats for a geolocation mission. Significant research has been completed at AFIT, as well as by other civilian, government, and military organizations on the feasibility and design of a CubeSat geolocation mission. The next step is to look at the geolocation algorithms, and then evaluate if the achievable performance brings enough value to be worthwhile.

2.2 Geolocation

RF geolocation is the process of determining the position of a signal emitter on the surface of the earth. Traditionally, it can be broken into "two components: measurements and estimate" [14]. Within those two primary components are the subprocesses of "detection, correlation, association, and estimation" [47]. "Detection" refers to the ability to distinguish the presence of a signal in the presence of noise, either background transmitted RF from unwanted sources or thermal noise in the receiver(s). After signal(s) have been detected, "correlation" is the process by which multiple incident signals can be compared in order to ensure that multiple receive platforms are processing and measuring from the same source. This can be accomplished through the use of a Cross Correlation Function (CCF). The measurement must then go through the "association" process to bin or sort multiple measurements to the same source for use in geolocation algorithms. All of these steps may not be required for every measurement technique and geolocation algorithm. This section will describe

the geolocation process and is broken into two parts, signal measurement techniques and geolocation algorithms. The problems associated with the process of detection, correlation and association will not be addressed individually and are instead assumed to occur perfectly.

2.2.1 Signal Measurement Techniques.

The first step in the classical approach to geolocation is to measure the relevant signal parameters. Depending upon the geolocation phenomenology in use, these measurements can include the signal time of arrival, frequency and phase. Further, these measurements can be combined with similar measurements from other receivers to produce TDOA, Frequency Difference of Arrival (FDOA), and AOA measurements. While an in-depth study and analysis of RF measurement techniques is outside the scope of this thesis, some background is required to understand the models employed. Additionally, this is not intended as a full survey of available methods and relative performance, but rather an overview of the methods this research leverages. The following sections will cover these methods and the expected performance for TDOA and FDOA as well as for AOA measurements.

2.2.1.1 Time and Frequency Difference of Arrival Measurements.

TDOA and FDOA are commonly used measurements that require two or more receivers. TDOA is, as the name implies, a measure of the time difference(s) between when the signal arrives at one receiver and when it arrives at one or more additional receivers located at some distance from the first. The difference in the time of arrival is due to the different ranges between the emitter and each receiver, which will be elaborated upon in Section 2.2.2.1. FDOA is a measurement of the difference(s) between the received frequencies of the SOI at each receiver. The received frequency

will be different if there is relative motion between the receivers, which in-turn induces a differential range-rate to the SOI due to the Doppler effect [20].

TDOA and FDOA measurements are obtained by comparing the incident waveforms at two or more receivers and calculating the time offset, the Differential Time Offset (DTO), and the frequency offset, the Differential Frequency Offset (DFO), between them. One of the seminal works on estimation of the DTO and DFO describes the Complex Ambiguity Function (CAF) as "the basis for joint estimation of the differential delay and differential frequency offset between two waveforms that contain a common component plus additive noise" [48]. The CAF is shown in equation (2) below, with τ representing the time delay, f representing the frequency offset, and $s_1(t)$ and $s_2(t)$ representing the two waveforms in question. The estimates correspond to the values of τ and f respectively, that cause $|A(\tau, f)|$ to peak during some interval of integration T [20].

$$A(\tau, f) = \int_0^T s_1(t) s_2^*(t+\tau) \exp(-j2\pi f t)\, dt \tag{2}$$

Given the how, the next question becomes, how well can the DTO and DFO be calculated? Stein first limits the applicability by stating that "in order for the desired lobe peak to be uniquely identified (very low probability of spurious noise lobes exceeding a detection threshold), the SNR in the output has to exceed about 10 dB" and continues by saying that "For given input signal-to-noise ratios (SNRs) and given input bandwidths, the integration time T determines the accuracy with which DTO or DFO can be measured". This behavior is quantified by the standard deviations of the DTO and DFO measurements given by equations (3) and (4) where T is the integration time, B is the noise bandwidth at the receivers, β is the "Root Mean Square (RMS) radian frequency", T_e is the "RMS integration time", and γ is the effective input SNR. The intermediate quantities β, T_e, and γ are given by

equations (5), (6), and (7) respectively, with B_s representing the signal bandwidth, T representing the length of the "gated segment" and γ_1 and γ_2 representing the SNR at receiver one and two respectively.

$$\sigma_{DTO} = \frac{1}{\beta}\frac{1}{\sqrt{BT\gamma}} \tag{3}$$

$$\sigma_{DFO} = \frac{1}{T_e}\frac{1}{\sqrt{BT\gamma}} \tag{4}$$

$$\beta = \frac{\pi}{\sqrt{3}}B_s \tag{5}$$

$$T_e = 1.8T \tag{6}$$

$$\gamma = 2\left[\frac{1}{\gamma_1} + \frac{1}{\gamma_2} + \frac{1}{\gamma_1\gamma_2}\right]^{-1} \tag{7}$$

As alluded to earlier, equations (3) and (4) exhibit a strong dependence upon received signal bandwidth and integration duration. High bandwidth, low duration signals, such as are commonly encountered in radar applications, can be measured very accurately with respect to DTO but less accurately with respect to DFO. Long duration, low bandwidth signals, such as commonly encountered in communications, yields the opposite result. This behavior suggests that different geolocation techniques may be more appropriate for different signal types.

The resulting estimates from equation (2) for τ and f are unbiased and the expected standard deviations developed above for DTO and DFO are the best performance that can be expected, i.e., they achieve the Cramer-Rao Lower Bound (CRLB). While these do represent a lower bound, Stein states that "it has been shown in re-

peated experiments that they can actually be achieved in reasonable implementation".

2.2.1.2 Angle of Arrival Measurement.

AOA measurement, as a type of RF Direction Finding (DF), is one of the oldest and most studied geolocation techniques. At its most basic form, DF is simply the determination of the direction from which a signal is incident upon a collector. Simple DF techniques have been in use since the late 1800s, were used extensively in WWI and played a critical role in the Battle of the Atlantic in WWII [13; 49; 39]. While early systems made use of simple mechanically rotated hoops of wire or simple dipole antennas, current AOA measurement techniques are much more sophisticated and generally rely on a either highly directive receiving antenna, nulling measurements using several antenna feeds, or phased arrays [20].

AOA measurement differs from TDOA and FDOA in that it can be accomplished from a single receiver platform. However, rather than a single antenna/receiver set, AOA measurements require multiple antennas and either multiple receivers or an RF switching front-end to feed multiple antenna outputs to a single receiver. The antennas can be arranged in either a linear array for one dimensional (1D) angle estimation or a planar array for two dimensional (2D) estimation. One specific type of planar array is the Uniform Circular Array (UCA), which is the type of array employed on the subject single-ball AOA sensor.

Although there are many ways in which to calculate an AOA, in practice the Multiple Signal Classification (MUSIC) algorithm is one of the most widely-used and studied methods as it has the benefit of a higher resolution capability than conventional beamforming methods, and is also power independent [2]. The fundamentals of the MUSIC algorithm were originally described by Schmidt in 1979 and widely published in 1986, in which the author describes the MUSIC algorithm as "capable of

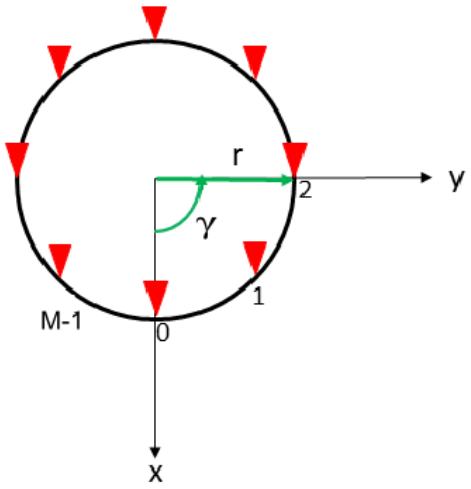

Figure 1. Uniform circular array geometry (adapted from [1])

providing asymptotically unbiased estimates of the number of signals, directions of arrival, strengths and cross correlations among the directional waveforms, polarizations, and strength of noise/interference" [50].

The ability of a UCA to resolve 2D angles of arrival is a function of the number of antenna elements M, radius of the UCA r, SNR, number of samples K, wavelength of the collected signal λ, and the incident angle of the signal planar wavefront upon the UCA. Equation (8) describes the phase delay at the n-th antenna element of a UCA arranged as shown in Figure 1. The source elevation angle is given by ε and is measured from the z-axis. Similarly, the source azimuth is given by ϕ, and is measured counterclockwise from the UCA x axis. Finally, γ is the angular position of element n, and r is the radius of the UCA [1]. This measurement system is shown in Figure 2.

$$a_n(\varepsilon, \phi) = exp\left(j\frac{2\pi}{\lambda} r \sin(\theta)\cos(\phi - \gamma_n)\right) \tag{8}$$

Understanding how the UCA reacts to an incoming wavefront is merely the first step in the MUSIC process. Next, the spatial covariance matrix R_{xx} of the collected

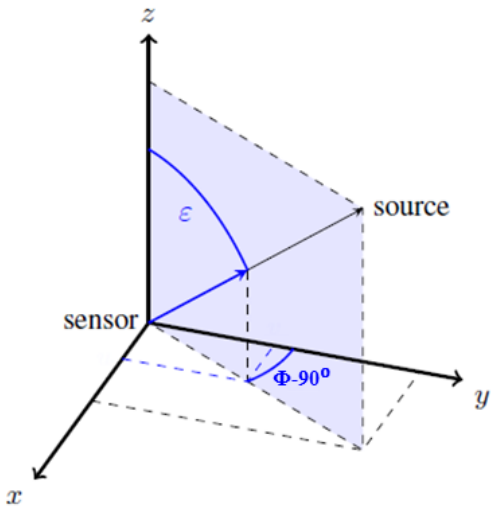

Figure 2. Uniform circular array coordinate system (adapted from [2])

signal data vector x is calculated. The MUSIC algorithm is based on the assumption that the incident signals and the noise are uncorrelated, and thus respective subspaces are disjoint and orthogonal. This fact can be leveraged by performing an eigende-composition of R_{xx} as shown in equation (9) with Q_s as the signal subspace and Q_n as the noise subspace. Recalling that the signal and noise subspaces are orthogonal, it is possible to construct a steering vector, which results in a 2D parameter search to maximize equation (9) [50; 51; 1]. The values of ε and ϕ that yield the largest peak of the probability distribution function P_{MUSIC}, are the estimated elevation and azimuth of the signal respectively.

$$\mathbf{R}_{xx} = \mathbf{QDQ}^H = \begin{bmatrix} \mathbf{Q}_s & \mathbf{Q}_n \end{bmatrix} \begin{bmatrix} \mathbf{D}_s & 0 \\ 0 & \sigma^2\mathbf{I} \end{bmatrix} \begin{bmatrix} \mathbf{Q}_s & \mathbf{Q}_n \end{bmatrix}^H \tag{9}$$

$$\mathbf{P}_{MUSIC}(\theta, \phi) = \frac{1}{\mathbf{A}^H(\theta, \phi)\mathbf{Q}_n\mathbf{Q}_n^H\mathbf{A}(\theta, \phi)} \tag{10}$$

While it is possible to generate a simulated signal and antenna response upon which to operate the algorithm [33], it is a computationally intensive, and often

an unnecessary step in modeling the performance of AOA measurement. Instead, multiple efforts have focused on determining the bounds of expected performance from ideal and realistic arrays. The bearing covariance for an ideal UCA as a function of the array parameters, SNR and the number of samples collected is shown in equation (11), where K denotes the number of samples, d is the inter-element spacing, or diameter of the UCA, M is the number of UCA elements, ε is the true elevation angle measured from the vertical in the sensor frame, and λ is the signal wavelength [2; 51; 52]. This formulation does not include bearing errors due to mismatches between the actual array transfer vector and the mathematical model thereof. These mismatches can occur for a variety of reasons including, but not limited to, non-uniform gain patterns, antenna coupling, and other phenomenon that result in "biased bearing estimates that depend on the signal direction of arrival itself" [2].

$$Cov\left(\phi,\varepsilon\right) = C_{\psi} = \frac{1}{KM^{3}SNR}\left(\frac{\lambda}{d}\right)^{2}\begin{bmatrix} \frac{1}{\cos^{2}(\varepsilon)} & 0 \\ 0 & \frac{1}{\sin^{2}(\varepsilon)} \end{bmatrix} \tag{11}$$

Although, the MUSIC algorithm in conjunction with a UCA is a very capable AOA generation arrangement, it does have limitations. First and foremost, the MUSIC algorithm is limited in the number of simultaneous signals that it can collect and process. The maximum allowable simultaneous signals is $M-1$. Another limitation is inherent in the UCA design itself. In order to correctly capture the phase difference of the incoming signals, the array segments must be no more than $\frac{1}{2}\lambda$ apart. This places a natural lower limit on the collection frequency due to size constraints, particularly on a CubeSat-scale collection platform.

2.2.2 Geolocation Algorithms.

The second step in the traditional approach to geolocation is to translate the collected signal to an emitter position. This can be accomplished in many different ways depending upon the collection platform/geometry and signal measurements available. Some of the most common geolocation algorithms include TDOA, F/T-DOA, and AOA. Each of these algorithms operates upon different information with the common goal of locating the transmitting emitter. This section will cover the formulation and application of these three algorithms.

2.2.2.1 Time Difference of Arrival.

TDOA is one of the most widely used algorithms for geolocation [33; 53; 54] and can be used in a variety of situations utilizing multiple sensors at differing baseline distances [33]. The TDOA geolocation algorithm utilizes the multiple TDOA measurements available from two or more receive platforms to form a pseudo-range problem, not dissimilar to that associated with Global Positioning System (GPS) position determination. In the TDOA formulation, the measured differences in the received times can be combined with the known speed of light c, to calculate the range difference to the emitter. According to Loomis [20], one TDOA measurement "gives rise to a locus of constant TDOA called an isochron", and in three dimensions, "an isochron is a hyperboloid of revolution about the axis joining two receivers". The intersection of these isochrons represents the estimated emitter position. A direct 2D fix requires a minimum of three collectors yielding two TDOA measurements and a direct three dimensional (3D) fix requires four collectors yielding a total of three TDOA measurements. However, it is possible to calculate a 3D fix from three collectors by including the surface of the earth as an added constraint. Additionally, it is possible to develop a position fix over time, in an under-constrained situation, by

taking advantage of relative movement between the collectors to resolve ambiguities [20]. The following is a description of the mathematical formulation of three and four-ball direct TDOA algorithms. Other techniques, often iterative and involving Taylor series linearization of the nonlinear geolocation problem exist [55], but require an initial guess, which can be provided by the direct solution.

The closed-form solution for three and four-ball TDOA geolocation was described by Ho and Chan [55] and utilized by Small [33], in a slightly modified form, for previous AFIT work. The development starts with the recognition that the difference in time of arrival between the first, or reference receiver, and the subsequent receivers two through n, τ, is related to the difference in their respective ranges to the emitter by the speed of light, as shown in equation (12). The true range from each receiver to the transmitter is given in equation (13). The combination of these two simple equations yields the emitter position [55]. Solving this nonlinear relationship is not easy however, and is the focus of Ho and Chan's work.

$$\begin{gathered} \Delta r_{i,1} = c\tau_{i,1} = r_i - r_1 \\ i = 2, 3, \ldots, n \end{gathered} \tag{12}$$

$$\begin{gathered} r_i^2 = (x_i - x_t)^2 + (y_i - y_t)^2 + (z_i - z_t)^2 \\ i = 1, 2, \ldots, n \end{gathered} \tag{13}$$

Beginning with the three ball case, it is first necessary to apply an additional constraint to allow for a 3D position fix. In the case of an emitter located on the surface of the earth at $[x_t, y_t, z_t]$, the radius of the earth, given by equation (14), serves as a convenient constraint. However, it must be noted that since the radius of the

earth is not constant, the true solution still requires either a good a priori estimate of the emitter location, or iteration of the solution to converge on the true location. Ho and Chan found that it was possible to converge upon the true radius within three or four iterations [56].

$$r_e^2 = x_t^2 + y_t^2 + z_t^2 \tag{14}$$

Combining equations (12) and (13) yields equation (15). For convenience, define an intermediate value K_i for each of the receivers as equation (16). It is then possible to convert equation (15) for each of the three receivers into a matrix form given in equation (17).

$$\begin{gathered} \Delta r_{i,1}^2 = r_i^2 - 2\Delta r_{i,1} r_1 + r_1^2 \\ i = 2, 3, \ldots, n \end{gathered} \tag{15}$$

$$\begin{gathered} K_i = x_i^2 + y_i^2 + z_i^2 \\ i = 1, 2, 3 \end{gathered} \tag{16}$$

$$\begin{bmatrix} x_1 & y_1 & z_1 \\ x_2 & y_2 & z_2 \\ x_3 & y_3 & z_3 \end{bmatrix} \begin{bmatrix} x_t \\ y_t \\ z_t \end{bmatrix} = \frac{1}{2} \begin{bmatrix} K_1 + r_e^2 - r_1^2 \\ K_2 + r_e^2 - r_1^2 - 2\Delta r_{2,1} r_1 - \Delta r_{2,1}^2 \\ K_3 + r_e^2 - r_1^2 - 2\Delta r_{3,1} r_1 - \Delta r_{3,1}^2 \end{bmatrix} \tag{17}$$

In order to solve for the emitter position, the matrix of satellite positions must be inverted, which allows the coordinates of interest to be expressed in terms of r_1, the range from the reference receiver to the target, as shown in equation (18) with $\widetilde{x}_t$, $\widetilde{y}_t$, and $\widetilde{z}_t$ representing the estimated emitter position.

$$\begin{bmatrix} \widetilde{x}_t \\ \widetilde{y}_t \\ \widetilde{z}_t \end{bmatrix} = \frac{1}{2} \begin{bmatrix} x_1 & y_1 & z_1 \\ x_2 & y_2 & z_2 \\ x_3 & y_3 & z_3 \end{bmatrix}^{-1} \begin{bmatrix} K_1 + r_e^2 - r_1^2 \\ K_2 + r_e^2 - r_1^2 - 2\Delta r_{2,1} r_1 - \Delta r_{2,1}^2 \\ K_3 + r_e^2 - r_1^2 - 2\Delta r_{3,1} r_1 - \Delta r_{3,1}^2 \end{bmatrix} \tag{18}$$

Substituting the resulting expressions for $\widetilde{x}_t$, $\widetilde{y}_t$, and $\widetilde{z}_t$ into the original range equation (13) with $i = 1$ yields a fourth-order polynomial in r_1, the roots of which can then be back substituted into equation (18) to determine the possible emitter position.

However, before that can happen, the coefficients of the quartic polynomial must be generated. The coefficients $\tilde{A}$, $\tilde{B}$, $\tilde{C}$, $\tilde{D}$, and $\tilde{E}$ in equation (19) can be produced more easily via the inclusion of a number of intermediate temporary variables. These temporary variables, defined in equations (20), (21), (22), (23), and (24) are employed in equations (25), (26), (27), (28), and (29) to calculate the necessary coefficients.

$$\tilde{A} r_1^4 + \tilde{B} r_1^3 + \tilde{C} r_1^2 + \tilde{D} r_1 + \tilde{E} = 0 \tag{19}$$

$$\begin{bmatrix} \alpha \\ \beta \\ \varphi \end{bmatrix} = \begin{bmatrix} K_1 + r_e^2 \\ K_2 + r_e^2 - \Delta r_{2,1}^2 \\ K_3 + r_e^2 - \Delta r_{3,1}^2 \end{bmatrix} \tag{20}$$

$$\begin{bmatrix} a_{11} & a_{12} & a_{13} \\ a_{21} & a_{22} & a_{23} \\ a_{31} & a_{32} & a_{33} \end{bmatrix} = \frac{1}{2} \begin{bmatrix} x_1 & y_1 & z_1 \\ x_2 & y_2 & z_2 \\ x_3 & y_3 & z_3 \end{bmatrix}^{-1} \tag{21}$$

$$\begin{bmatrix} A \\ D \\ G \end{bmatrix} = \begin{bmatrix} a_{11} & a_{12} & a_{13} \\ a_{21} & a_{22} & a_{23} \\ a_{31} & a_{32} & a_{33} \end{bmatrix} \begin{bmatrix} -1 \\ -1 \\ -1 \end{bmatrix} \tag{22}$$

$$\begin{bmatrix} B \\ E \\ H \end{bmatrix} = \begin{bmatrix} a_{12} & a_{13} \\ a_{22} & a_{23} \\ a_{32} & a_{33} \end{bmatrix} \begin{bmatrix} -2\Delta r_{2,1} \\ -2\Delta r_{3,1} \end{bmatrix} \tag{23}$$

$$\begin{bmatrix} C \\ F \\ I \end{bmatrix} = \begin{bmatrix} a_{11} & a_{12} & a_{13} \\ a_{21} & a_{22} & a_{23} \\ a_{31} & a_{32} & a_{33} \end{bmatrix} \begin{bmatrix} \alpha \\ \beta \\ \varphi \end{bmatrix} \tag{24}$$

$$\tilde{A} = A^2 + D^2 + G^2 \tag{25}$$

$$\tilde{B} = 2AB + 2DE + 2GH \tag{26}$$

$$\tilde{C} = -2x_1A - 2y_1D - 2z_1G + 2AC + 2DF + 2GI + B^2 + E^2 + H^2 - 1 \tag{27}$$

$$\tilde{D} = -2x_1B - 2y_1E - 2z_1H + 2BC + 2EF + 2HI \tag{28}$$

$$\tilde{E} = -2x_1C - 2y_1F - 2z_1I + C^2 + F^2 + I^2 + K^1 \tag{29}$$

The quartic polynomial in r_1 will yield at most four unique roots. The negative valued roots can be discarded outright, but each positive root needs to be checked to determine which more closely satisfies the constraint equations. Alternatively, any *a priori* knowledge of where the emitter is expected to be can be used to resolve remaining ambiguities.

The formulation of the four-ball TDOA equations is similar to that of the three,

but does not require the addition of the surface of the earth constraint as three TDOA measurements are sufficient to uniquely identify the emitter position in 3D space. The following formulation was employed by Small [33] and adapted from Ho and Chan [55]. Beginning with the relationship in equation (15) and combining it with equation (16) yields equation (30).

$$\begin{gathered} 2x_i x_t + 2y_i y_t + 2z_i z_t = K_i + r_e^2 - r_i^2 \\ i = 2, 3, 4 \end{gathered} \tag{30}$$

In matrix form, this yields equation (31), in which r_1 and the unknown emitter coordinates are the only unknown variables. This equation can then be solved for x_t, y_t, and z_t as functions of r_1 and then substituted into equation (13) to yield a quadratic in r_1 in equation (32) with A, B, and C defined in equations (33), (34), (35) respectively. The roots of this quadratic equation represent possible values of r_1.

$$\begin{bmatrix} \Delta r_{2,1}^2 \\ \Delta r_{3,1}^2 \\ \Delta r_{4,1}^2 \end{bmatrix} + 2r_1 \begin{bmatrix} \Delta r_{2,1} \\ \Delta r_{3,1} \\ \Delta r_{4,1} \end{bmatrix} = -2 \begin{bmatrix} x_{2,1} & y_{2,1} & z_{2,1} \\ x_{3,1} & y_{3,1} & z_{3,1} \\ x_{4,1} & y_{4,1} & z_{4,1} \end{bmatrix} \begin{bmatrix} x_t \\ y_t \\ z_t \end{bmatrix} + \begin{bmatrix} K_2 \\ K_3 \\ K_4 \end{bmatrix} - \begin{bmatrix} K_1 \\ K_1 \\ K_1 \end{bmatrix} \tag{31}$$

$$0 = Ar_1^2 + Br_1 + C \tag{32}$$

$$A = \alpha_1^2 + \alpha_2^2 + \alpha_3^2 - 1 \tag{33}$$

$$B = 2(\alpha_1\beta_1 + \alpha_2\beta_2 + \alpha_3\beta_3 - x_1\alpha_1 - y_1\alpha_2 - z_1\alpha_3 \tag{34}$$

$$C = K_1 - 2x_1\beta_1 - 2y_1\beta_2 - 2z_1\beta_3 + \beta_1^2 + \beta_2^2 + \beta_3^2 \tag{35}$$

In a similar manner as in the three-ball case, the introduction of intermediate, temporary variables will ease the calculation. The intermediate variables α and β are given in equations (36) and (37).

$$\begin{bmatrix} \alpha_1 \\ \alpha_2 \\ \alpha_3 \end{bmatrix} = - \begin{bmatrix} x_{2,1} & y_{2,1} & z_{2,1} \\ x_{3,1} & y_{3,1} & z_{3,1} \\ x_{4,1} & y_{4,1} & z_{4,1} \end{bmatrix}^{-1} \begin{bmatrix} \Delta r_{2,1} \\ \Delta r_{3,1} \\ \Delta r_{4,1} \end{bmatrix} \tag{36}$$

$$\begin{bmatrix} \beta_1 \\ \beta_2 \\ \beta_3 \end{bmatrix} = - \begin{bmatrix} x_{2,1} & y_{2,1} & z_{2,1} \\ x_{3,1} & y_{3,1} & z_{3,1} \\ x_{4,1} & y_{4,1} & z_{4,1} \end{bmatrix}^{-1} \frac{1}{2} \begin{bmatrix} \Delta r_{2,1}^2 - K_2 + K_1 \\ \Delta r_{3,1}^2 - K_3 + K_1 \\ \Delta r_{4,1}^2 - K_4 + K_1 \end{bmatrix} \tag{37}$$

The calculated values of r_1 must then be evaluated to determine the appropriate solution. Negative values may be immediately discarded and additional constraints such as proximity to the surface of the earth may be used to resolve any remaining ambiguities. Equation (38) gives the emitter position in Earth Centered Earth Fixed (ECEF) coordinates.

$$\begin{bmatrix} \widetilde{x}_t \\ \widetilde{y}_t \\ \widetilde{z}_t \end{bmatrix} = - \begin{bmatrix} x_{2,1} & y_{2,1} & z_{2,1} \\ x_{3,1} & y_{3,1} & z_{3,1} \\ x_{4,1} & y_{4,1} & z_{4,1} \end{bmatrix}^{-1} \left[\begin{bmatrix} \Delta r_{2,1} \\ \Delta r_{3,1} \\ \Delta r_{4,1} \end{bmatrix} r_1 + \tfrac{1}{2} \begin{bmatrix} \Delta r_{2,1}^2 - K_2 + K_1 \\ \Delta r_{3,1}^2 - K_3 + K_1 \\ \Delta r_{4,1}^2 - K_4 + K_1 \end{bmatrix} \right] \tag{38}$$

2.2.2.2 Angle of Arrival.

The AOA algorithm has its roots in early DF techniques for geolocation and navigation [13; 39]. These techniques consisted of using multiple AOAs, either from one

receiver in different locations or multiple spatially separate receivers, to triangulate an emitter's position. Historically, this was typically accomplished in two dimensions, as both emitter and receiver were near the surface of the earth. However, the general triangulation approach is extensible to three dimensions which opens the possibility of applying the technique using satellites. The AOA algorithm is particularly attractive for use on a CubeSat as it is possible to perform geolocation from a single moving platform capturing multiple AOAs over a period of time, making geolocation possible from a single collector. The remainder of this section will cover the basics of how the triangulation algorithm works, as well as some of the limitations and sources of error in its application.

In concept, the triangulation algorithm is very simple. First, measured AOAs are combined with the position of the receiver at the time of signal intercept and projected towards the emitter to create a Line of Bearing (LOB), or vector in 3D space, from the receiver in the direction of the emitter. The precise magnitude of projection is not critical so long as it extends beyond the maximum possible emitter range. Multiple LOBs to the emitter are created from spatially and temporally disparate locations, with the point of intersection indicating the position of the emitter [15; 3]. In two dimensions, this can be accomplished with two azimuth LOBs. In three dimensions, it requires two 2D LOBs incorporating azimuth (ϕ) and elevation (θ) angles [3]. A graphical representation of a simple 2D AOA geolocation scenario with three LOBs is shown in Figure 3.

In the case of perfect AOA and receiver position measurements, each LOB will precisely intersect at the emitter. However, in real-world applications this is not the case and LOBs are not likely to share a common intersection point. In this case, it is necessary to determine the *best* solution for the emitter position given the imperfect LOB information. This is accomplished by introducing a term, D, as the sum of

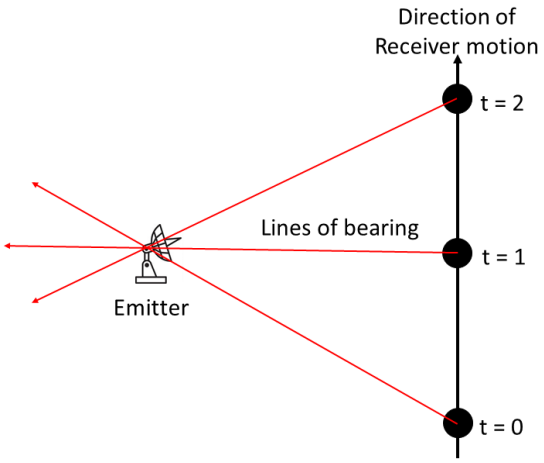

Figure 3. Simple 2D AOA triagulation

the squared distances from each LOB to a possible emitter location [3], as shown in equation (39). The distance from each LOB to any arbitrary point in 3D space is given by Boas [57] in equation (40) where s_t and s_i represent the Cartesian coordinates of the transmitter and i-th receiver respectively, per equations (41) and (42). The minimum distance between a line and a point is the vector perpendicular to the line which goes through the point in question. This is depicted in Figure 4.

$$D\left(s_t\right) = \sum_{i=1}^{N} d_i^2(s_t, LOB_i) \tag{39}$$

$$d_i = \left| (s_t - s_i) \times \frac{\overrightarrow{LOB}}{\left|\overrightarrow{LOB}\right|} \right| \tag{40}$$

$$s_t = \begin{bmatrix} x_t & y_t & z_t \end{bmatrix}^T \tag{41}$$

$$s_i = \begin{bmatrix} x_i & y_i & z_i \end{bmatrix}^T \tag{42}$$

In order to determine the *best* estimate for the emitter location, it is necessary to

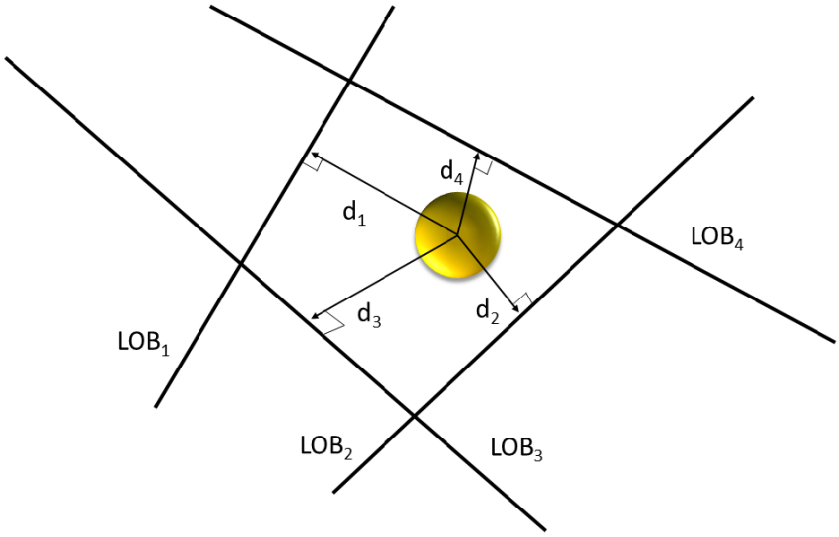

Figure 4. Distance from LOBs to point in three dimensional space (adapted from [3])

minimize D in equation (39) [3]. That is, find the point that has the smallest total sum of squared distances from the LOBs. Thus, this becomes a least squares problem as described in [33; 58] and formulated as follows. Let LOB_i have a start point v_i at the receiver location s_i and end point w_i. A unit vector, u_i along this LOB is then defined by equation (43). Equation (44) constructs a projection matrix $\mathbf{a}$ that projects any vector onto the plane perpendicular to LOB_i and passing through the origin. The intersection of the normal plane and the LOB is then given by equation (46). Creating matrix $\mathbf{A}$ as the sum of all projection matrices $\mathbf{a}$ per equation (45) and vector b as the summation of all points of intersection per equation (47) sets up the least squares problem. The solution to the least squares problem, given in equation (48), represents the estimated emitter position that minimizes D, with $\mathbf{A}^+$ indicating the Moore-Penrose pseudoinverse of $\mathbf{A}$.

$$u_i = \frac{\overrightarrow{LOB}}{\left|\overrightarrow{LOB}\right|} = \frac{(v_i - w_i)}{|v_i - w_i|} \tag{43}$$

$$\mathbf{a}_i = \begin{bmatrix} 1 & 0 & 0 \\ 0 & 1 & 0 \\ 0 & 0 & 1 \end{bmatrix} - u_i * u_i^T \tag{44}$$

$$\mathbf{A} = \sum_{i=1}^{N} \mathbf{a}_i \tag{45}$$

$$p_i = \mathbf{a}_i * w_i \tag{46}$$

$$b = \sum_{i=1}^{N} p_i \tag{47}$$

$$\begin{bmatrix} \widetilde{x}_t \\ \widetilde{y}_t \\ \widetilde{z}_t \end{bmatrix} = \mathbf{A}^{+} b \tag{48}$$

While the AOA algorithm is simple and powerful, it does have limitations and several potential sources of error. One of the limitations that needs to be considered is that as a triangulation technique, it is sensitive to collection geometries. Although two LOBs are sufficient to calculate an estimated position, if those LOBs are too closely spaced, in the presence of noise, there will be significant ambiguity as to the true intersection point. In contrast, two or more widely separated LOBs will result in a less ambiguous emitter position. This phenomenon is known as Geometric Dilution of Precision (GDOP) and is illustrated in Figures 5a and 5b with the yellow and black hatched regions indicating possible emitter locations. It is obvious that widely separated LOBs with uncertainty yield a smaller area of intersection than the same LOBs from closely spaced receivers. A satellite has the potential, depending upon pass geometry and contact times, to collect from multiple widely disparate locations

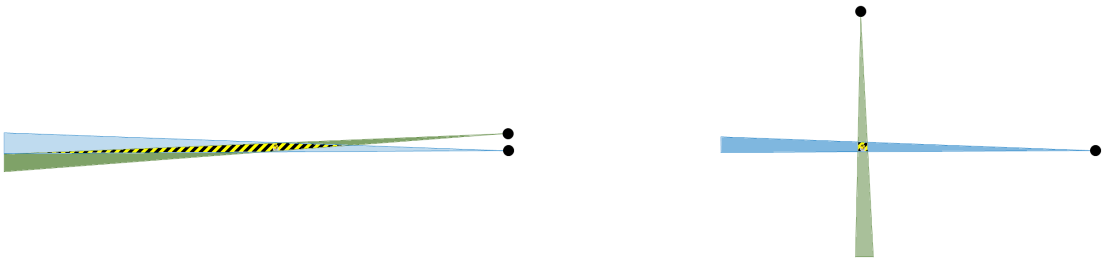

(a) Bad GDOP **(b) Good GDOP**

Figure 5. Comparison of bad and good GDOP collection geometry

yielding a beneficial GDOP.

Another requirement for accurate geolocation of the emitter using the AOA algorithm is precise receiver platform attitude knowledge [26; 7]. The measured azimuth and elevation angles are measured with respect to the platform's attitude, and if that attitude is not correctly known, then the translation of the LOBs to the ECEF frame of reference will include an unknown bias. As star trackers are the most accurate method of determining SV attitude, and the volume constraints of a CubeSat limit the employment of star trackers, this points to a potential disadvantage of the CubeSat platform.

The final consideration is related to the ability to estimate the resulting variance on an estimate derived from the AOA triangulation algorithm. It is typically possible to calculate the CRLB, or best statistically achievable performance, of TDOA and F/TDOA algorithms, but this in not the case with TDOA [3]. While it is true that the uncertainty associated with an estimated emitter position decreases with the number of LOBs [15], that decrease cannot be easily quantified with the algorithm as currently constructed. However, research into modified AOA techniques, such as employing Nonlinear Optimization (NLO), does provide that information. The use of such algorithms are outside of the scope of this effort and will not be covered in depth.

2.2.3 Geolocation Conclusion.

The preceding treatment of geolocation algorithms is not exhaustive. There are many different approaches presented in the literature to achieve the same final solution. Some algorithm formulations may be more suitable than others for specific signal types and collection scenarios, but the presented algorithms will be sufficient to answer the questions posed in Chapter I. The aforementioned algorithms will each provide an explicit solution in 3D space. However with the assumption that the emitter is located on the surface of the earth, it is possible to apply an additional constraint. The methods for application as well as fusion of multiple estimates will be briefly discussed in the following sections.

2.3 Surface of the Earth Constraint

A common constraint imposed in geolocation problems is that the emitter must lie on, or near, the surface of the earth. There are several commonly encountered techniques in the literature to accomplish this goal. For some geolocation problems, particularly in short range, low altitude, and/or simplified formulations, the surface of the earth is assumed to be a 2D flat plane [59]. Research focused on geolocating targets of interest from satellites typically introduce either a spherical earth model or use the World Geodetic System 1984 (WGS 84) reference ellipsoid for increased fidelity. The most fidelity is achieved through the use of a Digital Elevation Model (DEM). This section will introduce the different types of DEMs available and the characteristics of each type. Application of the surface of the earth constraint will be covered in section 3.5.

2.3.1 Digital Elevation Models.

Elevation models play an increasingly important role in many civilian and military applications. An elevation model can be as simple as a topographic map [60] or as complex as sub−meter resolution Light Detection and Ranging (LIDAR) data. However, until relatively recently, the large variety of different DEMs available made it difficult to work on a global scale due to the disparate nature of each country's approach, standards, and chosen datum(s) [60]. Additionally, large parts of the world, particularly those commonly obscured by heavy cloud cover, had no high accuracy elevation data [60]. Fortunately, with the completion of the Shuttle Radar Topography Mission, DEMs are now available with nearly complete global coverage. This section provides background on the common terminology and datums used in discussing DEMs, and the differences between the different DEM products.

DEM is the generic term for any digital terrain or surface model. A DEM is typically stored and visualized in a matrix format, with each cell representing a "post" of elevation data. There are two basic sub-types of DEM, Digital Terrain Model (DTM)s and Digital Surface Model (DSM)s. DTMs and DSMs are similar, but differ in one important respect. A DTM is a bare-earth representation of the surface of the earth whereas a DSM is a representation of the first reflective surface [61]. That is, a DTM is stripped of all man-made features such as buildings and vegetation such as trees while a DSM includes these features. Often, a DTM is produced from the same data set as a DSM, just with additional post-processing.

A common feature of all DEMs is that they must be referenced to a known datum in order to be useful. The particular datum(s) used varies from product to product, but all include a horizontal and vertical component. The horizontal component refers to the position on the surface of the earth in the common north/south, east/west sense. A commonly used horizontal datum is the WGS 84 reference ellipsoid. The

vertical datum is used to establish height or elevation, commonly above Mean Sea Level (MSL) [59]. The most used vertical datum is the Earth Gravitational Model 1996 (EGM 96) geoid. The EGM 96 geoid is defined as "the equipotential surface of the Earth's gravity field which best fits MSL if the sea were extended through the continents" [59]. It is described by a spherical harmonics series of degree and order 360 [4] and differs from the WGS 84 ellipsoid by up to 100 meters [59]. Figure 6 graphically depicts the difference between the EGM 96 geoid and the WGS 84 ellipsoid with areas in red indicating that EGM 96 is higher than WGS 84 and areas in purple indicating the opposite. Fortunately, translating between heights referenced to the EGM 96 geoid and the WGS 84 ellipsoid is a common occurrence and relatively straightforward. Figure 7 shows the relationship between the ellipsoidal height h, geoid height N, and orthometric height H. The mathematical relationship is given in equation (49). This research utilizes the ellipsoidal height for all altitudes. Also worth noting is that in actual practice, as well as in this research, Digital Terrain Elevation Data (DTED) data is usually sampled at a much higher resolution than the EGM 96 model, so it is necessary to perform a 2D interpolation over the surface. This will be expounded upon in section 3.5.

$$h = N + H \tag{49}$$

The two most commonly used DEMs in the DOD are DTED and Shuttle Radar Topography Mission (SRTM). The National Geospatial-Intelligence Agency (NGA) produces, controls and distributes DTED as well as DTED formatted SRTM data sets [62]. NASA also distributes SRTM data sets [5]. Fortunately, the two data types share many of the same characteristics which make it easy to use one in place of the other depending upon the needs of a specific application. Firstly, the two share the same terminology used to describe the resolution of the data. As mentioned above,

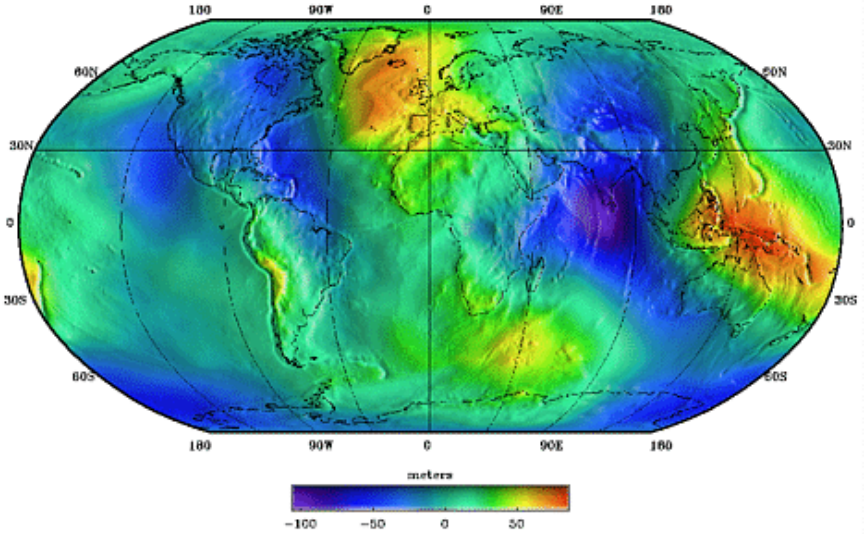

Figure 6. EGM 96 geoid [4]

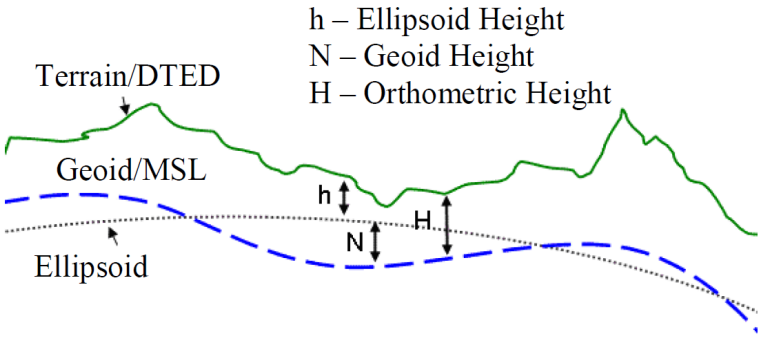

Figure 7. Relationship between ellipsoid, geoid and orthometric height [5]

DEMs can be visualized as posts of elevation data. The size, or "post-spacing", of the posts determines the resolution of the DEM. DTED and SRTM are available in three different post-spacings, indicated by a -0, -1, or -2. DTED/SRTM-0 is the lowest resolution data with 30 arc second post-spacing, DTED/SRTM-1 has an order of magnitude better resolution with 3 arc second post$-$spacing and DTED/SRTM-2 is higher yet at 1 arc second. Even higher resolution data is available via LIDAR collection at the High Resolution Terrain elevation (HRTe)$-3,-4$, and -5 levels, 0.4, 0.2, and 0.04 arc second respectively, but is typically only available in small areas [63]. Table 1 shows the post size for each level as a function of the latitude of the point of interest [8]. It must be noted that the cell dimensions are equal in width and height (arc seconds of longitude and latitude) at mid latitudes, up to 50° north and south, but deviate at higher latitudes. This is necessary in order to keep the posts nearly square as latitude lines come together at the poles. See Table 1 for post dimensions per given latitude. Another commonality between the two data sets is that they are referenced in the same way. Both use the WGS 84 ellipsoid as the horizontal datum and EGM 96 as the vertical datum [59; 64; 8]. Further, both standards use the southwest corner of an area or cell as the reference point and are arranged in the same file structure with the same naming convention. This makes it very easy to swap out one data set in favor of the other when conditions warrant.

Table 1. DTED post sizes (adapted from [8])

	DTED Level 0		DTED Level 1		DTED Level 2	
Position on Earth	Post Size (arc second)					
Latitude North/South (deg)	lat	lon	lat	lon	lat	lon
0 - 50	30	30	3	3	1	1
50 - 70	30	60	3	6	1	2
70 - 75	30	90	3	9	1	3
75 - 80	30	120	3	12	1	4
80 - 90	30	180	3	18	1	6

Despite the similarities, there are differences between the two products that make one more or less suitable than the other for some uses. These differences include bare earth versus surface model, collection method, and releasabilty. The most significant difference between the two products is that DTED is a DTM type product whereas SRTM is a DSM. DTED has been processed to remove all vegetation and man-made objects, which make it most useful in cases where the true terrain contours are of interest, or where the target of interest is likely obscured by heavy vegetative cover. In contrast, SRTM includes the highest return and thus preserves vegetation and man-made objects. This data set is of particular use in cases where the emitter may be positioned away from the surface of the earth. For example, on the top of a building, or installed on a tower [61]. The next major difference between the two data sets is the collection method. As the name implies, SRTM is derived from the data collected by the Shuttle Radar Topography Mission using Synthetic Aperture Radar (SAR) interferometry. The nature of SAR collection results in some areas of poor, or no, returns yielding data voids. SRTM voids were typically caused by either lack of line-of-sight, for example the back side of a steep slope, or "smooth areas such as smooth water or sand which scattered too little energy back to the radar to create an image" [60]. These voids can create problems, particularly if not correctly identified, which is why the Shuttle Radar Finished Topography (SRFT) product type was created. SRFT is based off of SRTM, but processed to remove spikes, wells, and small voids [60]. Additionally, ocean elevations were set to zero meters, and lakes and rivers were clearly delineated at a constant elevation [60]. This processing did result in the removal of some data cells, but the SRFT data set is still considered "good" and "has been vetted and approved by NGA as production quality" [63]. In contrast to SRTM, the DTED data can come from more than one collector and includes National Technical Means (NTM) collections. This inclusion of NTM data

partly drives the differing releasability of the two data sets. Only DTED−0 is publicly releasable, DTED levels 1 and 2 are Limited Distribution only [62]. Unlike DTED, SRTM and SRFT levels 0 and 1 are fully publicly releasable, level 2 coverage of the US and Africa is fully releasable, and level 2 global coverage will be released over the next year [65]. This makes SRTM and SRFT data particularly attractive for research and publishing purposes.

The inclusion of high fidelity DEMs is an exciting area of research. As DEMs become more prevalent and releasability improves, it is likely that they will find additional uses in civilian and military applications. The inclusion of DEMs in the geolocation problem is certainly a promising area and will be explored in the course of this research.

2.4 Geolocation Fusion Techniques

Fusion has been described as the "synergistic use of sensory data from multiple sensors to extract the greatest amount of information possible about the sensed environment" [47]. It is, in the most basic sense, combining multiple observations or measurements to create one, hopefully improved, measurement. Fusion is often employed in conjunction with distributed sensor networks, and has been the subject of increased study, particularly with focus shifting to network-centric warfare and intelligence gathering [6]. As a process, fusion "includes detection, correlation, estimation, and combination of data" [47]. This section focuses on the techniques used in the combination of data for fused estimates.

Before discussing specific fusion techniques, it is first necessary to discuss common terminology. An estimated geolocation has two components. Obviously one of these components is the estimated geolocation coordinates, $[\tilde{x}_t, \tilde{y}_t, \tilde{z}_t]$, indicated as the vector $\hat{\mathbf{x}}$ and commonly annotated with a subscript indicating which collector

the estimate is from. The second component of the estimate is the covariance, or uncertainty, associated with the measurement. The covariance is given by the matrix $\mathbf{P}$, again commonly annotated with a subscript indicating the associated collector. In addition to the covariance, another measure of confidence is commonly used. The Information Matrix, or Fisher Information Matrix (FIM), is indicated by the matrix $\mathbf{I}$. The FIM is a measure of the amount of information present in a measurement and is the inverse of the true, converged covariance [66], per equation (50) [67].

$$\mathbf{P} = \mathbf{I}^{-1} \tag{50}$$

One of the most important considerations when evaluating fusion techniques is whether or not the technique in question is consistent. In fact, Julier and Uhlmann state that "the fundamental requirement of an estimator is that it is able to fuse information from a number of noise corrupted sources to make consistent inferences about the state of a system" [68]. Consistency in the context of estimate fusion means that the "estimated covariance is always an upper-bound" [35]. In practical terms, a consistent estimate of covariance will result in a confidence ellipse or ellipsoid that contains the intended percentage of results. For example, a 100 run Monte Carlo simulation will result in 95 estimates within a consistent 95% ellipsoid. A non-consistent estimate would likely contain fewer than 95% of the estimates as it does not represent the true upper-bound of expected variance. In the absence of any correlation between measurements to be fused, consistency can be obtained through a variety of methods, including Kalman filtering [35; 66; 34; 6]. However, in the presence of unknown correlation, consistency can be more difficult to achieve. According to Niehsen, who pioneered one of the techniques for dealing with unknown correlation, "ignorance of cross correlations yields nonconservative Kalman filter estimates with overly confident estimation error variance" [69]. These correlations between estimates

can exist for a number of different reasons. One of the first and foremost reasons that estimates might be considered to be correlated is if there is a "lack of knowledge of the true system" [68]. A system may be particularly complex with difficult to quantify error sources, particularly second-order statistics [69]. Another potential reason is 'data incest' that can occur between nodes in distributed networks [66]. In the case of geolocating an RF emitter, it is possible that correlation of estimates will occur due to non-Gaussian errors introduced by the signal propagating from the same emitter and potentially through the same atmosphere to each collector. Regardless of the cause of estimate correlation, it must be considered to produce a consistent estimate. The following subsections describe and demonstrate some of the different methods employed to achieve consistency.

2.4.1 Kalman Filter.

The Kalman filter is one of the most widely used and studied methods for fusing multiple measurements. In fact, some have gone so far as to describe it as "one of the cornerstones of modern technology" [35]. A Kalman filter operates by considering information matrices and states, and combining them via simple convex addition as shown in equation (51). $\hat{\mathbf{x}}$, $\hat{\mathbf{x}}_1$, and $\hat{\mathbf{x}}_2$ indicate the fused estimate, source one estimate, and source two estimate respectively, with associated covariance matrices P, P_1, and P_2. It has been shown that in the case where there is both Gaussian system and measurement noise, "the Kalman filter is the optimal estimator in the mean square error sense for the state of a linear dynamic system" [69]. Optimal, in this instance, refers to the fact that the Kalman filter minimizes the trace of resulting fused covariance matrix [35] and is also optimal in the least squares sense, and the resulting error is orthogonal to the measurements used.

While the Kalman filter is an extremely powerful tool, it does have weaknesses.

An inherent assumption in the application of a Kalman filter is that"each information source can be expressed as a random variable with a known mean, covariance, and cross correlation with other sources" [68]. If these assumptions are not true, for example, if the sources are correlated, the estimates are not guaranteed to be consistent. Additionally, although a Kalman filter can be tuned to achieve consistency under certain conditions, this often results in an unstable filter that will diverge [68]. Neglecting instability, if a Kalman filter is utilized without full knowledge of second-order statistics, such as the cross correlations, it will result in an estimate with "overly confident estimation error variances" [69]. Graphically, this is demonstrated in Figure 8, where the Kalman filter fused ellipse is smaller than the overlap in the two individual source error ellipses. Despite these limitations, the Kalman filter is a convenient reference for this thesis, and is expected to perform well with models corrupted by Gaussian distributed noise.

$$\hat{\mathbf{x}} = \mathbf{P}\mathbf{P}_1^{-1}\hat{\mathbf{x}}_1 + \mathbf{P}\mathbf{P}_2^{-1}\hat{\mathbf{x}}_2 \tag{51a}$$

$$\mathbf{P}^{-1} = \mathbf{P}_1^{-1} + \mathbf{P}_2^{-1} \tag{51b}$$

2.4.2 Covariance Intersection.

One of the issues encountered when trying to fuse sensor data is the problem of unknown, or unquantified, measurement correlation. In the presence of such correlation, the Kalman filter convex combination estimates are non-conservative, and yield "overly confident estimation error variances" [69]. Covariance Intersection (CI) is a technique that was developed in an attempt to address this problem and produce consistent estimates independent of network structure in the presence of an unknown degree of correlation between sensor node measurements [66; 69; 68]. It has

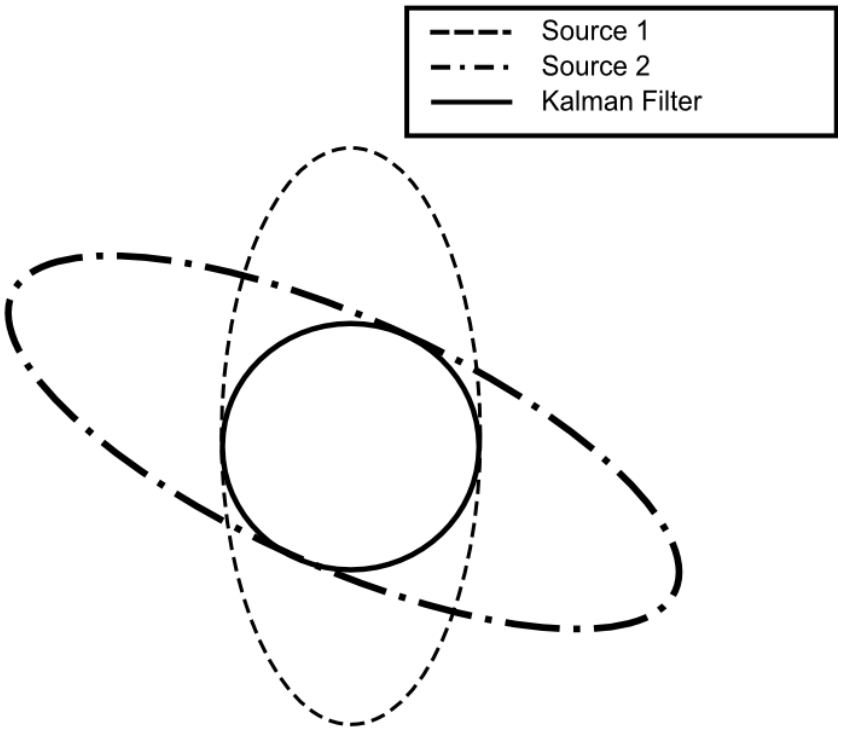

Figure 8. Graphical depiction of Kalman filter ellipse fusion

proven successful, and is widely used, particularly in distributed estimation [35]. CI is still based upon convex combinations of information matrices, but includes weighting terms in an attempt to account for the unknown correlation. These weighting terms are generally chosen such that they minimize either the trace or the determinant of the ellipsoid that fully encompasses the intersection of the ellipsoids corresponding to the covariances of the measurements [66]. It is perhaps best illustrated rather than described. Figure 9 notionally depicts the goal of the CI algorithm. There are multiple ways of achieving this goal. As mentioned, the optimal solution requires minimizing either the trace or determinant of the combined error covariance matrix. As this is numerically intensive, it is commonly estimated using the Fast Covariance Intersection algorithm. There are also improved CI algorithms that attempt to take advantage of the relative orientations of the error ellipsoids. The formulations of the "fast" and improved approaches are discussed below.

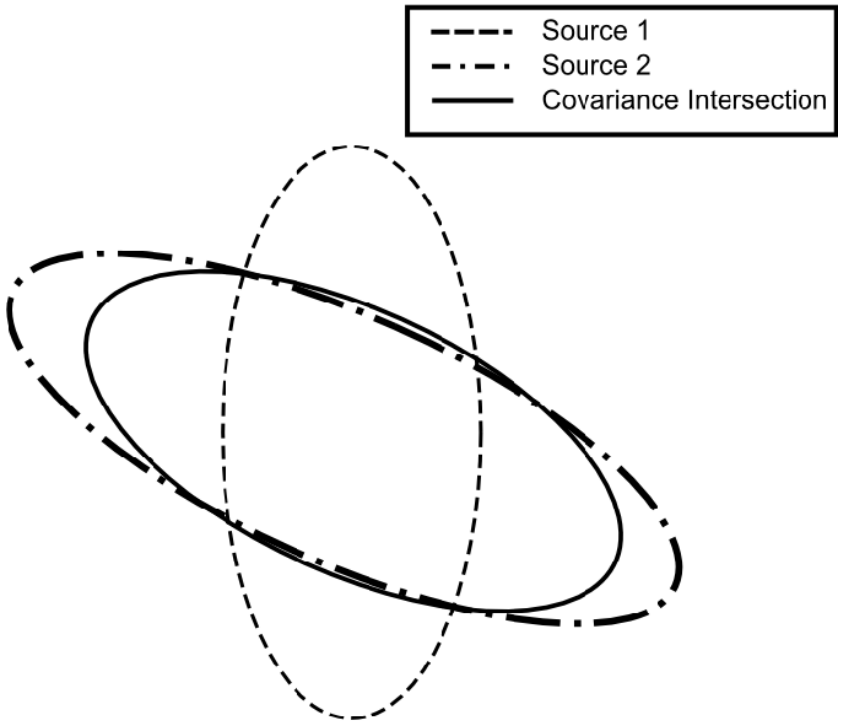

Figure 9. Graphical depiction of Covariance Intersection ellipse fusing

One of the downsides of the CI algorithm is that computing the weighting that minimizes the determinant or trace of the resulting covariance matrix requires a search along a 1D curve in n-squared-dimensional space. In order to avoid this computationally expensive operation, a "fast" CI algorithm was created by Niehsen [69]. This Fast CI algorithm can be used to produce weighting coefficients to minimize either the determinant or trace of the resulting covariance matrix.

Like the Kalman filter, the Fast CI algorithm is based upon convex combinations of the estimates [66]. However, it differs from the Kalman filter Convex combination, as shown in equation (51), in that it includes non-negative weighting factors ω_1 and ω_2 as shown in equation (52), with $\hat{\mathbf{x}}_1$ and $\hat{\mathbf{x}}_2$ as the estimates with associated covariance matrices $\mathbf{P}_1$ and $\mathbf{P}_2$ respectively.

$$\hat{\mathbf{x}} = \omega_1 \mathbf{P}\mathbf{P}_1^{-1}\hat{\mathbf{x}}_1 + \omega_2 \mathbf{P}\mathbf{P}_2^{-1}\hat{\mathbf{x}}_2 \tag{52a}$$

$$\mathbf{P}^{-1} = \omega_1 \mathbf{P}_1^{-1} + \omega_2 \mathbf{P}_2^{-1} \tag{52b}$$

$$\omega_1 + \omega_2 = 1 \tag{52c}$$

The calculation of ω_1 and ω_2, as developed by Niehsen, focuses on the trace of the resulting estimate covariance matrix [66]. Noting that if $trace(\mathbf{P}_1) \ll trace(\mathbf{P}_2)$, that is the error ellipsoid of estimate 1 is much smaller than that of estimate 2, then estimate 1 should be weighted more heavily and $\omega_1 \approx 1$. To that end, Niehsen proposed equation (53) as the appropriate relationship between ω_1 and ω_2, which naturally leads to the expression for ω_1 in equation (54) [66]. The same process can be used to estimate the minimization of the determinant, yielding an ω_1 given by equation (55).

$$\omega_1 \; trace(\mathbf{P}_1) - \omega_2 \; trace(\mathbf{P}_2) = 0 \tag{53}$$

$$\omega_1 = \frac{trace(\mathbf{P}_2)}{trace(\mathbf{P}_1) + trace(\mathbf{P}_2)} \tag{54}$$

$$\omega_1 = \frac{det(\mathbf{P}_2)}{det(\mathbf{P}_1) + det(\mathbf{P}_2)} \tag{55}$$

The preceding formulations rely on the estimation error variances, but it is also possible to construct them from a FIM perspective [66]. Using the relationship in equation (56), ω_1 can be described per equations (57) and (58). The FIM based equivalent of (52) is given in equation (59).

$$\mathbf{I} = \mathbf{P}^{-1} \tag{56}$$

$$\omega_1 = \frac{trace(\mathbf{I}_1)}{trace(\mathbf{I}_1) + trace(\mathbf{I}_2)} \tag{57}$$

$$\omega_1 = \frac{det(\mathbf{I}_1)}{det(\mathbf{I}_1) + det(\mathbf{I}_2)} \tag{58}$$

$$\mathbf{I}\hat{x} = \omega_1 \mathbf{I}_1 \hat{\mathbf{x}}_1 + \omega_2 \mathbf{I}_2 \hat{x}_2 \tag{59a}$$

$$\mathbf{I} = \omega_1 \mathbf{I}_1 + \omega_2 \mathbf{I}_2 \tag{59b}$$

$$\omega_1 + \omega_2 = 1 \tag{59c}$$

One of the weaknesses of the Fast CI algorithm is that it does not take the orientation of the respective covariances ellipses into account. An example from [66], illustrates this well. Consider the case where $\mathbf{I}_1 > \mathbf{I}_2 \Leftrightarrow \mathbf{P}_1 < \mathbf{P}_2$ with orientations shown in Figures 10 and 11. In Figure 10, where the source 1 covariance ellipse is wholly contained within the source 2 ellipse and the two ellipses are nearly collinear, the minimum combined covariance $\mathbf{P}$ is associated with an $\omega_1 = 1$. However, the Fast CI algorithm, either trace or determinant oriented, will return $\omega_1 \approx \frac{1}{2}$. While this is not optimal, it actually is a a more reasonable value if the two estimates are completely, or nearly completely, uncorrelated [66]. In this case the loss of performance is small. However, in a case such as depicted in Figure 11 where the covariances are nearly orthogonal, the Fast CI algorithm will return $\omega_1 \gg \frac{1}{2}$, which inappropriately ignores the significant information from source 2 due to the orthogonal orientation of the covariances. Taking the effect of the orientation into account is the goal of the

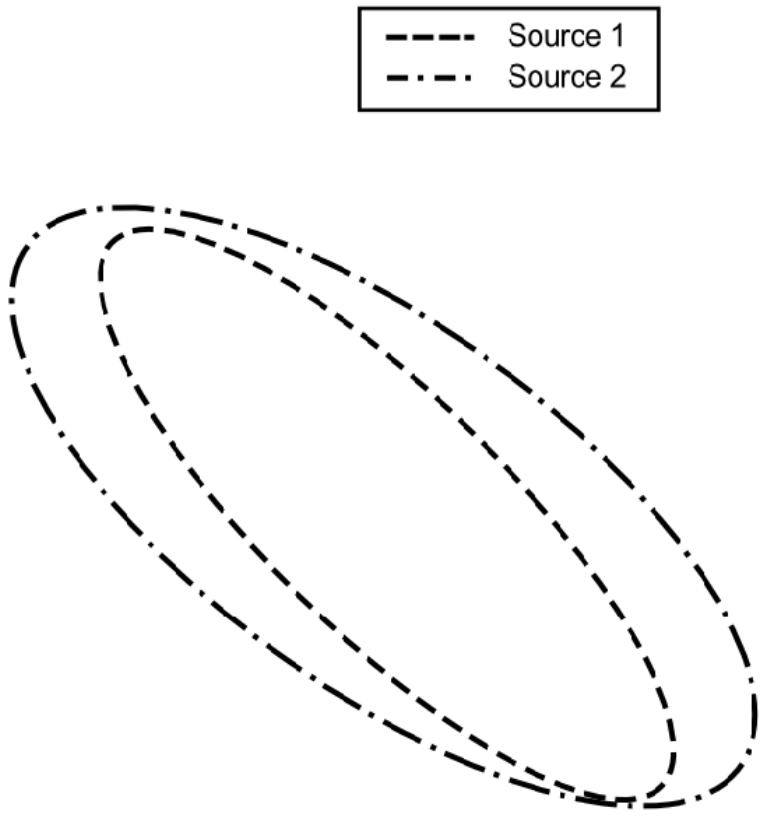

Figure 10. Unknown correlation with similar orientations

Improved Fast Covariance Intersection algorithm [66].

The development of the Improved Fast CI algorithm, as described by Fränken and Hüpper, starts with equations (55) and (58). From there, an ω_1 that is more symmetric is produced by introducing a new term α_1. This relationship is shown in equation (60) with α_1 defined by equation (61). In order to improve the performance in the scenarios such as shown in Figure 11, a correction factor β, given by equation (62), is applied to α to produce $\tilde{\alpha}$ per equation (63). The correction factor is a function of the angle between the covariance major semi-axes, and reaches a peak when the major semi-axes are orthogonal [47].

$$\omega_1 = \frac{1 - \alpha_1}{2} \tag{60}$$

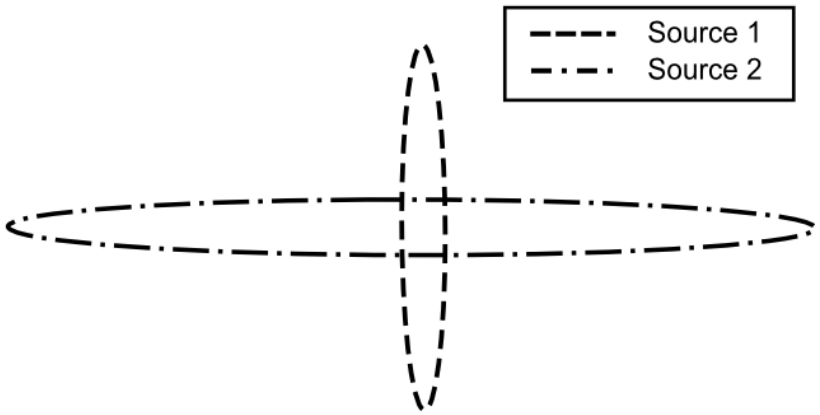

Figure 11. Unknown correlation with orthogonal orientations

$$\alpha_1 = \frac{\det(\mathbf{P}_1) - \det(\mathbf{P}_2)}{\det(\mathbf{P}_1) + \det(\mathbf{P}_2)} = \frac{\det(\mathbf{I}_2) - \det(\mathbf{I}_1)}{\det(\mathbf{I}_2) + \det(\mathbf{I_1})} \tag{61}$$

$$\beta = \frac{\det(\mathbf{I}_2) + \det(\mathbf{I}_1)}{\det(\mathbf{I}_2 + \mathbf{I}_1)} = \frac{\det(\mathbf{P}_1) + \det(\mathbf{P}_2)}{\det(\mathbf{P}_1 + \mathbf{P}_2)} \tag{62}$$

$$\tilde{\alpha}_1 = \beta\alpha_1 \tag{63}$$

According to Fränken and Hüpper, "the general orientation-dependent behavior of the correction factor is expected to be preserved for higher dimensions" due to the fact that the general form of $\tilde{\alpha}_1$, given in equation (64), "takes into account not only a measure of information assigned individually to each estimate, i.e. $det(\mathbf{I}_1)$ and $det(\mathbf{I}_2)$, but also $det(\mathbf{I}_1 + \mathbf{I}_2)$ as a measure of the joint information" [66]. This relationship, together with equation (65), yield a final equation for ω_1 taking into account the relative orientation of the two covariance ellipses in equation (66).

$$\tilde{\alpha} = \frac{det(\mathbf{I}_2) - det(\mathbf{I}_1)}{det(\mathbf{I}_2 + \mathbf{I}_1)} \tag{64}$$

$$\tilde{\omega}_1 = \frac{(1 - \tilde{\alpha}_1)}{2} \tag{65}$$

$$\tilde{\omega}_1 = \frac{det(\mathbf{I}_1 + \mathbf{I}_2) - det(\mathbf{I}_2) + det(\mathbf{I}_1)}{2\, det(\mathbf{I}_1 + \mathbf{I}_2)} \tag{66}$$

The performance of the Improved Fast CI algorithm compared against tradition Kalman filtering, channel filtering, minimum trace and determinant via nonlinear optimization, and the standard Fast CI algorithms was competitive in a scenario tested by Fränken and Hüpper, and exhibited higher performance in the case of "significant, yet unknown amount of independent information in the estimates to be fused" [66]. The Improved Fast CI algorithm is expected to perform well in cases with orthogonal covariance matrices, which might be expected to result from fusing of different geolocation phenomenologies.

2.4.3 Ellipsoid Intersection.

The Ellipsoid Intersection (EI) algorithm was recently created to address one of the weaknesses of the CI algorithm. That is, the tendency of the CI algorithm to "suffer from a decay of the modeled accuracy in terms of comparing the covariance of the fused estimate to the corresponding covariances of the prior estimate" [6]. Intuitively, and mathematically, one would anticipate an improvement in accuracy as information is merged, but this is not always the case with the CI algorithm. To that end, the EI state fusion algorithm attempts to create a fused estimate that is always of higher accuracy than the individual estimates to be fused [6]. It attempts to accomplish this by explicitly characterizing the unknown correlations via a novel parameterization of the estimates to be fused. It does this before creating a fused estimated that can then be based upon the independent portions of the estimates to

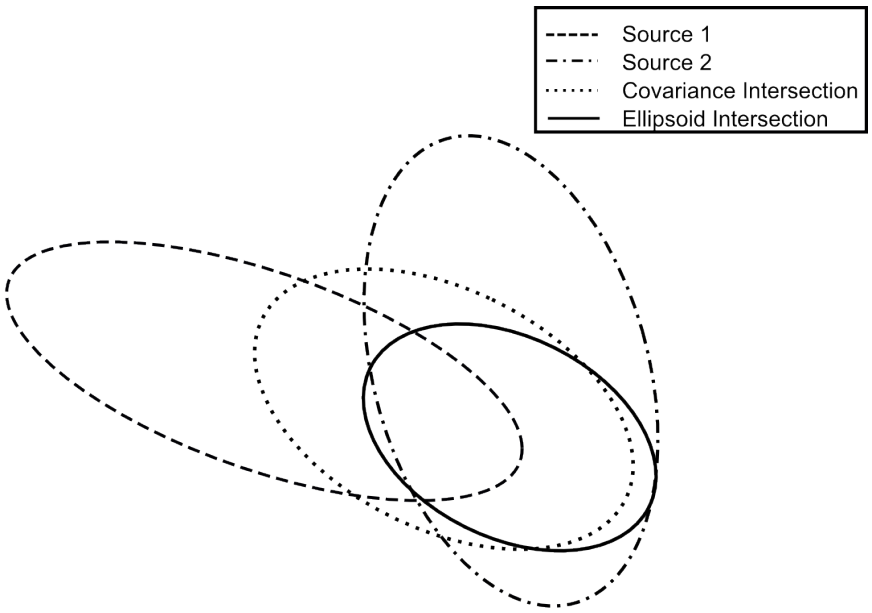

Figure 12. Comparison of CI and EI (adapted from [6])

be fused. The difference between EI and CI is illustrated in Figure 12. It is obvious in the case shown that the EI algorithm yields a significantly smaller covariance than the CI algorithm, and it is also smaller than either of the prior estimates. In this section, the computation of the EI geolocation estimate and associated covariance will be addressed.

On the surface, the EI algorithm is similar to the Kalman filter and CI algorithms in that it involves convex combinations of the source covariance matrices. However, the fused geolocation and covariance estimates include factors Γ, characterizing the mutual covariance, and γ, the mutual mean. The fused covariance and estimated position are given in equations (67) and (68), respectively.

$$P_f = \left(P_1^{-1} + P_2^{-1} - \Gamma^{-1}\right)^{-1} \tag{67}$$

$$\hat{x}_f = P_f \left(P_1^{-1}\hat{x}_1 + P_2^{-1}\hat{x}_2 - \Gamma^{-1}\gamma\right) \tag{68}$$

In order to carry through the calculation it is necessary to produce the mutual mean γ, which is itself a function of the mutual covariance Γ. The mutual covariance is given by equation (69) where D_Γ is a diagonal matrix constructed by comparing the values on the principal diagonal of I_n, an $n \times n$ identity matrix, and D_2, the diagonalized eigenvalues of the covariance matrix associated with source 2 and obtained by eigenvalue decomposition, and choosing the larger, per equation (70). T is a nonsingular matrix, equation (71), created from the eigenvectors of the source 1 covariance matrix, S_1, the eigenvectors of the source 2 covariance matrix, S_2, and the Cholesky decomposition of the eigenvalues of the source 1 covariance matrix, $D_1^{1/2}$. Once the mutual covariance is calculated, the mutual mean γ can be produced via equation (72) with the addition of factor η, given by equation (73). The approximation parameter ζ, is a small positive scalar value that can be tuned. However, Sijs and Lazar showed that the fusion result is relatively insensitive to ζ, and thus any value $<\approx 0.1$ is acceptable [6].

$$\Gamma = T D_\Gamma T^T \tag{69}$$

$$[D_\Gamma]_{qq} = \max\left\{1, [D_2]_{qq}\right\} \tag{70}$$

$$T = S_1 D_1^{1/2} S_2 \tag{71}$$

$$\gamma = \left(P_1^{-1} + P_2^{-1} - 2\Gamma^{-1} + 2\eta I_n\right)^{-1} \times \left(\left(P_2^{-1} - \Gamma^{-1} + \eta I_n\right)\hat{x}_1 + \left(P_1^{-1} - \Gamma^{-1} + \eta I_n\right)\hat{x}_2\right) \tag{72}$$

$$\eta = \begin{cases} 0 & \text{if } \left| [D_2]_{qq} - 1 \right| \geq 10\zeta \\ \zeta & \text{else} \end{cases}$$

Although the EI technique shows promise, and does result in fused estimates with a smaller associated covariance, it has not been formally shown to provide consistent estimates [6]. That being the case, it is important to check for consistency, which can be accomplished in a simulation environment through Monte Carlo analysis.

2.4.4 Largest Ellipsoid.

The Largest Ellipsoid (LE) algorithm is another fusion technique developed in an attempt to accommodate correlated estimates while avoiding the loss of performance inherent in the CI algorithm. While CI guarantees consistency by completely enclosing the region defined by the intersection of the source covariance ellipsoids, it accomplishes this by overestimating the intersection area [34]. The result is that CI is excessively conservative, Kalman filtering is over confident, and the true covariance lies somewhere in between. The LE algorithm is still based upon an estimation of the intersection area, but slightly underestimates it by attempting to compute the largest ellipsoid contained within the intersection rather than overestimating it [34].

The LE algorithm is similar to the other methods already discussed in that it is based on convex combinations of the estimates to be fused. However, it is somewhat unique in that it has a clear delineation between fusing the estimate and fusing the covariance matrices. In fact, the fused geolocation estimate is given by the standard Kalman filter solution in equation (51) and the fused covariance is given by equation (75) [34]. The overall solution is considered to be the estimate provided by the Kalman filter with the covariance matrix calculated by the LE algorithm. The method described by Benaskeur follows. First, the fused covariance matrix is created

through a series of geometrical transformations starting with a rotation of $\mathbf{P}_1$ to align with the Cartesian plane. This rotation is defined as shown in equation (76) for three dimensions, using the eigenvectors of the source 1 covariance matrix. This rotation matrix is then applied to both source covariance matrices per equation (79). The next step in the transformation is a scaling that "makes all of the eigenvalues of the matrix $\mathbf{P}_1^{sr}$ equal" [34]. This transformation $\mathbf{T}_s$, is shown in equation (78) where λ_{1_i} is the i^{th} eigenvalue of $\mathbf{P}_1$. Combining equations (77) and (78) yields the transformation matrices $\mathbf{P}_1^{sr}$ and $\mathbf{P}_2^{sr}$ given in equation (79). Eigenvalue decomposition is then performed on the two transformation matrices. The "eigenvectors of $\mathbf{P}_2^{sr}$ serve as the eigenvectors of the intersection ellipsoid" [34]. A diagonal matrix D is then produced according to equation (80) with κ_i given by equation (81). The intersection ellipsoid, in the transformed space, is then produced by combining the eigenvectors of $\mathbf{P}_2^{sr}$ and D, per equation (82). The final step is to simply reverse the transformations to move the covariance matrix back to the original space as shown in equation (74).

$$P_f = T_r^{-1} T_s^{-1} \hat{P}_f^{sr} T_s^{-T} T_r^{-T} \tag{74}$$

$$P_f = T_r^{-1} T_s^{-1} \begin{bmatrix} v_{2_1} & \dots & v_{2_n} \end{bmatrix} \mathbf{D} \begin{bmatrix} v_{2_1}^T \\ \vdots \\ v_{2_n}^T \end{bmatrix} T_s^{-T} T_r^{-T} \tag{75}$$

$$T_r = \begin{bmatrix} v_{1_1}^T & v_{1_2}^T & v_{1_3}^T \end{bmatrix}^T \tag{76}$$

$$\mathbf{P}_1^r = \mathbf{T}_r \mathbf{P}_1 \mathbf{T}_r^T \tag{77a}$$

$$\mathbf{P}_2^r = \mathbf{T}_r \mathbf{P}_2 \mathbf{T}_r^T \tag{77b}$$

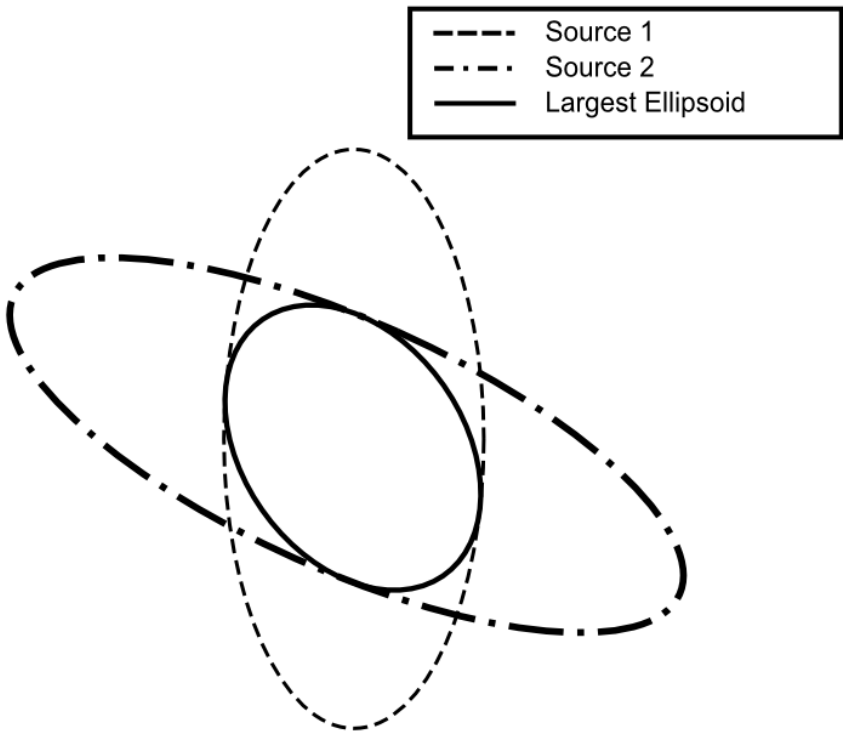

Figure 13. Graphical depiction of Largest Ellipsoid algorithm fusion

$$\mathbf{T}_s = \begin{bmatrix} 1 & 0 & 0 \\ 0 & \sqrt{\frac{\lambda_{1_1}}{\lambda_{1_2}}} & 0 \\ 0 & 0 & \sqrt{\frac{\lambda_{1_1}}{\lambda_{1_3}}} \end{bmatrix} \tag{78}$$

$$\mathbf{P}_1^{sr} = \mathbf{T}_s \mathbf{P}_1^r \mathbf{T}_s^T = \mathbf{T}_s \mathbf{T}_r \mathbf{P}_1 \mathbf{T}_r^T \mathbf{T}_s^T \tag{79a}$$

$$\mathbf{P}_2^{sr} = \mathbf{T}_s \mathbf{P}_2^r \mathbf{T}_s^T = \mathbf{T}_s \mathbf{T}_r \mathbf{P}_2 \mathbf{T}_r^T \mathbf{T}_s^T \tag{79b}$$

$$\mathbf{D} = \begin{bmatrix} \kappa_1 & 0 & 0 \\ 0 & \kappa_2 & 0 \\ 0 & 0 & \kappa_3 \end{bmatrix} \tag{80}$$

$$\kappa_i = \min(\lambda_{1_i}, \lambda_{2_i}) \tag{81}$$

$$\mathbf{P}_f^{sr} = \begin{bmatrix} v_{2_1} & v_{2_2} & v_{2_3} \end{bmatrix} \mathbf{D} \begin{bmatrix} v_{2_1}^T \\ v_{2_2}^T \\ v_{2_3}^T \end{bmatrix} \tag{82}$$

The LE fusion algorithm is relatively simple, computationally efficient, consistent, and results in a tighter covariance than the CI algorithm. Benaskeur showed via Monte Carlo simulation that LE "avoids the inconsistency of the simple fusion" and "the assumed covariance is much closer...than the one obtained by the covariance intersection method" [34]. It is expected that LE will likely give good results when applied to the geolocation fusion problem conducted herein.

2.4.5 Fusion Conclusions.

The previous subsections have covered Kalman filter, Fast Covariance Intersection, Improved Covariance Intersection, Ellipsoid Intersection and the Largest Ellipsoid fusion algorithms. While each technique is unique and has different advantages and disadvantages, they all have the same goal of obtaining "an estimate of an unknown variable from its available noise-corrupted observations" [34]. Furthermore, they all would seem to be reasonable techniques for fusing geolocation measurements and will be carried forward for the purposes of this thesis.

2.5 Summary

The preceding sections served to introduce and describe the current research status of the primary components of the geolocation problem including SV considerations, signal measurement, geolocation algorithms, DEMs, and estimate fusion techniques.

This information will serve as a basis for this research. The combination of SV considerations, signal measurement capabilities, and geolocation algorithms will allow for the performance of representative collectors to be modeled, the application of DEMs will allow for the addition of a high fidelity surface of the earth constraint, and the fusion techniques will allow for the estimates from multiple collectors to be combined in order to study the impact of augmentation. The next chapter will expound the precise methodology by which the principles described are applied to address the thesis proposition.

III. Methodology

This chapter will address the overall methodology of the simulations to include an overview of the overall process followed by more detailed explanations of the specific models utilized, the application of the surface of the earth constraint, and Measure of Performance (MOP)s.

3.1 Overall Strategy

Prior to discussing the individual components that make up the whole of the methodology, and describing each use case, it is useful to have an understanding of the overarching structure and strategy of this research. This section will provide a brief description of the steps utilized.

1. The first step is to import the applicable geometry from STK. This includes the SV position and velocity in ECEF coordinates, as well as the duration of time in the main beam of the emitter. For single-ball collectors, this is simply the time necessary for the main beam to sweep through the SV, but for multi-ball collectors, it is the time in which all of the SVs in the cluster were within the main beam simultaneously.

2. The next step is to use the true geometries to determine the actual, uncorrupted measurements that would be received in that collection scenario. The techniques used to calculate the true values, given the true SV positions and velocities and the true position of the emitter are shown below.

   (a) The true azimuth and elevation angles, from the SV to the emitter, are produced via the MATLAB ® function *ecef2aer* using the true emitter

location in ECEF coordinates, the SV position in terms of latitude, longitude, and altitude above the WGS 84 reference ellipsoid. The outputs are the azimuth and elevation angles in degrees, and the range in meters. In the case of multiple signal pulses received in one sweep through the main beam of the emitter, the true azimuth and elevation are considered to be the same for each of the pulses despite the small change in relative SV position.

(b) The true TDOA measurements are calculated as the differences in the instantaneous slant ranges between each receiver and emitter. A slant range is simply the Euclidean distance between the emitter and receiver in ECEF coordinates as presented in section 2.2.2.1 and given by equation (13). In this research, receiver 1 is considered to be the "master" to which receivers 2 through n are referenced. This produces $n-1$ TDOA measurements per equation (83). It must be noted that the TDOA geolocation algorithms actually work on the range differences, which are simply the TDOA measurements multiplied by the speed of light.

$$\begin{aligned} TDOA_{i,1} \cdot c &= r_i - r_1 \\ i &= 2, 3, \ldots, n \end{aligned} \tag{83}$$

3. The third step is to corrupt the true measurements to introduce the noise inherent in real-world measurements. This is accomplished by adding Gaussian distributed white noise, with a given standard deviation. The standard deviations for TDOA and FDOA measurements and AOA measurements were developed in sections 2.2.1.1 and 2.2.1.2 respectively. A generic form of this process is shown in equation (84) where ψ is the measurement in question, X is

a random number drawn from a normal distribution with zero mean and standard deviation σ. More tailored treatments for each of the measurements are presented in section 3.3.4.

$$\psi_{noisy} = \psi_{true} + \mathrm{X}\sigma_{\psi} \tag{84}$$

4. After all of the requisite measurements have been appropriately corrupted, an explicit geolocation is calculated. In the case of AOA geolocation this occurs at end of a pass, via the technique described in section 2.2.2.2. For TDOA geolocation, this occurs for each received pulse per the process described in section 2.2.2.1.

5. The explicit geolocation then provides a seed to start applying a surface of the earth constraint using the DEM data. A grid search in the area surrounding the seed point is conducted using terrain posts as potential emitter positions. The post that minimizes the chosen Figure of Merit (FOM), which will be discussed in section 3.5, is the estimated emitter position.

6. The aforementioned process is then repeated for a set number of "runs"; a run being defined as one pass by the SV of the emitter. The number of runs is sufficiently large that the resulting covariance of estimated emitter positions is nearly constant with additional runs. The metric used to evaluate convergence is the average per run change of the norm of the covariance eigenvalues over the previous ten runs. For this research, an average change of less than or equal to 0.05% is considered converged.

7. The next step in the process is performing the data fusion. Each geolocation "agent" will have an associated average estimated position and covariance matrix. These estimates are fused using the techniques described in section 2.4. In

this research, the term "agent" refers a receiver or set of receivers that provides a geolocation estimate. For example, one SV with an AOA geolocation payload is an agent, as is a cluster of three SVs performing TDOA geolocation.

8. Finally, the consistency of the estimates produced by the different fusion techniques is evaluated. Each agent will have a covariance matrix generated over the course of all of the runs, and each run will also have an associated position estimate. Consistency is checked by fusing the position estimate and covariance matrix for each agent for each run and then determining the percentage of times that the true emitter location falls within the fused error ellipsoid. While estimate consistency is not the primary MOP, it is a useful indicator of whether or not the MOPs are valid.

3.2 Problem Scenarios

Three distinct scenarios are utilized in this research to demonstrate geolocation performance, and improvement due to fusion, in different situations. The scenarios differ in terms of available collector geometries and the ruggedness of terrain.

The first scenario is the simplest. It features the emitter of interest located slightly east of the AFIT campus. The terrain is relatively flat and collection geometries are unlimited, meaning that an airborne collector can fly at any heading or altitude. The primary purpose of this scenario is to explore the effect of relative collector headings on cross-platform geolocation performance. For example, the AOA SV collector at a set orbital inclination and Right Ascension of the Ascending Node (RAAN) can be combined with the collections of an airborne AOA collector flying at headings parallel, perpendicular, and intermediate angles to the ground track of the SV.

The second scenario is intended to demonstrate an operationally realistic collection scenario, complete with limitations on where the airborne collector(s) can fly. The

emitter is located at the Tripoli International Airport in Libya and airborne collectors are limited to flying within international airspace, 12 nm or greater from the Libyan coast. A flight path paralleling the Libyan coast over the Mediterranean maximizes the collection opportunity of the airborne collectors.

The final scenario was chosen to test performance in mountainous terrain, which will also serve to stress the DEM surface of the earth constraint application. In this scenario the emitter is located on top of a mountain ridge in the Hindu Kush mountains of north-eastern Afghanistan, near the border of Pakistan. This limits the collection geometries from an airborne emitter in a similar manner as in scenario two, due to the restriction of not violating Pakistani airspace. Although DEM data is included, the effect of terrain masking due to blocked line-of-sight is not included. The addition of terrain masking is a recommendation for future research.

3.3 Models

3.3.1 Emitter.

The precise characteristics of the emitter of interest are not the focus of this research, however it is necessary to define characteristics to simulate, which do impact the resulting geolocation performance. For this reason, the Air Route Surveillance Radar-4 (ARSR-4) was chosen as a useful reference emitter as it shares many characteristics with other similar surveillance radars. The ARSR-4 is an Federal Aviation Administration (FAA)/Air Force long range search radar operating in the L band with parameters shown in Table 2. This research utilizes the ARSR-4 as a reference, but does not require strict adherence to operational characteristics. For example, the Equivalent Isotropic Radiated Power (EIRP) and PRF can be adjusted to emulate more challenging emitters.

The actual simulation of the emitter and SV geometries occur in STK® and

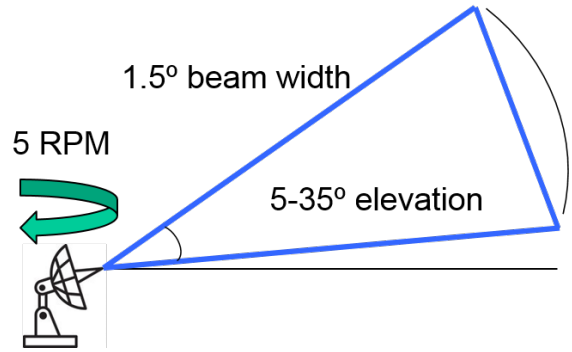

Figure 14. Reference emitter geometry [7]

MATLAB ®. The geometry of the beam, including azimuth and elevation beam widths and the emitter rotation in azimuth, are modeled in the STK® simulation from which all collection geometries are derived. These geometric features are shown in Figure 14. It should be noted that the beam elevation range results in a "donut hole" centered directly above the emitter where no collection can take place. A depiction of this is shown in Figure 15. The frequency, bandwidth, power, and PRF characteristics of the signal are included in the MATLAB ® portion of the simulation, and will be further elaborated upon in section 3.3.3.

Table 2. ARSR-4 parameters

Parameter	Value
Center frequency	1315 MHz
Bandwidth	100 MHz
Radiated power	6.5 - 65 kW
Transmit antenna gain	45 dBi
Azimuth beam width	1.5 deg
Elevation beam width	5-35 dec
Antenna polarization	RHCP
Azimuth rotation	5 RPM
Pulse repetition frequency	72/216 Hz

3.3.2 Geometry.

Modeling collector geometry and signal intercept times and durations is a critical component of the overall simulation effort. This research utilizes STK® to generate the collector movement and transmitter rotation. The precise collector positions and velocities, in the ECEF coordinate frame, for each signal collection are then exported. For simplification, and to reduce the total number of test cases, several standard collector flight paths are defined in this section and will be reused as needed. The standard orbital collection geometries will be addressed first, followed by the airborne collection geometries.

Defining orbital collection parameters is, in some ways, eased by the rigid Keplerian restrictions inherent in orbital mechanics. This research focuses on the realm commonly inhabited by CubeSats, namely LEO circular orbits. An altitude of 500 kilometers is used to provide reasonable coverage and orbital lifetime [70; 7]. The standard inclination used in this research is 63.4°, also known as critically inclined [71]. A critically inclined orbit has the benefit of not suffering from rotation of perigee, the specifics of which are outside the scope of this research. The "donut hole" described in section 3.3.1 provides a convenient reference point. Three basic passes are defined for ascending and descending portions of the orbit in order to bracket the expected performance. It must be noted that these passes do not represent successive revolutions, but rather represent the range of geolocation performance expected from the spectrum of possible geolocation geometries. The first pass has a ground path that directly passes over the target location. The second pass is tangent to the donut hole and represents the best case collection from an SNR and received pulse perspective. The third pass is near the edge of the emitter cone and represents a worst case pass. A simple depiction of the ascending and descending passes over AFIT, Libya, and Afghanistan are shown in Figures 15, 16 and 17 respectively.

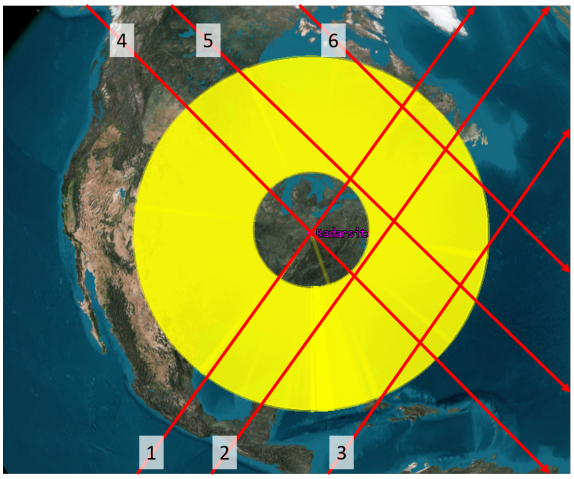

Figure 15. AFIT orbital collection pass geometries

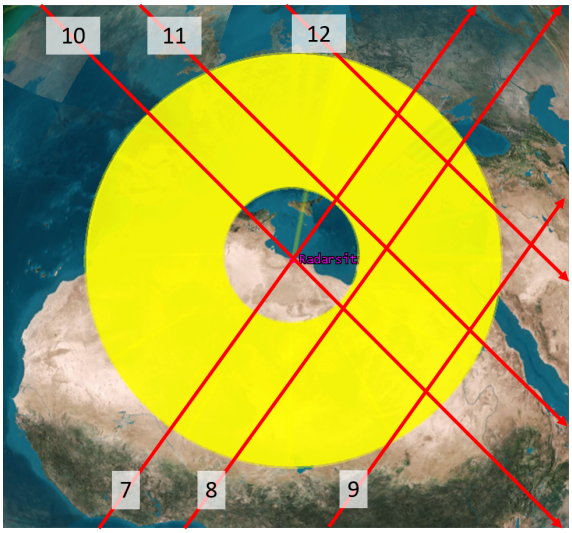

Figure 16. Libya orbital collection pass geometries

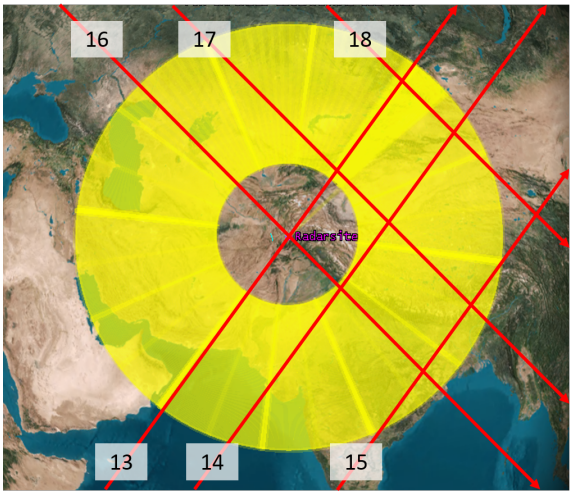

Figure 17. Afghanistan Orbital Collection Pass Geometries

The airborne collector parameters are more flexible than the orbital parameters. Geolocation payloads can be hosted on a wide range of airframes from small UAVs to large, high altitude platforms such as the U-2 and Global Hawk. In order to limit the scope of the research, only three classes of airborne collectors, generally termed Aerial Vehicle (AV)s in this research, are represented. The first class is the relatively low and slow, medium capability UAV typified by the MQ-1 Predator in service with the US Air Force, and the Boeing Insitu ScanEagle in service with the US Army, Navy and Marine Corps[10]. The second class is composed of higher altitude and airspeed manned aircraft such at the MC-12 Liberty and the final class is a high altitude and airspeed aircraft such at the U-2. The approximate cruise airspeed and service ceiling for each of the aircraft is shown in Table 3.

Table 3. Aircraft parameters [9; 10; 11; 12]

Aircraft	Cruise Speed (kts)	Ceiling (m)
ScanEagle	48	5944
MQ-1	70	7620
MC-12	200	10668
U-2	415	21300

This research does not attempt to precisely capture the true mission performance of these airborne collectors. Instead, it seeks to generalize the operational parameters of altitude and speed while employing a nominal geolocation payload which may or may not represent realistic operational capabilities. To that end, the operational aircraft parameters were generalized to create the aforementioned three classes of reference airborne collector, the details of which are shown below in Table 4.

Table 4. Reference airborne collector parameters

Reference Collector	Speed (kts)	Altitude (m)	Payload Type
Low Altitude UAV	60	1500	TDOA
Mid Altitude Aircraft	200	6000	AOA
High Altitude Aircraft	400	21000	AOA

One of the primary strengths of airborne collectors is operational flexibility, which includes the ability to fly at any arbitrary heading. However, for purposes of this research it is necessary to limit the collection headings, which will vary by scenario. Scenario one, with the emitter located near AFIT gives the most opportunity for flexibility as there are no external limitations such as airspace with which to contend. To that end, three distinct collection headings will be employed for the AFIT scenario. The first heading is tangent with the AOA orbital collector. The second is normal to the orbital collector, and the third is at a 45° angle to the orbital collector. The same three headings are duplicated 5 nautical miles to the east of the transmitter. These paths are shown in Figure 18. The next two scenarios are more limited due to the realistic operational airspace considerations. The second scenario, collecting an emitter located at the Tripoli International Airport, utilizes only one heading; a course parallel to the Libyan coast and approximately 20 and 100 nm offshore. This collection geometry is depicted in Figure 19. The third and final scenario is similarly limited. The airborne collectors fly approximately parallel to the border of Pakistan at a distance of 20 and 100 nm as shown in Figure 20.

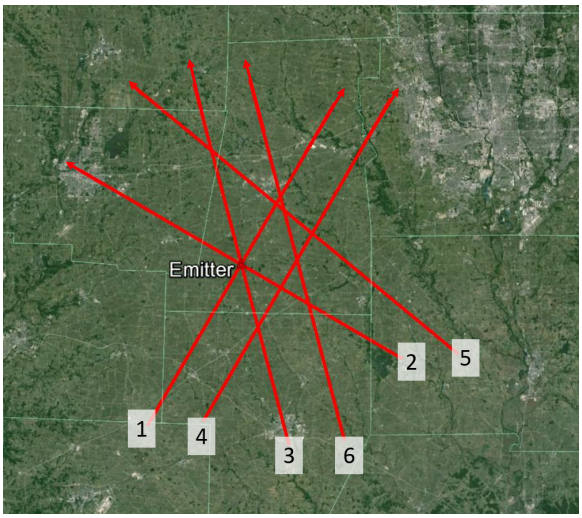

Figure 18. AFIT airborne collector geometry

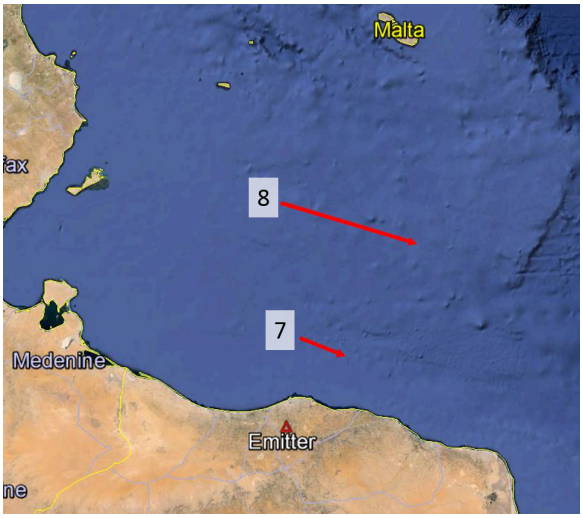

Figure 19. Libya airborne collector geometry

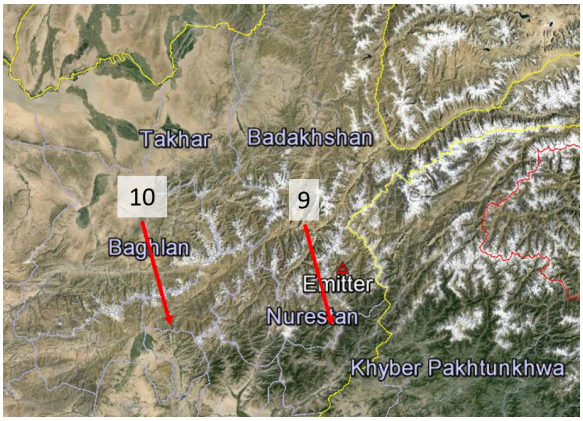

Figure 20. Afghanistan airborne collector geometry

3.3.3 Signal Propagation.

The implementation of a dynamic signal propagation model is an important component of this research. While the emitter transmits at constant power, the actual power received at the collector is not constant due to the variable path loss of the signal. Using the position data of the collector at time of intercept, it is possible to calculate the range between the emitter and collector, determine the free space loss, and calculate the received SNR. The overall received SNR is given by equation (85). This section will describe the components that go into the SNR calculation as well as how those component tie into the rest of the simulation.

$$SNR = EIRP + G_{Rx} - L_{combined} - N_{combined} \tag{85}$$

The first step is to calculate the EIRP. In fact, the EIRP is the best way to compare emitters with different powers and antenna gains. The EIRP is given by equation (86) [45] where P_{tx} is the transmitter power, in Decibel-Watts (dBW), G_{tx} is the emitter antenna gain, in Decibel-isotropic (dBi), and L_{tx} represents the line losses in the transmitter in dB.

$$EIRP = P_{tx} + G_{tx} - L_{tx} \tag{86}$$

The next step is to calculate the combined losses, which include the path loss between the emitter and collector, the pointing loss due to any mismatch in the collection antenna gain pattern and the incident signal, and receiver losses including line and filtering losses. A breakdown of the these losses, including whether they are dynamic or constant and the associated values is shown in Table 5.

The most significant portion of the combined losses is the path loss. Path loss is due to the range between the emitter and collector, and the medium the RF travels

Table 5. Signal propagation losses

Loss	Dynamic/Constant	Value (dB)
FSPL	Dynamic	variable
Atmospheric attenuation	Constant	0.5
Pointing	Constant	1.0
Receiver filter	Constant	0.7648
Receiver line	Constant	1.0

through over that range, and is frequency dependent. Path loss can be broken into two components; Free Space Path Loss (FSPL) and atmospheric attenuation. Both are functions of the signal frequency and range from the emitter to the collector. However, it was previously determined that the atmospheric attenuation at the ARSR-4 operational frequency is relatively invariant, and may be simplified as a small constant loss [7; 26], so this research does not include an atmospheric attenuation model. The FSPL variation, however, is significant and is included dynamically for each collection using equation (87), [45], with r indicating the range, and λ representing the signal wavelength.

$$FSPL_{dB} = 10\log_{10}\left(\frac{4\pi r}{\lambda}\right)^2 \tag{87}$$

The next component to be addressed is the system noise. System noise is described by the system noise temperature, T_{sys} and is given by equation (88), with the Boltzmann constant, $k = 1.380650 \times 10^{-23}$, T_{sys} representing the system noise temperature, and B_{noise} representing the noise bandwidth. The system noise temperature is a function of the receiver hardware and thus depends upon a specific design. This research utilizes system noise temperatures representative of commercially available receiver hardware. Additional details are available in the limited distribution addendum to this research.

$$N_{combined} = 10\log_{10}(kT_{sys}B_{noise}) \tag{88}$$

The final component required to calculate the received SNR are the receive antenna gains, as discussed in section 2.1.3. The gains employed in this research are based upon those specified in previous AFIT research [7; 31] and are shown in Table 6.

Table 6. Collection antenna properties

Parameter	Collector		
	AOA	TDOA	F/TDOA
Receiver antenna gain (dB)	3.0	2.5	2.5

3.3.4 Signal Measurement Noise.

The application of signal measurement noise is an important aspect of this research. In a perfect scenario, without measurement noise, the geolocation problem becomes trivial and it is possible to perfectly locate the emitter position. Unfortunately, such perfect measurement is an impossibility and all signal measurements have uncertainty, as discussed and developed in section 2.2.1. Fortunately, the distribution of signal measurement error is known, and can be simulated. Musicki and Koch noted that "In the measurement space, TDOA and FDOA true value uncertainties, given the measurement, are Gaussian" [14]. In a similar manner, the AOA measurements produced via the MUSIC algorithm are Gaussian with zero mean [51]. The fact that the signal measurements of interest have Gaussian distribution with zero mean and known standard deviations allows for a stochastic modeling approach [33]. This section will describe how the measurement "corruption" mentioned in section 3.1 is implemented for AOA, TDOA and FDOA measurements.

Corruption of true AOA measurements occurs via the general process described

by equation (84) wherein a random number drawn from a normal distribution with zero mean is multiplied by the standard deviation for the given conditions and added to the true angles of arrival. The standard deviations for azimuth and elevation measurements are drawn from the MUSIC covariance matrix, C_ψ, calculated per equation (11). The standard deviation of the azimuth measurement, $\sigma_{azimuth}$, and $\sigma_{elevation}$, the standard deviation of the elevation measurement, are equal to the square root of the upper left and lower right matrix entries respectively. In this research the matrix C_ψ is calculated for each sweep through the main beam with dynamic SNR calculation and K equal to the number of pulses received during that sweep through. The estimated azimuth and elevation angles are then calculated per equations (89a) and (89b), respectively. In these equations, X is a random number drawn from a normal distribution with zero mean, and thus may be negative, resulting in a normal distribution of measurements centered on the true value.

$$\phi_{estimate} = \phi_{true} + \mathrm{X}\sigma_{\phi,measurement} \tag{89a}$$

$$\theta_{estimate} = \theta_{true} + \mathrm{X}\sigma_{\theta,measurement} \tag{89b}$$

TDOA measurement corruption is more involved than the AOA corruption as the measurement requires multiple collection platforms to produce. This results in two separate components of error. The first component is the actual measurement based off of the CAF introduced in section 2.2.1.1. The standard deviation of this component, given in equation (3), is a function of the input SNR, RMS radian frequency, noise bandwidth, and integration time.

The second component is a side effect of the requirement for multiple collection platforms. In order to measure a difference in the times of arrival, each pair of collectors must share a common clock synchronization. If the clock synchronization

has any offset or bias, it will affect the measured TDOA. Previous research has illustrated methods for dealing with and minimizing asynchronization, most of which depend upon "hacking" an internal clock to GPS time [31; 33; 38]. The accuracy achieved with this method is variable, depending upon implementation and internal clock type (crystal or atomic), but most fall in the $30-50$ ns range. For this research, a normally distributed offset with mean zero and standard deviation, σ_t, of 50 ns is used to match the system proposed by DiGiacomo [31].

The total TDOA measurement corruption then follows the structure established in equation (84), albeit with the inclusion of an additional term. The estimated TDOA measurement is shown in equation (90) with σ_{DTO} given by equation (3), and X_1 and X_2 representing random numbers independently drawn from a normal distribution with zero mean. This research calculates σ_{DTO} at each sweep through of the main beam based upon the dynamic SNR. The TDOA measurements from each pulse recieved during that sweep through are then corrupted via equation (90) and serve as inputs to the TDOA geolocation algorithm.

$$TDOA_{estimate} = TDOA_{true} + \mathrm{X}_1\sigma_{DTO} + \mathrm{X}_2\sigma_t \tag{90}$$

3.3.5 Collection Platform Noise.

Signal measurements are critical to RF geolocation, but the SV that hosts the payload is literally the backbone. Regardless of RF performance, SV parameters can greatly impact the overall geolocation accuracy of the system. In particular, the SV attitude, position, and velocity play significant roles in AOA, TDOA, and FDOA respectively. Although spacecraft design details are outside of the scope of this research, it is necessary to include some measures of spacecraft performance and the effect on geolocation performance. Section 2.1.1, describes the expected attitude,

position, and velocity knowledge from a CubeSat SV. This section will briefly describe how these factors are included in the simulation.

SV attitude is defined by SME-SMAD as "the three-dimensional orientation of a vehicle with respect to a specified reference frame" [71]. This 3D knowledge of vehicle orientation is essential to performing AOA geolocation as all azimuth and elevation angle measurements are made in the vehicle reference frame and must then be converted to the ECEF frame. SV attitude knowledge error results in a bias between the measured LOB and the translated LOB that in-turn leads to an inaccurate geolocation estimate. In order to include the effects of imperfect attitude knowledge on the AOA geolocation results, further noise is introduced to the azimuth and elevation estimates. This is accomplished by once again following the pattern established by equation (84) and adding random, Gaussian noise to the estimates as shown in equation (91). It should be noted that this treatment is an acknowledged weakness of this research. SV attitude knowledge is unlikely to be truly random due to the filtering that typically takes place in an Attitude Determination and Control Subsystem (ADCS) system. However, assuming an attitude determination system that is bias free, this treatment should represent a worst-case scenario. Improving this model to more accurately represent real attitude knowledge is a recommended topic for future research.

$$\phi_{final} = \phi_{estimate} + \mathrm{X}\sigma_{\phi,attitude} \tag{91a}$$

$$\theta_{final} = \theta_{estimate} + \mathrm{X}\sigma_{\theta,attitude} \tag{91b}$$

While attitude errors have a negative impact on AOA geolocation accuracy, it has no impact on TDOA accuracy, outside of a potential loss in SNR due to antenna gain pattern mismatch. Position knowledge however, has an impact on all geolocation

algorithms and is the primary SV driver of TDOA accuracy. Position knowledge is a 3D problem and as such needs to be accounted for properly in the model. This research uses ECEF coordinates for SV position which makes it easy to independently corrupt the x, y, and z coordinates of the SV via the same general process as used on the signal measurements and attitude knowledge as shown in equation (92). It must be noted the position knowledge model has the same caveat as the attitude knowledge model in that the true position uncertainty is unlikely to be random normally distributed. This is particularly true in the case of the orbital collectors which can utilize orbital propagation techniques to improve position knowledge. Additionally, the position knowledge error included in this research is in absolute terms. In reality, the absolute and relative position knowledge of each collector in a TDOA arrangement should be treated separately, particularly in cases where a cross-link allows for improved relative position knowledge. The absolute position knowledge technique utilized in this research should provide a reasonable worst-case scenario but future enhancements should include a discrete absolute/relative position model.

$$x_{corrupt} = x_{true} + \mathrm{X}\sigma_x \tag{92a}$$

$$y_{corrupt} = y_{true} + \mathrm{X}\sigma_y \tag{92b}$$

$$z_{corrupt} = z_{true} + \mathrm{X}\sigma_z \tag{92c}$$

The preceding section described the inclusion of attitude, position, and velocity knowledge errors in the simulation. The standard deviations used to corrupt the true values are based upon prior research described in section 2.1.1. The values utilized in this research are consolidated in Table 7. These should be considered "tuning" parameters that may be adjusted to match the expected performance from

any collector design.

Table 7. Collector attitude and position standard deviations

Component	Platform				
	AOA SV	AOA AV	3-ball TDOA SV	4-ball TDOA SV	TDOA AV
Attitude (deg)	0.1	0.025	NA	NA	NA
Position (m)	10	10	2.0	0.5	10

3.4 Measures of Performance

In order to quantify geolocation performance, it is necessary to define appropriate metrics or MOPs. Traditionally, the Root Mean Square Error (RMSE), shown in equation (93), [72; 73; 74; 75], and average miss distance, given by equation (94) [76; 77] are the most commonly used metrics, although uncertainty ellipse/ellipsoid area and volume, given by equations (95a) and (95b) [16] with a, b, and c representing the semi-axis lengths, are also occasionally used. In each of these equations, $[\tilde{x}_t, \tilde{y}_t, \tilde{z}_t]$ represents the estimated emitter position and $i = 1 \ldots n$ where n is the total number of position estimates. While these measures are useful as basic performance metrics, they do not capture the shape of the error ellipse, in 2D, or error ellipsoid, in 3D. This is problematic from a user perspective in that different shaped error ellipsoids, of a threat emitter for example, are more useful than others. For instance, a circular error ellipse with a 1 km radius has an ellipse area of 3.14 km^2; the same area as an ellipse with a semi-major axis of 10 km and a semi-minor axis of 0.1 km. Despite the identical areas, the geolocation estimate of the first estimate, shown in red in Figure 21, is a more useful estimate than that of the second case, shown in blue, particularly for targeting or threat avoidance purposes. In order to address this concern, this research introduces two new MOPs.

$$RMSE = \sqrt{\frac{\sum_{i=1}^{n} \left(\| [\widetilde{x}_{t,i}, \widetilde{y}_{t,i}, \widetilde{z}_{t,i}] - [x_t, y_t, z_t] \| \right)^2}{n}} \tag{93}$$

$$miss_i = \| [\widetilde{x}_{t,i}, \widetilde{y}_{t,i}, \widetilde{z}_{t,i}] - [x_t, y_t, z_t] \| \tag{94a}$$

$$miss_{average} = \frac{\sum_{i=1}^{n} miss_i}{n} \tag{94b}$$

$$Area_{ellipse} = \pi ab \tag{95a}$$

$$Volume_{ellipsoid} = \frac{4}{3}\pi abc \tag{95b}$$

The first new MOP is simply the Semi-Major Axis (SMA) length, that is, the maximum of the three semi-axis lengths. This represents a worst case scenario, the furthest an emitter can be from the estimated position at the given confidence level. This technique is straight forward and effective for 2D ellipses, but can break down when applied to the 3D ellipsoids encountered in a three dimensional geolocation problem. This breakdown primarily occurs when the ellipsoid major axis is not co-incident to the surface of the earth in that area. In this case, another approach is needed. By including a DEM-based surface of the earth model it is possible to determine the intersection between the error ellipsoid and the ground. A search is then completed over all of the DEM posts within the ellipsoid to identify the two posts with the greatest Euclidean separation. This distance is termed the Maximum Post-to-Post Separation (MPTPS) and is demonstrated in Figure 22. As the MPTPS spans the entire intersection, it is most analogous to the major axis length and a value

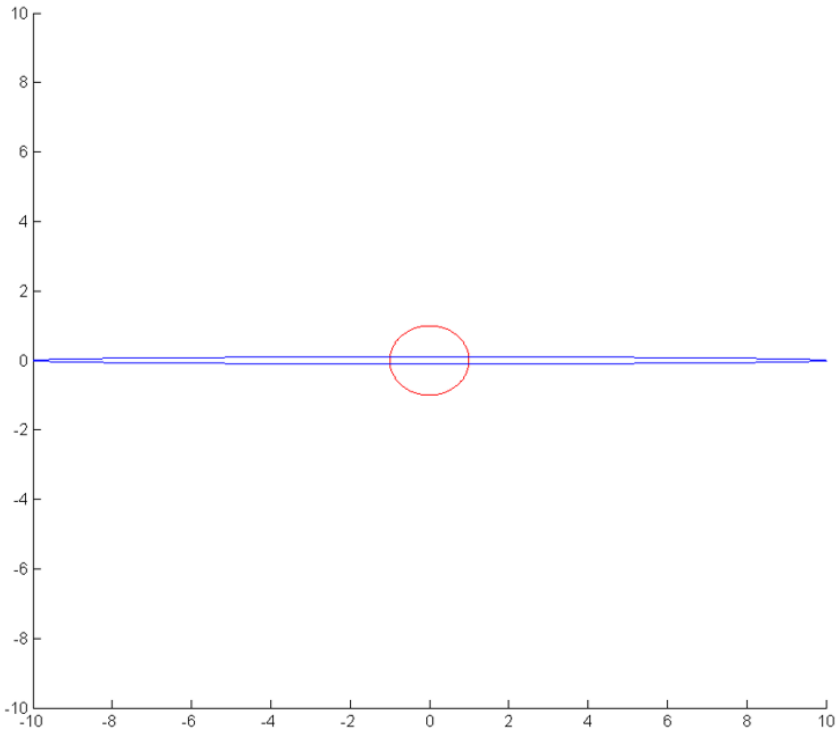

Figure 21. Comparison of ellipses of equal area

of $\frac{1}{2}$ of the MPTPS is an appropriate comparison versus the semi-major axis.

In the estimate fusion cases, it is necessary to include two additional metrics to bolster the SMA and MPTPS MOPs described above. The ellipsoid consistency and ellipse consistency are measures of how accurately the fusion method in question produces a fused uncertainty ellipsoid with the desired confidence level. The ellipsoid consistency is specifically the percent of estimates that fall within the 3D fused ellipsoid. In contrast, the ellipse consistency is the percent of estimates that fall within the ellipse produced by projecting the 3D ellipsoid onto the 2D plane of the surface of the earth in the East-North-Up (ENU) reference frame. Thus, estimates that lie directly above or below the ellipsoid are not consistent in the ellipsoid sense, but are consist in the ellipse sense. The ellipsoid consistency is expected to be the more appropriate metric for estimates with significant variation in all axes, but the ellipse consistency may be appropriate for ground constrained estimates that have relatively little vari-

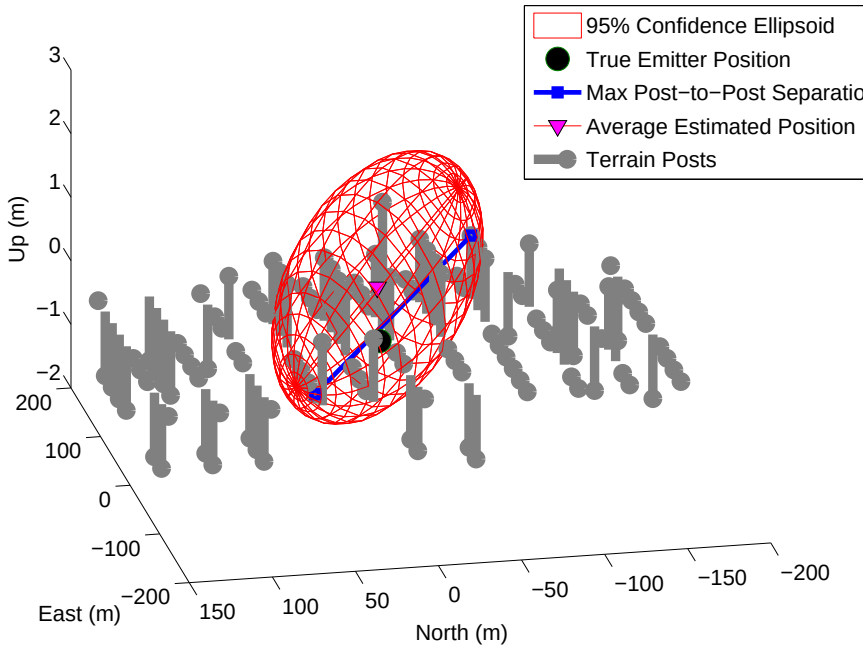

Figure 22. Demonstration of maximum post-to-post spacing

ation in the "up" direction. In order for the SMA and MPTPS MOPs to be valid for comparison purposes, particularly in the fused estimate cases, the consistency must fall within an acceptable range.

In order to allow for comparison against previous research, this effort will retain the commonly used metrics as well as introducing the semi-major axis and MPTPS metrics described above and tabulated in Table 8. These metrics, when validated as appropriately consistent, will allow for an objective comparison of performance between the various geolocation agents, scenarios and fusion techniques against a given emitter.

Table 8. Measures of performance

Measures of Performance
Root Mean Square Error (m)
Average Miss Distance (m)
Ellipsoid Volume (m^3)
SMA Length (m)
Max Post-to-Post Separation (m)

3.5 Application of Surface of the Earth Constraint

A key component of this research is the application of a surface of the earth constraint. Existing research commonly refers to surface of the earth constraints, but most use either a simplified spherical or ellipsoidal earth model, or a simple flat plane assumption. The research that does include terrain data or DEM based constraints approach the problem from a generalized CRLB perspective, and do not develop an algorithm for implementation [67]. However, Fowler did show that, in general, "by knowing something about the emitter's z_e it is possible to achieve better performance than is possible to not only improve the emitter's altitude but to also improve the down-range performance" [67]. In fact, in some cases the addition of terrain data alone yielded better results than precise knowledge of the emitter location. This is due to the fact that the terrain data provides additional data, such as the terrain slope, that is unavailable in the known elevation case [67]. Intuitively, this should be the case as terrain information adds significantly to the FIM, which is inversely proportional to the CRLB per equation (50).

Given the fact that incorporating a DEM based surface of the earth constraint will improve performance, the next challenge is to determine the most appropriate way to implement the constraint. Section 3.1 briefly described the basic approach taken in this research; namely, an explicit solution is used as a seed for an explicit grid search over the available DEM for the solution that minimizes the selected FOM. The following section provides the specifics of this implementation.

1. The process starts, as mentioned above, with the explicitly calculated emitter geolocation as a seed. For AOA agents, one pass by an emitter yields a single geolocation which will serve as the seed location. In contrast, TDOA and F/TDOA agents can produce an estimated geolocation at every pulse. In those cases, the seed position is the average of all of the position estimates determined

in one pass. In either instance, the estimated geolocation is in ECEF coordinates, which much be translated to a latitude, longitude, and elevation. This research utilizes the MATLAB ® function *ecef2lla* for this task. The latitude and longitude of this estimated position serve as the center of the initial search area.

2. The next step is to define the search area. The goal is a box centered at the estimated latitude and longitude with a defined width and height. This research utilizes a box height and width of $0.01°$, or $36''$, which was found to be an acceptable compromise between speed and coverage, but has not yet been optimized and thus should not be considered as the optimal value. At a SRTM-1 /SRFT-1 / DTED-1 level, defined in 2.3.1, this nominally results 12×12 post search area.

3. After defining the area, the next step is to pull in DEM data for the defined search area. This research utilizes SRFT data sets due to the greater releasability compared to DTED and lack of data voids compared to SRTM. However, as they are formatted identically, it is possible to easily replace the SRFT data sets with DTED should the need arise. In order to acquire the SRFT data for the search area, the built-in MATLAB ® function *dted* is utilized. This function crops the desired area, defined by the latitude and longitude range vectors, shown in equation (96), from the large $1° \times 1°$ SRFT file. A similar function, *egm96geoid*, is used to acquire the corresponding EGM 96 data in the search area.

$$LATLIM = [lat_{est} - 0.5box_{height} \quad lat_{est} + 0.5box_{height}] \tag{96a}$$

$$LONLIM = [lon_{est} - 0.5box_{width} \quad lon_{est} + 0.5box_{width}] \tag{96b}$$

4. The SRFT and EGM 96 data is then used to define the terrain data in term of height above the WGS 84 ellipsoid. This is accomplished via equation (49), described in section 2.3.1. This translation must be performed for every post, which is complicated by the fact that EGM 96 has a much greater sampling distance and thus must be interpolated within the area of interest. A bicubic interpolation of EGM 96 data at each of the post latitudes and longitudes results in the necessary values to complete the translation.

5. After translation of the terrain data, a grid search to determine which post is the best solution to the geolocation problem given the known signal measurements is performed. However, this process requires a FOM, Φ, to be minimized. For AOA geolocation, the FOM is the sum of squared distances from the post in question to each of the LOBs, given by equation (97), where $[x_p, y_p, z_p]$ is the vector of ECEF coordinates of the current post, and i represents each main beam sweep through from 1 to n. The TDOA FOM is the sum of squared range errors over all of the pulses collected as given in equation (98) with $r_{2,1}$ and $r_{3,1}$ representing the actual range differences between the collectors and emitter, given by equation (99), $TDOA_{2,1}$ and $TDOA_{3,1}$ representing the measured time differences of arrival, and i represents each pulse received from 1 to n. The FOM must be calculated for each position, with the lowest or minimal valued post representing the best emitter location.

$$\Phi_{AOA}\left([x_p, y_p, z_p]\right) = \sum_{i=1}^{n} \left(\left| ([x_p, y_p, z_p] - [x_i, y_i, z_i]) \times \frac{\overrightarrow{LOB_i}}{\left|\overrightarrow{LOB_i}\right|} \right| \right)^2 \tag{97}$$

$$\Phi_{TDOA}\left([x_p, y_p, z_p]\right) = \sum_{i=1}^{n} \left((r_{2,1_i} - TDOA_{2,1_i} \cdot c)^2 + (r_{3,1_i} - TDOA_{3,1_i} \cdot c)^2 \right) \tag{98}$$

$$r_{2,1_i} = |[x_{2_i}, y_{2_i}, z_{2_i}] - [x_p, y_p, z_p]| - |[x_{1_i}, y_{1_i}, z_{1_i}] - [x_p, y_p, z_p]| \tag{99a}$$

$$r_{3,1_i} = |[x_{3_i}, y_{3_i}, z_{3_i}] - [x_p, y_p, z_p]| - |[x_{1_i}, y_{1_i}, z_{1_i}] - [x_p, y_p, z_p]| \tag{99b}$$

6. After the best fit post position in the search area has been identified, it is necessary to perform a check to determine if the given post position is at the outside edge of the search area. A location near the edge indicates that there may be a better solution outside of the current search area. An outside boundary of two posts is defined, as shown in yellow in Figure 23, and if the predicted solution falls within the boundary, a new search area is defined centered at that point and the process begins again. In this manner, the search area is "walked" onto the target location. An example of this process is shown in Figure 24 where the initial search area is centered on the explicit solution, and a ground constrained solution is found near the edge. The solution results in the definition of a new search area, shown in green. This area is then searched yielding solution near the edge which necessitates a third search area, shown in blue. The process stops when the best ground constrained solution is near the center of the blue search area. In practice, this process will continue indefinitely until it converges upon a solution. The converged solution serves as the estimated emitter solution

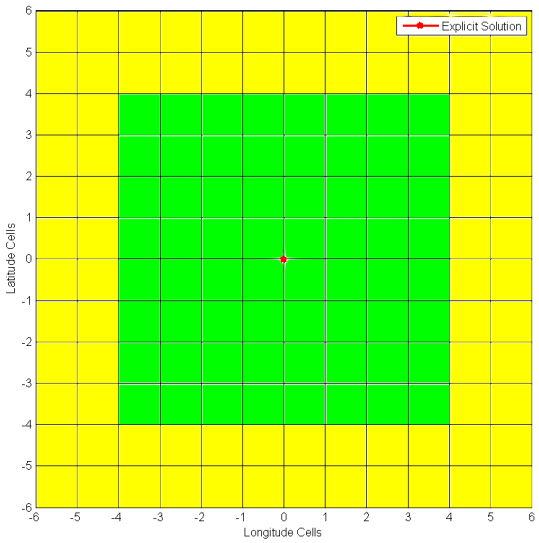

Figure 23. DEM search area with boundary area

for the current pass at the SRFT-1 level.

7. The SRFT-1 level geolocation then serves as a starting point for further refinement. This refinement uses the same steps as described above, but utilizes SRFT-2 data with a post spacing of 1", which corresponds to $\approx$ 30 meters at mid latitudes. The search area is a 10" square centered at the final SRFT-1 post solution yielding a 10×10 post search area. The SRFT-2 post that minimizes the FOM is set as *the* ground constrained position estimate.

8. The steps described above are repeated for each pass, producing a ground constrained position estimate at each step. The collection of position estimates is the output to the analysis process.

This application of a surface of the earth constraint is simple and robust. The performance will be evaluated as part of this research by comparing the MOPs for the same scenario with and without the surface of the earth constraint. One potential weakness of this technique is the potential for the ground constrained solution to inappropriately converge on a particular terrain feature such as a peak or bowl. In

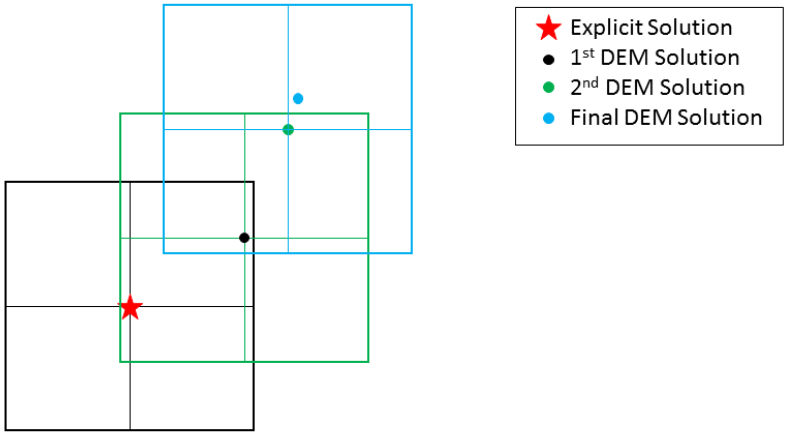

Figure 24. Example of dynamic DEM search

order to avoid this, the search area may require tuning based upon seed location accuracy and terrain variability.

3.6 Covariance and Fusion

In order to quantify the variability in estimated emitter geolocations, and then use that variability as part of the estimate fusion process, it is necessary to create a statistical representation of the set of estimated positions. As geolocation is inherently a three dimensional problem, the 3×3 covariance matrix P, shown in equation (100) is utilized in this research to quantify estimate variability. The estimate covariance matrix, P, is produced for each geolocation agent, for each set of runs. The individual cells are calculated using equation (101), substituting the appropriate variables for $\tilde{x}$, $\tilde{y}$, $\tilde{z}$, $\bar{\tilde{x}}$, $\bar{\tilde{y}}$, and $\bar{\tilde{z}}$, where the bar indicates the average value [78].

$$P = cov\left(\tilde{x}, \tilde{y}, \tilde{z}\right) = \begin{bmatrix} \sigma_{\tilde{x}}^2 & \sigma_{\tilde{y}\tilde{x}} & \sigma_{\tilde{z}\tilde{x}} \\ \sigma_{\tilde{x}\tilde{y}} & \sigma_{\tilde{y}}^2 & \sigma_{\tilde{z}\tilde{y}} \\ \sigma_{\tilde{x}\tilde{z}} & \sigma_{\tilde{y}\tilde{z}} & \sigma_{\tilde{z}}^2 \end{bmatrix} \tag{100}$$

$$\sigma_{\tilde{x}\tilde{y}} = \operatorname{cov}(\tilde{x}, \tilde{y}) = \sum_{i=1}^{N} \frac{(\tilde{x}_i - \bar{\tilde{x}})(\tilde{y}_i - \bar{\tilde{y}})}{N} \tag{101}$$

The total number of runs completed is variable, depending upon how many estimated positions are required to yield a constant covariance matrix. As the eigenvalues of the covariance matrix are a measure of spread in the data, the magnitude of the vector containing the eigenvalues can serve as a metric. Specifically, the incremental change in the covariance matrix eigenvalues between runs, as given by equation (102) with $\lambda(P_{1:i})$ indicating the eigenvalues of the covariance matrix up to the current run and $\lambda\left(P_{1:(i-1)}\right)$ indicating the eigenvalues up to the previous run. When the average of per run changes for the last ten runs is below a set threshold, the covariance is considered to be converged. This research uses a 0.5% threshold. As equal numbers of runs are more convenient to work with, more runs than are required to meet the threshold were completed such that all agents reach or exceed the threshold and meet or exceed a minimum number of runs.

$$\Delta\lambda(P) = \frac{|[\lambda_{1:3}(P_{1:i})] - [\lambda_{1:3}(P_{1:i-1})]|}{|[\lambda_{1:3}(P_{1:i-1})]|} \tag{102}$$

The resulting covariance matrices are used to generate a graphical depiction of the error ellipsoid at a desired confidence level. This research utilizes a 95% confidence level, which aligns with previous research as well as the defacto DOD standard [16]. It is necessary to define a desired confidence level because without some level of uncertainty, the error ellipsoid will be unnecessarily large. In fact, a 100% confidence level would theoretically require an infinitely large error ellipsoid. In contrast, a lower confidence level will result in a smaller error ellipsoid, but potentially less useful information. A graphical comparison of a 50% and a 95% error ellipsoid on the same 200 run data set is shown in Figure 25.

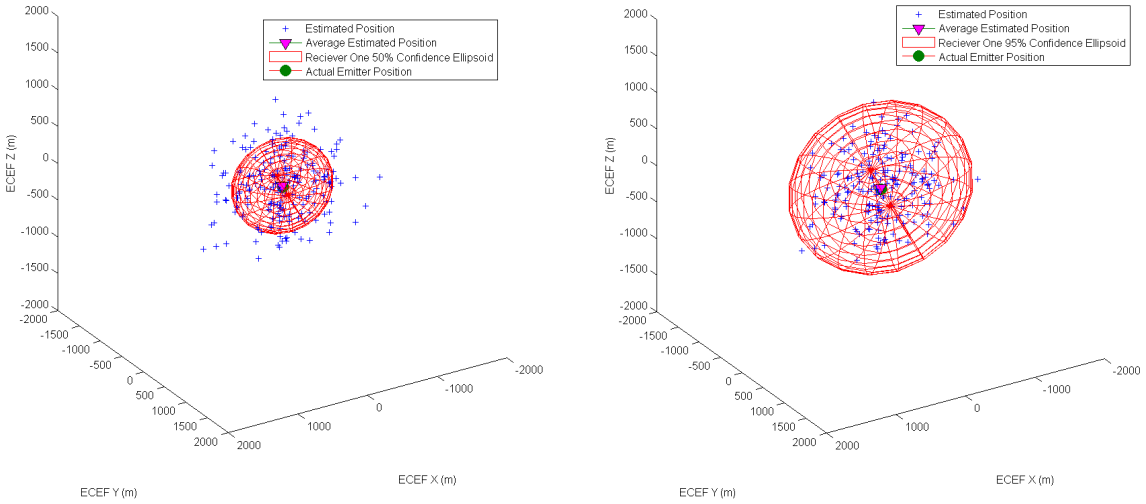

(a) 50% **Confidence level** **(b)** 95% **Confidence level**

Figure 25. Comparison of confidence Levels

In general, error ellipsoid axes lengths are a strict function of the eigenvalues of the covariance matrix, and the orientation of the ellipsoid is dependent upon the eigenvectors. However, it is necessary to apply a scale factor derived from the chi-squared distribution for the desired confidence level and number of degrees of freedom. This factor can be calculated, or, for most common probability levels, determined via a lookup table. The χ^2 value associated with a 3D 95% confidence level is 7.815.

The covariance matrices calculated for each of the data sets are the foundation of the fusion process. For each scenario with multiple collectors, the corresponding estimate covariance matrices are fused per the techniques described in section 2.4. These fusion algorithms produce an estimate and uncertainty which can then be compared. Additionally, a consistency check is performed to determine a) if an appropriate percentage of runs result in the true emitter position lying within the developed error ellipsoid and b) if the the same is true for the fused error ellipsoid centered at the fused position estimate.

3.7 Summary

The preceding chapter covered the overall methodology used in this research as well specific model details, the MOPs used to evaluate performance, fusion of multiple estimates, and the technique for application of the surface of the earth constraint. Taken together, these components yield an accurate and robust model to evaluate the utility of the proposed augmentation. The next chapter will present the results from each scenario.

IV. Results

This chapter will present the results of the simulations performed via the methodology described in the previous chapter. The results have been divided into three scenarios; scenario one with the emitter located near AFIT, scenario two with the emitter located at the Tripoli Airport in Libya, and scenario three with the emitter located in the mountains of northeastern Afghanistan. Each scenario will include the results of each geolocation agent individually as well as the resulting performance from fusing multiple geolocation agents together.

4.1 Scenario One

Scenario one, with the emitter near AFIT, is intended to serve as a "geolocation sandbox" to provide the widest flexibility of collection agent types and geometries. The airspace is unrestricted and the terrain relatively flat. This fact will be leveraged to draw conclusions regarding overall patterns of performance prior to looking at more specific collection situations in the following scenarios. To this end, the section contains the most detailed treatment of the geolocation performance whereas the subsequent scenarios will focus upon scenario specific behavior and aberrations.

4.1.1 Single Geolocation Agent Performance.

In order to quantify the utility in using a CubeSat hosted AOA geolocation payload as an augmentation for existing systems, it is first necessary to establish a baseline performance level for each of the geolocation agents. The single agent results will also serve to establish the effectiveness of the surface of the earth constraint. The following subsections will present the single agent MOPs and plots for the satellite and aircraft AOA, satellite and aircraft three-ball TDOA and satellite based four-ball

TDOA geolocation agents respectively.

4.1.1.1 AOA Satellite Performance.

To begin, it is important to understand the expected performance of the single-ball AOA CubeSat that has been proposed as an augmentation system. Six different geometries, numbered $1-6$ as described in subsection 3.3.2, were considered with the collector and emitter as described in Chapter III and the transmitter operating at a power of $6.5kW$ and a PRF of $216Hz$. The respective performance, as measured by the MOPs discussed in subsection 3.4 are shown in Tables 9 and 10 for the unconstrained and SRFT-2 based ground constrained formulations respectively.

Examining the MOPs reveals several patterns of performance. First, the best performance occurs on geometries 2 and 4. This is not unexpected as those passes have the highest number of received pulses and also benefit from a higher received SNR than passes 3 and 6. Another useful observation is that adding an SRFT-2 based surface of the earth constraint increases performance by every measure. The greatest improvement was to ellipsoid volume with reductions of two to three orders of magnitude. More significantly, the RMSE and average miss distance were also reduced by an average of 12% and 15% respectively. The 95% confidence ellipsoid SMA and MPTPS, which are particularly of interest per subsection 3.4, saw more modest improvements, averaging 6% and 5% respectively. It should be noted that in one case, pass 4, the SMA actually had a very slight increase.

Shifting to the graphical representation of the simulation results, Figures 26 to 31 show the geolocation solutions for the first 100 runs in reference to the SRFT terrain with the true emitter position, average estimated position and MPTPS marked. Note that in some cases the MPTPS is not available due to the high computational load associated with performing the $(n-1)^n$ search over the terrain posts encompassed

Table 9. Unconstrained AOA satellite performance against AFIT target

Geometry	Measure of Performance				
	RMSE (m)	Avg Miss (m)	Volume (m^3)	SMA (m)	MPTPS (m)
1	694	608	3.21E+09	1686	3109
2	414	377	1.11E+09	832	1477
3	1861	1703	9.04E+10	4054	8039
4	690	617	3.01E+09	1696	3341
5	361	329	7.62E+08	717	1311
6	2933	2402	6.65E+10	7940	13127

Table 10. Ground constrained AOA satellite performance against AFIT Target

Geometry	Measure of Performance				
	RMSE (m)	Avg Miss (m)	Volume (m^3)	SMA (m)	MPTPS (m)
1	636	544	1.77E+07	1635	3083
2	343	302	4.17E+06	757	1427
3	1672	1476	2.70E+08	4053	7823
4	655	567	1.41E+07	1702	3225
5	302	265	3.49E+06	663	1247
6	2432	2007	3.62E+08	6605	11386

within a large error ellipsoid. The graphical depictions illustrate some of the characteristics of the of the DEM based surface of the earth constraint. The first obvious behavior is that the solutions "stick" to the terrain resulting in a much thinner ellipsoid. This behavior is responsible for the remarkable reduction in ellipsoid volume discussed earlier. Additionally, since a surface model rather than a terrain model is being used, some additional noise in the "up" direction can be expected from vegetation and structures as seen in this data. However, the ground constrained ellipsoids are still an order of magnitude less thick in the up direction than the non-ground constrained counterparts. Another observation, best observed in Figure 31, is that the surface of the earth constraint forces the ellipsoid to an orientation coincident with the surface of the earth. This may have the effect of increasing the MPTPS in cases where the ellipsoid would otherwise be orientated at an angle closer to normal to the

surface of the earth. Finally, the orientation of the ellipsoids should be noted. In pass geometries 1 and 4, which pass directly over the emitter, the ellipsoids are oriented in the direction of travel of the collector. In contrast, the other geometries exhibit error ellipses that are closer to normal to the direction of travel of the collector. These orientation patterns will be useful in the discussion of fusion performance. Overall, the satellite based AOA geolocation agent appears to exhibit good performance. Next, the aircraft based AOA geolocation agent performance will be examined.

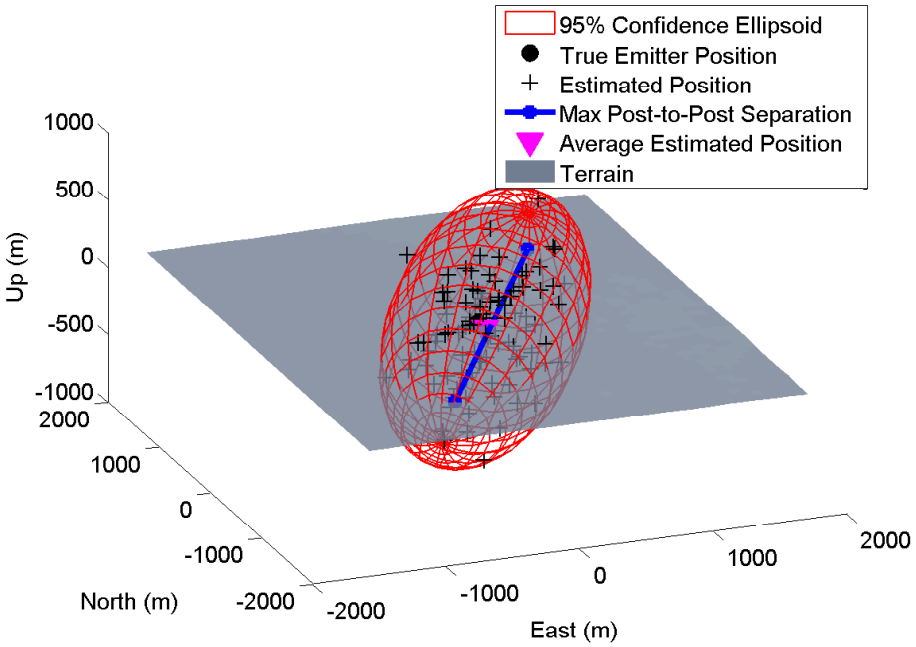

(a) No ground constraint

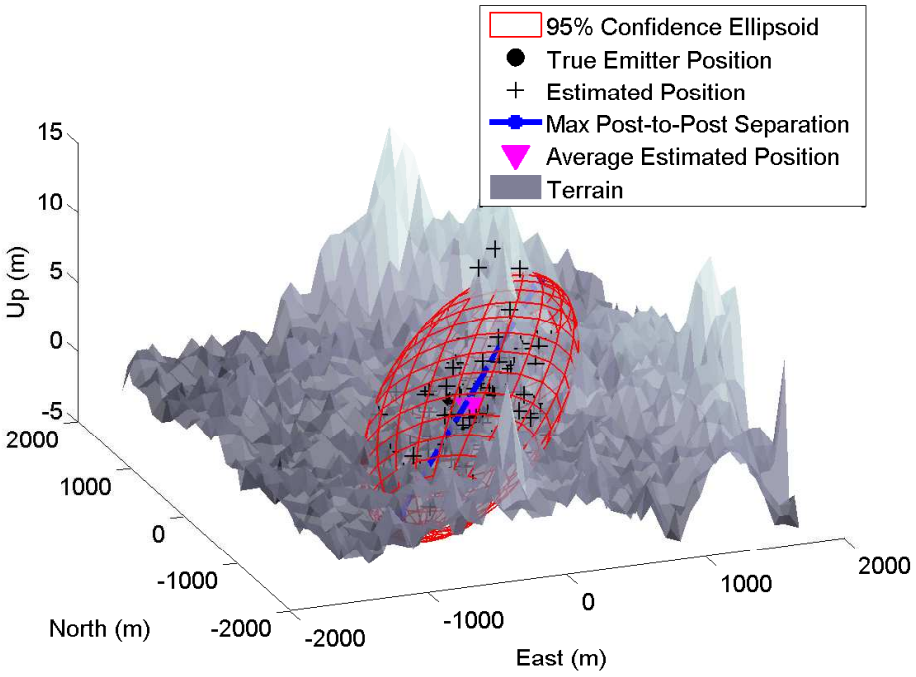

(b) Ground constrained

Figure 26. AOA satellite geometry 1 against AFIT target

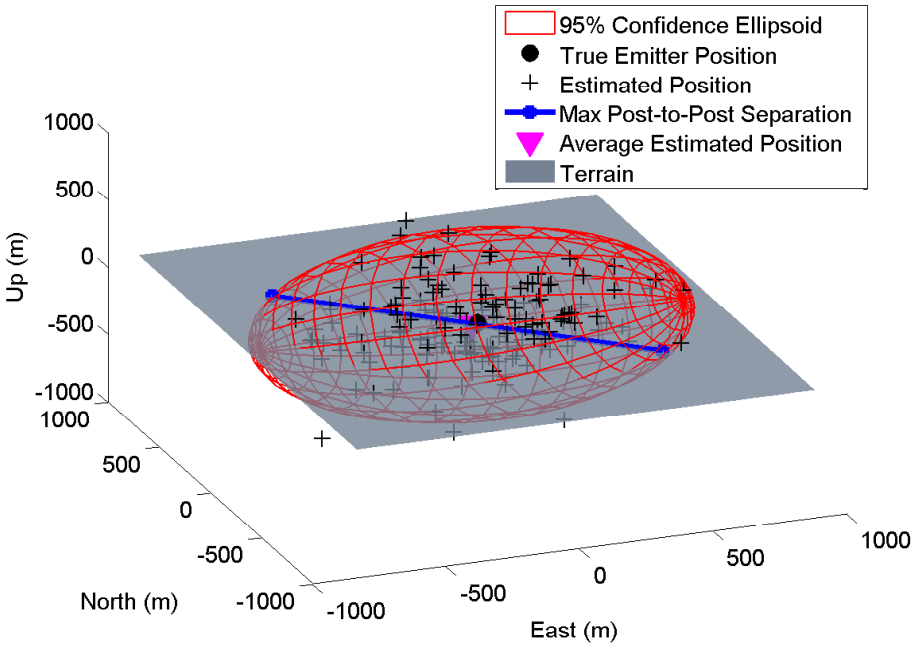

(a) No ground constraint

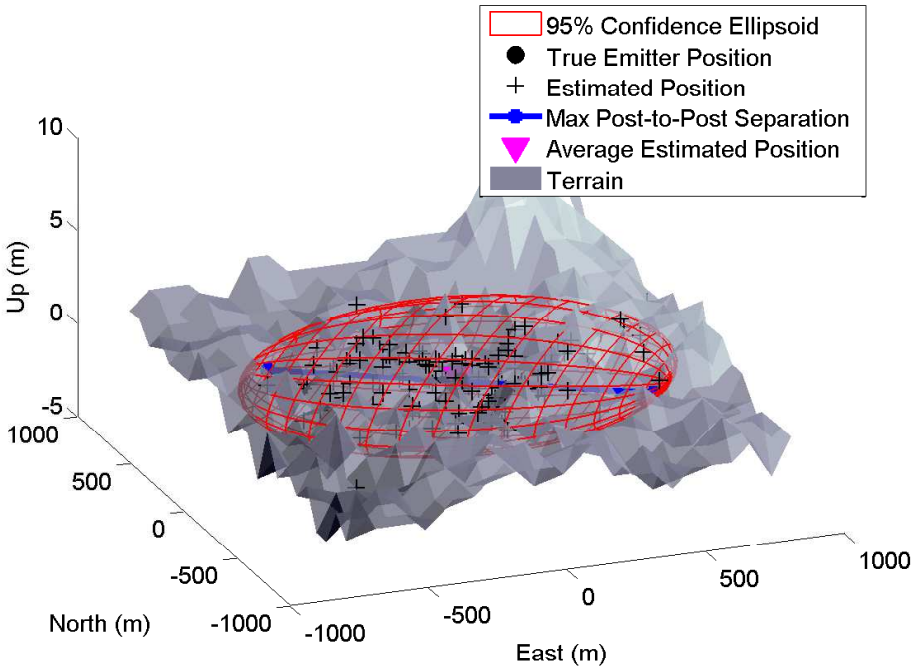

(b) Ground constrained

Figure 27. AOA satellite geometry 2 against AFIT target

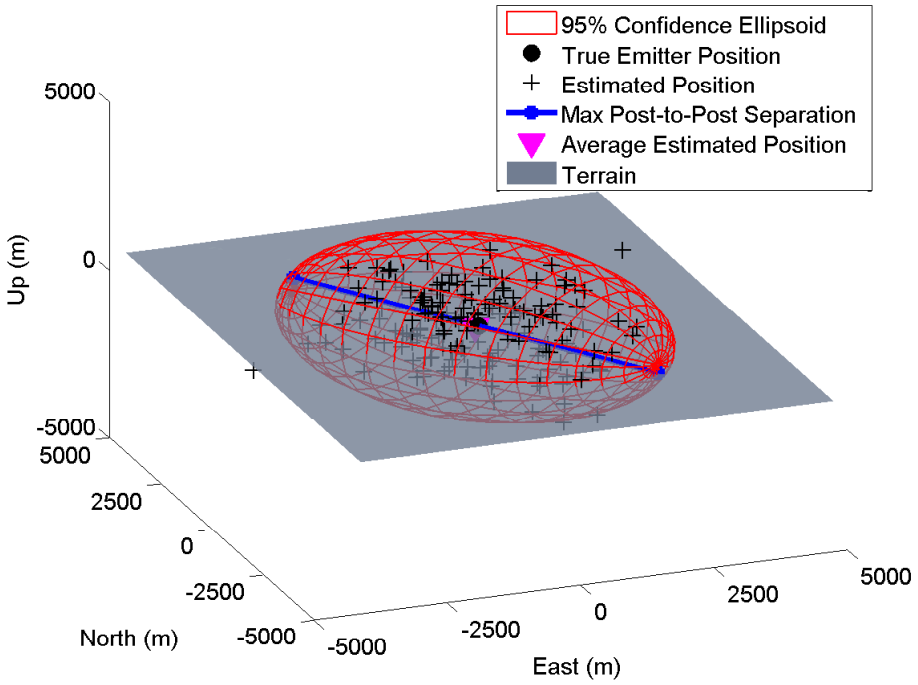

(a) No ground constraint

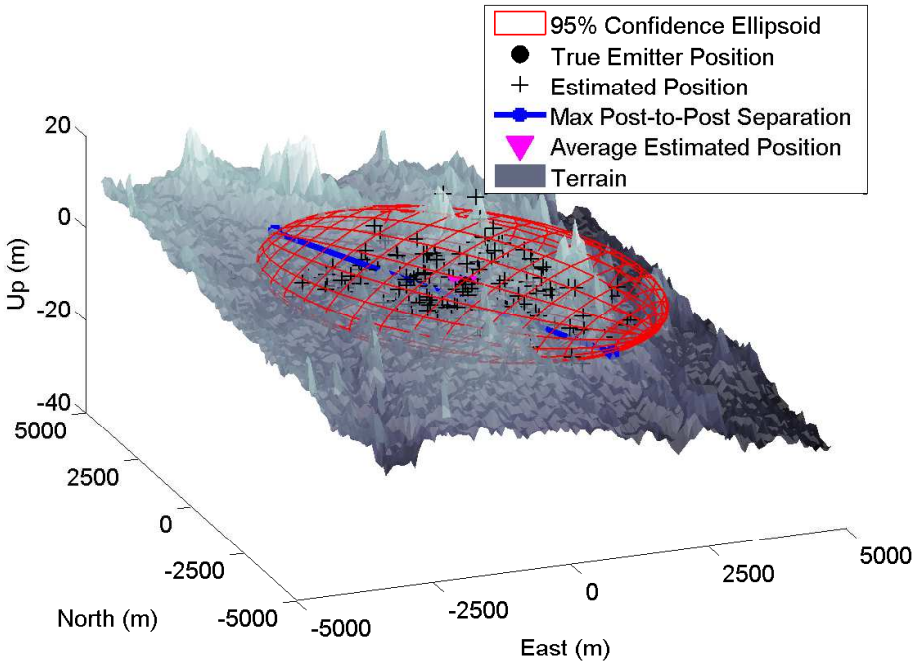

(b) Ground constrained

Figure 28. AOA satellite geometry 3 against AFIT target

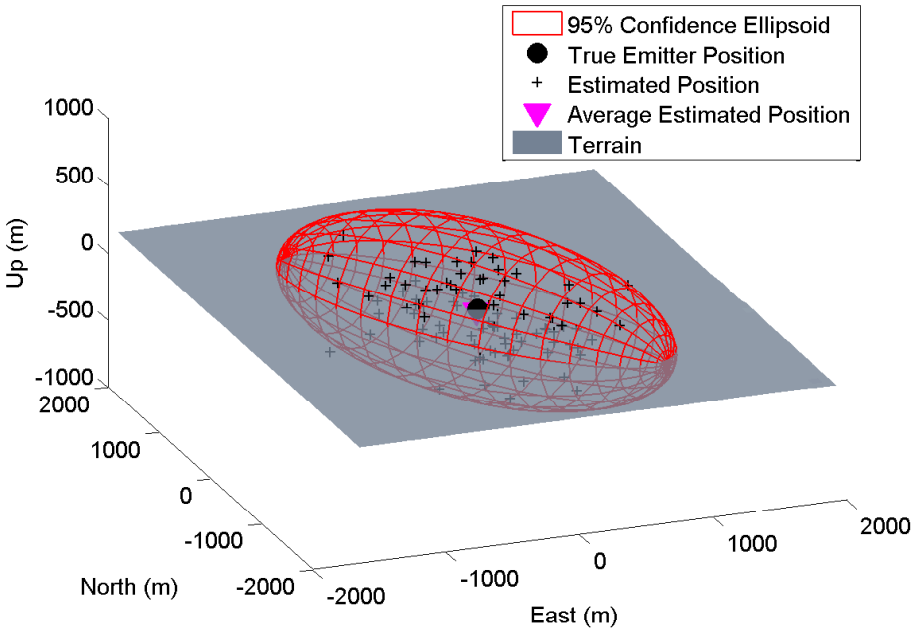

(a) No ground constraint

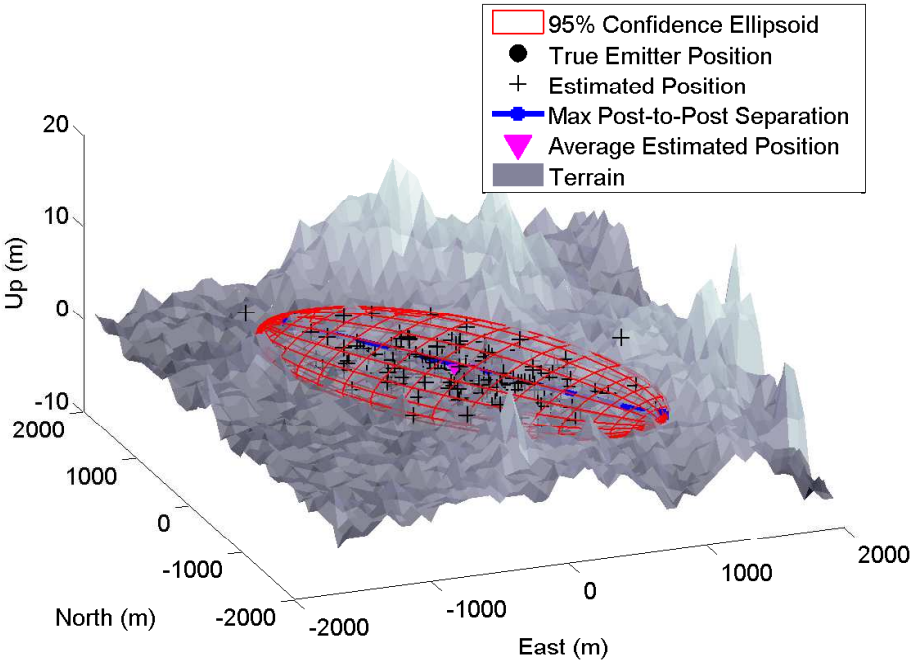

(b) Ground constrained

Figure 29. AOA satellite geometry 4 against AFIT target

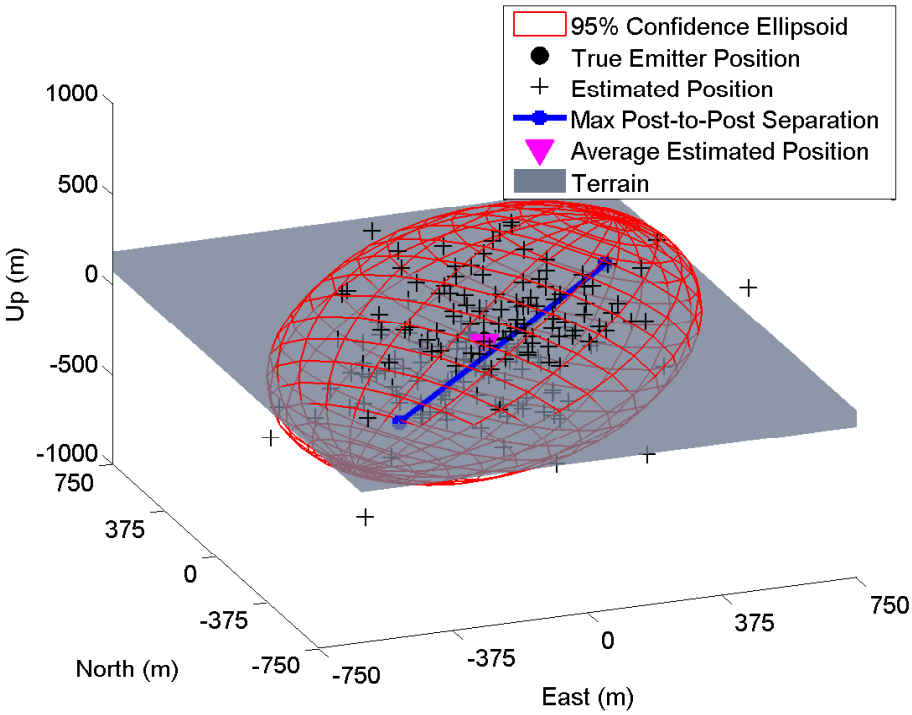

(a) No ground constraint

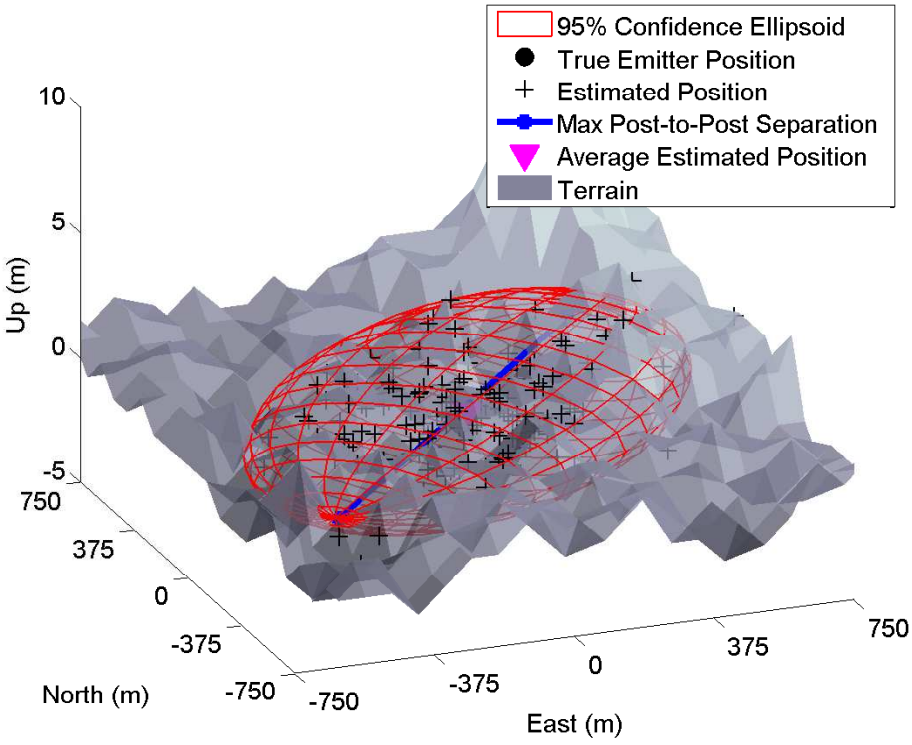

(b) Ground constrained

Figure 30. AOA satellite geometry 5 against AFIT target

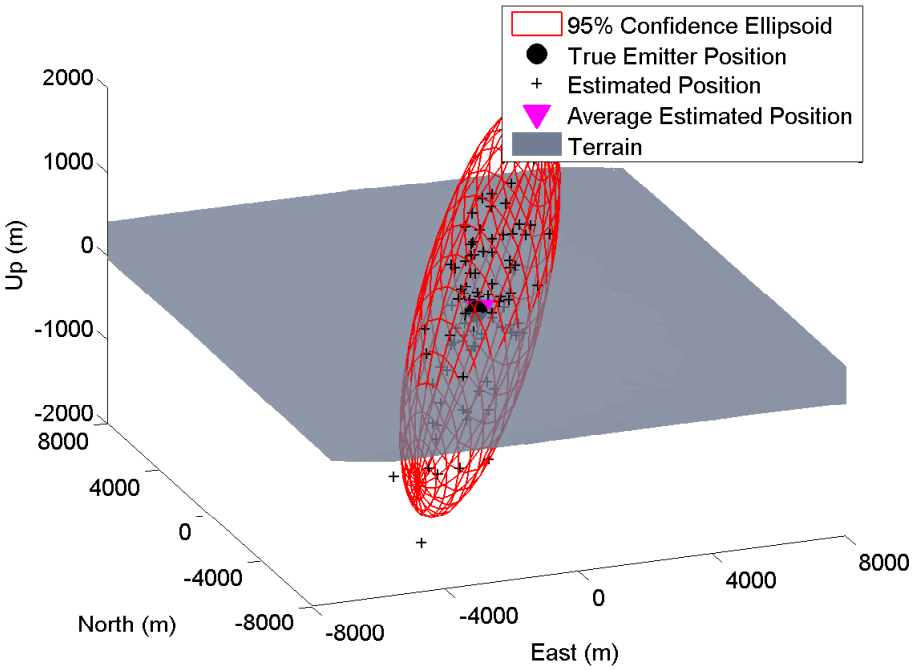

(a) No ground constraint

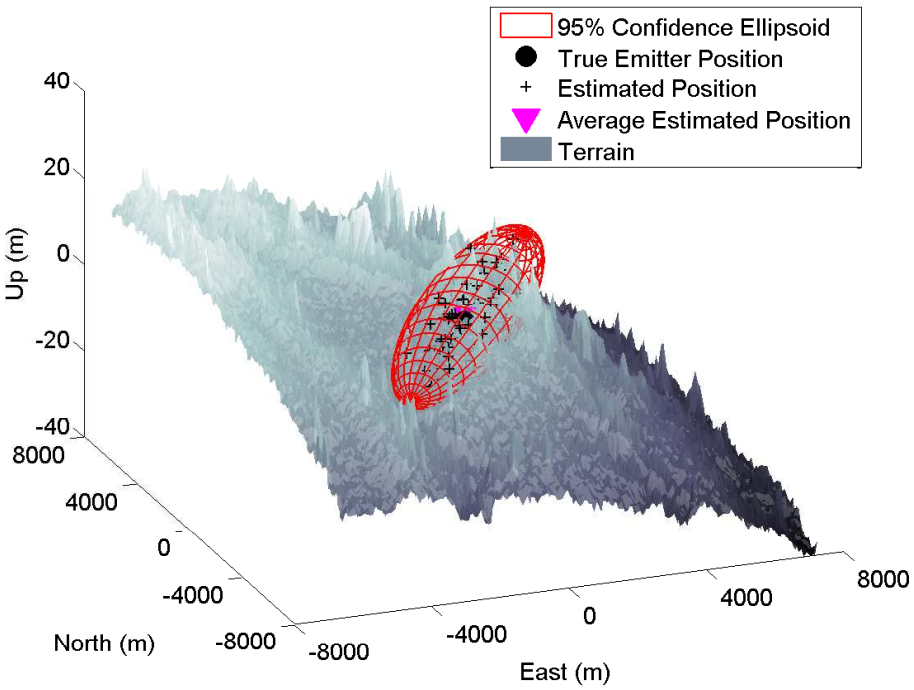

(b) Ground constrained

Figure 31. AOA satellite geometry 6 against AFIT target

4.1.1.2 AOA Aircraft Performance.

The aircraft based AOA agents share many of the same collection characteristics as the satellite based agent. The primary differences are that the aircraft have an attitude knowledge error five times higher than that of the satellite and that the aircraft are much closer to the emitter, resulting in a higher SNR and less distance over which angular errors propagate. It is expected that these differences will manifest in differing MOP values.

Based upon the performance shown in Tables 11 and 12, the performance boost provided by the later more than compensates for the loss due to the former. Despite the improved performance when compared to the SV based solution, some of the same performance patterns are visible. Pass geometries 1 through 3, which pass directly overhead the emitter have better performance than geometries 4 through 6 which are offset to the east. The ground constrained solutions again results in improved performance in most cases, albeit not as significant as that seen in the SV based AOA agent. The average improvement to the RMSE and average miss distance is 5% and 8% respectively. The ground constrained SMA however was worse for pass geometries 1 through 3 and only slightly improved for pass geometries 4 through 6. This may suggest that the inclusion of a surface of the earth constraint is more beneficial for less accurate cases where the distributions of unconstrained estimates spans a significantly greater distance than the post spaces of the DEM being used to apply the surface of the earth constraint.

Shifting again to the graphical depiction of the geolocation solutions shown in Figures 32 to 37, it is again noted that AOA collectors passing directly overhead produce ellipsoids oriented along the path of motion. The collector offset to the east produce ellipsoids follow the pattern observed in the SV based AOA agents with the exception of pass geometry 4 which is not oriented normal to its direction of travel.

This may be a result of the small offset, but will need to be considered in the latter scenarios.

Table 11. Unconstrained AOA aircraft performance against AFIT target

Geometry	Measure of Performance				
	RMSE (m)	Ave Miss (m)	Volume (m^3)	SMA (m)	MPTPS (m)
1	38	34	5.24E+05	94	156
2	35	32	4.59E+05	85	94
3	36	32	4.58E+05	87	93
4	65	58	2.30E+06	162	233
5	66	58	1.96E+06	167	170
6	66	58	2.43E+06	163	170

Table 12. Ground constrained AOA aircraft performance against AFIT target

Geometry	Measure of Performance				
	RMSE (m)	Ave Miss (m)	Volume (m^3)	SMA (m)	MPTPS (m)
1	39	32	1.72E+04	101	156
2	36	32	1.47E+04	94	113
3	36	30	1.89E+04	95	93
4	59	51	6.16E+04	150	143
5	57	49	4.88E+04	150	71
6	60	52	6.56E+04	153	143

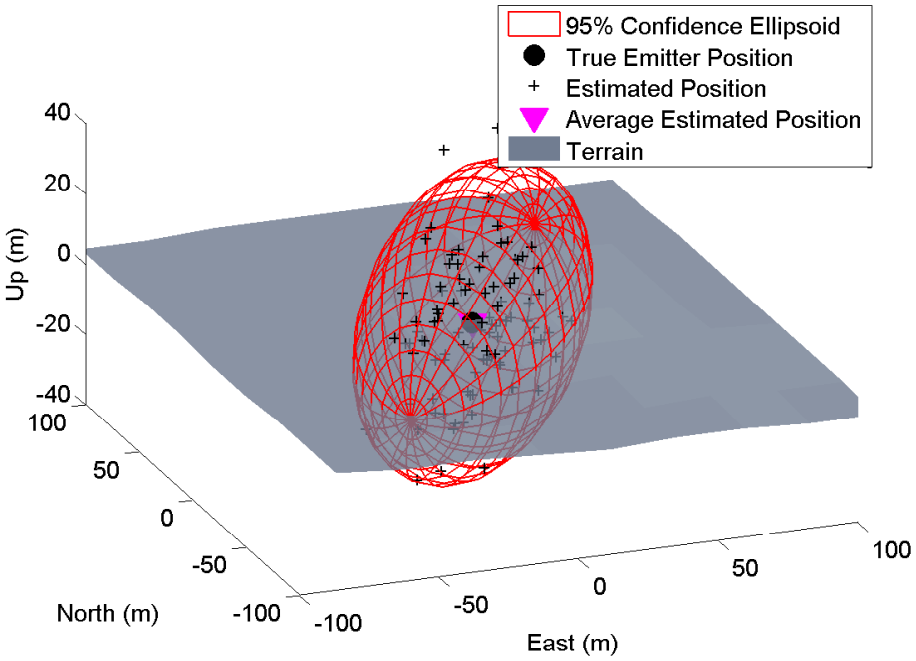

(a) No ground constraint

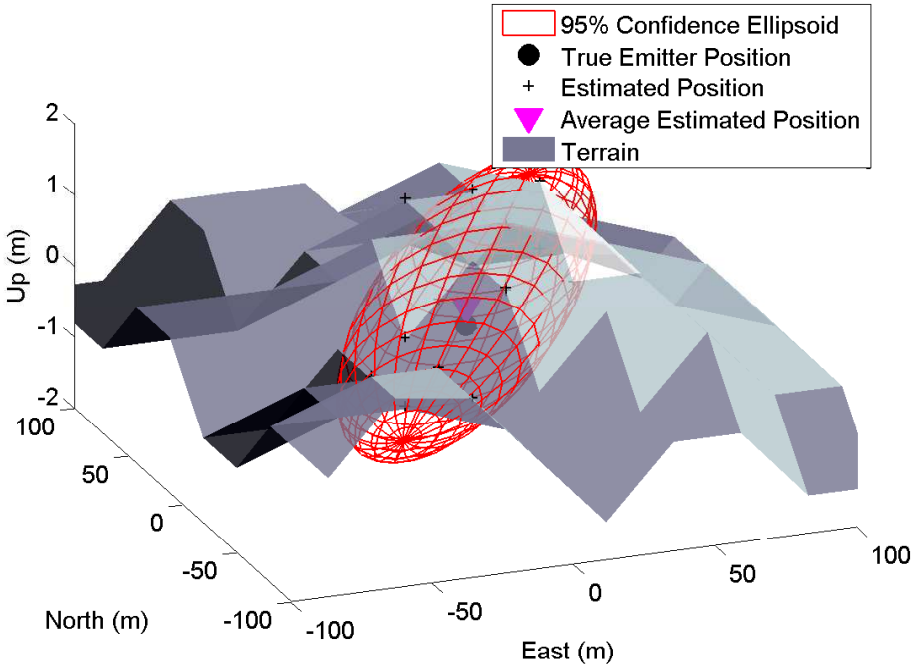

(b) Ground constrained

Figure 32. AOA aircraft geometry 1 against AFIT target

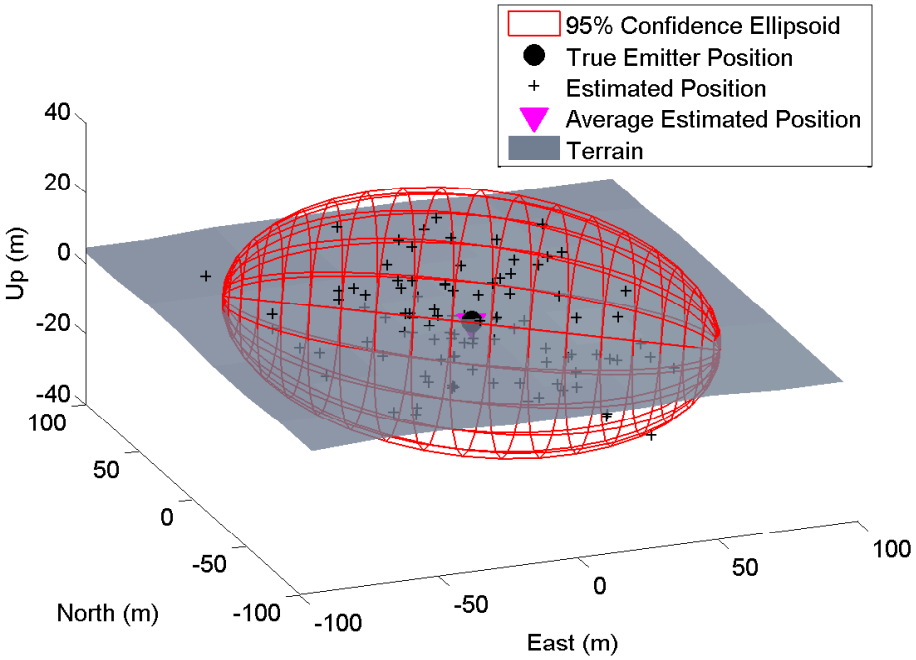

(a) No ground constraint

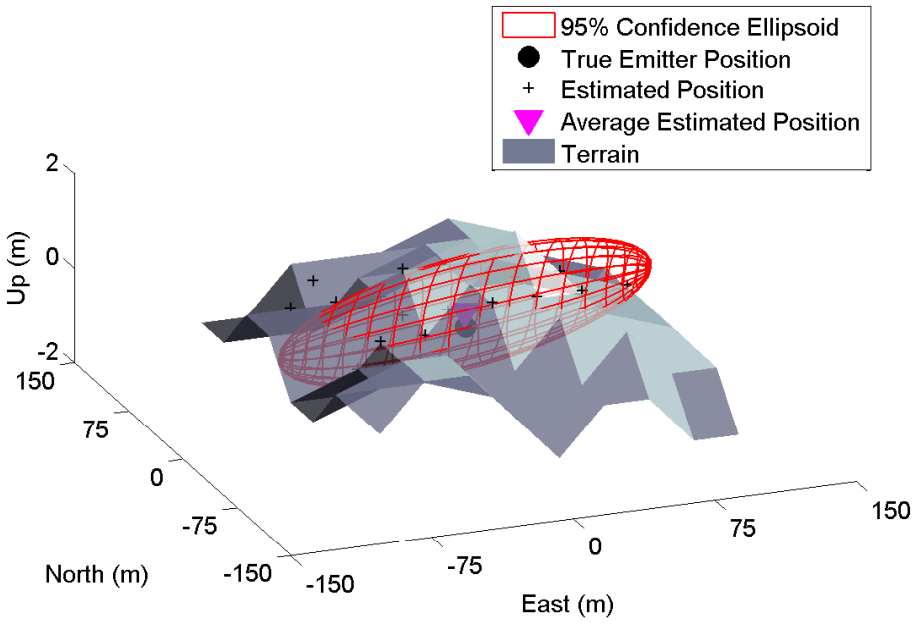

(b) Ground constrained

Figure 33. AOA aircraft geometry 2 against AFIT target

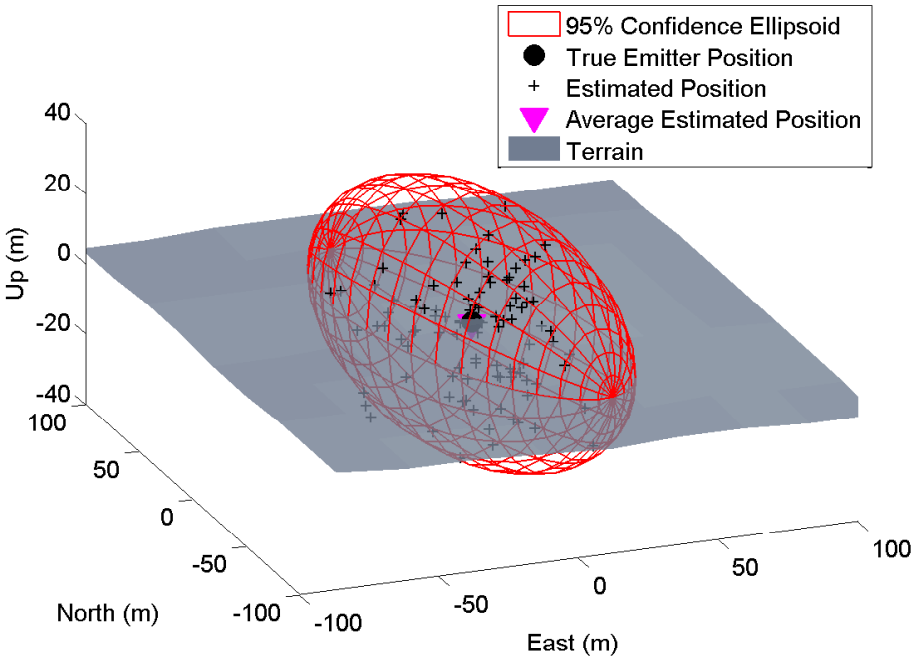

(a) No ground constraint

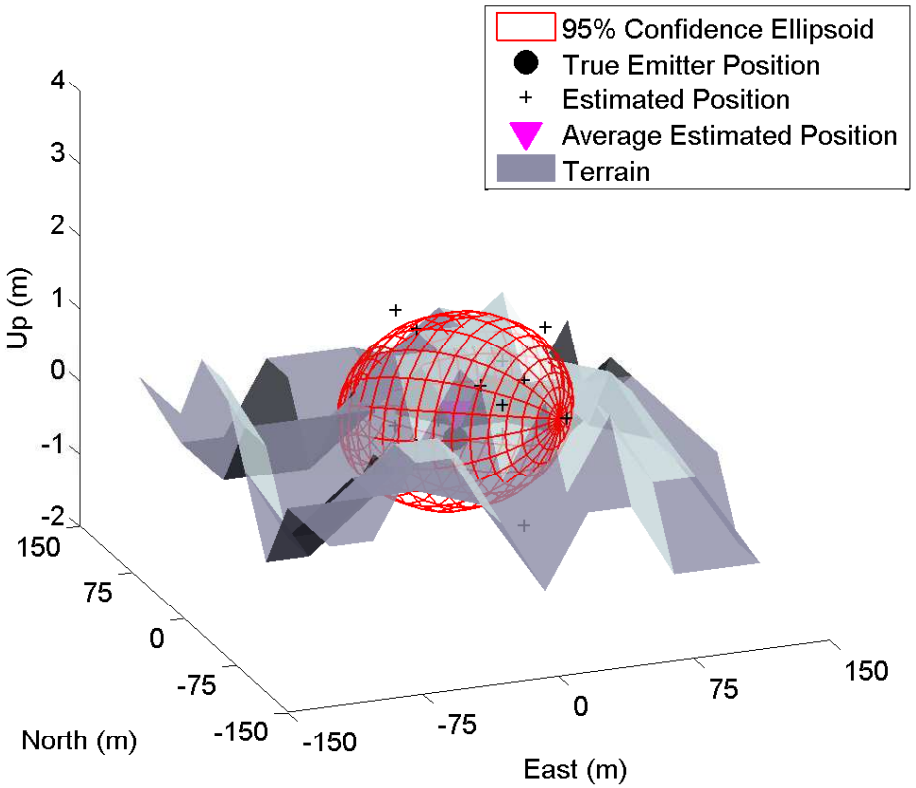

(b) Ground constrained

Figure 34. AOA aircraft geometry 3 against AFIT target

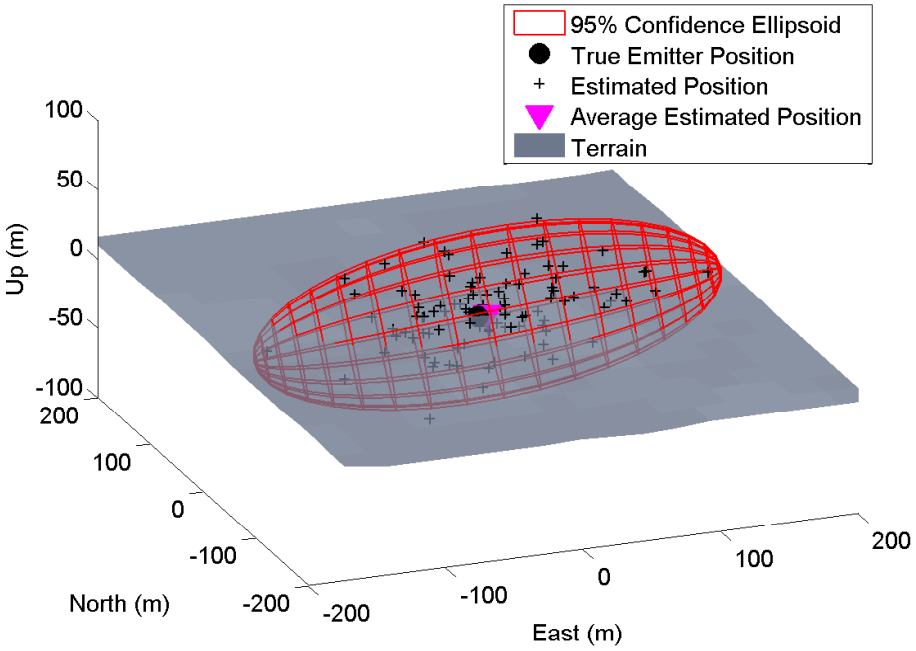

(a) No ground constraint

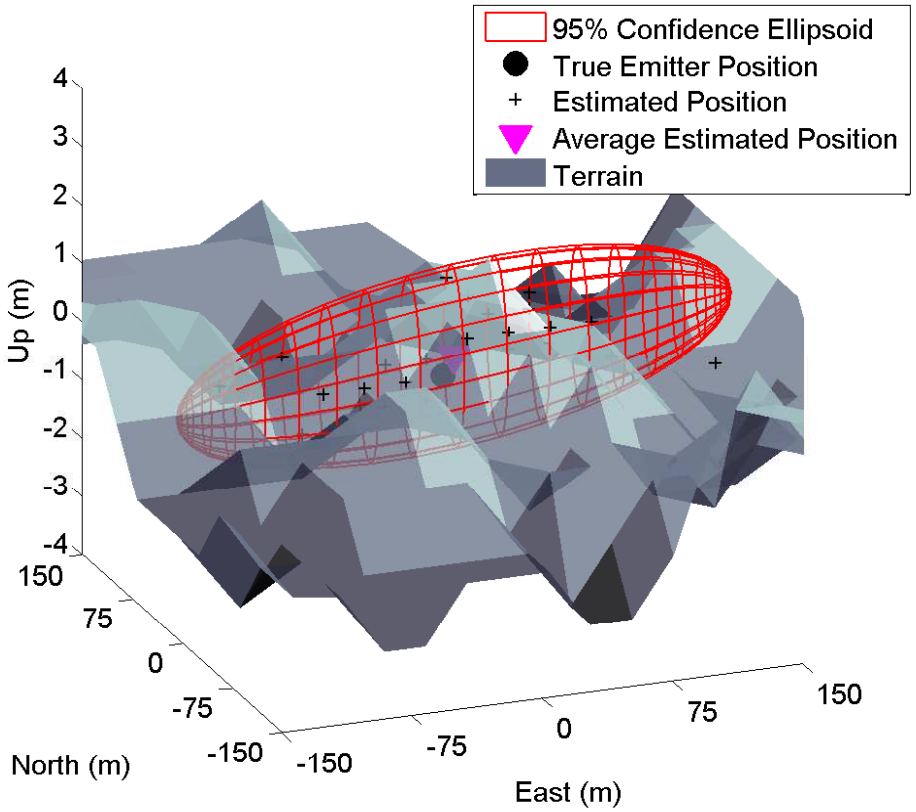

(b) Ground constrained

Figure 35. AOA aircraft geometry 4 against AFIT target

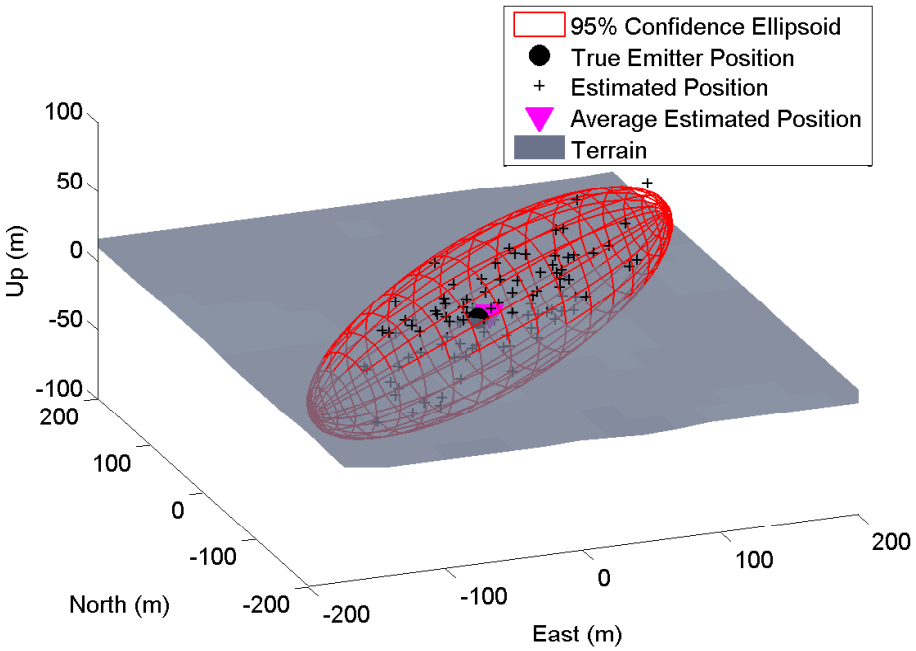

(a) No ground constraint

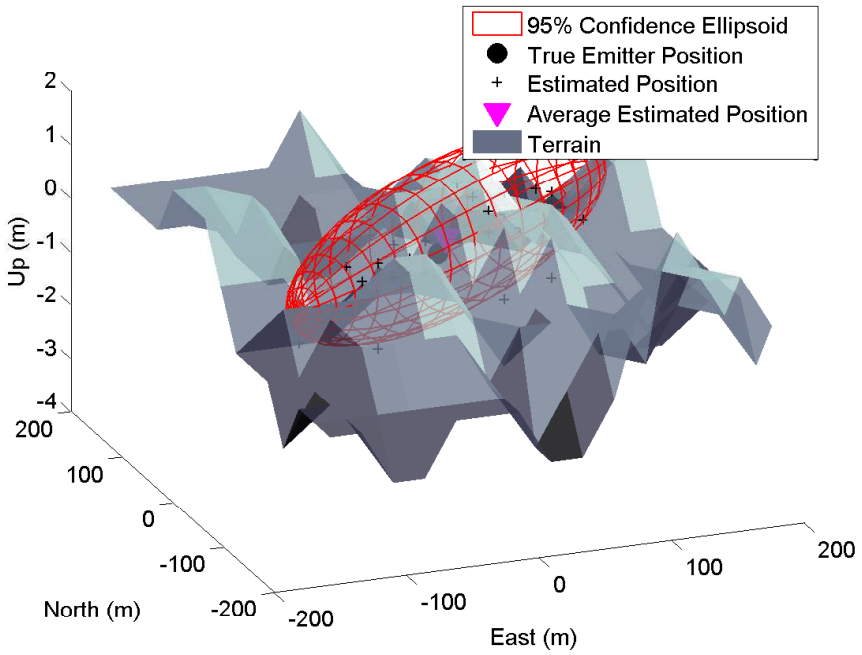

(b) Ground constrained

Figure 36. AOA aircraft geometry 5 against AFIT target

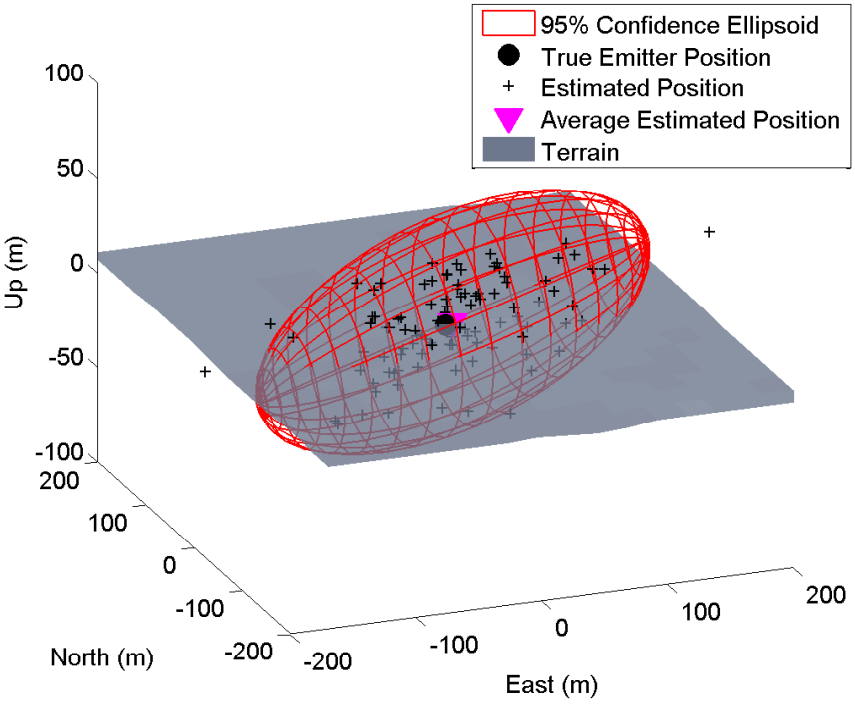

(a) No ground constraint

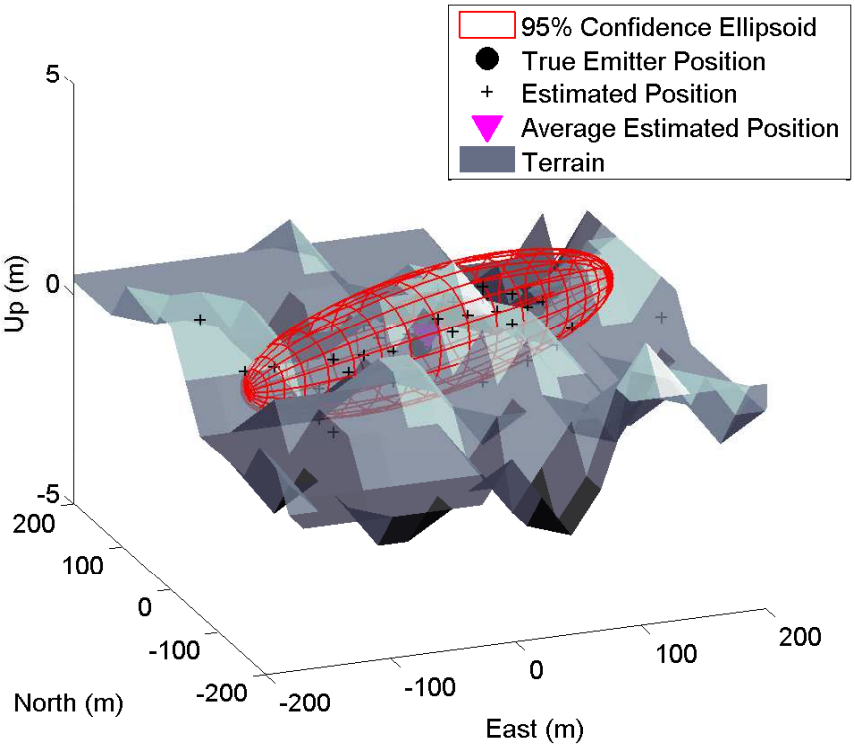

(b) Ground constrained

Figure 37. AOA aircraft geometry 6 against AFIT target

4.1.1.3 Three-ball TDOA Satellite Performance.

The three-ball SV based TDOA agent is the first collection agent with a different phenomenology to be considered. Tables 13 and 14 show the unconstrained and ground constrained solutions respectively. It should be noted that since the three-ball TDOA formulation contains an explicit ground constraint using the radius of the earth at the target position, "unconstrained" and "ground constrained" are slight misnomers. Rather, it is more appropriate to consider the ground constraint to be an additional level of fidelity applied post facto to a rough surface of the earth constraint. Overall, the performance provided by the three-ball TDOA agent is comparable, to slightly worse, than that provided by the AOA SV, particularly in the unconstrained case. However, very large improvements in most of the MOPs result from adding the DEM based surface of the earth constraint. In particular, the RMSE and average miss distance are improved by an average of 83% and 82% respectively with a similar reduction to the SMA. Much of this improvement can likely be attributed to the fact that "unconstrained" results tend to lie slightly below the surface of the earth. This phenomenon may be partially attributed to the difference between the WGS 84 ellipsoid and the true terrain height. The effect can be seen clearly in Figures 38a, 39a, 40a, 41a, 42a and 43a. The result of this offset is significantly increased missed distances and poor consistency which is remedied by the application of the high fidelity DEM based surface of the earth constraint. Another side effect of this offset is that the MPTPS MOP becomes a poor measure of the solution span. For example, Figure 40a shows a MPTPS resulting from the ellipsoid barely making contact with the DEM. This MPTPS does not span the true emitter position or the average estimated position and thus indicates that the solution is much better than it actually is. This behavior lends doubt as to the suitability of the MPTPS as a good universal metric of geolocation quality.

The patterns exhibited in the graphical representations of the geolocation solutions diverge slightly from the behavior noted in the AOA agents. The three-ball TDOA agent results in ellipsoids that are generally aligned with the direction of travel of the collector regardless of whether the pass geometry in question is directly over the emitter or offset. The one exception is shown in Figure 43 where the ellipsoid is oriented closer to normal to the direction of collector travel.

Table 13. Unconstrained three-ball TDOA satellite performance against AFIT target

Geometry	Measure of Performance				
	RMSE (m)	Ave Miss (m)	Volume (m^3)	SMA (m)	MPTPS (m)
1	1850	1486	1.47E+13	5141	2103
2	1944	1688	2.57E+14	4803	3894
3	9371	7512	1.23E+18	24322	NA
4	1810	1409	7.88E+12	5034	2415
5	2380	2000	1.16E+15	6329	3228
6	19200	16144	2.66E+20	40142	NA

Table 14. Ground constrained three-ball TDOA satellite performance against AFIT target

Geometry	Measure of Performance				
	RMSE (m)	Ave Miss (m)	Volume (m^3)	SMA (m)	MPTPS (m)
1	587	486	3.86E+10	1597	2803
2	295	265	5.28E+09	676	1252
3	820	661	8.32E+10	2267	3506
4	558	457	1.59E+10	1527	2641
5	282	244	4.11E+09	657	1243
6	651	525	4.28E+10	1795	2913

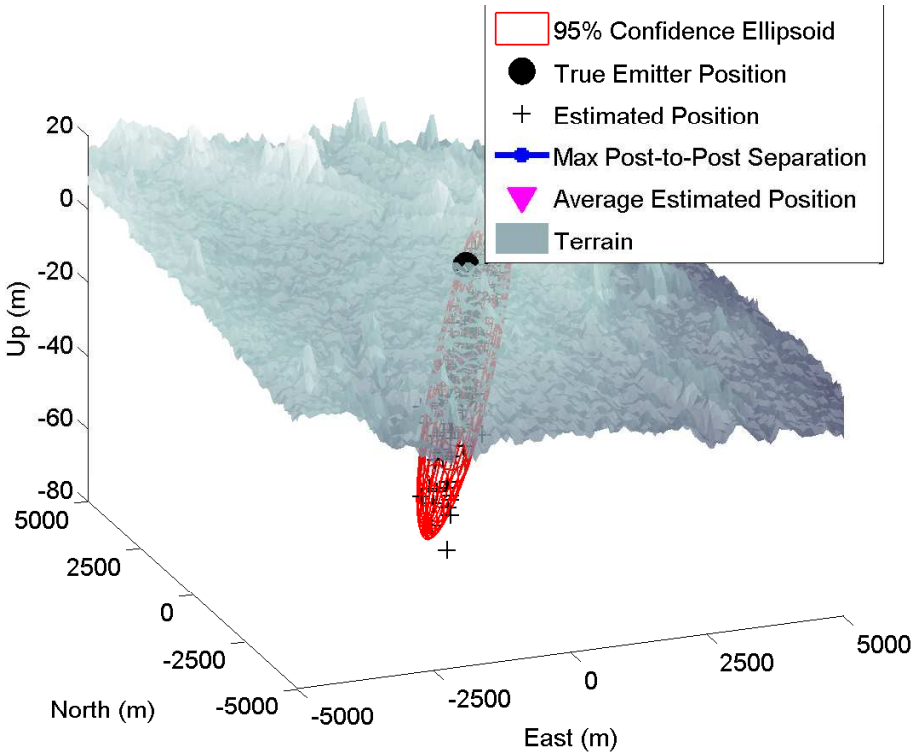

(a) No ground constraint

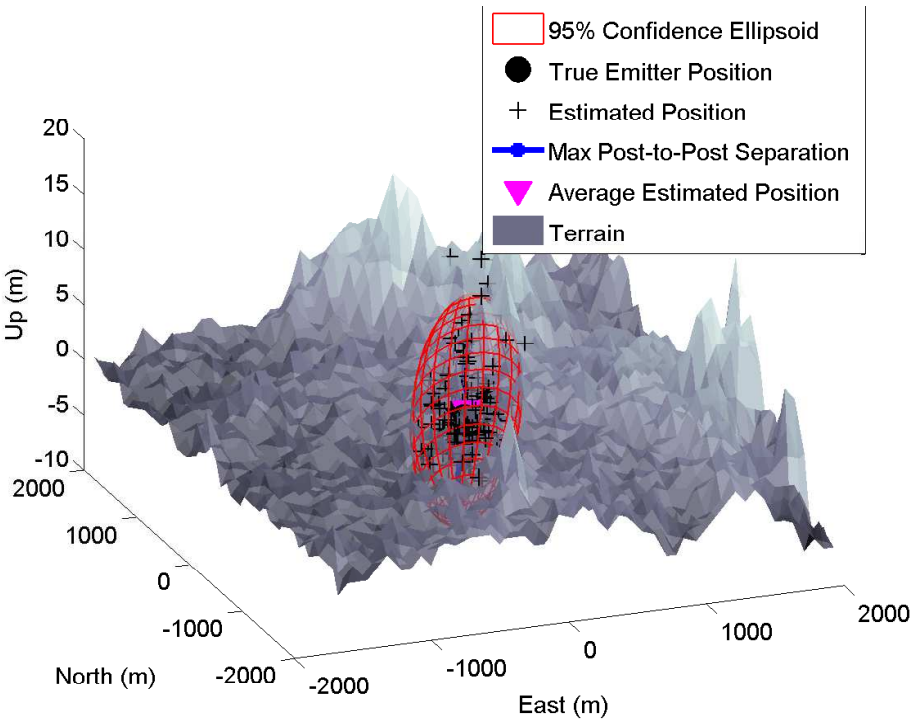

(b) Ground constrained

Figure 38. Three-ball TDOA satellite geometry 1 against AFIT target

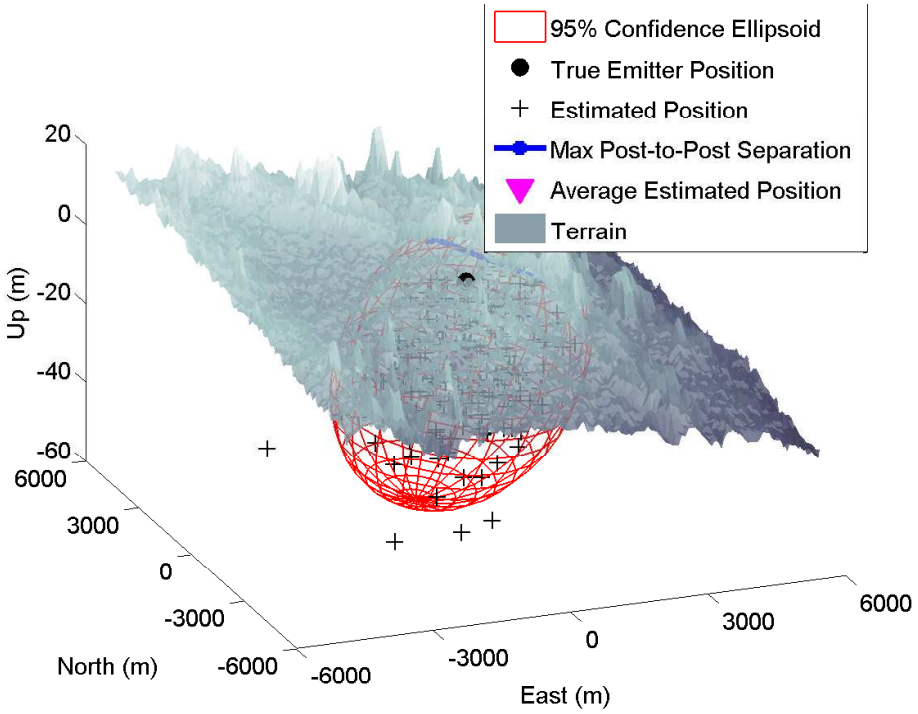

(a) No ground constraint

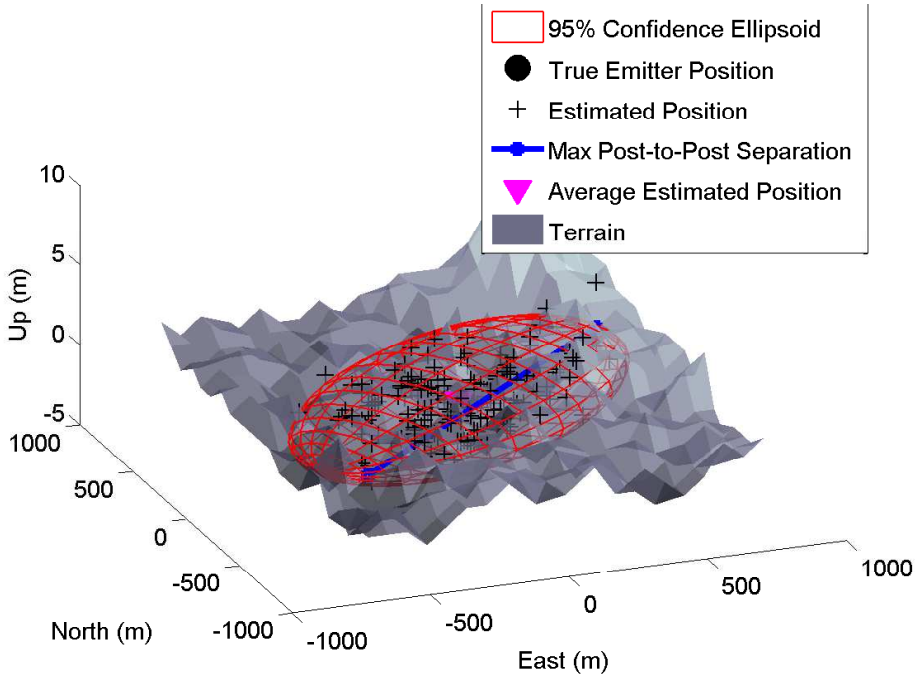

(b) Ground constrained

Figure 39. Three-ball TDOA satellite geometry 2 against AFIT target

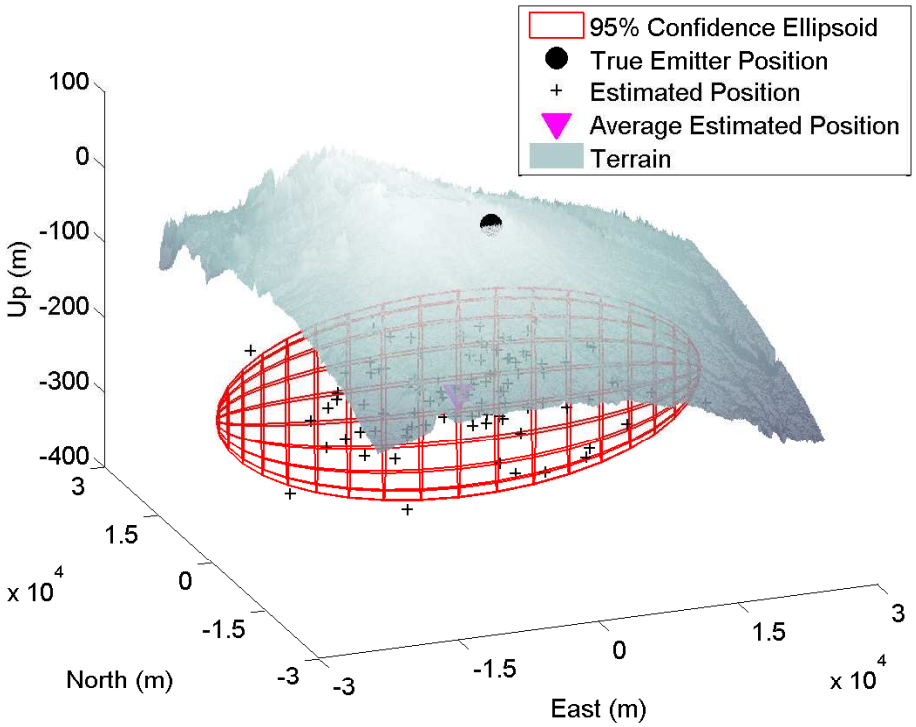

(a) No ground constraint

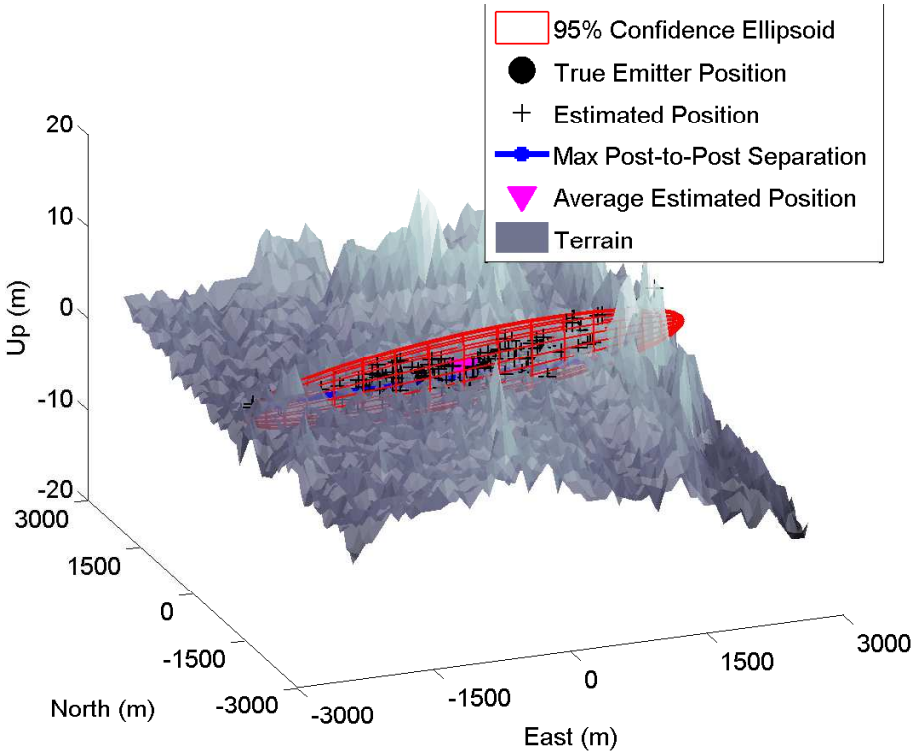

(b) Ground constrained

Figure 40. Three-ball TDOA satellite geometry 3 against AFIT target

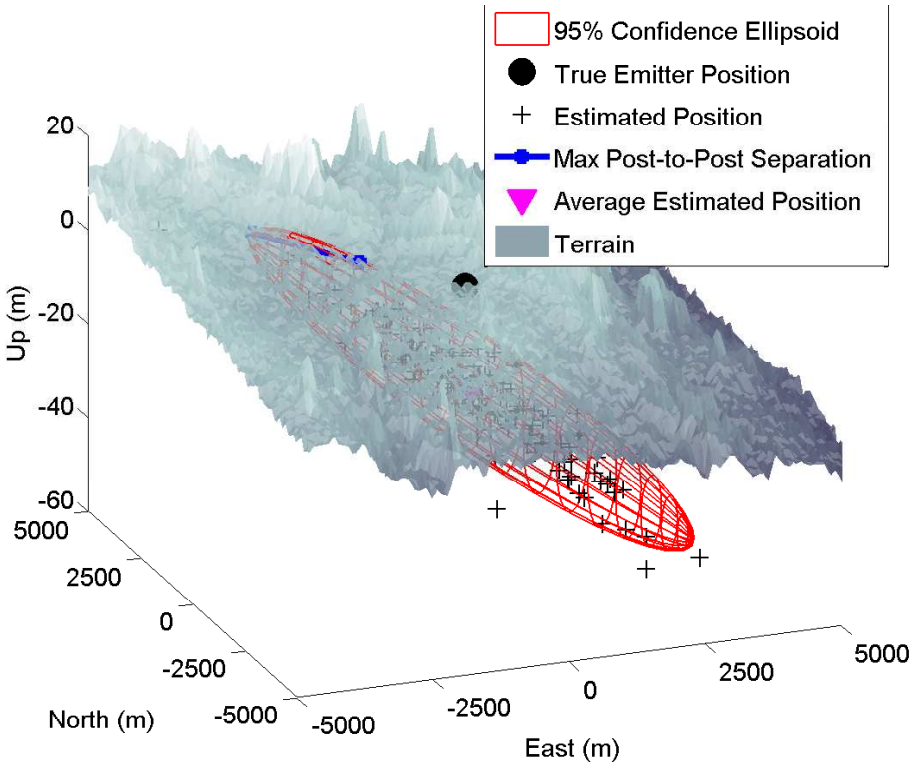

(a) No ground constraint

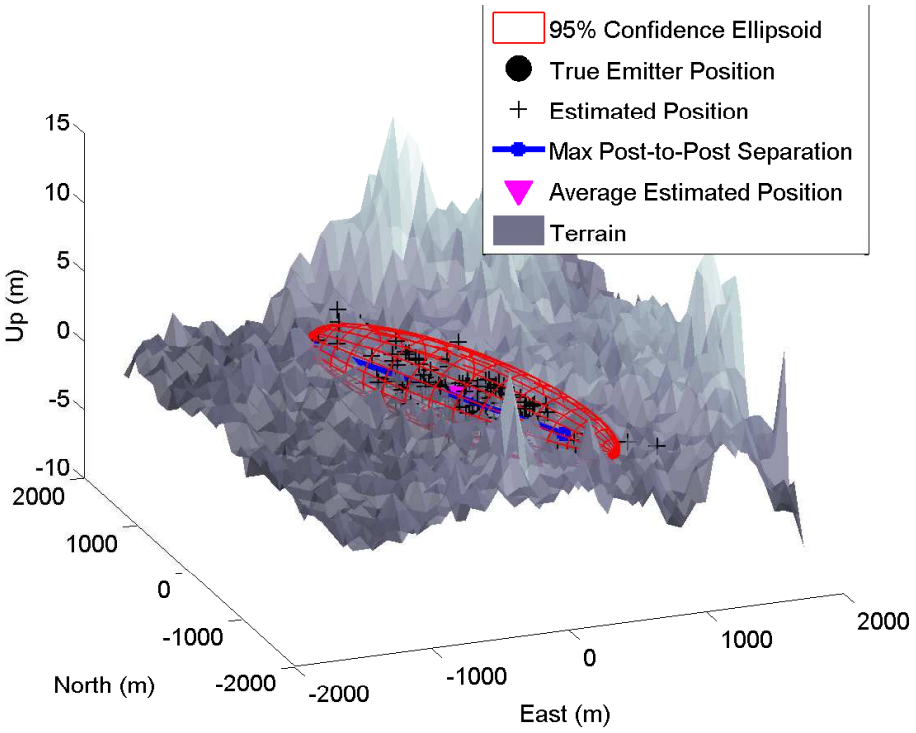

(b) Ground constrained

Figure 41. Three-ball TDOA satellite geometry 4 against AFIT target

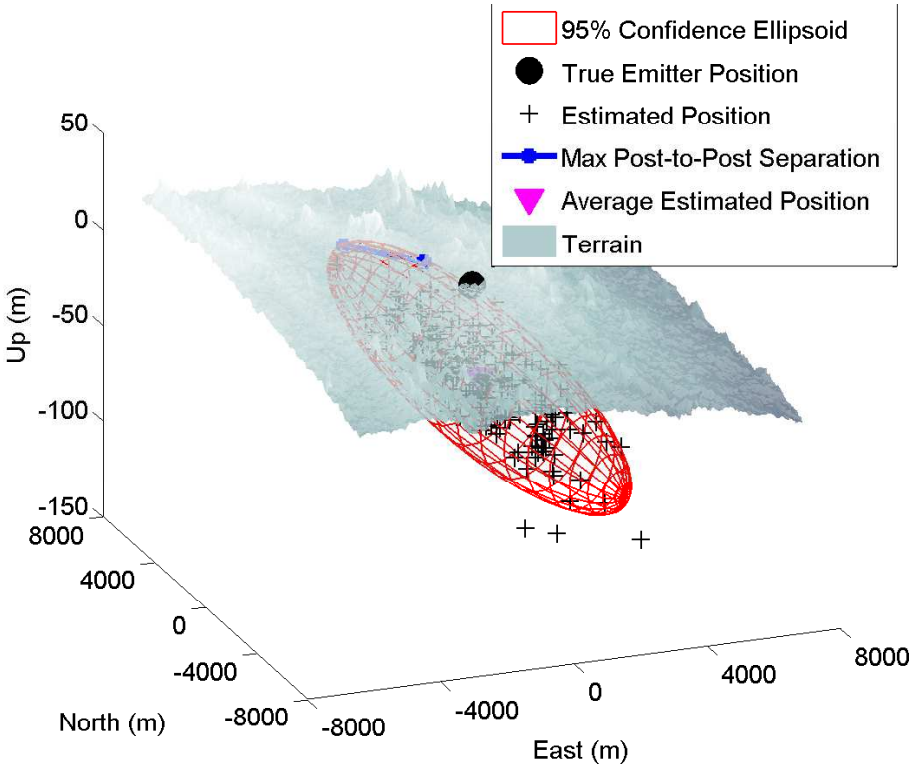

(a) No ground constraint

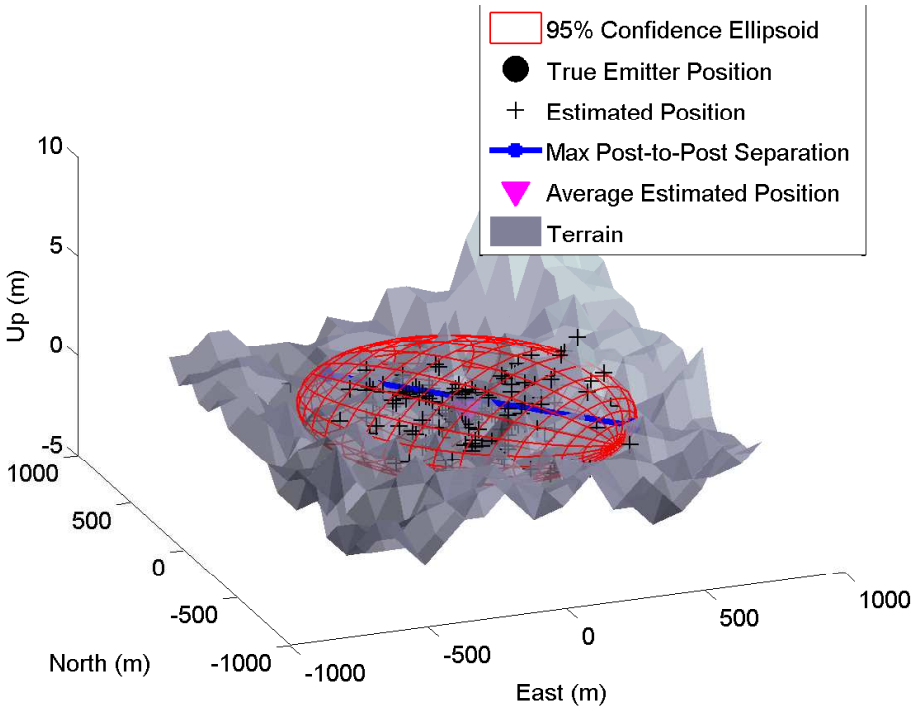

(b) Ground constrained

Figure 42. Three-ball TDOA satellite geometry 5 against AFIT target

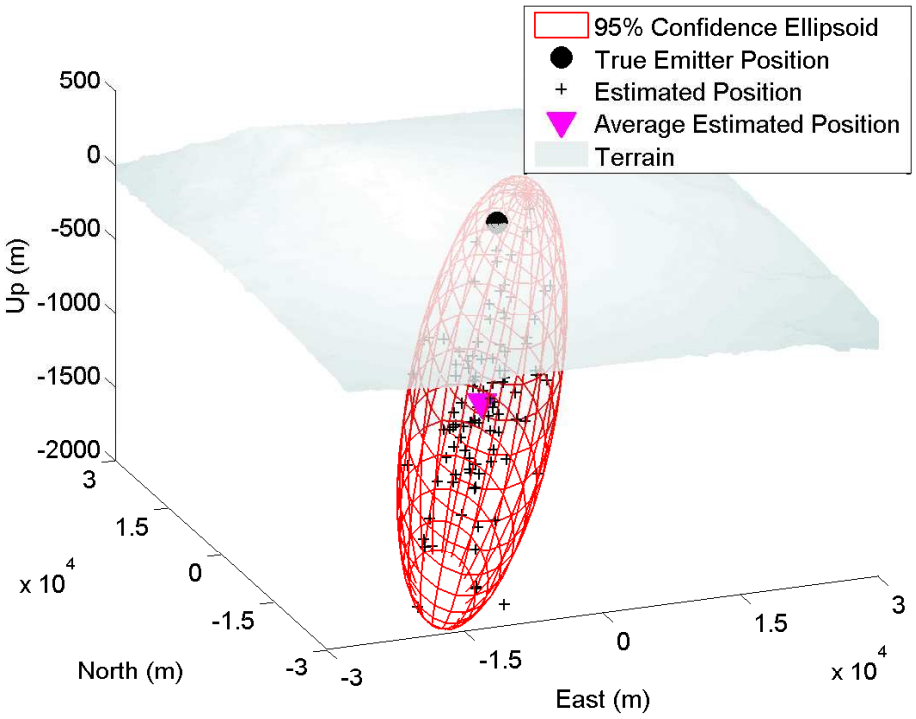

(a) No ground constraint

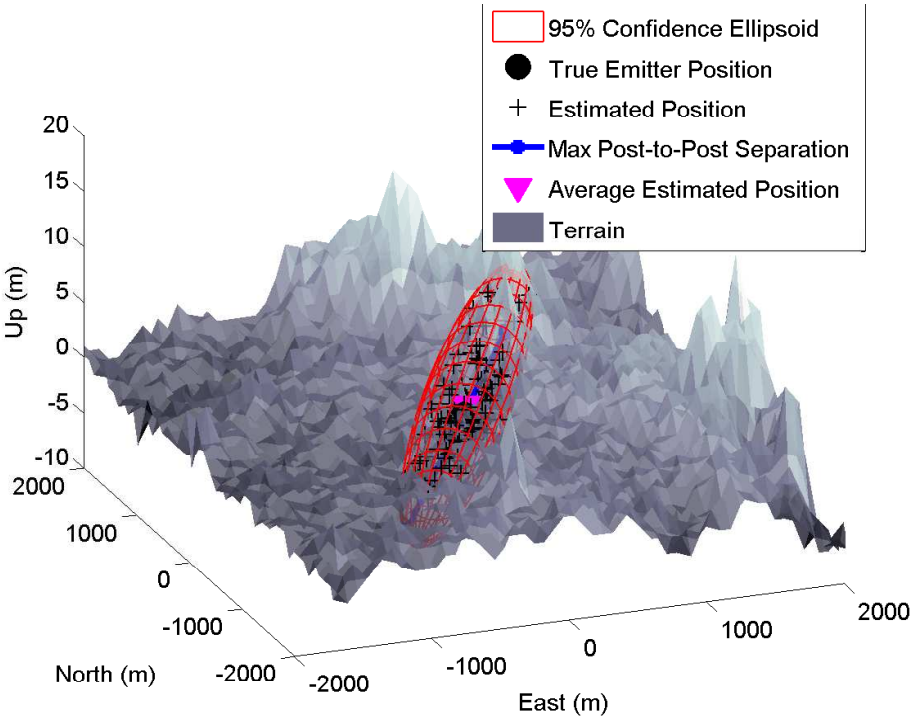

(b) Ground constrained

Figure 43. Three-ball TDOA satellite geometry 6 against AFIT target

4.1.1.4 Three-ball TDOA Aircraft Performance.

The UAV based three-ball TDOA geolocation agent yielded worse performance than the satellite based versions. This is counter-intuitive, but may potentially be ascribed to the collection geometry challenges encountered with a cluster of three UAVs. The narrow beam width of the emitter combined with the low altitude of the collectors requires a close spacing that still collects relatively few pulses. Additionally, the difference in range between the center of the earth and the UAV and the center of the earth and the emitter is very small. Due to the inaccuracy of the unconstrained solution, only the ground constrained solution is presented here. Further study is needed to optimize and more thoroughly evaluate the performance and suitable application of the three-ball TDOA UAV solution.

Table 15. Ground constrained three-ball TDOA UAV performance against AFIT target

Geometry	Measure of Performance				
	RMSE (m)	Avg Miss (m)	Volume (m^3)	SMA (m)	MPTPS (m)
1	8007	3989	2.76E+17	17785	29114
2	1511	1139	4.77E+12	4013	6739
3	12454	4030	2.28E+19	29353	37968

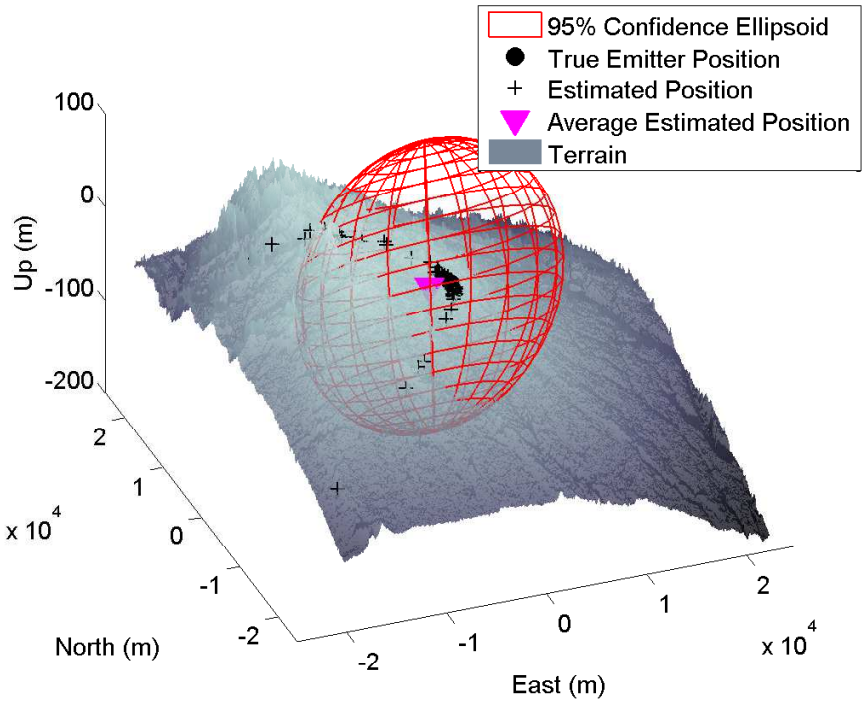

Figure 44. Three-ball TDOA UAV geometry 1 against AFIT target

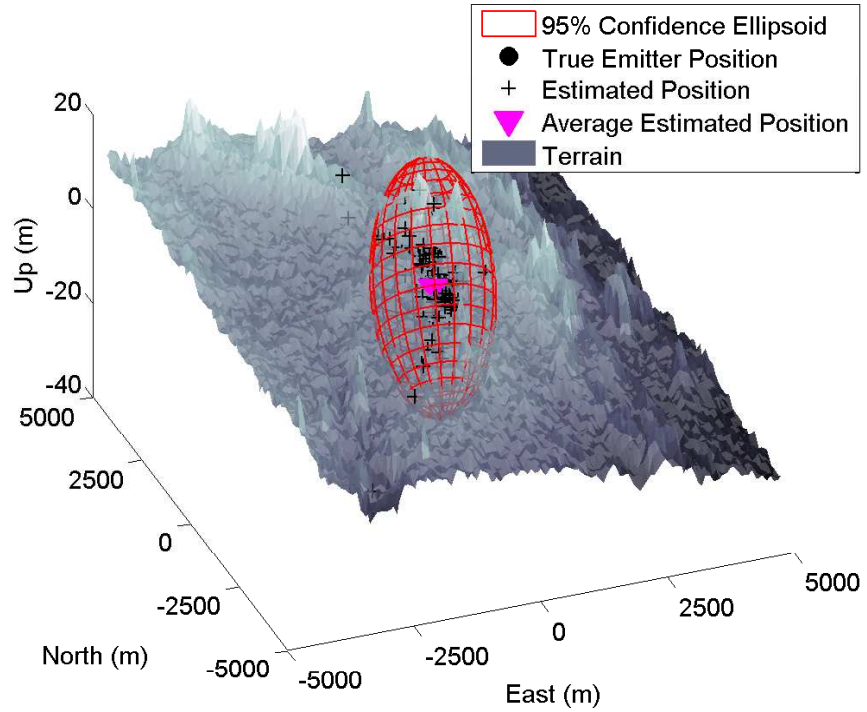

Figure 45. Three-ball TDOA UAV geometry 2 against AFIT target

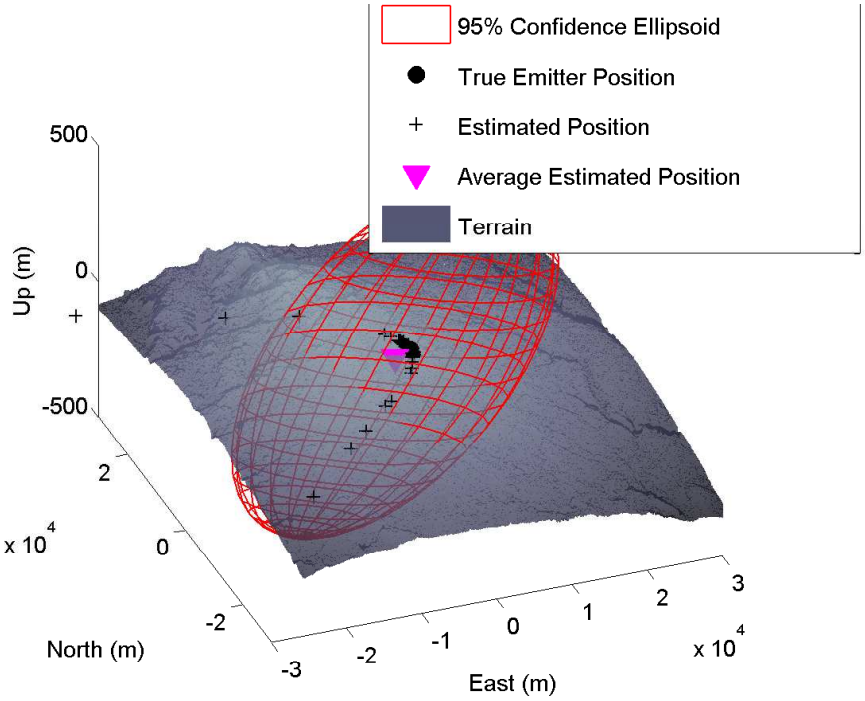

Figure 46. Three-ball TDOA UAV geometry 3 against AFIT target

4.1.1.5 Four-ball TDOA Satellite Performance.

Four-ball TDOA is the final geolocation phenomenology included in this research. The performance of this algorithm was highly variable depending upon collection duration, geometry and application of the surface of the earth constraint. The MOPs for the AFIT scenario are shown in Tables 16 and 17 for the unconstrained and ground constrained cases respectively. The first thing of note is that the unconstrained performance is very poor compared to the other geolocation techniques previously discussed with miss distances in the tens of kilometers and ellipsoid SMAs in the hundreds of kilometers. The ground constrained solutions however are greatly improved with miss distances on some passes in the hundreds of meters. Overall, the average improvements in RMSE, average miss distance, and SMA due to the addition of the DEM based surface of the earth constraint are 75%, 82% and 73% respectively, which is very significant. However, it should be noted that a subjective observation was made

that the precise process by which the surface of the earth constraint was applied could greatly affect the final geolocation solution. Specifically, the search box size and the maximum allowed number of search iterations seemed to have the largest impact. Making the search box too large and allowing for an infinite number of iterations resulted in solutions occasionally "wandering" very far from the initial guess and true emitter location. Conversely, too small of a search area and/or reduced numbers of iterations resulted in cases where the initial guess was unable to converge to a final solution. The proper tuning the surface of the earth constraint is an area that should certainly be researched further.

The graphical depictions of the four-ball TDOA geolocations are shown in Figures 47 to 52. The first observation is that the four-ball TDOA agent produces ellipsoids with a high eccentricity. That is, the ellipsoids are very long in comparison to width and height. In fact, in the extreme the ellipsoid take on the appearance of a knife edge as illustrated in Figure 53 where it is possible to see the curvature of the earth in the ground constrained solutions. The knife edge nature of the ellipsoids may have some benefit when it comes time to perform geolocation estimate fusion.

In addition to tuning the application of the surface of the earth constraint, there is ample room for future study on optimal cluster spacing and relative position for collecting narrow beamwidth emitters. Further development of the algorithm itself, in order to recognize and discard poor geolocations would also be valuable as the current formulation is negatively impacted by a relatively small number of estimates that are very far from the true emitter location.

Table 16. Unconstrained four-ball TDOA satellite performance against AFIT target

Geometry	Measure of Performance				
	RMSE (m)	Avg Miss (m)	Volume (m^3)	SMA (m)	MPTPS (m)
1	12927	10435	1.95E+10	36259	NA
2	54281	45107	5.64E+13	117205	NA
3	112711	91728	2.38E+14	254685	NA
4	16249	13285	3.53E+10	44896	NA
5	8545	7270	7.39E+11	21311	NA
6	131160	114693	9.92E+14	217262	NA

Table 17. Ground constrained four-ball TDOA satellite performance against AFIT target

Geometry	Measure of Performance				
	RMSE (m)	Avg Miss (m)	Volume (m^3)	SMA (m)	MPTPS (m)
1	670	550	1.21E+07	1849	NA
2	305	253	1.37E+06	830	NA
3	54520	28028	4.44E+10	148321	NA
4	2966	2339	1.52E+08	8296	NA
5	4378	3506	2.04E+08	12231	NA
6	31094	9211	1.14E+10	45090	NA

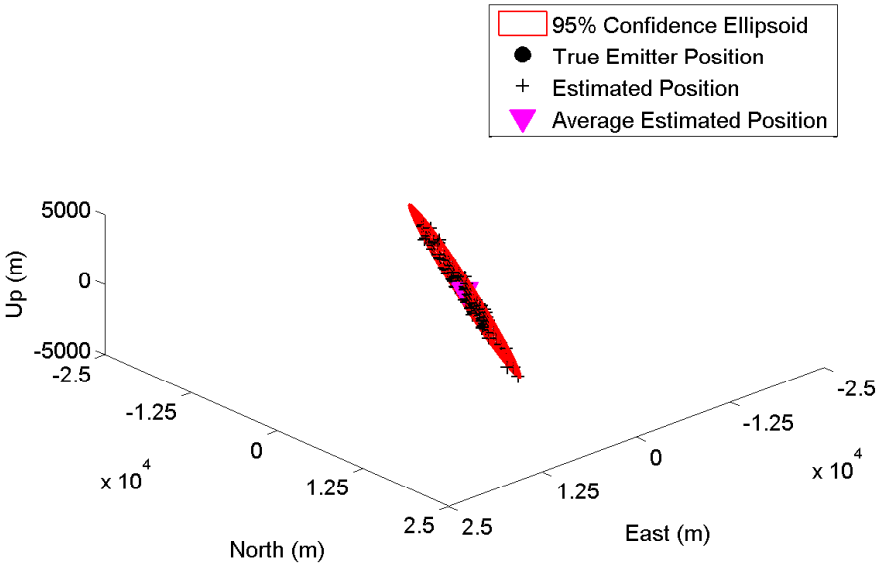

(a) No ground constraint

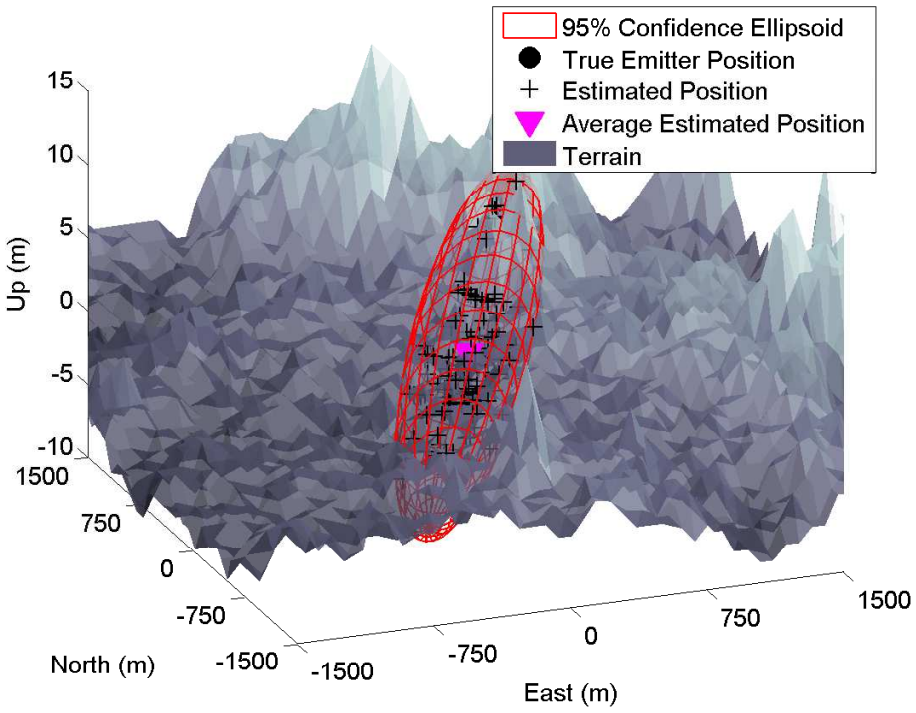

(b) Ground constrained

Figure 47. Four-ball TDOA satellite geometry 1 against AFIT target

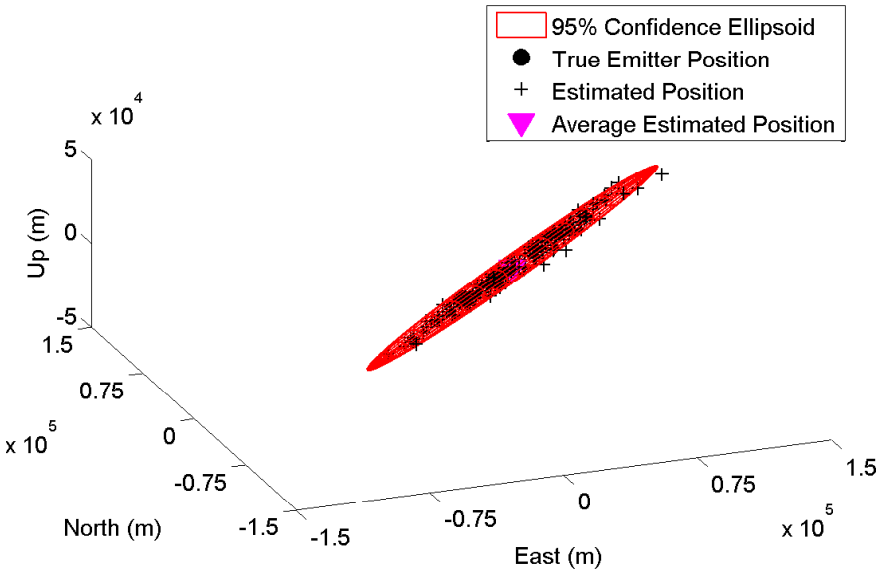

(a) No ground constraint

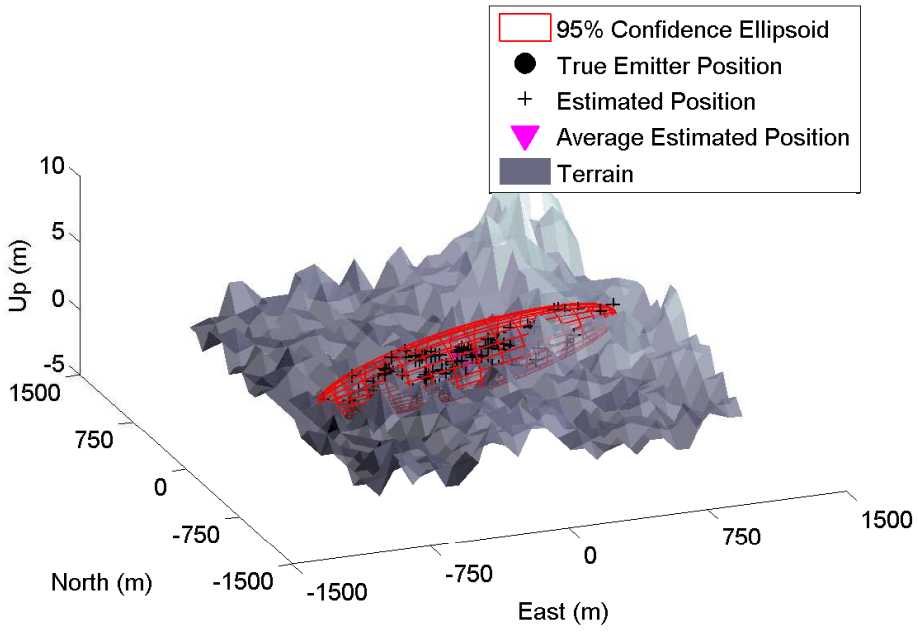

(b) Ground constrained

Figure 48. Four-ball TDOA satellite geometry 2 against AFIT target

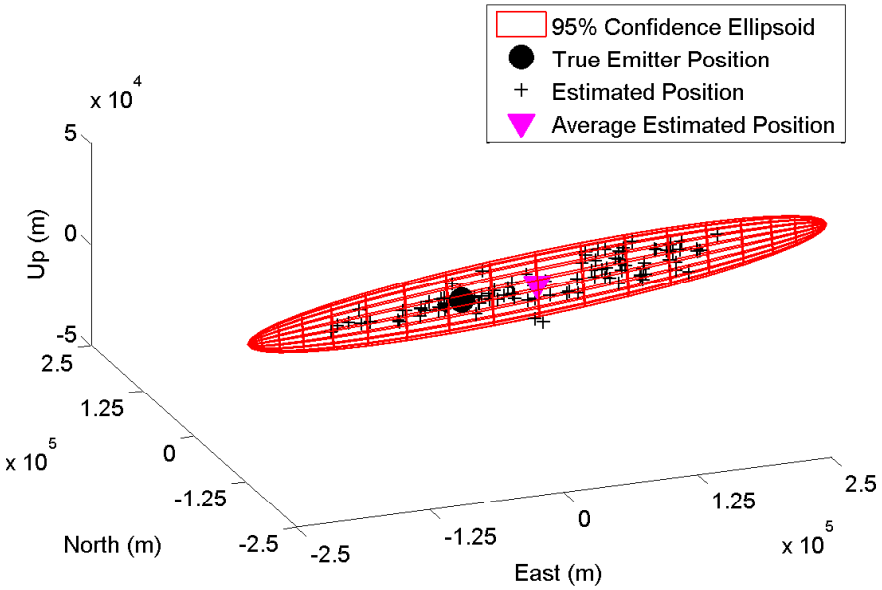

(a) No ground constraint

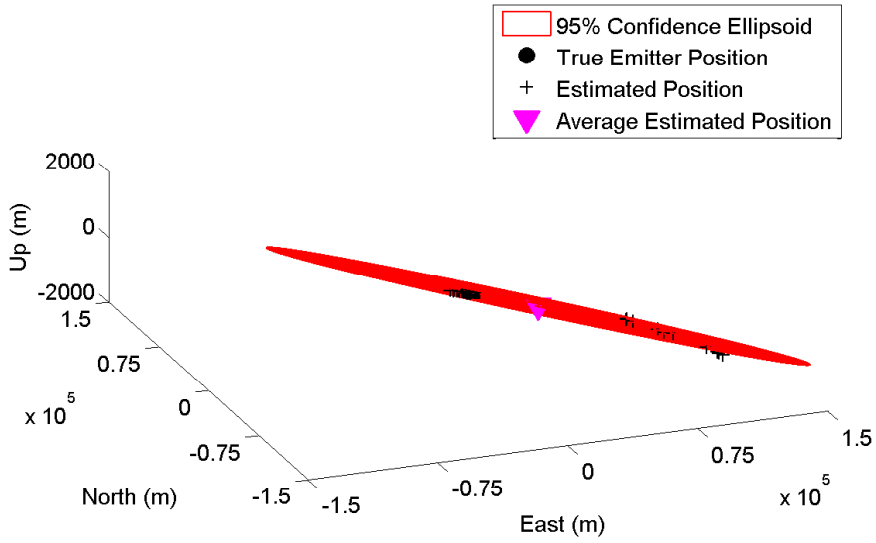

(b) Ground constrained

Figure 49. Four-ball TDOA satellite geometry 3 against AFIT target

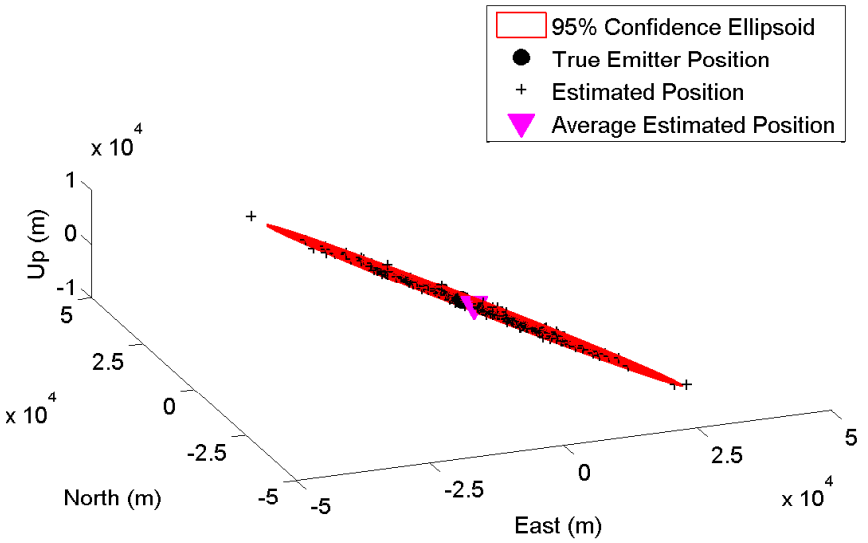

(a) No ground constraint

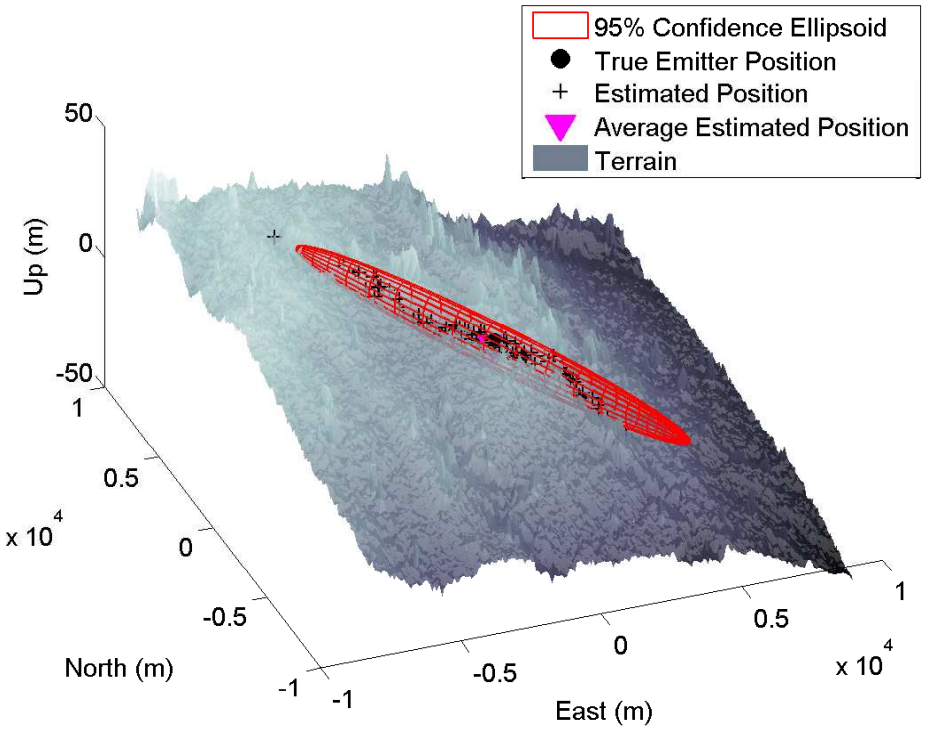

(b) Ground constrained

Figure 50. Four-ball satellite geometry 4 against AFIT target

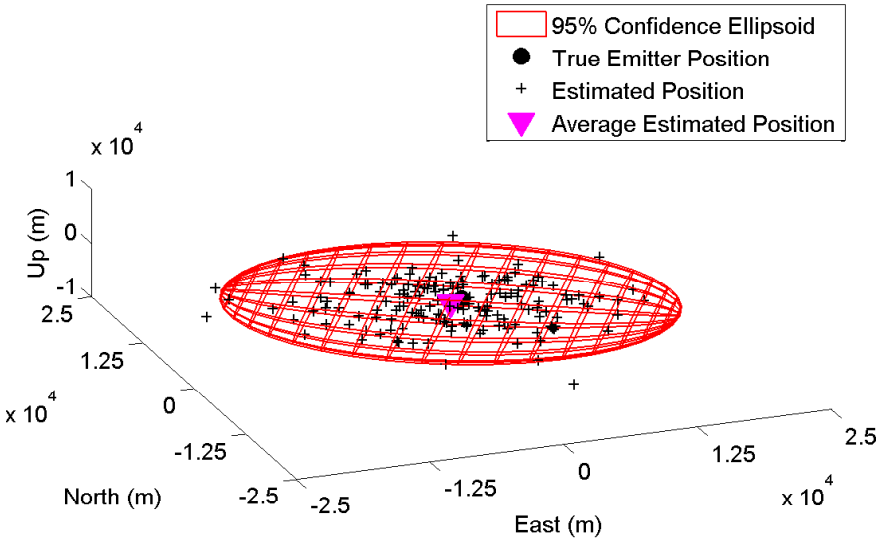

(a) No ground constraint

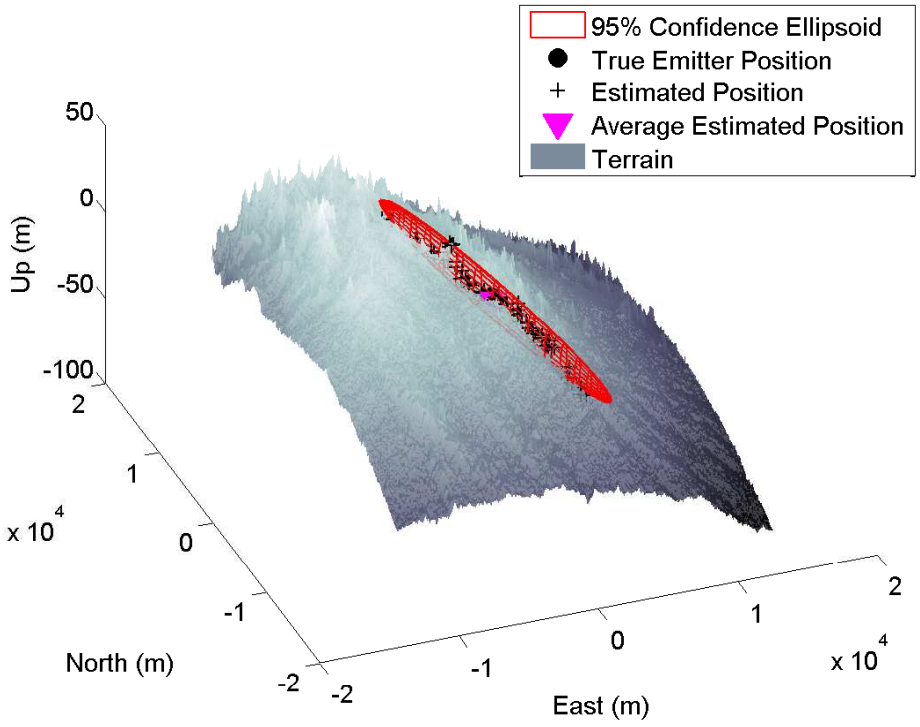

(b) Ground constrained

Figure 51. Four-ball TDOA satellite geometry 5 against AFIT target

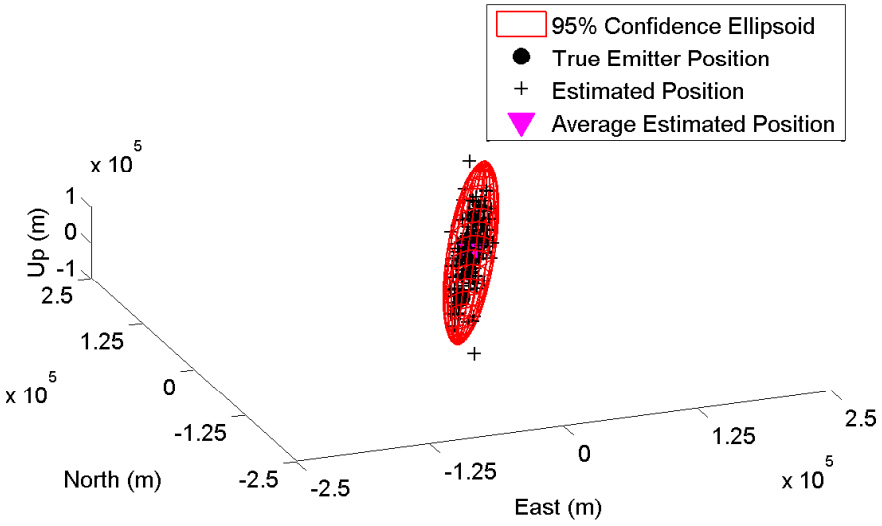

(a) No ground constraint

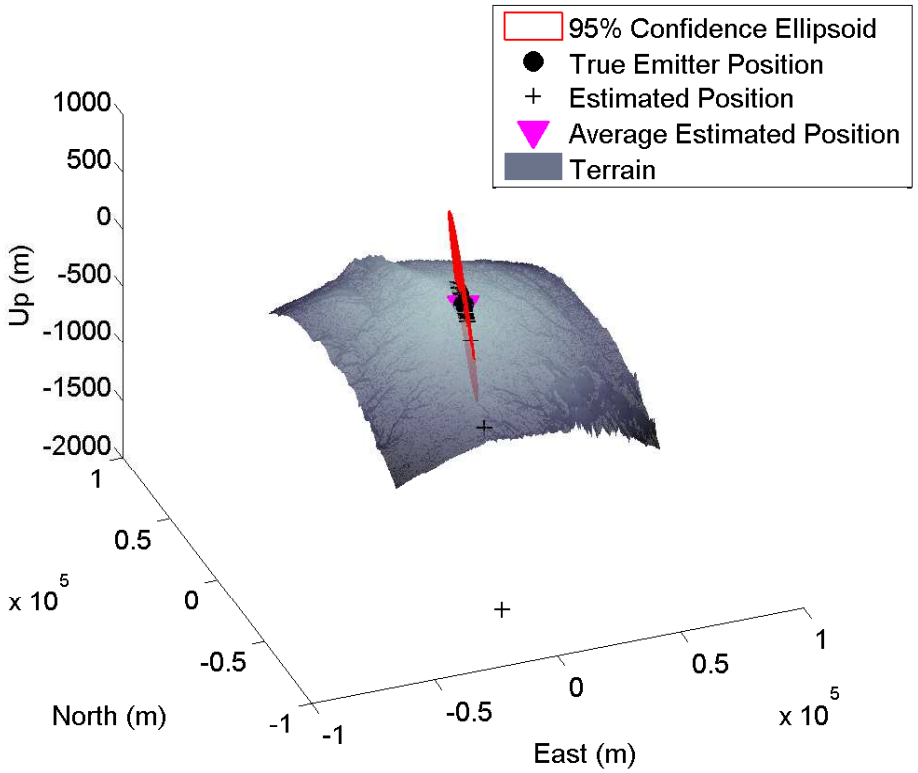

(b) Ground constrained

Figure 52. Four-ball TDOA satellite geometry 6 against AFIT target

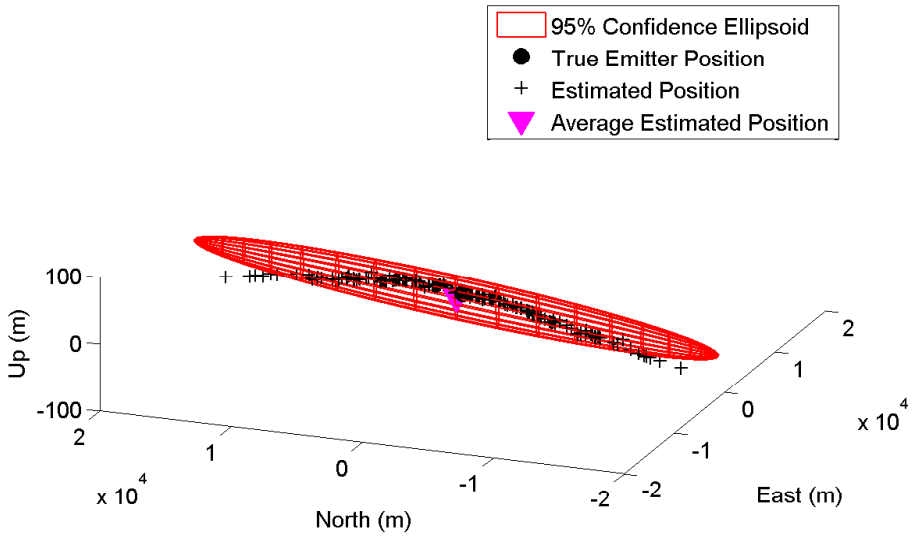

Figure 53. Side view of unconstrained TDOA satellite geometry 6

The preceding subsections describing the geolocation performance of the various agents serve as a basis from which to work and quantify the performance improvements due to fusing multiple geolocation estimates. The following section will show the performance improvement as well as discuss the fusion consistency of the different fusion techniques employed.

4.1.2 Fused Geolocation Performance.

In order to show the utility of using a single-ball AOA SV as an augmentation platform, it is necessary to determine the situations in which the augmentation is valuable, and quantify that improvement. This section will examine each of the fusion permutations and present the resulting accuracy and consistency metrics. When discussing fusion, each case represents the fusion of two geolocation agents. Within a case, there are $n \times m$ different combinations, where n is the number of collector one pass geometries and m is the number of collector two pass geometries. Within each combination of pass geometries, there are two permutations; unconstrained and

ground constrained. Each permutation represents a sequence of fusion events. In this research, 100 fusion events were completed for each permutation in order to develop the average MOP statistics. The intent will be to first examine all of the fusion algorithms for one case, and then down-select to the most promising algorithm for the remainder of the cases.

4.1.2.1 AOA Satellite Augmenting AOA Satellite.

The first case to look at is the fusion of one AOA SV with another AOA SV. Each of these agents has six pass geometries, which yields 36 different combinations. As both agents have constrained and unconstrained solutions, this yields a total of 72 permutation; 36 each for unconstrained and ground constrained. Each permutation represents a fusion sequence, and every fusion sequence was completed with each of the six fusion techniques for a total of 432 fusion sequences. In order to reduce the amount of data to analyze, the average improvement and consistency for each of the fusion algorithms across every combination of pass geometry were calculated and are listed in Table 18. For brevity, only the average miss and SMA improvements were tabulated as the RMSE tended to follow the same pattern as the average miss. Additionally, it was not practical to calculate the fused MPTPS due to the computational intense nature of the measurement and the large number of fusion events to be completed. From this data it is obvious that overall, fusing an additional AOA SV collection agent improves geolocation accuracy. However, it must be noted that improvements highlighted herein are the average across all of the pass geometry combinations, there are in fact some combinations that show no improvement and others that show reduced performance. In order to determine which combinations are most useful, it is necessary to look at the improvements at each individual combination. Of the fusion techniques utilized, the LE and Kalman filter show the best improvements,

as well as consistency results near 95%. The Kalman filter results will be used to demonstrate and can be seen in Table 19 along with the associated fusion sequence consistency for each combination in Table 20. The equivalent tables for the remainder of the fusion techniques are located in Appendix B, section 2.1.0.16.

Examining the data reveals several patterns. First, fusing two passes with the same geometry shrinks the fused SMA compared to either of the source SMAs but does not have a significant impact on the RMSE or average miss distance. For example, fusing pass geometry 1 with pass geometry 1 yields a 29% reduction in SMA but results in no change to the average miss distance or RMSE. The next pattern is that the greatest benefit from fusion occurs when adding augmentation to a poor geolocation solution. For example, in the ground constrained case there is an 90% improvement in SMA when fusing pass 6, a relatively poor performance pass, with pass 2, a relatively high performance pass. In contrast, fusing pass 2 with pass 4, another high performance pass, yields an improvement of only 10%. The final observable pattern is that the orientation of the individual ellipsoids has a noticeable effect on the size of the fused ellipsoid when using the Kalman filter fusion technique. Two estimates with ellipsoids that are nearly orthogonal produce a small fused ellipsoid than two similar sized ellipsoids that are coincident.

Table 18. Average AOA SV and AOA SV fusion results against AFIT target

Fusion Technique	Miss Improvement	SMA Improvement	Ellipsoid Consistency	Ellipse Consistency
Non-Ground Constrained				
Largest Ellipsoid	35%	37%	90%	96%
New Det CI	-	-	-	-
Fast Det CI	30%	27%	96%	99%
Fast Trace CI	32%	27%	96%	99%
Ellipsoid Intersection	34%	43%	91%	98%
Kalman filter	35%	43%	91%	98%
Ground Constrained				
Largest Ellipsoid	35%	35%	91%	96%
New Det CI	-	-	-	-
Fast Det CI	30%	28%	95%	99%
Fast Trace CI	32%	27%	97%	99%
Ellipsoid Intersection	-	-	-	-
Kalman filter	35%	42%	91%	97%

Table 19. Improvement from Kalman filter fusion based augmentation of AOA SV by AOA SV against AFIT target

	Ground Constrained						Non-Ground Constrained					
Average RMSE												
	AOA SV Pass to be Augmented						AOA SV Pass to be Augmented					
AOA SV Pass	1	2	3	4	5	6	1	2	3	4	5	6
1	-1%	25%	66%	47%	12%	77%	-1%	27%	67%	45%	14%	78%
2	60%	-2%	80%	53%	26%	87%	56%	-2%	78%	50%	26%	87%
3	11%	1%	0%	15%	5%	59%	11%	1%	0%	14%	6%	62%
4	46%	10%	67%	6%	20%	80%	45%	17%	68%	6%	23%	82%
5	58%	35%	83%	63%	0%	88%	55%	35%	82%	59%	1%	88%
6	11%	7%	41%	25%	1%	3%	5%	8%	41%	23%	5%	3%
Average Miss												
	AOA SV Pass to be Augmented						AOA SV Pass to be Augmented					
AOA SV Pass	1	2	3	4	5	6	1	2	3	4	5	6
1	0%	27%	66%	46%	10%	77%	0%	28%	68%	44%	13%	76%
2	60%	-3%	79%	51%	27%	86%	55%	-2%	78%	49%	26%	85%
3	9%	0%	-2%	13%	4%	57%	10%	0%	-1%	13%	6%	58%
4	44%	9%	67%	3%	19%	78%	43%	17%	68%	4%	22%	80%
5	56%	36%	83%	62%	0%	87%	53%	36%	82%	59%	1%	87%
6	13%	7%	42%	22%	2%	3%	6%	7%	41%	21%	5%	3%
Average SMA												
	AOA SV Pass to be Augmented						AOA SV Pass to be Augmented					
AOA SV Pass	1	2	3	4	5	6	1	2	3	4	5	6
1	29%	26%	66%	55%	9%	77%	29%	32%	65%	54%	11%	79%
2	66%	29%	82%	60%	33%	90%	66%	29%	80%	59%	33%	91%
3	16%	2%	29%	8%	4%	65%	16%	3%	29%	8%	4%	69%
4	53%	11%	61%	29%	24%	82%	54%	16%	61%	29%	29%	85%
5	63%	41%	84%	70%	29%	90%	62%	42%	83%	70%	29%	91%
6	7%	12%	43%	31%	2%	29%	2%	14%	40%	31%	2%	29%

Table 20. Kalman filter geolocation fusion consistency for augmentation of AOA SV by AOA SV against AFIT target

		Ground Constrained						Non-Ground Constrained					
		Ellipsoid Consistency Augmented AOA SV Pass						Ellipsoid Consistency Augmented AOA SV Pass					
		1	2	3	4	5	6	1	2	3	4	5	6
AOA SV Pass	1	76%	91%	91%	95%	96%	91%	74%	93%	95%	97%	97%	94%
	2	91%	74%	93%	90%	94%	94%	93%	74%	93%	93%	93%	92%
	3	91%	93%	74%	96%	97%	92%	95%	93%	67%	95%	95%	94%
	4	95%	90%	96%	75%	95%	98%	97%	93%	95%	72%	95%	96%
	5	96%	94%	97%	95%	75%	92%	97%	93%	95%	95%	75%	95%
	6	91%	94%	92%	98%	92%	76%	94%	92%	94%	96%	95%	73%
		Ellipse Consistency Augmented AOA SV Pass						Ellipse Consistency Augmented AOA SV Pass					
		1	2	3	4	5	6	1	2	3	4	5	6
AOA SV Pass	1	84%	97%	96%	100%	99%	98%	93%	100%	100%	100%	100%	99%
	2	97%	92%	98%	98%	99%	97%	100%	93%	98%	99%	100%	98%
	3	96%	98%	94%	98%	99%	100%	100%	98%	97%	99%	100%	100%
	4	100%	98%	98%	92%	99%	99%	100%	99%	99%	93%	98%	99%
	5	99%	99%	99%	99%	95%	99%	100%	100%	100%	98%	95%	99%
	6	98%	97%	100%	99%	99%	93%	99%	98%	100%	99%	99%	91%

4.1.2.2 AOA Satellite Augmenting AOA Aircraft.

The next case is the fusion of an AOA SV geolocation agent with an AOA AV agent. The same process used for the previous fusion analysis will be used to evaluate the fusion performance. The AOA AV agent in question is the mid altitude manned aircraft with an AOA geolocation payload.

Table 21 shows the average improvements from fusing the individual agent estimates. Unlike the previous scenario, this fusion shows very little improvement, and in one case, a very significant decay of performance. The only two fusion techniques that show even a modest improvement are the LE and Kalman filter, at just 1% in the unconstrained case and 3% in the ground constrained case. The most likely reason for the very small improvement is the fact that the AOA AV agent results are significantly more accurate than the AOA SV agent results. For instance, the pass geometry 1 AOA AV had an SMA of 94 meters whereas the equivalent AOA SV pass had an SMA of 1686 meters. The worst case, the unconstrained Ellipsoid Intersection, suffered from a nearly threefold increase in the average miss distance over the first 100 runs while maintaining approximately the same SMA but with a 37% ellipsoid consistency. This indicates that the algorithm is failing to correctly determine the fused position. In conjunction with the high ellipse consistency, this likely indicates that the estimated position was either above or below the true emitter position.

Table 22 shows the improvements for each pass combination and Table 23 shows the corresponding consistencies. While there are no strong patterns, the greatest improvements are associated with AV pass geometry 4, which is offset from the emitter and at the same heading as pass geometries 1 through 3.

Based upon these results, an AOA SV geolocation agent does not appear to have much utility in augmenting a mid-altitude AOA AV platform. However, more challenging cases will be presented in the Libya and Afghanistan scenarios which may

show a more significant improvement.

Table 21. Average AOA SV and AOA AV fusion results against AFIT target

Fusion Technique	Miss Improvement	SMA Improvement	Ellipsoid Consistency	Ellipse Consistency
Non-Ground Constrained				
Largest Ellipsoid	1%	0%	95%	100%
New Det CI	-	-	-	-
Fast Det CI	0%	0%	94%	100%
Fast Trace CI	0%	0%	95%	100%
Ellipsoid Intersection	-271%	1%	37%	100%
Kalman filter	1%	1%	95%	100%
Ground Constrained				
Largest Ellipsoid	3%	0%	92%	99%
New Det CI	-	-	-	-
Fast Det CI	1%	0%	91%	99%
Fast Trace CI	1%	0%	91%	99%
Ellipsoid Intersection	-	-	-	-
Kalman filter	3%	3%	91%	99%

Table 22. Improvement from Kalman filter fusion based augmentation of AOA AV by AOA SV against AFIT target

Ground Constrained

RMSE

AOA SV Pass \ AOA Aircraft Pass	1	2	3	4	5	6
1	4%	7%	5%	13%	1%	-4%
2	7%	7%	5%	10%	1%	-9%
3	2%	3%	4%	9%	1%	-7%
4	4%	3%	4%	11%	4%	-6%
5	3%	6%	2%	9%	4%	-4%
6	2%	2%	3%	8%	-1%	-8%

Average Miss

AOA SV Pass \ AOA Aircraft Pass	1	2	3	4	5	6
1	0%	4%	4%	14%	-1%	-2%
2	4%	4%	7%	14%	1%	-2%
3	-2%	2%	5%	11%	-1%	-6%
4	0%	1%	5%	14%	2%	-3%
5	-1%	5%	6%	13%	4%	-2%
6	-2%	0%	4%	10%	-3%	-6%

Average SMA

AOA SV Pass \ AOA Aircraft Pass	1	2	3	4	5	6
1	0%	4%	2%	3%	1%	2%
2	2%	9%	3%	5%	3%	3%
3	0%	1%	0%	1%	0%	0%
4	1%	7%	2%	4%	3%	3%
5	2%	9%	4%	6%	3%	4%
6	0%	1%	0%	1%	0%	1%

Non-Ground Constrained

RMSE

AOA SV Pass \ AOA Aircraft Pass	1	2	3	4	5	6
1	1%	-1%	2%	12%	-2%	-1%
2	4%	-3%	1%	10%	1%	-6%
3	1%	-3%	3%	9%	-2%	-4%
4	2%	-3%	2%	9%	2%	-3%
5	1%	-1%	3%	8%	2%	-1%
6	1%	-2%	3%	8%	-2%	-4%

Average Miss

AOA SV Pass \ AOA Aircraft Pass	1	2	3	4	5	6
1	-1%	-1%	0%	11%	-3%	2%
2	2%	-2%	0%	9%	0%	-1%
3	-1%	-2%	1%	9%	-3%	0%
4	0%	-2%	0%	10%	1%	0%
5	-1%	0%	2%	8%	1%	0%
6	-1%	-1%	1%	8%	-4%	-1%

Average SMA

AOA SV Pass \ AOA Aircraft Pass	1	2	3	4	5	6
1	0%	1%	0%	2%	1%	2%
2	1%	1%	1%	2%	3%	3%
3	0%	0%	0%	0%	0%	0%
4	1%	0%	0%	2%	3%	2%
5	1%	1%	1%	4%	3%	3%
6	0%	0%	0%	1%	0%	0%

Table 23. Kalman filter geolocation fusion consistency for augmentation of AOA AV by AOA SV against AFIT target

		Ground Constrained						Non-Ground Constrained					
		Ellipsoid Consistency AOA Aircraft Pass						Ellipsoid Consistency AOA Aircraft Pass					
		1	2	3	4	5	6	1	2	3	4	5	6
AOA SV Pass	1	86%	91%	91%	97%	94%	88%	94%	95%	94%	94%	96%	93%
	2	86%	91%	91%	97%	94%	89%	95%	95%	94%	97%	96%	93%
	3	86%	91%	91%	97%	93%	88%	94%	95%	94%	94%	96%	93%
	4	86%	91%	91%	97%	94%	88%	94%	95%	94%	94%	96%	93%
	5	86%	91%	91%	97%	94%	90%	95%	95%	94%	97%	98%	93%
	6	86%	91%	91%	97%	93%	88%	94%	95%	94%	94%	96%	93%
		Ellipse Consistency AOA Aircraft Pass						Ellipse Consistency AOA Aircraft Pass					
		1	2	3	4	5	6	1	2	3	4	5	6
AOA SV Pass	1	100%	95%	99%	100%	100%	97%	100%	99%	100%	99%	100%	100%
	2	100%	95%	99%	100%	100%	98%	100%	99%	100%	100%	100%	100%
	3	100%	95%	99%	100%	100%	97%	100%	99%	100%	99%	100%	100%
	4	100%	95%	99%	100%	100%	97%	100%	99%	100%	99%	100%	100%
	5	100%	95%	99%	100%	100%	98%	100%	99%	100%	100%	100%	100%
	6	100%	95%	99%	100%	100%	97%	100%	99%	100%	99%	100%	100%

4.1.2.3 AOA Satellite Augmenting Three-ball TDOA Satellites.

The fusion of the AOA SV and three-ball TDOA geolocation agents is the next case to consider. In the same manner as the two previous cases, the average increase in performance due to fusion is shown in Table 24. In this case, there is a significant improvement in most MOPs for the majority of fusion techniques with the exception of the EI algorithm. The EI algorithm provided poor results, with both unconstrained and ground constrained fused position estimates significantly worse than either of the individual agents for most combinations. Between the two agents, the ground constrained provided worse results than the unconstrained. This behavior is similar to that noted in the previous AOA cases.

Another observation is that unlike the previous AOA cases, the unconstrained CI solutions have unusually low ellipsoidal consistency, as does the EI algorithm. This weakness disappears in the ground constrained case, from which we can conclude that the CI and EI algorithms are ill-suited to estimates that are spatially separated, as is in the case of the three-ball TDOA solutions below the surface of the earth. The exact cause of this behavior, and potential methods to prevent the degradation, are recommended areas for future study.

The individual combination fusion results shown in Table 25 with corresponding fusion sequence consistency for each combination shown in Table 26 help illustrate the pass combinations that benefit most from geolocation fusion. From an SMA perspective, the greatest improvements correspond to a "high quality" augmentation pass with a collector traveling nearly orthogonal to the augmented pass. For instance, three-ball TDOA pass geometry 3 with AOA SV pass geometry 5 results in a 76% reduction in the SMA. The same behavior is encountered in the fusion between TDOA pass 6 and AOA pass 2. However, it is difficult to determine what portion, if any, of the improvement is attributable to the orientation rather than the sizes of the fused

covariances as the two variables are largely confounded. For example, looking at the fusion of TDOA pass 1 with AOA passes 2 and 5, which have similar accuracy shows an a difference in reduction of SMA size of only 1%. Similar behavior is exhibited by the Fast Determinant and Fast Trace Covariance Intersection algorithms. Only the Largest Ellipsoid algorithm exhibits a significant difference, with the fused result from the 1-5 combination yielding a 65% improvement whereas the 1-2 combination results in a 54% improvement.

The results shown here indicate that the AOA SV geolocation agent is likely a good augmentation to a three-ball TDOA SV agent with the largest benefit occurring where the three-ball TDOA performance is otherwise marginal.

Table 24. Average AOA SV and three-ball TDOA SV fusion results against AFIT target

Fusion Technique	Miss Improvement	SMA Improvement	Ellipsoid Consistency	Ellipse Consistency
Non-Ground Constrained				
Largest Ellipsoid	75%	80%	95%	100%
New Det CI	-	-	-	-
Fast Det CI	55%	49%	36%	99%
Fast Trace CI	74%	70%	81%	99%
Ellipsoid Intersection	-2079%	77%	5%	99%
Kalman filter	75%	77%	10%	99%
Ground Constrained				
Largest Ellipsoid	32%	26%	92%	99%
New Det CI	-	-	-	-
Fast Det CI	24%	18%	97%	99%
Fast Trace CI	26%	19%	97%	100%
Ellipsoid Intersection	-	-	-	-
Kalman filter	32%	36%	94%	99%

Table 25. Improvement from Kalman filter fusion based augmentation of three-ball TDOA SV by AOA SV against AFIT target

	Ground Constrained						Non-Ground Constrained					
RMSE												
	Three-ball TDOA Satellite Pass						Three-ball TDOA Satellite Pass					
AOA SV Pass	1	2	3	4	5	6	1	2	3	4	5	6
1	30%	15%	67%	46%	19%	35%	70%	69%	93%	82%	79%	95%
2	57%	25%	66%	53%	28%	65%	85%	82%	95%	84%	86%	97%
3	10%	7%	25%	6%	4%	24%	55%	42%	85%	42%	47%	91%
4	45%	20%	57%	19%	7%	56%	81%	73%	93%	68%	74%	96%
5	60%	31%	73%	63%	33%	64%	86%	85%	96%	87%	88%	97%
6	3%	6%	41%	20%	4%	14%	26%	22%	86%	67%	60%	84%
Average Miss												
	Three-ball TDOA Satellite Pass						Three-ball TDOA Satellite Pass					
AOA SV Pass	1	2	3	4	5	6	1	2	3	4	5	6
1	28%	17%	65%	46%	20%	32%	68%	70%	93%	81%	78%	95%
2	57%	26%	63%	50%	27%	62%	84%	82%	95%	82%	85%	97%
3	9%	9%	25%	6%	2%	20%	53%	41%	83%	38%	46%	90%
4	42%	20%	56%	19%	4%	54%	79%	72%	92%	64%	73%	96%
5	58%	31%	72%	59%	32%	60%	85%	84%	95%	85%	87%	97%
6	1%	8%	38%	19%	3%	12%	25%	22%	85%	65%	60%	84%
Average SMA												
	Three-ball TDOA Satellite Pass						Three-ball TDOA Satellite Pass					
AOA SV Pass	1	2	3	4	5	6	1	2	3	4	5	6
1	30%	13%	70%	52%	21%	33%	71%	69%	94%	84%	80%	96%
2	65%	32%	69%	58%	25%	69%	88%	85%	97%	86%	88%	98%
3	14%	4%	23%	7%	1%	20%	55%	49%	86%	38%	47%	91%
4	53%	29%	60%	27%	7%	61%	84%	70%	93%	68%	75%	96%
5	64%	30%	76%	67%	37%	67%	88%	86%	97%	90%	90%	98%
6	8%	3%	47%	25%	7%	10%	24%	19%	87%	69%	65%	83%

Table 26. Kalman filter geolocation fusion consistency for augmentation of three-ball TDOA SV by AOA SV against AFIT target

		Ground Constrained						Non-Ground Constrained					
		Ellipsoid Consistency						Ellipsoid Consistency					
		Three-ball TDOA Satellite Pass						Three-ball TDOA Satellite Pass					
		1	2	3	4	5	6	1	2	3	4	5	6
AOA SV Pass	1	93%	93%	97%	90%	94%	92%	1%	4%	3%	0%	16%	37%
	2	92%	95%	92%	91%	96%	94%	0%	5%	1%	2%	13%	50%
	3	90%	96%	94%	91%	94%	95%	0%	5%	0%	1%	11%	12%
	4	95%	95%	97%	94%	93%	94%	0%	2%	3%	1%	12%	33%
	5	93%	94%	96%	93%	97%	93%	0%	6%	0%	0%	14%	47%
	6	93%	97%	94%	91%	95%	95%	0%	4%	0%	1%	10%	18%
		Ellipse Consistency						Ellipse Consistency					
		Three-ball TDOA Satellite Pass						Three-ball TDOA Satellite Pass					
		1	2	3	4	5	6	1	2	3	4	5	6
AOA SV Pass	1	99%	100%	100%	99%	98%	99%	99%	99%	100%	100%	99%	100%
	2	99%	100%	100%	99%	99%	99%	98%	98%	99%	99%	98%	99%
	3	99%	100%	97%	100%	99%	100%	99%	100%	100%	100%	100%	99%
	4	100%	100%	100%	100%	99%	99%	99%	99%	99%	100%	98%	99%
	5	99%	100%	100%	99%	99%	99%	99%	99%	100%	100%	100%	99%
	6	100%	100%	100%	100%	100%	99%	100%	97%	100%	100%	99%	100%

4.1.2.4 AOA Satellite Augmenting Three-ball TDOA Aircraft.

The three-ball TDOA UAV geolocation agent fused with the AOA SV agent is the next case. The three-ball TDOA UAV was run with ground constraint only, so the focus of analysis is on the fusion of the ground constrained estimates. The fusion was accomplished in the same manner as previously discussed with average results as shown in Table 27. In this case, the addition of the AOA SV agent yields a significant improvement to all of the MOPs with the Largest Ellipsoid and Kalman filter yielding the largest improvement. The fact that the fusion improves performance is not surprising as the AOA SV agent achieves better performance than the three-ball TDOA UAV agent for all pass geometries.

The individual combination fusion results and corresponding fusion sequence consistency for each combination, using Kalman filter fusion, are shown in Tables 28 and 29, respectively. The results for remainder of the fusion techniques are available in Appendix B, section 2.1.0.19. The largest improvements noted are associated with three-ball TDOA pass geometries 1 and 3, which correspond to the passes with the worst performance.

Table 27. Average AOA SV and three-ball TDOA AV fusion results against AFIT target

Fusion Technique	Miss Improvement	SMA Improvement	Ellipsoid Consistency	Ellipse Consistency
Non-Ground Constrained				
Largest Ellipsoid	NA	NA	NA	NA
New Det CI	NA	NA	NA	NA
Fast Det CI	NA	NA	NA	NA
Fast Trace CI	NA	NA	NA	NA
Ellipsoid Intersection	NA	NA	NA	NA
Kalman filter	NA	NA	NA	NA
Ground Constrained				
Largest Ellipsoid	72%	81%	83%	91%
New Det CI	-	-	-	-
Fast Det CI	68%	75%	83%	91%
Fast Trace CI	70%	75%	95%	99%
Ellipsoid Intersection	-	-	-	-
Kalman filter	72%	80%	95%	99%

Table 28. Improvement from Kalman filter fusion based augmentation of three-ball TDOA AV by AOA SV against AFIT target

		Ground Constrained		
		RMSE		
		Three-ball TDOA Satellite Pass		
		1	2	3
AOA SV Pass	1	92%	62%	95%
	2	96%	78%	97%
	3	79%	33%	87%
	4	92%	65%	95%
	5	96%	80%	98%
	6	75%	23%	84%
		Average Miss		
		Three-ball TDOA Satellite Pass		
		1	2	3
AOA SV Pass	1	87%	58%	86%
	2	92%	74%	92%
	3	63%	28%	63%
	4	86%	61%	87%
	5	93%	78%	94%
	6	63%	26%	60%
		Average SMA		
		Three-ball TDOA Satellite Pass		
		1	2	3
AOA SV Pass	1	91%	72%	94%
	2	96%	81%	97%
	3	77%	31%	86%
	4	90%	61%	94%
	5	96%	83%	98%
	6	63%	62%	77%

Table 29. Kalman filter geolocation fusion consistency

		Ground Constrained		
		Ellipsoid Consistency		
		Three-ball TDOA Satellite Pass		
		1	2	3
AOA SV Pass	1	77%	80%	75%
	2	93%	92%	93%
	3	95%	95%	94%
	4	67%	84%	71%
	5	93%	93%	96%
	6	62%	81%	57%
		Ellipse Consistency		
		Three-ball TDOA Satellite Pass		
		1	2	3
AOA SV Pass	1	75%	82%	73%
	2	98%	95%	97%
	3	100%	96%	98%
	4	75%	88%	76%
	5	97%	96%	97%
	6	100%	96%	100%

4.1.2.5 AOA Satellite Augmenting Four-ball TDOA Satellites.

The final case in the AFIT scenario is the fusion of the four-ball TDOA SV agent and the AOA SV agent geolocation estimates. This case also shows significant improvement in the MOPs from estimate fusion, as shown in Table 31, particularly in the unconstrained permutations. This is likely due to the inaccuracy of the unconstrained four-ball TDOA solution as noted in section 4.1.1.5. One unique observation is that this case is the first in which there has been a significant difference in the performance of the largest Ellipsoid and Kalman filter fusion techniques. A side-by-side comparison of the two techniques, applied to ground constrained solutions, is shown in Table 30. The data shows that in some instances the Largest Ellipsoid algorithm returns a smaller SMA, while in others the Kalman filter returns the smaller SMA. This is graphically illustrated in Figures 54 and 55 where Figure 54 depicts the fusion of pass geometry 1 for each agent and Figure 55 depicts the fusion of AOA SV pass geometry 1 with Four-ball TDOA SV pass geometry 4.

The general pattern of improvement is similar to that seen before where the poorest estimates benefit the most from augmentation. In this case, pass geometries 3 and 6 benefit the most from fusion.

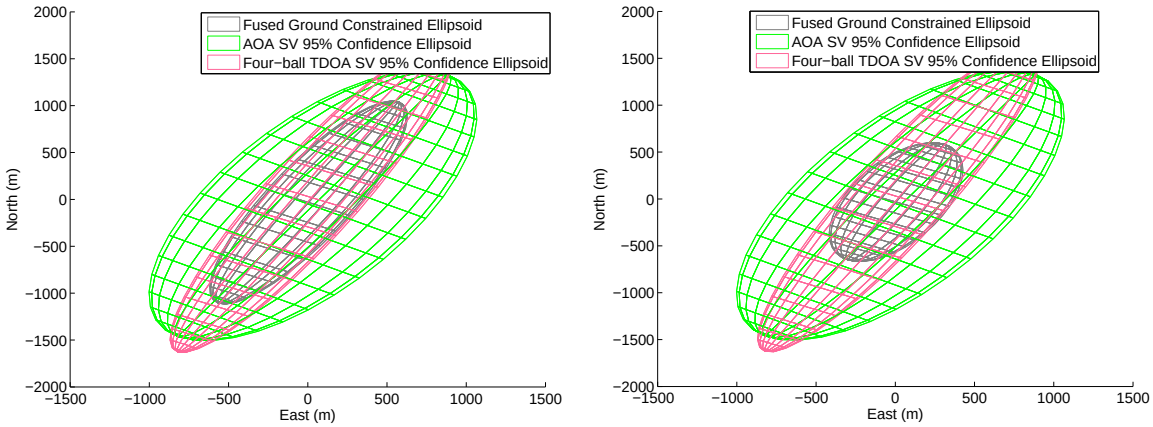

(a) Kalman filter fusion **(b) Largest Ellipsoid fusion**

Figure 54. Comparison of fused ellipsoids

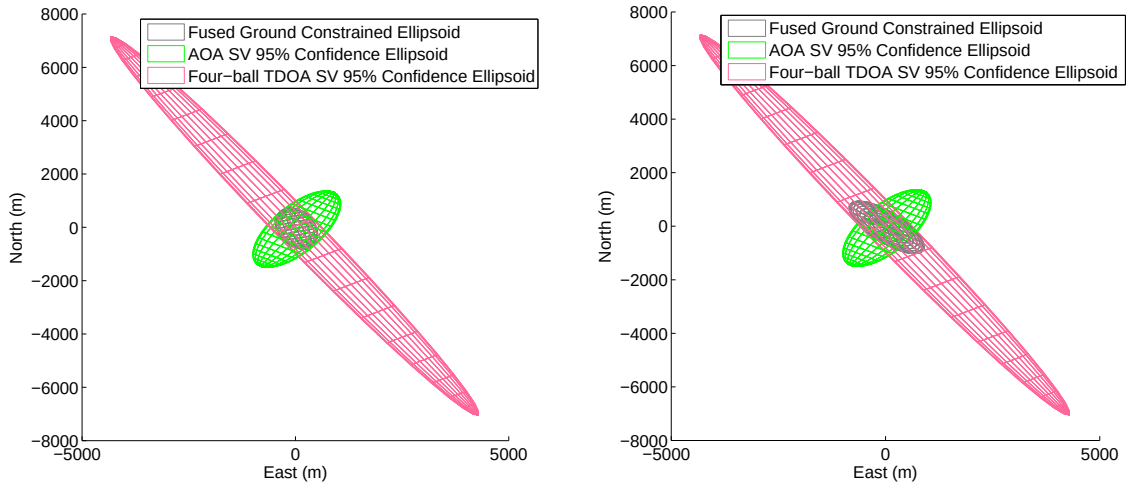

(a) Kalman filter fusion **(b) Largest Ellipsoid fusion**

Figure 55. Comparison of fused ellipsoids

Table 30. Detailed comparison of Kalman filter and Largest Ellipsoid fusion performance for augmentation of 4-ball TDOA SV with AOA SV against AFIT target

		Kalman Filter							Largest Ellipsoid					
RMSE														
		Four-ball TDOA Satellite Pass							Four-ball TDOA Satellite Pass					
		1	2	3	4	5	6		1	2	3	4	5	6
AOA SV Pass	1	38%	26%	100%	89%	93%	98%	1	38%	26%	100%	89%	93%	98%
	2	65%	37%	99%	90%	94%	99%	2	65%	37%	99%	90%	94%	99%
	3	19%	2%	98%	58%	70%	96%	3	19%	2%	98%	58%	70%	96%
	4	58%	32%	99%	81%	88%	99%	4	58%	32%	99%	81%	88%	99%
	5	65%	37%	100%	92%	95%	99%	5	65%	37%	100%	92%	95%	99%
	6	9%	10%	99%	79%	85%	96%	6	9%	10%	99%	79%	85%	96%
Average Miss														
		Four-ball TDOA Satellite Pass							Four-ball TDOA Satellite Pass					
		1	2	3	4	5	6		1	2	3	4	5	6
AOA SV Pass	1	37%	25%	99%	88%	92%	95%	1	1%	-38%	99%	91%	92%	97%
	2	63%	38%	99%	89%	93%	98%	2	45%	20%	99%	89%	93%	97%
	3	22%	2%	97%	56%	69%	90%	3	-168%	-70%	99%	59%	71%	88%
	4	56%	32%	99%	80%	87%	97%	4	-3%	4%	99%	85%	86%	95%
	5	64%	36%	99%	91%	95%	98%	5	52%	21%	99%	92%	94%	98%
	6	10%	12%	98%	78%	85%	89%	6	-265%	-96%	99%	81%	86%	94%
SMA														
		Four-ball TDOA Satellite Pass							Four-ball TDOA Satellite Pass					
		1	2	3	4	5	6		1	2	3	4	5	6
AOA SV Pass	1	34%	31%	100%	91%	93%	97%	1	63%	0%	99%	85%	92%	98%
	2	69%	38%	99%	91%	94%	99%	2	60%	22%	100%	93%	95%	98%
	3	19%	5%	98%	58%	71%	94%	3	0%	0%	98%	51%	68%	94%
	4	60%	33%	99%	80%	88%	98%	4	41%	0%	99%	92%	94%	98%
	5	68%	41%	100%	94%	96%	99%	5	71%	32%	100%	92%	95%	99%
	6	9%	11%	99%	81%	86%	92%	6	25%	0%	96%	61%	81%	97%

Table 31. Average AOA SV and four-ball TDOA SV fusion results against AFIT target

Fusion Technique	Miss Improvement	SMA Improvement	Ellipsoid Consistency	Ellipse Consistency
Non-Ground Constrained				
Largest Ellipsoid	96%	97%	95%	100%
New Det CI	-	-	-	-
Fast Det CI	95%	93%	95%	100%
Fast Trace CI	95%	95%	95%	100%
Ellipsoid Intersection	93%	96%	95%	100%
Kalman filter	96%	96%	95%	100%
Ground Constrained				
Largest Ellipsoid	47%	69%	92%	99%
New Det CI	-	-	-	-
Fast Det CI	64%	63%	92%	99%
Fast Trace CI	68%	65%	92%	99%
Ellipsoid Intersection	-	-	-	-
Kalman filter	71%	73%	92%	99%

Table 32. Improvement from Kalman filter fusion based augmentation of four-ball TDOA by AOA SV against AFIT target

	Ground Constrained						Non-Ground Constrained					
RMSE												
	Three-ball TDOA Satellite Pass						Three-ball TDOA Satellite Pass					
AOA SV Pass	1	2	3	4	5	6	1	2	3	4	5	6
1	38%	26%	100%	89%	93%	98%	95%	99%	99%	98%	93%	99%
2	65%	37%	99%	90%	94%	99%	98%	99%	100%	98%	95%	100%
3	19%	2%	98%	58%	70%	96%	92%	97%	98%	91%	81%	99%
4	58%	32%	99%	81%	88%	99%	97%	99%	99%	96%	93%	100%
5	65%	37%	100%	92%	95%	99%	98%	99%	100%	98%	96%	100%
6	9%	10%	99%	79%	85%	96%	79%	95%	98%	96%	81%	98%
Average Miss												
	Three-ball TDOA Satellite Pass						Three-ball TDOA Satellite Pass					
AOA SV Pass	1	2	3	4	5	6	1	2	3	4	5	6
1	37%	25%	99%	88%	92%	95%	95%	99%	99%	98%	93%	99%
2	63%	38%	99%	89%	93%	98%	98%	99%	100%	98%	95%	100%
3	22%	2%	97%	56%	69%	90%	92%	96%	98%	91%	80%	99%
4	56%	32%	99%	80%	87%	97%	97%	99%	99%	96%	92%	99%
5	64%	36%	99%	91%	95%	98%	98%	99%	100%	98%	96%	100%
6	10%	12%	98%	78%	85%	89%	79%	95%	98%	96%	81%	98%
Average SMA												
	Three-ball TDOA Satellite Pass						Three-ball TDOA Satellite Pass					
AOA SV Pass	1	2	3	4	5	6	1	2	3	4	5	6
1	34%	31%	100%	91%	93%	97%	95%	99%	99%	98%	93%	99%
2	69%	38%	99%	91%	94%	99%	98%	99%	100%	98%	96%	100%
3	19%	5%	98%	58%	71%	94%	93%	97%	98%	91%	82%	98%
4	60%	33%	99%	80%	88%	98%	98%	99%	99%	96%	92%	99%
5	68%	41%	100%	94%	96%	99%	98%	99%	100%	99%	97%	100%
6	9%	11%	99%	81%	86%	92%	79%	94%	97%	97%	81%	96%

Table 33. Kalman filter geolocation fusion consistency for augmentation of four-ball TDOA SV by AOA SV against AFIT target

		Ground Constrained						Non-Ground Constrained					
		Ellipsoid Consistency						Ellipsoid Consistency					
		Three-ball TDOA Satellite Pass						Three-ball TDOA Satellite Pass					
		1	2	3	4	5	6	1	2	3	4	5	6
AOA SV Pass	1	89%	91%	91%	94%	95%	90%	95%	96%	93%	97%	96%	94%
	2	94%	91%	91%	97%	97%	90%	96%	95%	94%	98%	96%	92%
	3	89%	91%	90%	95%	93%	89%	95%	95%	94%	96%	96%	93%
	4	93%	91%	90%	95%	93%	88%	95%	95%	95%	94%	96%	93%
	5	92%	91%	92%	97%	99%	90%	95%	96%	95%	97%	97%	94%
	6	84%	91%	90%	97%	92%	88%	94%	95%	94%	95%	97%	93%
		Ellipse Consistency						Ellipse Consistency					
		Three-ball TDOA Satellite Pass						Three-ball TDOA Satellite Pass					
		1	2	3	4	5	6	1	2	3	4	5	6
AOA SV Pass	1	100%	97%	99%	100%	100%	97%	100%	99%	100%	100%	100%	100%
	2	100%	98%	99%	100%	100%	98%	100%	99%	100%	100%	100%	99%
	3	100%	94%	99%	100%	99%	98%	100%	99%	100%	99%	100%	100%
	4	100%	95%	99%	99%	100%	98%	100%	99%	100%	99%	100%	100%
	5	100%	97%	99%	100%	100%	98%	100%	99%	100%	100%	100%	99%
	6	100%	95%	99%	100%	100%	98%	100%	99%	100%	99%	100%	100%

The preceding fusion results were intended to provide a relatively detailed description of the fusion behavior in a permissive environment. The next two scenarios will focus on more tailored applications.

4.2 Scenario Two

This scenario, with the emitter located at the Tripoli Airport in Libya is designed to test the geolocation fusion performance in an operational representative environment. As much of the performance may be similar to that observed in Scenario One, this discussion will focus on highlighting the differences and unique aspects of limited collection opportunities. The full set of results, as presented for scenario one, are available in Appendix A.

4.2.1 Single Geolocation Agent Performance.

Most of the geolocation agents utilized in the Libya collection scenario are the same as those employed against the target located near AFIT with the exception of the addition of a high altitude manned aircraft, described in subsection 4.2.1.2, and the removal of the three-ball TDOA UAV cluster. The three-ball TDOA UAV cluster was removed as the greater standoff distance required and the low altitude nature of the reference UAV platform precluded collection of the SOI.

4.2.1.1 AOA Satellite Performance.

The AOA SV geolocation agent exhibited similar performance against the Libya target as the target near AFIT. Applying the surface of the earth constraint improved performance in all cases and the best performance came from the pass geometries 8 and 11 which are analogous in relative position to pass geometries 2 and 4 in scenario one. The numerical MOPs are shown in Tables 34 and 35, and the graphical depictions

are available in Appendix A, subsection 1.1.0.7.

Table 34. Unconstrained AOA satellite performance against Libya target

Geometry	Measure of Performance				
	RMSE (m)	Avg Miss (m)	Volume (m^3)	SMA (m)	MPTPS (m)
7	713	629	3.78E+09	1710	3341
8	433	399	1.24E+09	896	1585
9	2343	1972	3.85E+10	6305	11270
10	679	594	3.14E+09	1636	3227
11	406	372	9.68E+08	869	1386
12	1567	1357	2.09E+10	4091	7589

Table 35. Ground constrained AOA satellite performance against Libya target

Geometry	Measure of Performance				
	RMSE (m)	Avg Miss (m)	Volume (m^3)	SMA (m)	MPTPS (m)
7	643	541	1.10E+08	1667	3222
8	361	319	4.60E+07	810	1555
9	2096	1665	5.50E+08	5696	10693
10	618	513	9.92E+07	1622	3151
11	322	283	3.61E+07	725	1333
12	1438	1213	2.77E+08	3840	7411

4.2.1.2 AOA Aircraft Performance.

The AOA Aircraft collectors for the Libya scenario differ slightly from those employed in Scenario One against the emitter located near AFIT. Instead of six mid altitude collectors flying both above and slightly offset of the target, there are only two collectors and they are restricted to flying offset of target in international airspace over the Mediterranean. The mid-altitude collector is flying parallel to the coast approximately 20 nautical miles offshore, and the high altitude collector is flying on a parallel heading approximately 100 nautical miles offshore as depicted in Figure 19.

The MOPs for the unconstrained and ground constrained cases are shown in Tables 36 and 37 respectively. As expected, the geolocation performance is degraded

from that shown in the AFIT scenario due to the greater slant range to the target which results in both a lower SNR as well as a greater distance over which the angular error will propagate. The graphical representations can be seen in Figures 70 and 71 in Appendix A. Similar to the AOA AV collectors in the AFIT scenario, the ellipsoids are oriented with the SMA primarily along the average line-of-sight vector from the collector to the emitter.

Table 36. Unconstrained AOA aircraft performance against Libya target

Geometry	Measure of Performance				
	RMSE (m)	Avg Miss (m)	Volume (m^3)	SMA (m)	MPTPS (m)
7	454	368	1.15E+08	1213	1892
8	1010	814	1.87E+15	2562	4078

Table 37. Ground constrained AOA aircraft performance against Libya target

Geometry	Measure of Performance				
	RMSE (m)	Avg Miss (m)	Volume (m^3)	SMA (m)	MPTPS (m)
7	388	320	1.39E+07	1041	1892
8	855	701	1.37E+12	2194	3815

4.2.1.3 Three-ball TDOA Satellite Performance.

Scenario Two employs the same three-ball TDOA satellite cluster as used in the AFIT scenario. The pass geometry is analogous as well, with pass 7 corresponding to the same position relative to the emitter as pass 1 in the AFIT scenario and so on. The geometries in questions were shown previously in Figure 16.

The performance achieved against the emitter in Libya is similar to that achieved against the emitter near AFIT, and is tabulated in Tables 38 and 41. The graphical depictions are shown in Figures 72 to 77 in Appendix A. The same pattern of solutions without additional DEM constraint lying below the surface of the earth is present in the Libya scenario as was present in the AFIT scenario. Additionally, the terrain

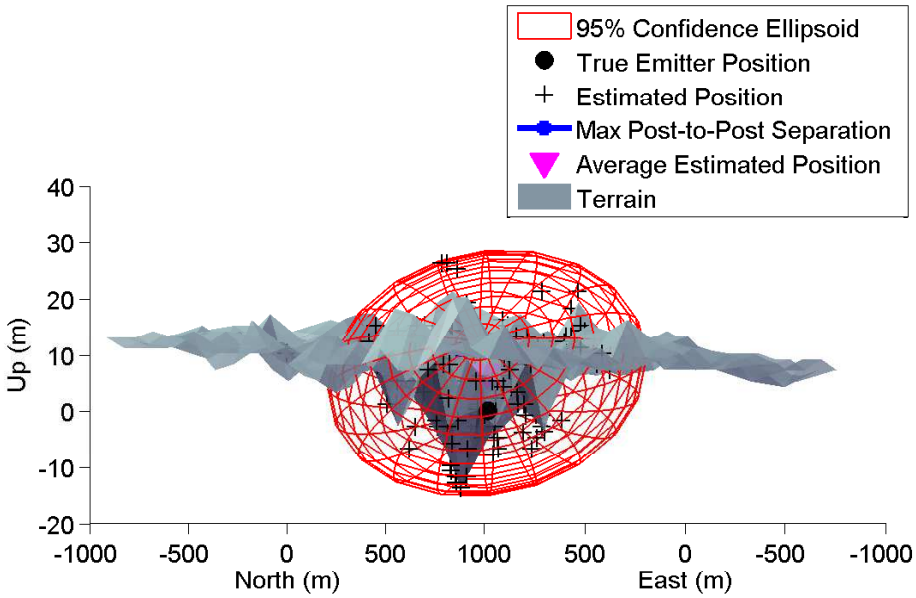

Figure 56. "Well" in Libya terrain data

near the emitter location exhibits an unusual "well" effect which may either indicate that there was physically a large a hole in the aircraft parking ramp when the SRTM data was collected, or that the surface qualities resulted in a poor collection. The well is approximately $20 - 25$ meters below the surround terrain, and can be seen in the ground constrained geolocation solution for pass geometry 8 in Figure 56. Regardless of the cause, the presence of the well highlights the fact that terrain data is not without noise and should be utilized with caution.

Table 38. Unconstrained three-ball TDOA satellite performance against Libya target

Geometry	Measure of Performance				
	RMSE (m)	Avg Miss (m)	Volume (m^3)	SMA (m)	MPTPS (m)
7	1734	1413	9.29E+12	4835	NA
8	1715	1465	8.48E+13	4357	632
9	5527	4516	9.64E+16	14132	NA
10	2089	1678	1.36E+13	5737	NA
11	2731	2257	5.68E+15	7329	7846
12	7061	5951	1.35E+18	17591	NA

Table 39. Ground constrained three-ball TDOA satellite performance against Libya target

Geometry	Measure of Performance				
	RMSE (m)	Avg Miss (m)	Volume (m^3)	SMA (m)	MPTPS (m)
7	782	625	2.36E+12	2158	4014
8	332	294	6.76E+11	738	1386
9	445	378	3.71E+11	1208	2304
10	864	702	3.35E+12	2391	4415
11	252	221	2.24E+11	582	1036
12	403	331	2.38E+11	1098	2041

4.2.1.4 Four-ball TDOA Satellite Performance.

The final geolocation agent employed in the Libya scenario is the four-ball TDOA SV cluster. The magnitudes of the geolocation performance are similar to that observed in the AFIT scenario although there is some variability. The large increase in performance due to the application of the higher fidelity surface of the earth constraint is still present, and the error ellipsoids are still very long and slender.

The tabulated performance is shown in Tables 40 and 41 for the unconstrained and ground constrained cases respectively and the graphical depiction is shown by Figures 78 to 83 in Appendix A.

Table 40. Unconstrained four-ball TDOA satellite performance against Libya target

Geometry	Measure of Performance				
	RMSE (m)	Avg Miss (m)	Volume (m^3)	SMA (m)	MPTPS (m)
7	27627	21855	5.77E+11	70815	NA
8	75730	59761	8.88E+13	209887	NA
9	13684	11443	3.80E+11	36649	NA
10	24803	20621	6.65E+11	60841	NA
11	66505	62781	9.58E+14	106162	NA
12	10885	9054	4.16E+11	28005	NA

Table 41. Ground constrained four-ball TDOA satellite performance against Libya target

Geometry	Measure of Performance				
	RMSE (m)	Avg Miss (m)	Volume (m^3)	SMA (m)	MPTPS (m)
7	8724	2795	4.67E+08	24310	NA
8	6108	1333	1.72E+07	1229	NA
9	5761	4600	2.16E+08	16080	NA
10	2904	2446	2.00E+08	8055	NA
11	10608	6027	1.49E+09	29291	NA
12	8600	6945	6.79E+08	24096	NA

4.2.2 Fused Geolocation Performance.

Now that the single geolocation agent performance has been quantified, it is possible to examine the results of applying geolocation estimate fusion. Again, it is expected that these results will be very similar to those observed in the AFIT scenario, so the basic results will be presented and only expounded upon in the case of unique or unexpected behavior. Full results, including the full permutation set performance and consistency, are included in Appendix B.

4.2.2.1 AOA Satellite Augmenting AOA Satellite.

The first case is an AOA SV agent augmented with another AOA SV agent. In order to quantify the general performance, the average improvements to miss distance and SMA size along with the corresponding fusion sequence consistency for each combination were tabulated for each of the fusion techniques. This tabulation is shown in Table 42. The performance observed closely match that of the same fusion in the AFIT scenario. In fact, all of the improvements to the average miss distance and SMA size match the equivalent MOP from the AFIT scenario to within 2%. However, this is a small difference in the measured consistencies, particularly in the ground constrained case. The ellipsoid consistency for both the LE and Kalman filter

techniques dropped below 90%, and in the Kalman filter case, is over 20% lower than the equivalent AFIT value. One potential explanation may be that "well" in the terrain data is causing more extreme outliers than would otherwise be expected in a ground constrained case.

As in the AFIT scenario, using an AOA SV geolocation platform to augment another AOA SV geolocation platform appears to have promise. The MOPs show significant improvements, and consistency is adequate in most cases, although further study may be required in that area.

Table 42. Average AOA SV and AOA SV fusion results against Libya target

Fusion Technique	Miss Improvement	SMA Improvement	Ellipsoid Consistency	Ellipse Consistency
Non-Ground Constrained				
Largest Ellipsoid	36%	38%	94%	97%
New Det CI	-	-	-	-
Fast Det CI	29%	27%	97%	99%
Fast Trace CI	32%	27%	98%	99%
Ellipsoid Intersection	36%	46%	91%	99%
Kalman Filter	36%	46%	91%	99%
Ground Constrained				
Largest Ellipsoid	37%	37%	84%	94%
New Det CI	-	-	-	-
Fast Det CI	31%	27%	94%	100%
Fast Trace CI	33%	27%	95%	100%
Ellipsoid Intersection	-	-	-	-
Kalman filter	37%	45%	70%	99%

4.2.2.2 AOA Satellite Augmenting AOA Aircraft.

The next fusion test case is the AOA SV agent fused with the two realistic AOA aircraft. This case is of particular interest in that the airborne collection aircraft are employed differently than in the AFIT scenario. Both aircraft are further offset from the emitter, and the high altitude collector is operating at a much higher altitude than

the airborne collectors employed in the AFIT scenario. Additionally, the geometry of collection is limited.

The average performance improvements, as shown in Table 43, are significantly greater than those achieved in the AFIT scenario. This is due to the fact that the increased slant range between the airborne AOA collectors and the emitter yielded larger ellipsoids than those produced in scenario one. In fact, the AOA AV ellipsoids were of similar magnitude to those produced by the AOA SV agent. The improvements shown here, as well as in the pass-by-pass performance metrics in Appendix B indicate that the single-ball AOA CubeSat may be a good candidate for improving the performance of operational airborne collectors. As previously noted, the greatest improvement from estimate fusion is obtained by fusing the best available data to a poor or marginal estimate. In this case, AOA SV pass geometries 2 and 5 increase performance the most, especially when applied to high altitude aircraft collections.

Table 43. Average AOA SV and AOA AV fusion results against Libya target

Fusion Technique	Miss Improvement	SMA Improvement	Ellipsoid Consistency	Ellipse Consistency
Non-Ground Constrained				
Largest Ellipsoid	44%	40%	96%	99%
New Det CI	-	-	-	-
Fast Det CI	19%	17%	96%	99%
Fast Trace CI	38%	27%	99%	100%
Ellipsoid Intersection	25%	48%	80%	100%
Kalman filter	44%	48%	96%	100%
Ground Constrained				
Largest Ellipsoid	45%	33%	87%	98%
New Det CI	-	-	-	-
Fast Det CI	26%	16%	82%	100%
Fast Trace CI	38%	23%	89%	100%
Ellipsoid Intersection	-	-	-	-
Kalman filter	45%	44%	58%	100%

4.2.2.3 AOA Satellite Augmenting Three-ball TDOA Satellites.

The fusion of the AOA SV and three-ball TDOA SV is the next case. Overall the performance improvements, tabulated in Table 44, are similar to those seen in the AFIT scenario.

Table 44. Average AOA SV and three-ball TDOA SV fusion results against Libya target

Fusion Technique	Miss Improvement	SMA Improvement	Ellipsoid Consistency	Ellipse Consistency
Non-Ground Constrained				
Largest Ellipsoid	82%	85%	18%	100%
New Det CI	-	-	-	-
Fast Det CI	61%	57%	62%	99%
Fast Trace CI	67%	66%	90%	100%
Ellipsoid Intersection	-	-	-	-
Kalman Filter	82%	84%	16%	100%
Ground Constrained				
Largest Ellipsoid	34%	25%	91%	100%
New Det CI	-	-	-	-
Fast Det CI	19%	14%	94%	99%
Fast Trace CI	10%	17%	96%	100%
Ellipsoid Intersection	-	-	-	-
Kalman filter	34%	39%	78%	99%

4.2.2.4 AOA Satellite Augmenting Four-ball TDOA Satellites.

The final fusion case in scenario two is the combination of estimates from an AOA SV agent and a four-ball TDOA SV agent. The average performance improvements are shown in Table 45. These results match relatively closely with the performance seen in the AFIT scenario. However, there are some deviations, particularly in the ground constrained cases where the results outperform their AFIT equivalents. This is likely due to the fact the ground constrained four-ball TDOA solutions in the Libya scenario are worse than those achieved in the AFIT scenario. This result should be

re-evaluated to determine the cause of the observed performance difference.

Table 45. Average AOA SV and three-ball TDOA SV fusion results against Libya target

Fusion Technique	Miss Improvement	SMA Improvement	Ellipsoid Consistency	Ellipse Consistency
Non-Ground Constrained				
Largest Ellipsoid	96%	96%	87%	85%
New Det CI	-	-	-	-
Fast Det CI	96%	94%	96%	95%
Fast Trace CI	96%	94%	96%	98%
Ellipsoid Intersection	95%	95%	96%	88%
Kalman filter	96%	95%	95%	88%
Ground Constrained				
Largest Ellipsoid	91%	77%	68%	98%
New Det CI	-	-	-	-
Fast Det CI	89%	74%	88%	100%
Fast Trace CI	89%	75%	91%	100%
Ellipsoid Intersection	-	-	-	-
Kalman filter	91%	78%	61%	99%

4.2.2.5 Scenario Two Conclusions.

Scenario Two demonstrated that the observations developed in the AFIT geolocation "sandbox" translate to another location and operationally relevant scenario. One of the unique takeaways is that a single-ball AOA satellite is more useful as an augmentation to realistic airborne collectors than the best case results from the AFIT scenario suggested.

4.3 Scenario Three

Scenario Three was chosen as an operationally relevant scenario that would provide a stress test to the application of the surface of the earth constraint. The emitter is placed near the top of a ridge line in the Hindu Kush mountains in northeastern Afghanistan. This section will report the results from single agent and multiple agent fusions while highlighting differences due to the mountainous terrain. The full suite of results including figures and pass-by-pass fusion and consistency metrics can be found in Appendices A and B respectively.

4.3.1 Single Geolocation Agent Performance.

As with the previous two scenarios, this section will document the performance of each geolocation agent independently to establish a baseline from which to judge the improvements from estimate fusion.

4.3.1.1 AOA Satellite Performance.

The single-ball AOA SV geolocation agent results are tabulated in Table 46. The unconstrained performance is very similar to that observed in the AFIT and Libya scenarios. This is not unexpected as the 3D solution is independent of the terrain. The ground constrained results however, are where the real interest lies. In an area with widely varying terrain elevations a surface of the earth constraint may serve to improve geolocation accuracy, or if incorrectly applied, may result in divergent estimates. In this case, the addition of the DEM based surface of the earth model significantly improved geolocation accuracy. The average improvements to the RMSE, average miss distance, SMA, and MPTPS were 16%, 22%, 17%, and 8% respectively. This level of improvement is impressive in of itself, but what is even more impressive is that it allows for results that are more precise than those developed for the flat

terrain present in the AFIT and Libya scenarios. The percent improvement, due to the application of the surface of the earth constraint in the mountainous terrain, was greater than than that in the flat terrain by at least 4% in RMSE, 6% in average miss distance, 9% in SMA, and 3% in MPTPS.

The graphical depictions of the geolocation solutions for each pass geometry can be found in section 1.2.0.11 of Appendix A. An example of the difference between unconstrained and ground constrained is shown in Figure 57.

Based upon these results, it appears that the addition of a surface of the earth constraint for space based AOA geolocation agents is worthwhile.

Table 46. Unconstrained AOA satellite performance against Afghanistan target

Geometry	Measure of Performance				
	RMSE (m)	Avg Miss (m)	Volume (m^3)	SMA (m)	MPTPS (m)
13	647	577	3.08E+09	1508	2036
14	430	393	1.23E+09	844	1514
15	1650	1416	2.17E+10	4331	6006
16	728	650	3.50E+09	1778	2739
17	414	375	1.09E+09	845	1199
18	1686	1443	2.56E+10	4410	5998

Table 47. Ground constrained AOA satellite performance against Afghanistan target

Geometry	Measure of Performance				
	RMSE (m)	Avg Miss (m)	Volume (m^3)	SMA (m)	MPTPS (m)
13	467	410	1.13E+09	1055	1712
14	372	334	5.27E+08	813	1570
15	1478	1131	1.13E+10	3853	5115
16	676	588	1.34E+09	1688	2723
17	339	298	4.82E+08	644	1203
18	1327	936	1.20E+10	3285	4816

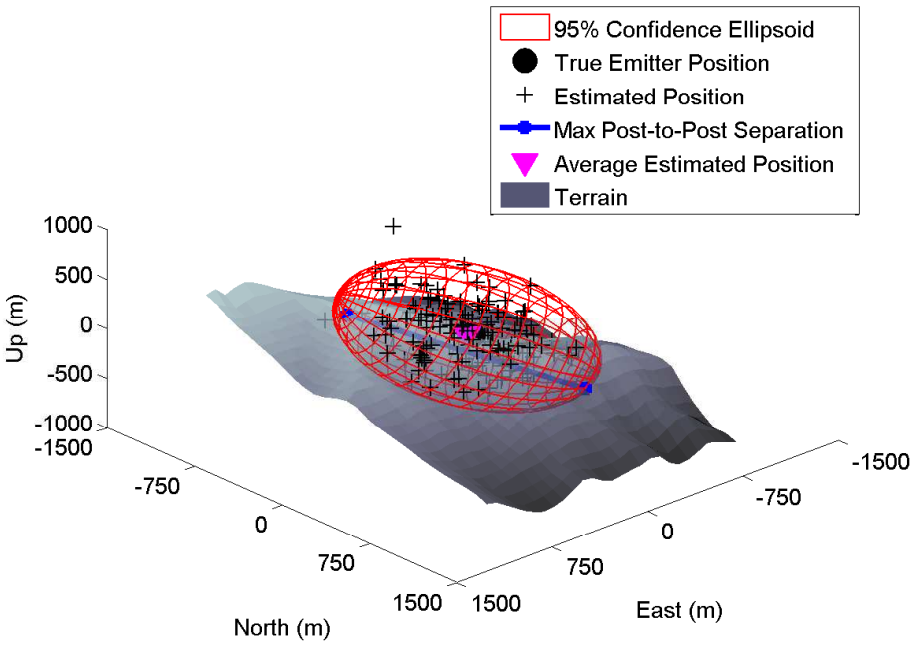

(a) No ground constraint

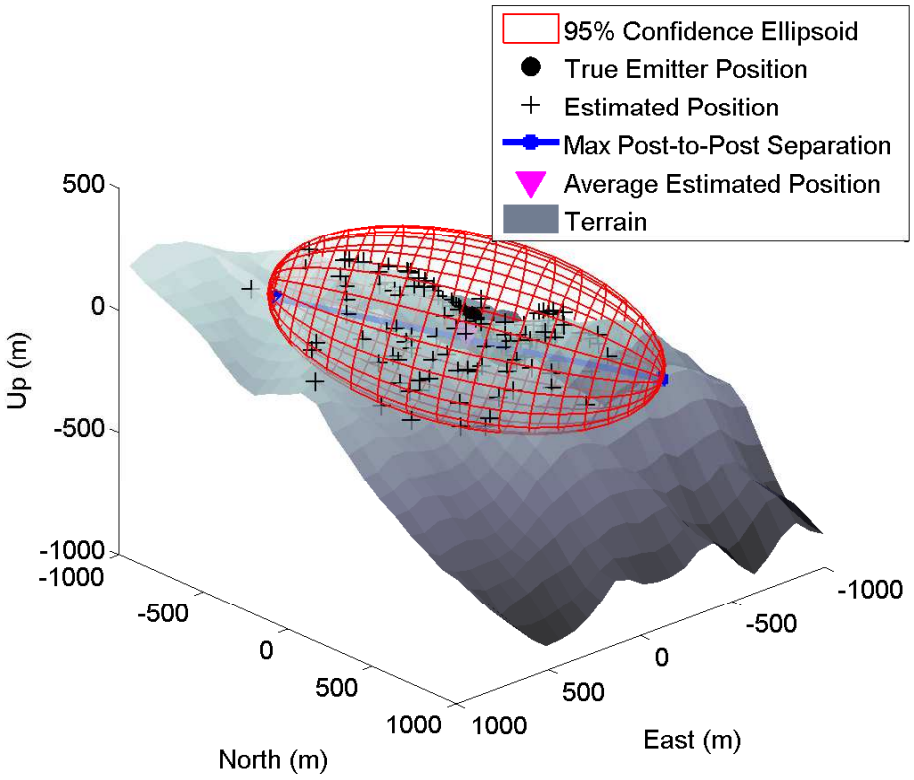

(b) Ground constrained

Figure 57. AOA satellite geometry 14 against Afghanistan target

4.3.1.2 AOA Aircraft Performance.

The next geolocation agent to evaluate is the AOA aircraft. The collection aircraft in this scenario are limited in a similar manner as those in the Libya scenario. In order to stay out of Pakistani airspace, the mid-altitude collector is offset from the border by approximately 15 nautical miles and the high altitude collector is offset by approximately 90 nautical miles.

The resulting performance of these two collectors is given in Tables 48 and 49, for the unconstrained and ground constrained cases respectively, and compares favorably with the AFIT and Libya scenario performance. The mid-altitude collector case has performance between that of the AFIT and Libya analogs, which is expected as the slant range lies between each case. The high altitude collector performs very similarly to the same collector in the Libya scenario in the unconstrained case. When a ground constraint is applied however, the performance improved to a greater extent. In fact, the RMSE and average miss distance improved by 46% and 17% respectively. The SMA and MPTPS saw more modest improvements of 17% and 2% respectively. One interesting behavior to note is the fact that the MPTPS for the mid-altitude case actually increased by 43%. This behavior is due to the fact that the ground constraint forces the ellipsoid to intersect with the ground whereas the unconstrained ellipsoid only intersects a small portion of the ridgeline. This behavior is illustrated in 90 in Appendix A. Considering this behavior, along with the improvements in the other MOPs, indicates that applying the surface of the earth constraint has the effect of pulling in most of the estimates towards the average, but doesn't prevent, and in some cases can actually promote, outliers.

Table 48. Unconstrained AOA aircraft performance against Afghanistan target

Geometry	Measure of Performance				
	RMSE (m)	Avg Miss (m)	Volume (m^3)	SMA (m)	MPTPS (m)
9	55	49	1.53E+09	130	84
10	997	831	1.48E+15	2604	2482

Table 49. Ground constrained AOA aircraft performance against Afghanistan target

Geometry	Measure of Performance				
	RMSE (m)	Avg Miss (m)	Volume (m^3)	SMA (m)	MPTPS (m)
9	52	46	6.73E+08	115	120
10	810	449	1.23E+15	2167	2430

4.3.1.3 Three-ball TDOA Satellite Performance.

The three-ball TDOA SV geolocation agent is also employed in the Afghanistan scenario. The tabulated performance for unconstrained and ground constrained cases is shown in Tables 50 and 51. Overall, the performance is very similar to that observed in the AFIT and Libya scenarios. There is a significant improvement due to the application of the high fidelity DEM based surface of the earth constraint, 84% for RMSE and average miss distance and 85% for SMA length, but this improvement is similar to that observed in the previous two scenarios. It is worth noting that unlike many of the cases, the average ellipsoid volume increased dramatically. This is due to the fact that the highly 3D nature of the surrounding terrain introduces more variance in the up direction than is present in the three-ball TDOA algorithm without the high fidelity DEM based surface of the earth constraint.

4.3.1.4 Three-ball TDOA Aircraft Performance.

The Afghanistan scenario employs one three-ball TDOA UAV geolocation agent that flies along the same heading as the mid-altitude AOA AV collector. The observed performance is similar to that observed in the AFIT scenario and exhibits a significant

Table 50. Unconstrained three-ball TDOA satellite performance against Afghanistan target

Geometry	Measure of Performance				
	RMSE (m)	Avg Miss (m)	Volume (m^3)	SMA (m)	MPTPS (m)
13	1874	1536	1.13E+13	5197	5371
14	1752	1498	1.19E+14	4420	4423
15	5737	4792	9.33E+16	13193	23083
16	2122	1704	1.68E+13	5890	1224
17	2825	2321	2.88E+15	7325	7633
18	9565	8281	9.27E+18	19464	31916

Table 51. Ground constrained three-ball TDOA satellite performance against Afghanistan target

Geometry	Measure of Performance				
	RMSE (m)	Avg Miss (m)	Volume (m^3)	SMA (m)	MPTPS (m)
13	411	353	1.16E+14	1002	1725
14	320	280	6.32E+13	674	1252
15	396	332	3.87E+13	1010	1017
16	738	534	4.37E+14	1966	1548
17	323	285	4.32E+13	764	1119
18	461	362	1.05E+14	1141	1310

improvement from the application of a surface of the earth constraint. The tabulated performance is shown in Tables 52 and 53, and the graphical representations are shown in Appendix A, subsection 1.2.0.14.

Table 52. Unconstrained three-ball TDOA UAV performance against Afghanistan target

Geometry	Measure of Performance				
	RMSE (m)	Avg Miss (m)	Volume (m3)	SMA (m)	MPTPS (m)
9	4262	3136	2.45E+18	8417	NA

Table 53. Ground constrained three-ball TDOA UAV performance against Afghanistan target

Geometry	Measure of Performance				
	RMSE (m)	Avg Miss (m)	Volume (m3)	SMA (m)	MPTPS (m)
9	3620	2087	2.29E+18	7694	NA

4.3.1.5 Four-ball TDOA Satellite Performance.

The final geolocation agent is the four-ball TDOA SV. The tabulated performance is shown in Tables 54 and 55 and is generally worse than the performance observed in the previous two scenarios. The improvement realized by the addition of the surface of the earth constraint is relatively minor compared to the other geolocation phenomenologies and in some instance actually decreases geolocation performance. It was noted in the course of this research that the four-ball TDOA geolocation solution was very sensitive to search area. Further improvements are required to prevent the ground constrained solution from *walking-off* of the correct solution, or alternatively, identifying and discarding poor estimates.

Table 54. Unconstrained four-ball TDOA satellite performance against Afghanistan target

Geometry	Measure of Performance				
	RMSE (m)	Avg Miss (m)	Volume (m^3)	SMA (m)	MPTPS (m)
13	23729	18880	4.68E+11	61317	NA
14	19254	15262	2.10E+11	51640	NA
15	142534	135123	5.57E+11	127228	NA
16	105990	104930	6.46E+11	53208	NA
17	74975	68396	9.31E+11	114693	NA
18	9596	7562	1.97E+10	26290	NA

Table 55. Ground constrained four-ball TDOA satellite performance against Afghanistan target

Geometry	Measure of Performance				
	RMSE (m)	Avg Miss (m)	Volume (m^3)	SMA (m)	MPTPS (m)
13	28124	21769	1.07E+11	73744	NA
14	62875	49605	1.02E+13	148753	NA
15	90743	79517	1.06E+15	213334	NA
16	21827	17301	1.35E+11	60294	NA
17	75720	68111	3.47E+14	117520	NA
18	11007	9761	7.73E+11	25040	NA

4.3.2 Fused Geolocation Performance.

Now that the individual geolocation agent performance has been quantified as a baseline, the fusion results can be explored. This section will cover each of the fusion combinations, highlighting differences and unique behaviors as applicable. The full set of results, including the full set of permutations and associated consistency, are included in Appendix B.

4.3.2.1 AOA Satellite Augmenting AOA Satellite.

Once again, the first fusion case to examine is the combination of two AOA SV geolocation agents. The average performance increase due to estimate fusion for each fusion technique is shown in Table 56. These results are similar to those seen in the AFIT and Libya scenarios with the exception of lower than expected ellipsoid consistency in the ground constrained cases. Ideally, the ellipsoid consistency should be at or near 95%. The fact that it is not, but the ellipse consistency is still high indicates that the estimated positions are likely falling either above or below the ellipsoid.

On a per pass basis, the greatest improvements attributable to fusion correspond to augmenting a relatively poor estimate with a relatively good estimate. This matches the behavior identified in the AFIT and Libya scenarios. It is also worth noting that this case is one of the only ground constrained test cases that did not result in the Ellipsoid Intersection algorithm failing and producing nonsensical results. This is likely due to the fact that ground constrained solutions on terrain with large vertical variation, such as the mountainous terrain in this scenario, result in covariance with greater vertical variation than ground constrained solutions on flat terrain.

Table 56. Average AOA SV and AOA SV fusion results against Afghanistan target

Fusion Technique	Miss Improvement	SMA Improvement	Ellipsoid Consistency	Ellipse Consistency
Non-Ground Constrained				
Largest Ellipsoid	34%	38%	92%	97%
New Det CI	-	-	-	-
Fast Det CI	27%	27%	96%	100%
Fast Trace CI	30%	26%	98%	100%
Ellipsoid Intersection	34%	45%	92%	98%
Kalman filter	34%	45%	91%	98%
Ground Constrained				
Largest Ellipsoid	31%	33%	88%	97%
New Det CI	-	-	-	-
Fast Det CI	25%	24%	92%	99%
Fast Trace CI	28%	23%	93%	99%
Ellipsoid Intersection	30%	41%	85%	98%
Kalman filter	31%	41%	85%	98%

4.3.2.2 AOA Satellite Augmenting AOA Aircraft.

The next case is the fusion of AOA SV and AOA AV geolocation agent estimates. The average improvements shown in Table 57 indicate that there are improvements, but not as great as those identified in the Libya scenario. However, closer inspection reveals that there is a great disparity in the improvement experienced by the two different AOA AV collectors. The mid-altitude collector is minimally improved while the high altitude collector is greatly improved, up to 70% in some cases. This adds additional support to the assertion made in the Libya scenario that a single-ball AOA geolocation payload is a worthwhile augmentation to certain classes of airbreathing collectors.

Table 57. Average AOA SV and AOA AV fusion results against Afghanistan target

Fusion Technique	Miss Improvement	SMA Improvement	Ellipsoid Consistency	Ellipse Consistency
Non-Ground Constrained				
Largest Ellipsoid	28%	31%	94%	99%
New Det CI	-	-	-	-
Fast Det CI	21%	19%	94%	99%
Fast Trace CI	25%	23%	95%	99%
Ellipsoid Intersection	-36%	31%	63%	99%
Kalman filter	28%	31%	93%	99%
Ground Constrained				
Largest Ellipsoid	36%	22%	80%	98%
New Det CI	-	-	-	-
Fast Det CI	16%	21%	93%	98%
Fast Trace CI	16%	21%	94%	98%
Ellipsoid Intersection	-	-	-	-
Kalman filter	16%	29%	91%	98%

4.3.2.3 AOA Satellite Augmenting Three-ball TDOA Satellites.

The next fusion test case is the combination of the AOA SV augmenter and a three-ball TDOA SV geolocation agent. The average results of this combination are shown in Table 58. The results of this fusion are slightly worse than those exhibited in the AFIT and Libya scenarios. It should also be noted that the unconstrained cases present the same ellipsoid consistency deficiency, where the observed consistency is well below 95%, observed in the Libya scenario. This is indicative that the radius of earth constraint incorporated into the three-ball TDOA algorithm is causing the estimated solution to lie above or below the true emitter location. This hypothesis is confirmed by inspection of one of the non-ground constrained solution sets, as shown in Figure 58, that shows the plane of unconstrained solutions resting just below the true emitter position.

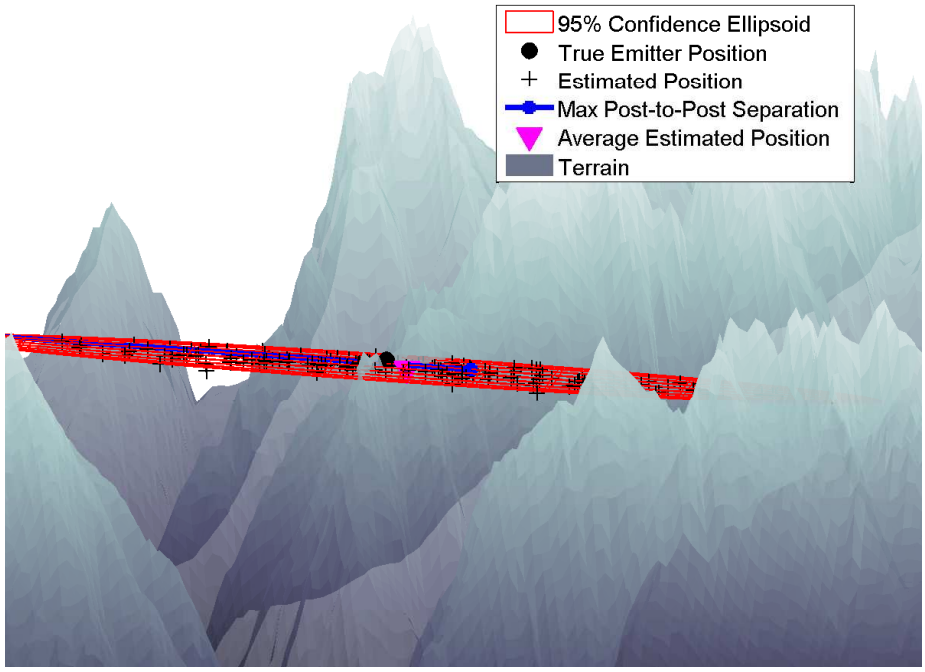

Figure 58. Zoomed-in three-ball TDOA solution

Table 58. Average AOA SV and three-ball TDOA SV fusion results against Afghanistan target

Fusion Technique	Miss Improvement	SMA Improvement	Ellipsoid Consistency	Ellipse Consistency
Non-Ground Constrained				
Largest Ellipsoid	78%	80%	9%	99%
New Det CI	-	-	-	-
Fast Det CI	51%	46%	40%	99%
Fast Trace CI	77%	75%	86%	100%
Ellipsoid Intersection	-	-	-	-
Kalman filter	78%	80%	10%	100%
Ground Constrained				
Largest Ellipsoid	24%	21%	93%	100%
New Det CI	-	-	-	-
Fast Det CI	16%	10%	94%	100%
Fast Trace CI	22%	12%	96%	100%
Ellipsoid Intersection	18%	33%	82%	100%
Kalman filter	24%	33%	88%	100%

4.3.2.4 AOA Satellite Augmenting Three-ball TDOA Aircraft.

The AOA SS augmenter was also used in conjunction with a three-ball TDOA AV geolocation agent. The average improvements are shown in Table 59. One unique behavior noted is that the EI algorithm did not suffer from the break-down identified in the AFIT and Libya scenarios. This is likely due to the fact that the ground constrained solutions in mountainous terrain maintain significant vertical variance that is not present in the previous scenarios.

Table 59. Average AOA SV and three-ball TDOA UAV fusion results against Afghanistan target

Fusion Technique	Miss Improvement	SMA Improvement	Ellipsoid Consistency	Ellipse Consistency
Non-Ground Constrained				
Largest Ellipsoid	78%	79%	96%	93%
New Det CI	-	-	-	-
Fast Det CI	76%	73%	96%	100%
Fast Trace CI	77%	74%	97%	100%
Ellipsoid Intersection	78%	79%	95%	100%
Kalman filter	78%	79%	95%	100%
Ground Constrained				
Largest Ellipsoid	74%	78%	81%	93%
New Det CI	-	-	-	-
Fast Det CI	71%	76%	89%	99%
Fast Trace CI	73%	76%	91%	99%
Ellipsoid Intersection	74%	81%	83%	99%
Kalman filter	74%	81%	83%	99%

4.3.2.5 AOA Satellite Augmenting Four-ball TDOA Satellites.

The final fusion case in scenario three is the combination of estimates from an AOA SV agent and a four-ball TDOA SV agent. The average performance improvements are shown in Table 60. These results are similar to those in the Libya scenario although the ground constrained improvements are somewhat higher. This is not

unexpected as the four-ball TDOA SV single agent results were not as good as those in the Libya and AFIT scenarios. This is likely due to the difficulty encountered in applying the surface of the earth constraint in mountainous terrain.

Table 60. Average AOA SV and four-ball TDOA SV fusion results against Afghanistan target

Fusion Technique	Miss Improvement	SMA Improvement	Ellipsoid Consistency	Ellipse Consistency
Non-Ground Constrained				
Largest Ellipsoid	97%	97%	79%	93%
New Det CI	-	-	-	-
Fast Det CI	97%	97%	96%	100%
Fast Trace CI	97%	97%	96%	100%
Ellipsoid Intersection	96%	97%	74%	99%
Kalman Filter	97%	97%	95%	99%
Ground Constrained				
Largest Ellipsoid	98%	98%	85%	96%
New Det CI	-	-	-	-
Fast Det CI	97%	98%	89%	99%
Fast Trace CI	97%	98%	89%	99%
Ellipsoid Intersection	96%	98%	68%	97%
Kalman filter	98%	98%	87%	97%

4.3.2.6 Scenario Three Conclusion.

This scenario has demonstrated single agent and fused geolocation performance in mountainous terrain. The results show that a surface of the earth constraint can improve geolocation performance even more so in mountainous area than flat terrain. As a corollary, the method by which the ground constraint is applied is important, and an incorrectly applied or tuned method can cause more harm than good.

4.4 Consolidated Results

In order to facilitate an analysis of the data presented in the previous sections, it it is useful to examine some of the consolidated performance metrics from all three scenarios. In particular, the improvements due to the application of a high-fidelity surface of the earth constraint and geolocation estimate fusion are of interest, as well as the corresponding fused estimate consistency.

The first area of interest is the improvement due to the application of a high-fidelity DEM-based surface of the earth constraint. Table 61 tabulates the improvements in average miss distance and SMA length. Several basic patterns are apparent. The first is that the inclusion of the DEM-based constraint increases geolocation performance in nearly every case with the exception of the airborne AOA collectors against the AFIT target. The second observation is that the TDOA algorithm performance benefits the most from the constraint. Finally, it is notable that the greatest AOA performance increase is associated with the mountainous terrain present in the Afghanistan scenario.

Table 61. Improvement due to surface of the earth constraint

	AFIT		Libya		Afghanistan	
Agent	Avg Miss	SMA	Avg Miss	SMA	Avg Miss	SMA
AOA SV	15%	6%	16%	8%	22%	17%
AOA AV	8%	-0.5%	14%	14%	37%	14%
Four-ball TDOA SV	82%	73.2%	74%	65.7%	12%	4%
Three-ball TDOA SV	82%	83.4%	78%	79.0%	84%	85%
Three-ball TDOA AV	-	-	NA	NA	33%	9%

The next area of interest is the improvement due to fusing geolocation estimates. The numerical results for each scenario are reported in in sections 4.1 to 4.3 as well as Appendix B, but it is useful to consider graphical representations in order to observe patterns and draw general conclusions. Figure 63 shows the reduction in average miss

distance, SMA length and corresponding ellipsoid and ellipse consistency for each of the fusions in the AFIT scenario. Of note is the fact that the improvement to the airborne AOA geolocation estimates is negligible and that the TDOA agents benefit the most from augmentation. This is not unexpected as the TDOA geolocation agent uncertainty ellipsoids are the largest, and thus have the most to gain from augmentation. Similarly, Figure 60 shows the graphical depiction of the improvement due to estimate fusion in the Libya scenario. Many of the same patterns are present, but an important difference is the significant improvement in average miss distance and SMA associated with the airborne AOA geolocation agent solutions. This is due to the restricted collection geometries and increased slant range associated with the airborne collectors in the Libya scenario. Finally, Figure 61 shows the performance improvement due to estimate fusion in the Afghanistan scenario. Again, similar patterns are present including the fact that TDOA geolocation solutions are most improved by augmentation and that there are significant improvements to the airborne AOA geolocation agent solutions. Another pattern of note throughout all three scenarios, and visible in the aforementioned figures, is the fact that the average ellipsoidal consistency associated with the ground constrained geolocation solutions tends to be lower than that of the unconstrained solutions. This may be due to the fact that the ground constrained ellipsoid is relatively thin in the "up" direction making it more likely that solutions will lie directly above or below the ellipsoid. This is supported by the fact that the associated 2D ellipse consistency is higher in all cases than than 3D ellipsoid consistency.

Building off the consolidated performance increases in each scenario, it is useful to consider the average achieved consistency for each fusion algorithm across all three scenarios. To this end, Tables 62 and 63 tabulate the average achieved ellipsoid and ellipse consistency respectively. Once again, it is possible to use this consolidated

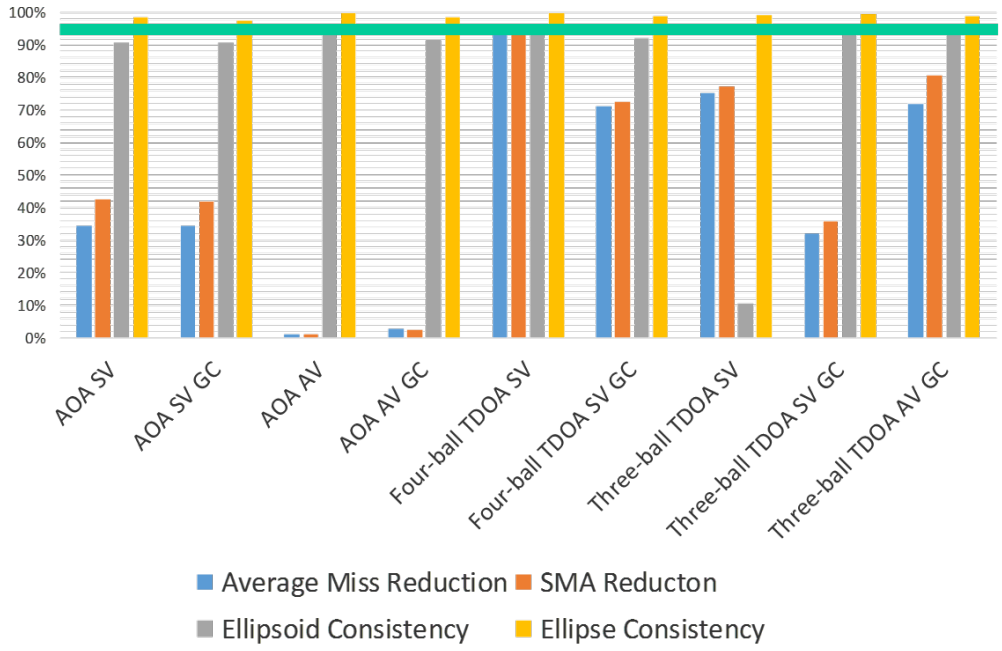

Figure 59. Average improvement due to estimate fusion against AFIT target using Kalman filter

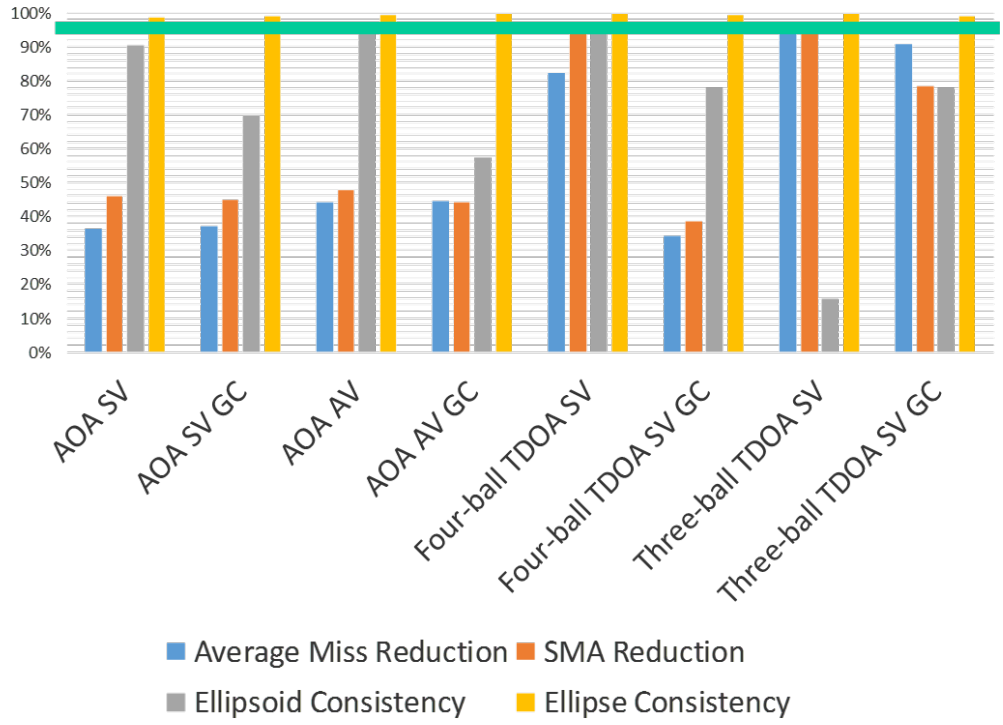

Figure 60. Average improvement due to estimate fusion against Libya target using Kalman filter

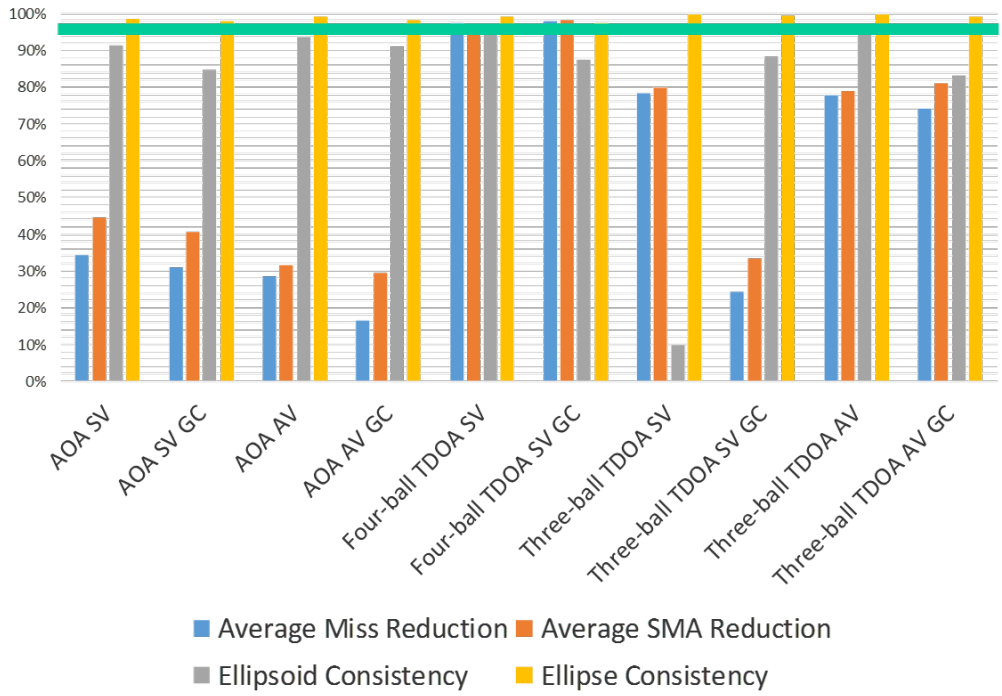

Figure 61. Average improvement due to estimate fusion against Afghanistan target using Kalman filter

data to observe patterns and draw general conclusions. The first item of note in the ellipsoid consistency is the relative performance of the selected fusion techniques. Both the Fast Trace and Fast Determinant CI algorithms have average consistencies at or above the target 95% level in most unconstrained cases. Likewise, the Kalman filter meets the desired 95% level in all but the cases augmenting AOA satellite and three-ball TDOA satellite agents. In contrast, the LE and EI algorithms have more variable consistency with the EI algorithm failing entirely to fuse the three-ball TDOA satellite agent estimate with the augmenting AOA satellite agent estimate. This pattern is repeated in the ground constrained cases, with the notable exception of a general reduction in consistency in most cases. However, it should be noted that the ellipsoid consistency of the three-ball TDOA satellite agent actually increased significantly. This is likely due to the fact that the ground constrained solutions introduce more variance in the "up" direction than is present in the "unconstrained"

solutions, which are nearly planar due to the explicit radius of the earth constraint included in the three-ball geolocation algorithm. The final observation is the fact that the EI algorithm fails in nearly all of the ground constrained test cases. Finally, moving to the ellipse consistency, the primary observation is that in all cases the ellipse consistency is higher than that of the corresponding ellipsoid. This is expected as the ellipse consistency measurement is 2D and includes estimates that would otherwise lie above or below the ellipsoid. It should also be noted that there is less variation between ground constrained and unconstrained ellipse consistency than there is in ellipsoid consistency.

Table 62. Average ellipsoid consistency across all scenarios

Unconstrained					
	Fusion Algorithm				
Augmented Agent	LE	Fast Det CI	Fast Trace CI	EI	Kalman filter
AOA SV	92%	96%	97%	91%	91%
AOA AV	95%	95%	96%	60%	95%
Four-ball TDOA SV	88%	96%	96%	75%	95%
Three-ball TDOA SV	11%	46%	86%	-	11%
Three-ball TDOA AV	78%	96%	97%	95%	95%
Ground Constrained					
	Fusion Algorithm				
Augmented Agent	LE	Fast Det CI	Fast Trace CI	EI	Kalman filter
AOA SV	88%	94%	95%	-	82%
AOA AV	87%	89%	91%	-	80%
Four-ball TDOA SV	76%	91%	92%	-	81%
Three-ball TDOA SV	93%	95%	96%	-	87%
Three-ball TDOA AV	82%	91%	93%	90%	88%

4.5 Summary

This chapter presented the results for individual geolocation agents as well as multi-agent estimate fusions in three distinct target scenarios. In addition to the

Table 63. Average ellipse consistency across all scenarios

Unconstrained					
		Fusion Algorithm			
Augmented Agent	LE	Fast Det CI	Fast Trace CI	EI	Kalman filter
AOA SV	97%	99%	100%	98%	98%
AOA AV	99%	99%	100%	99%	99%
Four-ball TDOA SV	89%	98%	99%	95%	95%
Three-ball TDOA SV	97%	99%	100%	-	100%
Three-ball TDOA AV	99%	99%	99%	99%	99%

Ground Constrained					
		Fusion Algorithm			
Augmented Agent	LE	Fast Det CI	Fast Trace CI	EI	Kalman filter
AOA SV	96%	99%	99%	-	98%
AOA AV	99%	99%	99%	-	99%
Four-ball TDOA SV	98%	99%	99%	-	99%
Three-ball TDOA SV	100%	100%	100%	-	99%
Three-ball TDOA AV	95%	98%	99%	98%	98%

numerical MOPs, as provided in the preceding sections, a number of general patterns were observed and noted, such as the orientations of error ellipsoids, relative performance of different geolocation agents, and the effect of terrain variation on the ground constrained estimates. Several of these observations warrant elaboration.

The first observation was the general pattern of ellipsoid orientation. AOA geolocation agents produced error ellipsoids that were oriented with the SMA along the average line-of-sight vector. Collectors that passed directly overhead yielded ellipsoids with the SMA along the path of travel while offset collectors, for example pass geometries 2, 3, 5, and 6 against the AFIT target, yielded ellipsoids with the SMA approximately normal to the path-of-travel as shown in Figure 62. Three-ball TDOA geolocation agents showed the same general pattern, but were not as sensitive to offset. For instance, against the AFIT target, pass geometries 2 and 5 yielded ellipsoids that were still predominantly in-line with collector movement, whereas pass geome-

tries 3 and 6 were approximately normal to the path-of-travel. It is also worth noting that the three-ball TDOA ellipsoids had higher eccentricity than those produced by AOA collectors. Lastly, four-ball TDOA geolocation agents showed the same pattern as the three-ball collectors, but with even greater eccentricity.

The next observation is also related to the orientation of the uncertainty ellipsoids. When fusing multiple estimates, the relative orientation of the ellipsoids does have an impact. The magnitude of the impact varies with fusion algorithm with the CI techniques being most effected and the Kalman filter being the least, but overall the fusion of two estimates with dissimilar ellipsoid orientations yields more accurate fused estimates with a smaller fused uncertainty ellipsoid than the fusion of two estimates with similar ellipsoid orientations . For example, fusing an AOA SV pass geometry 2 with a pass geometry 1 yields a smaller combined ellipsoid than fusing with a pass geometry 4, despite the fact that pass 1 and 4 individually have similar sized uncertainty ellipsoids. This pattern is visible in Figure 63 and holds for the other collection phenomenologies as well. However, it is important to stress that the impact is related to the relative orientation of the estimate uncertainty ellipsoids, and not the relative orientation of the collection passes. For instance, three-ball SV pass geometries 2 and 6 are dissimilar, the former is an ascending pass while the later is a descending, but the uncertainty ellipsoids generated from each are similar in orientation. The precise magnitude of the effect is difficult to ascertain due to the fact that ellipsoid orientation and size are confounded in this research, but it is a notable pattern and should be the subject of future research.

There was also an observation related to the application of the surface of the earth constraint. It was noted in multiple cases, predominantly those employing four-ball TDOA agents, that the application of a surface of the earth constraint yielded a relatively tight grouping of estimates with a small number far removed. This indicates

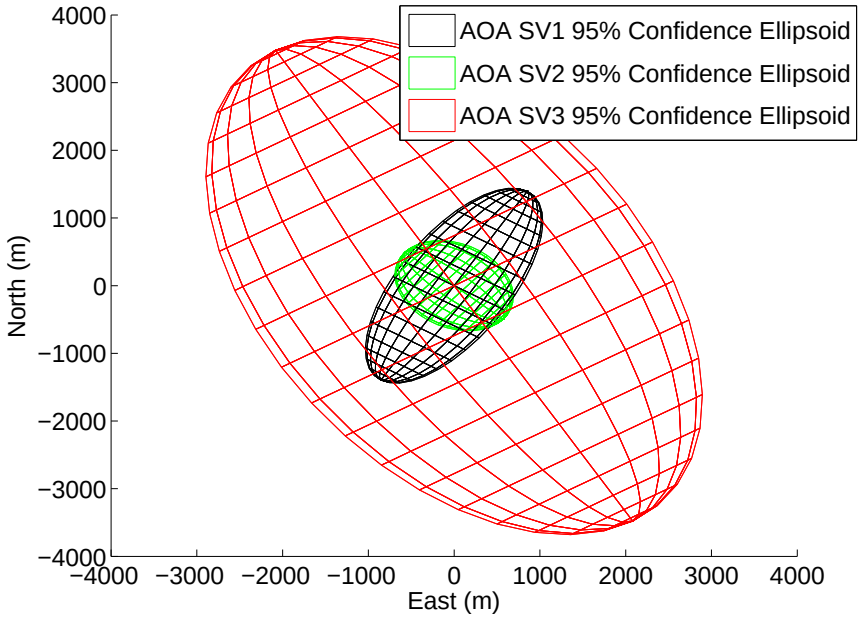

(a) AOA satellite passes 1, 2, and 3

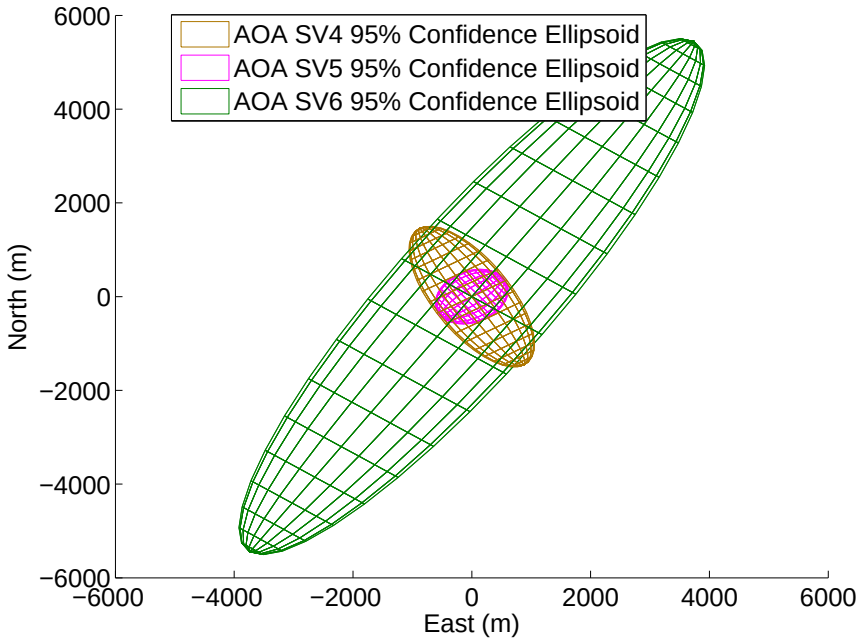

(b) AOA satellite passes 4, 5, and 6

Figure 62. Ellipsoid orientations

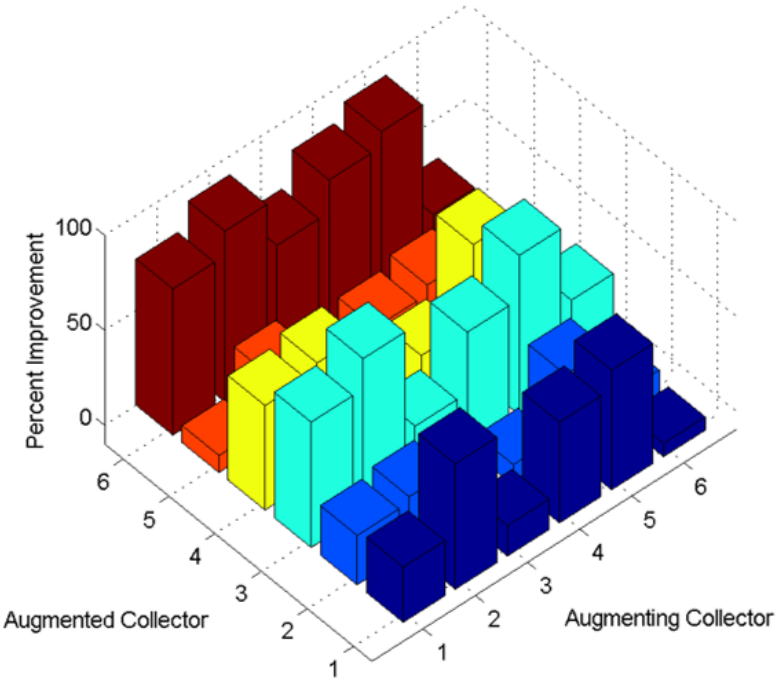

Figure 63. Example of geometry dependent SMA improvmentMA improvement

that the method of application periodically causes an estimate to diverge further from truth. Further research should be conducted to increase the sophistication of both the geolocation algorithms and the application of the DEM based surface of the earth constraint to intelligently discard erroneous solutions.

The final observation is in regards to the proposed MPTPS MOP. While the MPTPS was originally envisioned as an effective way to capture the amount of intersection between the ground and the uncertainty ellipsoid, in practice it has shown to be of limited utility with significant drawbacks. Foremost among the drawbacks is the fact that it is a computationally expensive MOP to calculate. Furthermore, the MPTPS is not a good metric when there is little intersection between the ground and uncertainty ellipsoid as was observed with the unconstrained three-ball TDOA agents. Finally, it is of limited utility due to the fact that when the MPTPS is valid, it usually closely parallels the SMA, which is easily calculated. Considering the drawbacks and marginal gain, the MPTPS is not recommended for future use as an MOP.

V. Conclusion

The goal of this research was to evaluate the military utility of an AOA geolocation payload on a CubeSat operating in either a tipping-and-cuing or cross-platform collection capacity. To accomplish this goal, the performance of a proposed single-ball AOA CubeSat was modeled, along with three and four-ball TDOA satellite, AOA aircraft and three-ball TDOA aircraft representative reference collectors. The individual performance of each collection agent was analyzed to set a baseline before augmenting each individual agent with estimates from the AOA SV agent via a number of different fusion algorithms. The single agent and fused results were quantified using a number of established MOPs including the average miss distance, RMSE, ellipsoid volume and ellipsoid SMA, as well as the newly proposed MPTPS MOP. A total of three different scenarios were considered in order to test the performance in operationally representative situations and terrain types. Additionally, a high fidelity DEM based surface of the earth constraint was developed and employed in an attempt to improve geolocation performance.

This chapter will present the conclusions based upon the results presented in Chapter IV, focusing on the proposed surface of the earth constraint, the effectiveness of the employed fusion algorithms, and finally an overall evaluation of the military utility of a single-ball AOA CubeSat as an augmentation to existing platforms. Additionally, recommendations for future research to improve or build upon this work will be discussed.

5.1 Surface of the Earth Constraint

This research has demonstrated the power and utility of a high fidelity DEM based surface of the earth constraint. The application of such a constraint utilizing

SRFT-2 data resulted in near universal improvement to geolocation MOPs. The only instances in which application of the constraint had no positive impact were the cases at the opposite ends of the accuracy spectrum. Very accurate 3D solutions with an average miss distances on the order of one to two times the post spacing of the terrain data saw no improvement. Very inaccurate 3D solutions would occasionally diverge even further when allowed to iterate in search of a better constrained solution. Additionally, in some cases, predominantly in scenario three, it was noted that the application of a surface of the earth constraint resulted in a small number of solutions diverging from the true solution. This indicates that the precise method by which the ground constraint is applied, particularly in mountainous terrain, is an important consideration. Although the specific technique presented in this work may not be the optimal solution, and is computationally expensive, it can serve as a basis for comparison and future optimization studies.

5.2 Fusion Technique Efficacy

This research examined six different fusion techniques, described in section 2.4, in an effort to determine which is most suitable for fusing geolocation estimates from dissimilar collection platforms and geolocation phenomonologies. The performance of each algorithm as measured by the MOPs and the resulting consistency of fused estimates was reported in Chapter IV. The conclusions drawn from this data, both in regards to individual algorithms as well as general guidelines for use, follow. The primary criterion are the flexibility and robustness of the algorithm and the achieved consistency. Recall that the desired consistency is 95% and that an achieved consistency greater than that value indicates that the uncertainty ellipsoid is excessively conservative, that is, the ellipsoid is larger than it needs to be, which will be reflected in the SMA and MPTPS MOPs. Alternatively, an achieved consistency less than 95%

indicates that the uncertainty ellipsoid underestimates the true variance. As this is a statistical process, and only a finite sample size was used, the consistency is unlikely to be precisely 95%, so the range of 93% to 97% is considered to be acceptable.

The Kalman filter fusion technique proved to be one of the most flexible and robust fusion algorithms. The algorithm was able to reliably fuse all estimates regardless of covariance orientation and shape. Unlike some of the algorithms tested, the Kalman filter was able to process the nearly 2D covariance associated with the three-ball TDOA algorithm and ground constrained estimates in flat target areas. It is also robust to highly 3D covariance, or covariance with significant variance in all three axes, such as that associated with non-ground constrained estimates as well as ground constrained estimates in mountainous terrain. One of the expected downsides of the Kalman filter is that the estimates and the associated uncertainty produced may be excessively confident in the presence of any unknown or unquantified measurement correlation resulting in an underestimate of the true covariance. As this research employed Gaussian white noise in a stochastic model, correlation was not expected, but this is an area recommended for future research. Regardless, the Kalman filter applied to the test cases described produced fused estimates with associated covariance and uncertainty ellipsoids smaller than either of the individual estimates while maintaining good consistency.

Three distinct forms of the CI fusion algorithm were tested; the Fast Determinant, Fast Trace and the Improved or New Fast formulations. Both of the "legacy" fast formulations performed well, and were very robust in that they were able to handle all of the estimates. However, as expected, they were both excessively consistent; meaning that they overestimate the true covariance ellipsoids. The Improved Fast Formulation was designed to ameliorate that issue. However, this research encountered difficulties in applying the Improved Fast formulation. At this point, additional work is required

to confirm or reject that particular algorithm before any performance conclusions can be made.

The Ellipsoid Intersection algorithm was designed in an attempt create an algorithm that would always produce a fused estimate with a smaller uncertainty than either of the individual estimates alone. This research showed that the algorithm, while novel, suffers from a lack of robustness. In some cases, particularly those with significant estimate variation in all three axes, such as non-ground constrained AOA, it produces good estimates with a smaller uncertainty ellipsoid than either source individually. However, in other cases, particularly ground constrained and three-ball TDOA, the technique produces nonsensical estimates with the fused estimate located at extremely long distances from either source estimate. It is possible that this technique could be adapted to overcome this issue, but the possibility was not explored in this research. As such, the Improved Fast technique is not recommended.

The final fusion technique employed was the LE algorithm. Recalling from Chapter II that the LE algorithm was developed with the goal of slightly underestimating the area of intersection of the covariance ellipsoids instead of slightly overestimating as in CI, this algorithm performed largely as expected. The fused estimates resulting from this technique are the same as those produced by the Kalman filter with fused covariance that is typically only slightly larger.

Based upon this research, the Kalman filter and Largest Ellipsoid algorithms appear to be the best choices. The final answer is contingent upon the the exact nature of the geolocation scenario and fusion methodology. For uncorrelated geolocation estimates, the Kalman filter is the optimal fusion technique, in the presence of any correlation, the Largest Ellipsoid algorithm may be better suited.

5.3 Evaluation of Military Utility

The overarching goal of this research was to evaluate whether or not there is military utility in the use of a single-ball AOA geolocation payload hosted on a CubeSat as an augmentation to existing platforms. Based upon the scenarios completed, it appears that there is military value when the system to be augmented has similar or worse geolocation performance than the augmenter. Additionally, it was observed that the greatest improvements result from the addition of an augmenting estimate with an uncertainty ellipsoid oriented in a different direction than that associated with the estimate to be augmented. Overall, improvements due to augmentation on the order of 30% or greater were common throughout the analyzed scenarios. The only geolocation agents that did not benefit were the airborne collectors that were very near the emitter. However, in operationally representative scenarios where it is undesirable, impracticable, or impossible to fly in close proximity to the emitter, the addition of the single-ball AOA satellite provided a compelling improvement to the geolocation MOPs. Furthermore, as this research showed augmentation has the greatest impact when applied to less precise geolocation solutions, this system may be particularly useful when employed near the periphery of an existing systems' capability to "fill in" and keep the fused geolocation performance constant. Ultimately, the true performance of the operational system(s) to be augmented must be included and the resulting performance weighted against the added cost and complexity of adding an augmentation system. As one of the strengths of the CubeSat platform is relatively low cost and complexity, it is expected that the cost/benefit ratio will be favorable.

5.4 Recommendations for Future Study

This research uncovered a number of areas for additional study. Some of these areas stem from the assumptions utilized in this research, while other are a direct result of noted behaviors, weaknesses, and predicted extrapolations. Overall, the recommended areas of study can be binned into three groups; general signal measurement and geolocation algorithm topics, the application of a surface of the earth constraint, and estimate fusion.

The first area of opportunity is in the realm of signal measurement and geolocation algorithms. Three significant assumptions were made in this area with each representing a research opportunity. Foremost among these assumptions was the neglection of co-channel interference. In real-world applications, there are likely to be other systems transmitting in the same frequency range as the SOI. Each of these represents a potential source of co-channel interference that would reduce the effective SNR for the geolocation algorithm. An effort should be made to include the effect of interference on geolocation performance as well as processing techniques to reduce the impact. The next assumption that must be addressed is that the process of association occurs perfectly. This researched assumed that either there was a single emitter, or that it was possible to identically determine from which of multiple emitters the signal emanated. Again, in the real world, it is very possible for there to be multiple emitters of the SOI within view of the SV at any given time. This is also important due to the fact that one of the limitations of the MUSIC algorithm is that it is only able to resolve $m-1$ signals where m is the number of antenna elements. Depending upon the SOI and the region of the world, it may be possible to have more emitters than space available for antenna elements on a CubeSat which, in the very least, necessitates alternative methods for determining the signal source. The final suggested area of research in this realm is comparing the performance of theoretical or modeled

antenna and receiver sets and the true performance. A CubeSat form factor is likely to require compromises which may yield lesser than predicted performance. Research should be completed to characterize the true achievable performance.

The next area of recommended future study is the application of a DEM based surface of the earth constraint. This research represents a first iteration attempt, but there may be more practical, accurate, and computationally efficient approaches. Furthermore, since this is an area of research that is not well represented in published literature, there is ample room to explore new potential solutions. One specific suggestion is to develop a method to check the line of sight between any given position on the surface of the earth and the collection platform. By eliminating positions with obstructed line-of-sight, the possible locations of the emitter would be reduced. This capability could also be used to realistically reduce the number of signal captures resulting from the emissions being blocked by terrain. Another area that requires further study is to determine the best way to introduce a surface of the earth constraint in mountainous terrain. It may be necessary to introduce larger search boxes or search boxes that dynamically scaled depending upon the elevation variability so as to avoid the solution becoming "trapped" on a peak or in a valley where the immediately surrounding terrain yields a worse FOM. To this end, the inclusion of a large area DTED-0 level search may be beneficial. Alternatively, a modified particle filter approach may have merit. There are also opportunities to combine a surface of the earth constraint with other geolocation algorithms. The Direct Position Determination (DPD) algorithm presented by Small [33] is one algorithm that could benefit from the inclusion of terrain data. Similarly, the NLO AOA algorithm, as described by Hartzell, could incorporate a DEM in a manner similar to that used by Fowler [67].

The final area of recommended study is to explore alternative fusion techniques.

This research explored several of the most common types of generalized estimate fusion techniques, but was unable to make an exhaustive study. The extended and unscented Kalman filters are other techniques often utilized in the literature [79; 80; 34; 22], and should be investigated. Similarly, the Hough transform function technique is promising for fusing estimates from different geolocation phenomenologies [21; 81] and should be able to incorporate a DEM constraint. Finally, the consistency of fused estimates should be further explored, particularly in regards to correlation between measurements. This may be an attractive target for hardware testing.

5.5 Final Conclusions

In summary, the work presented herein represents a strong start to determining whether or not a single-ball AOA CubeSat has military utility. At this point, indications are good, however, further study and refinement are necessary before reaching a definitive conclusion. The next stage is addressing the simplifying assumptions, incorporating more sophisticated geolocation algorithms, and developing the framework in which augmentation will occur so that a definitive technique may be chosen.

Appendices

EVALUATION OF THE MILITARY UTILITY OF EMPLOYING AN ANGLE OF ARRIVAL PAYLOAD HOSTED ON A CUBESAT AS AN AUGMENTATION TO EXISTING GEOLOCATION SYSTEMS

A. Libya and Afghanistan Figures

1.1 Libya Single Geolocation Agent Figures

1.1.0.7 AOA Satellite Performance.

The following are the graphical depictions of the AOA SV geolocation agent solutions for the Libya scenario.

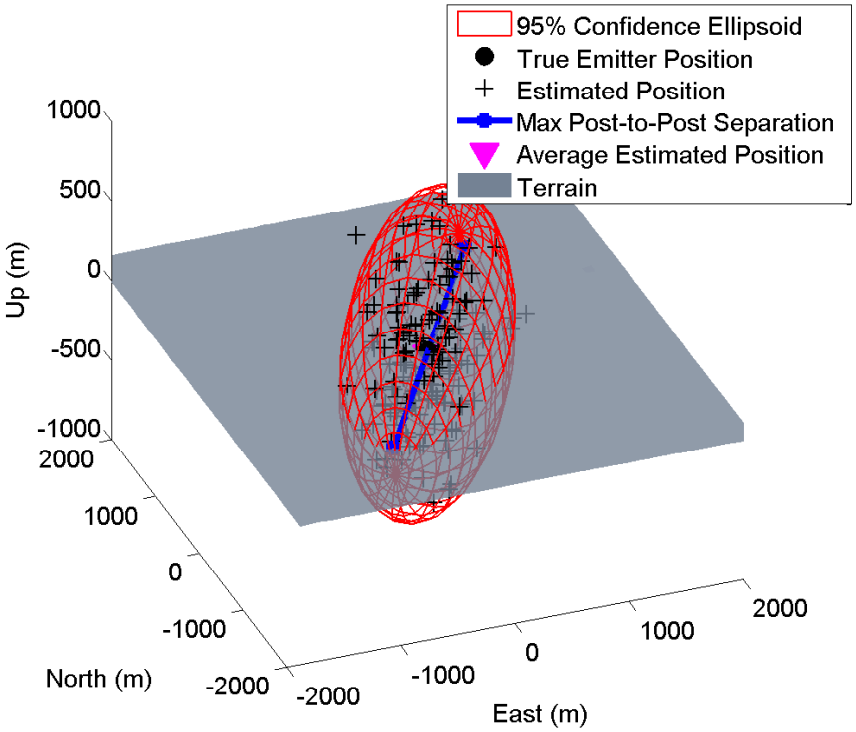

(a) No ground constraint

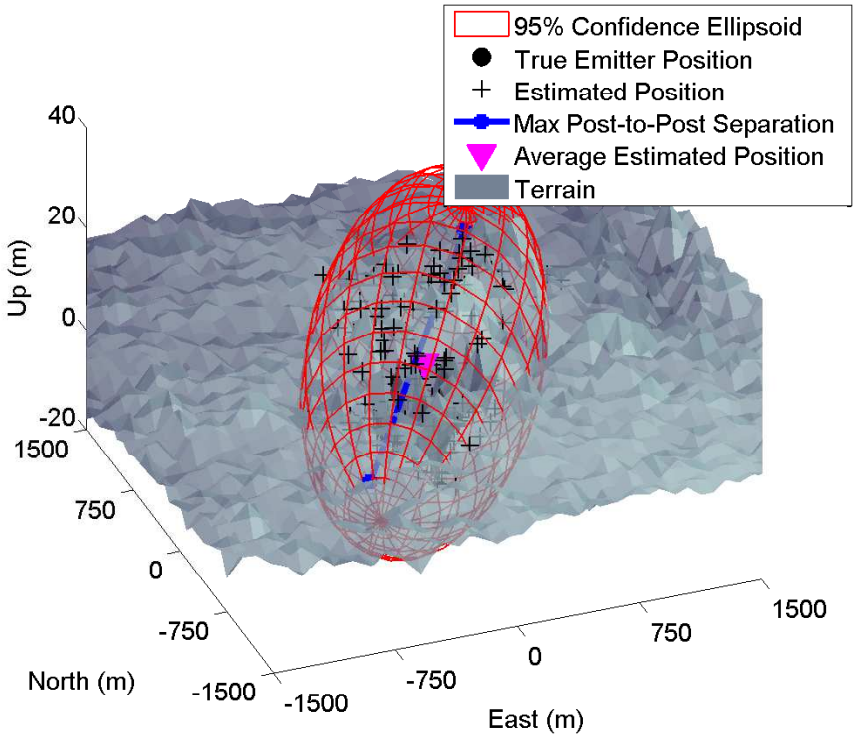

(b) Ground constrained

Figure 64. AOA satellite geometry 7 against Libya target

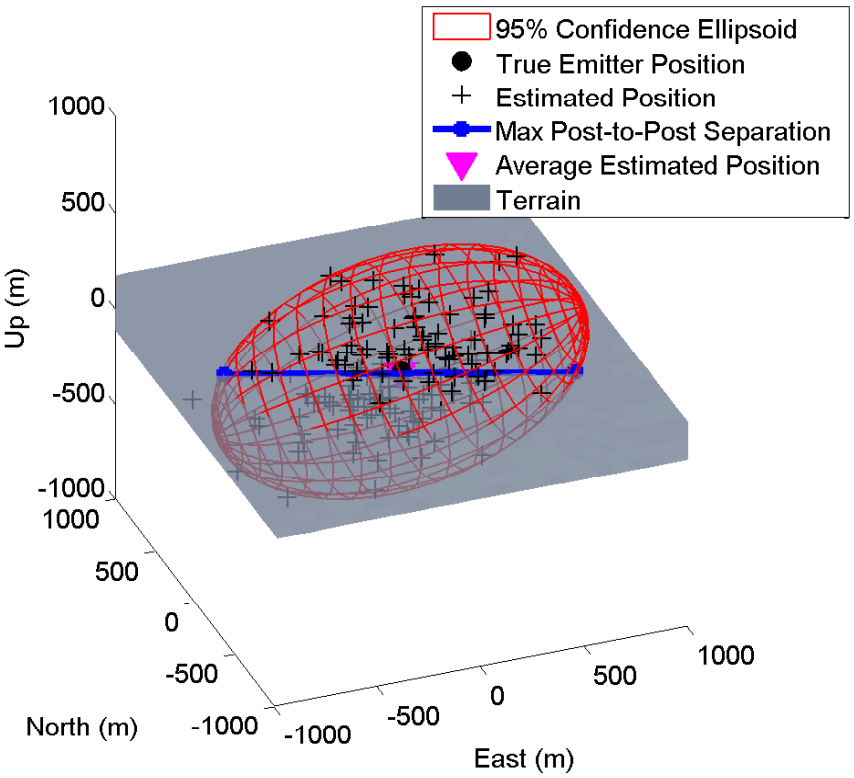

(a) No ground constraint

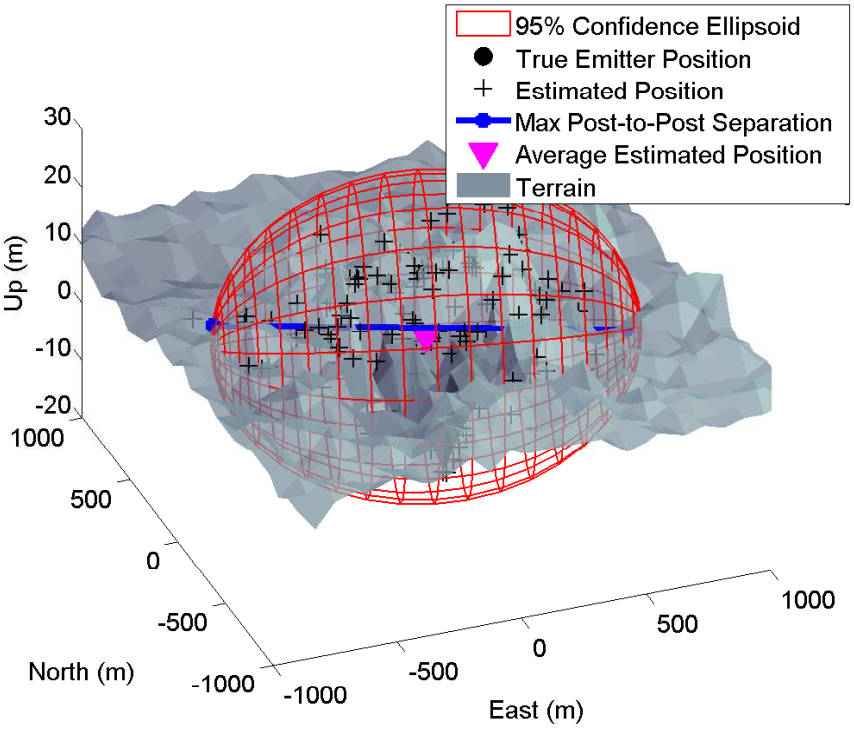

(b) Ground constrained

Figure 65. AOA satellite geometry 8 against Libya target

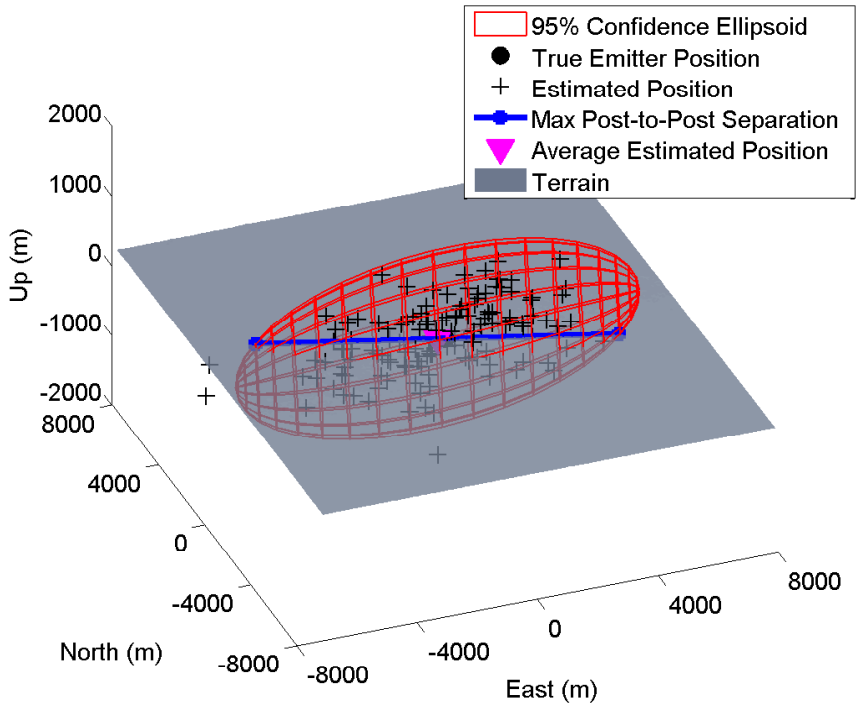

(a) No ground constraint

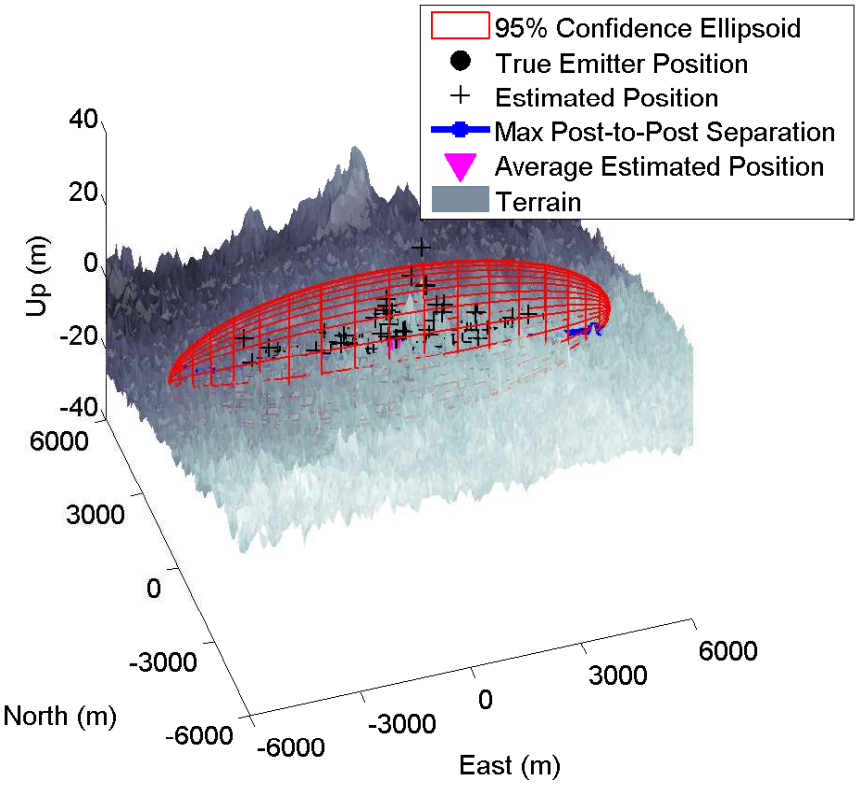

(b) Ground constrained

Figure 66. AOA satellite geometry 9 against Libya target

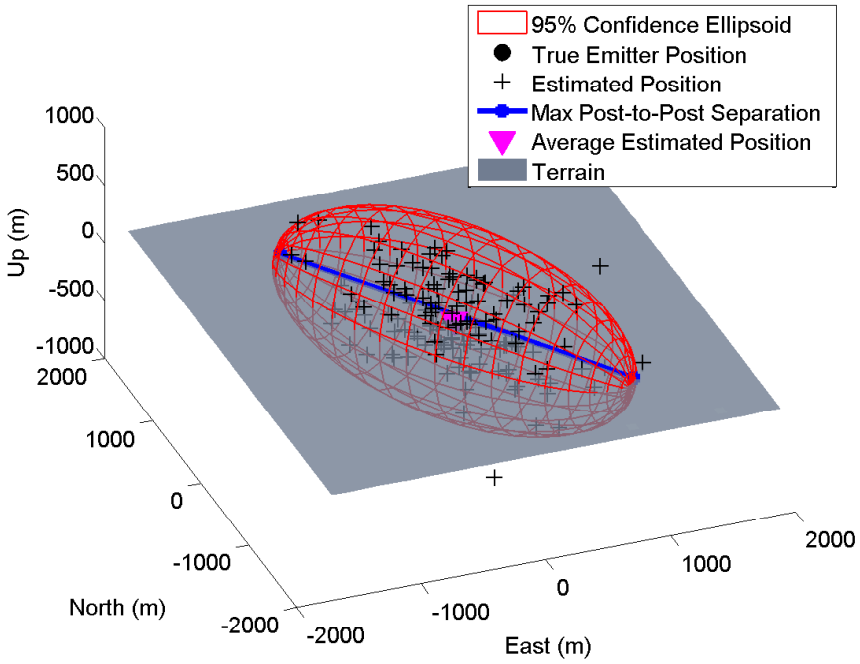

(a) No ground constraint

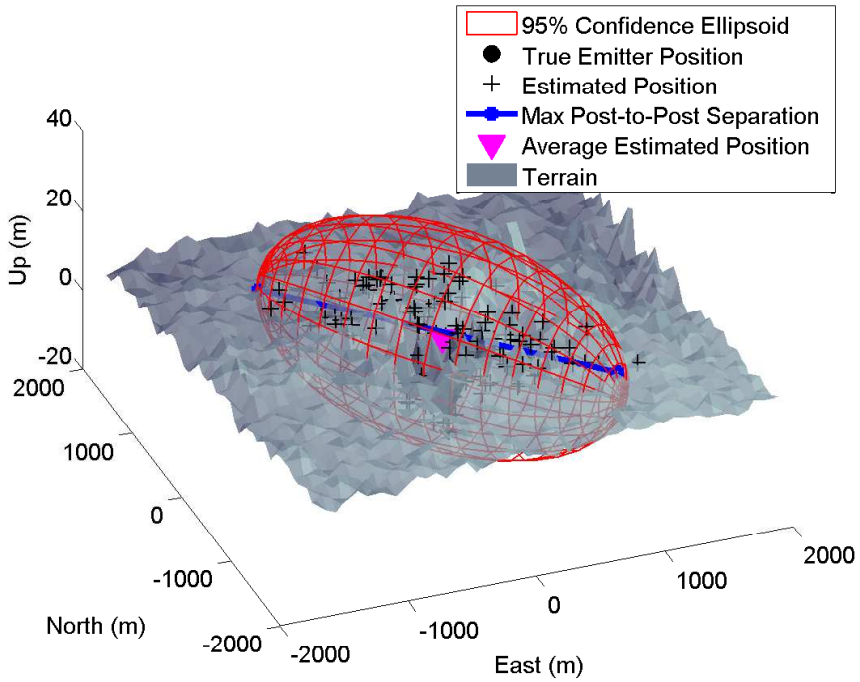

(b) Ground constrained

Figure 67. AOA satellite geometry 10 against Libya target

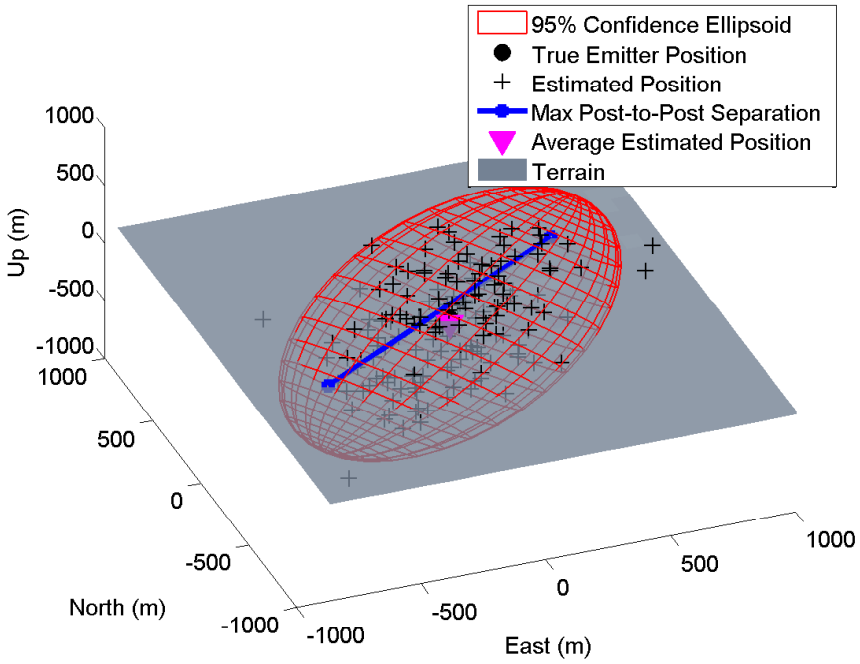

(a) No ground constraint

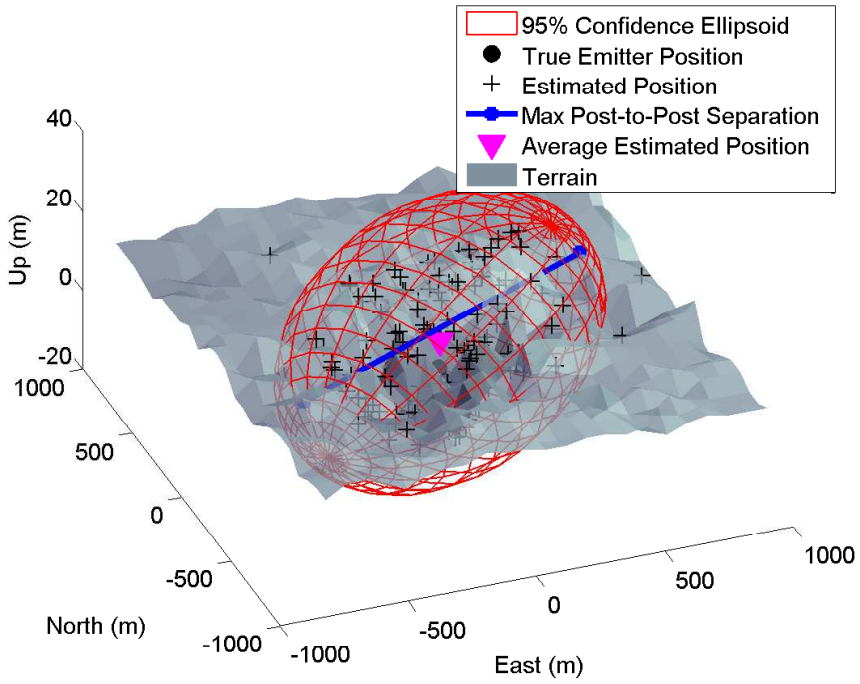

(b) Ground constrained

Figure 68. AOA satellite geometry 11 against Libya target

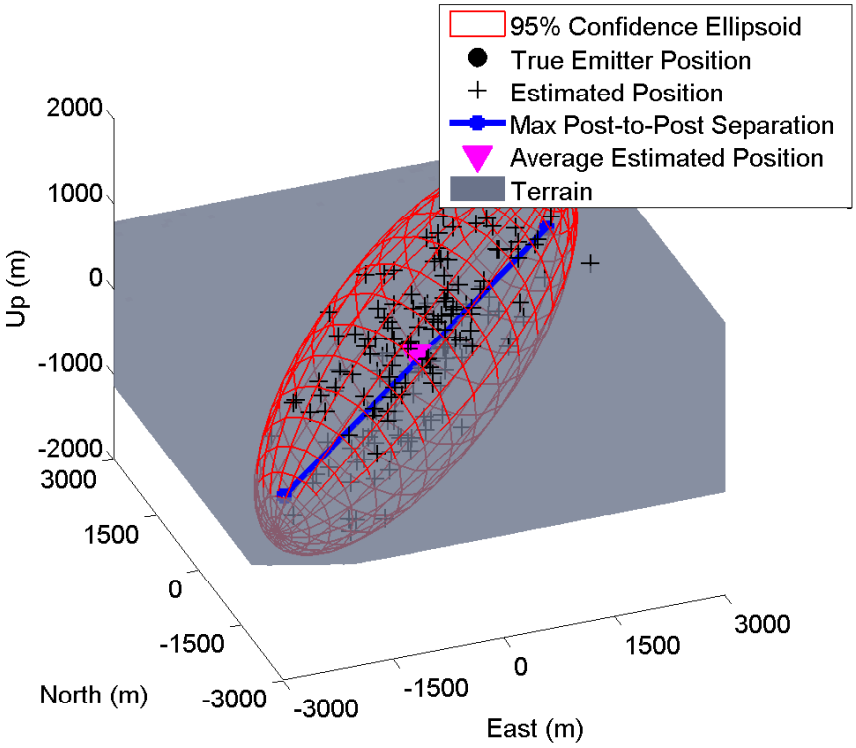

(a) No ground constraint

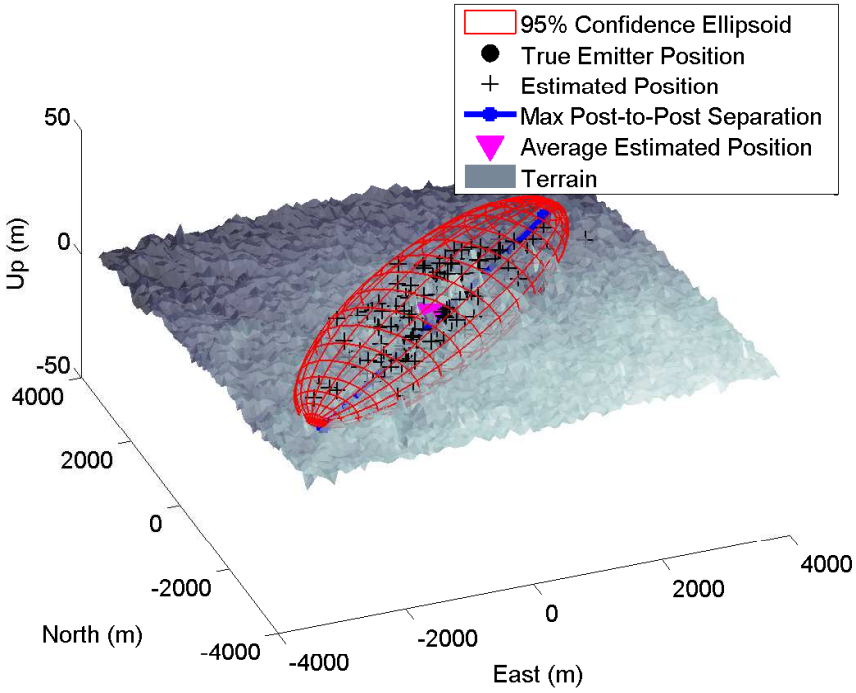

(b) Ground constrained

Figure 69. AOA satellite geometry 12 against Libya target

1.1.0.8 AOA Aircraft Performance.

The following are the graphical representations of the AOA aircraft geolocation agent solutions for the Libya scenario.

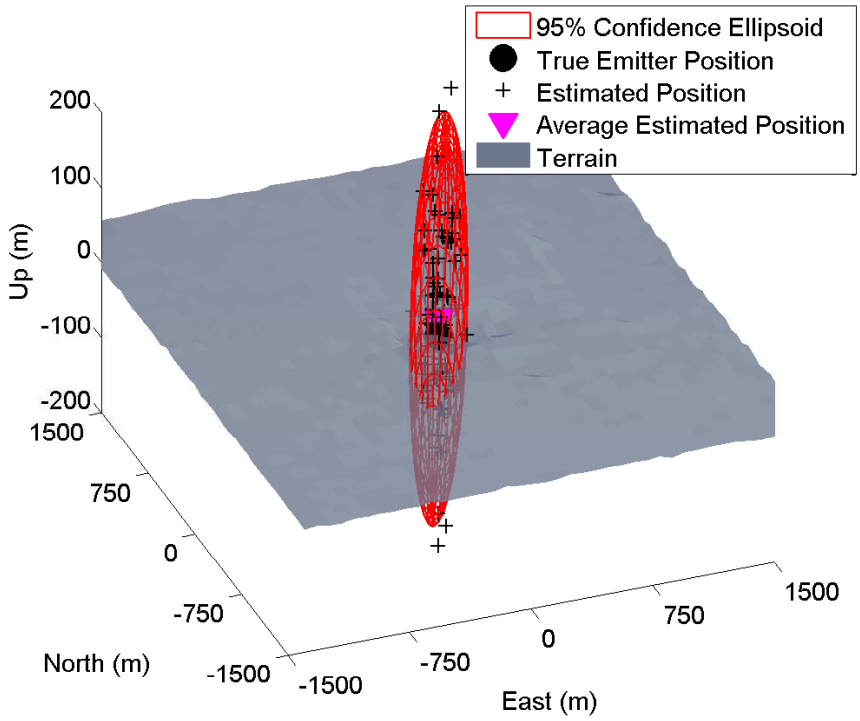

(a) No ground constraint

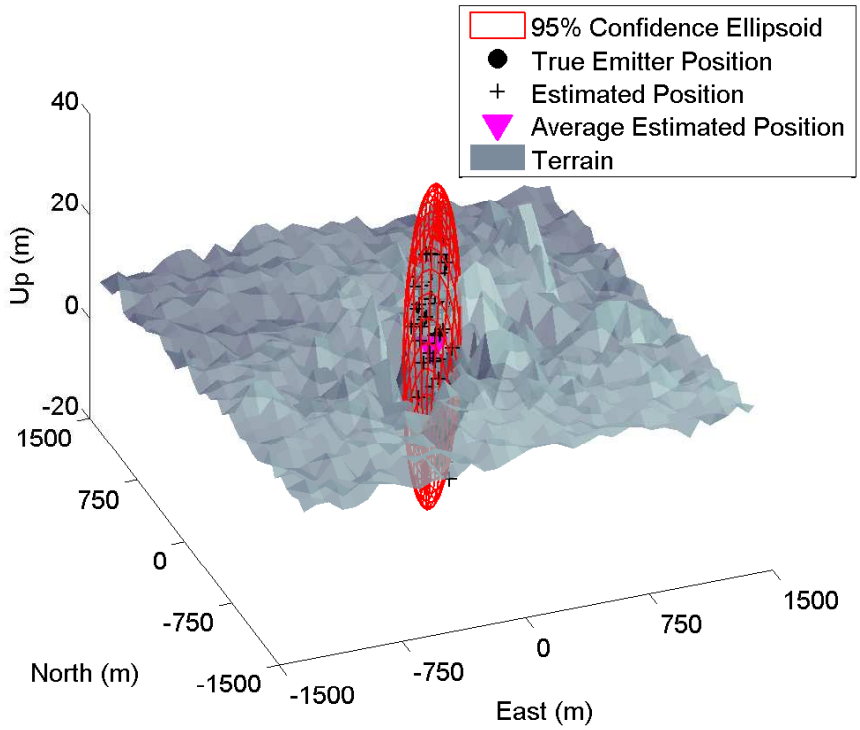

(b) Ground constrained

Figure 70. AOA aircraft geometry 7 against Libya target

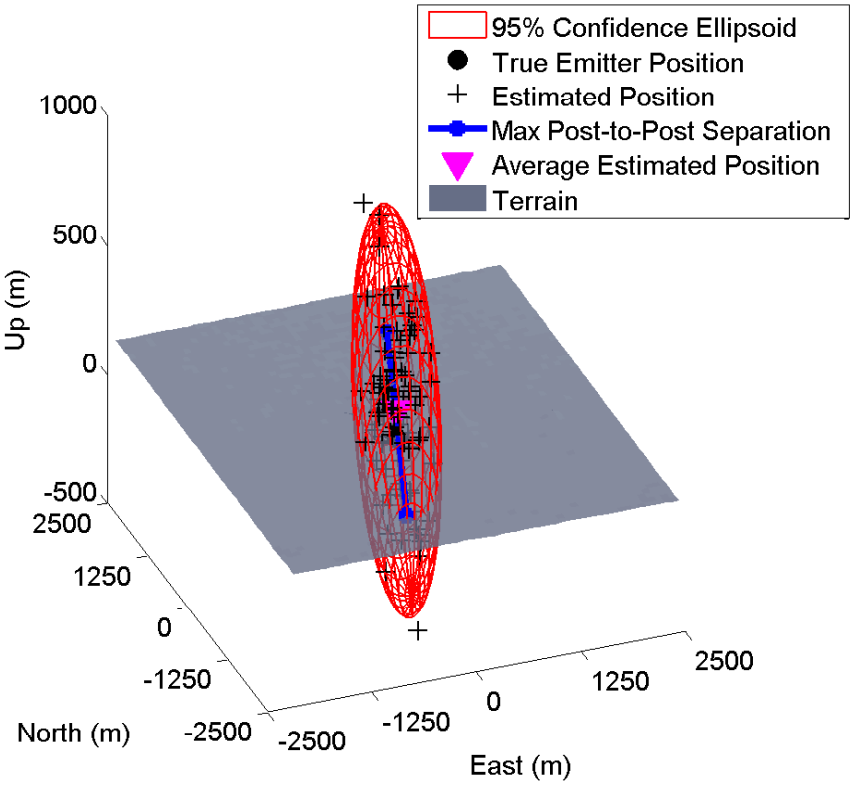

(a) No ground constraint

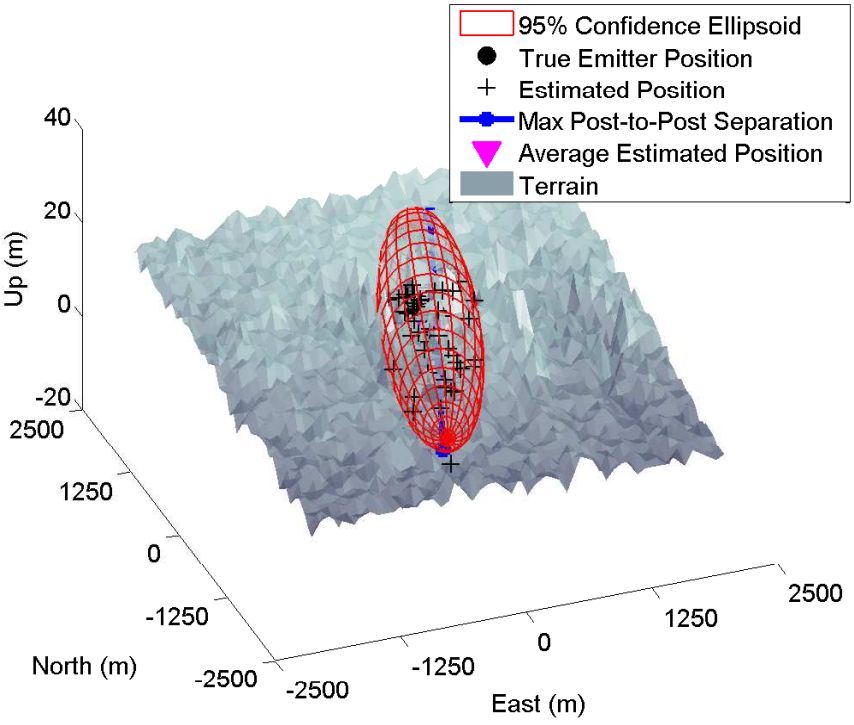

(b) Ground constrained

Figure 71. AOA aircraft geometry 8 against Libya target

1.1.0.9 Three-ball TDOA Satellite Performance.

The following are the graphical depictions of the three-ball TDOA SV geolocation agents solutions for the Libya scenario.

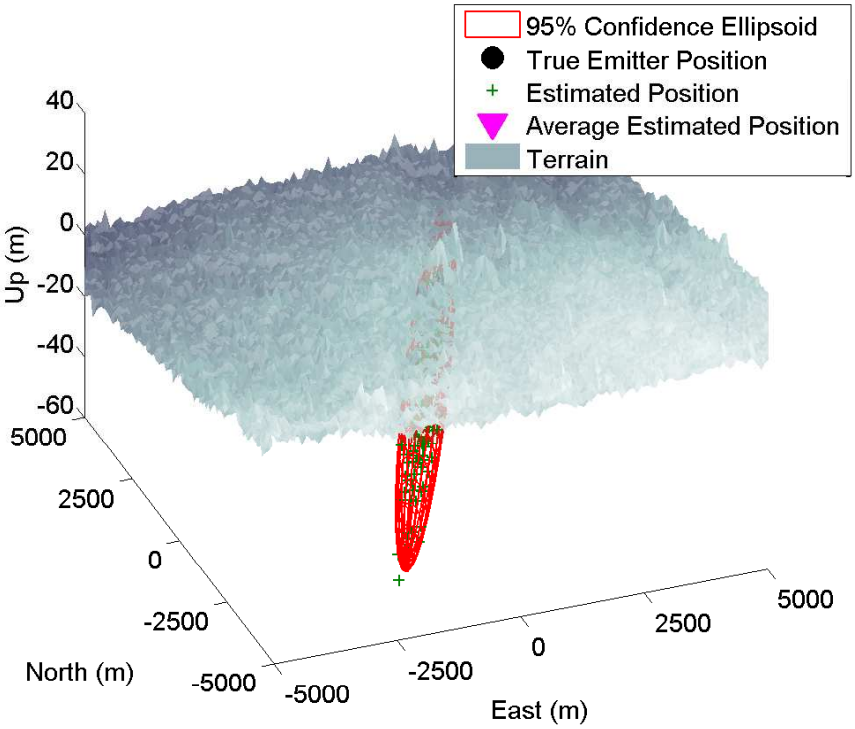

(a) No ground constraint

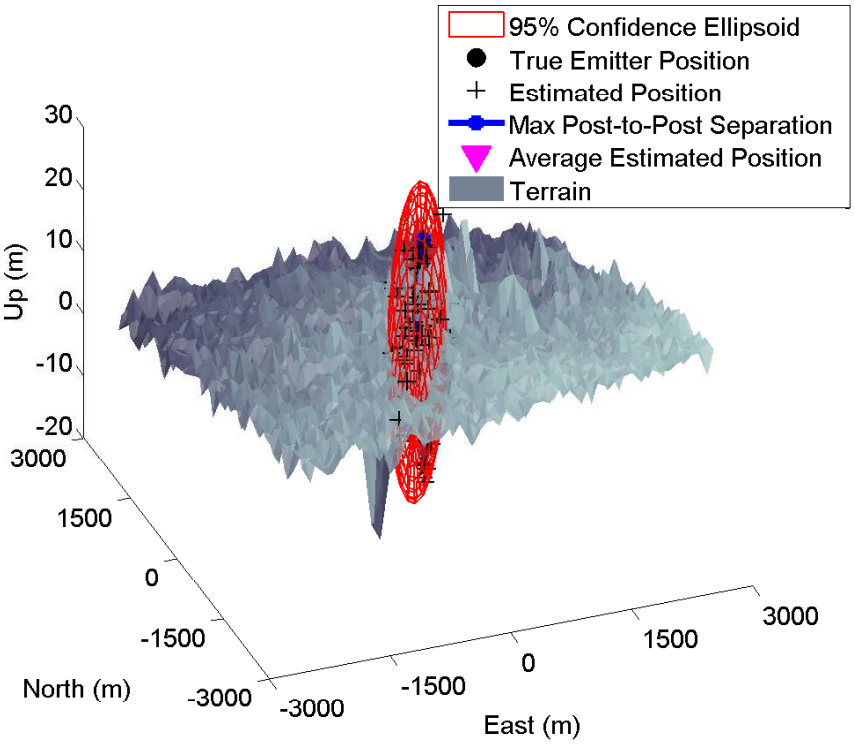

(b) Ground constrained

Figure 72. Three-ball TDOA satellite geometry 7 against Libya target

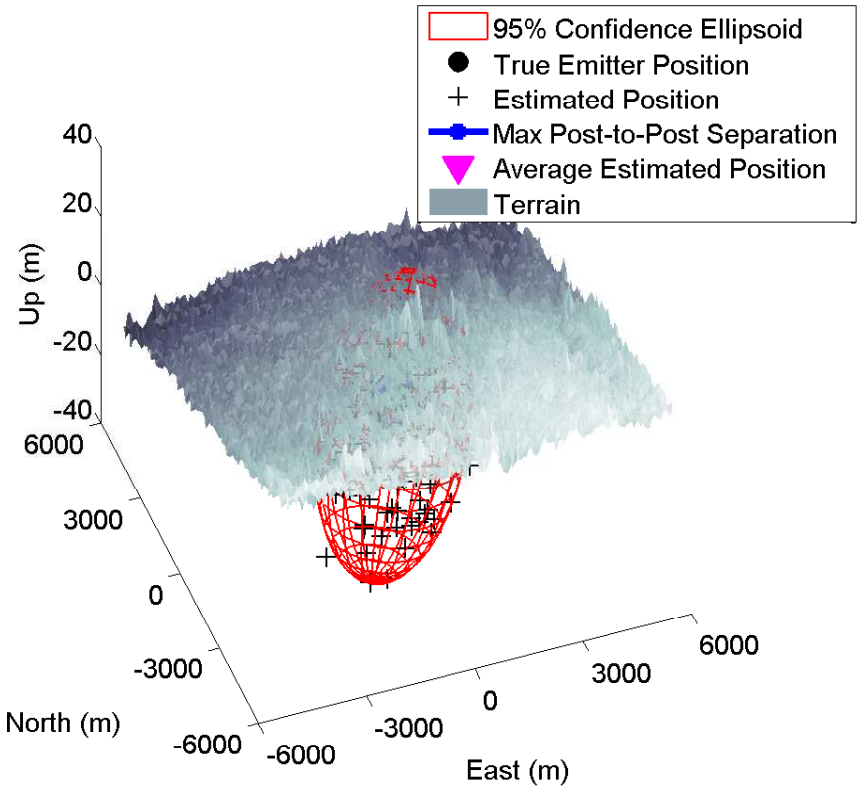

(a) No ground constraint

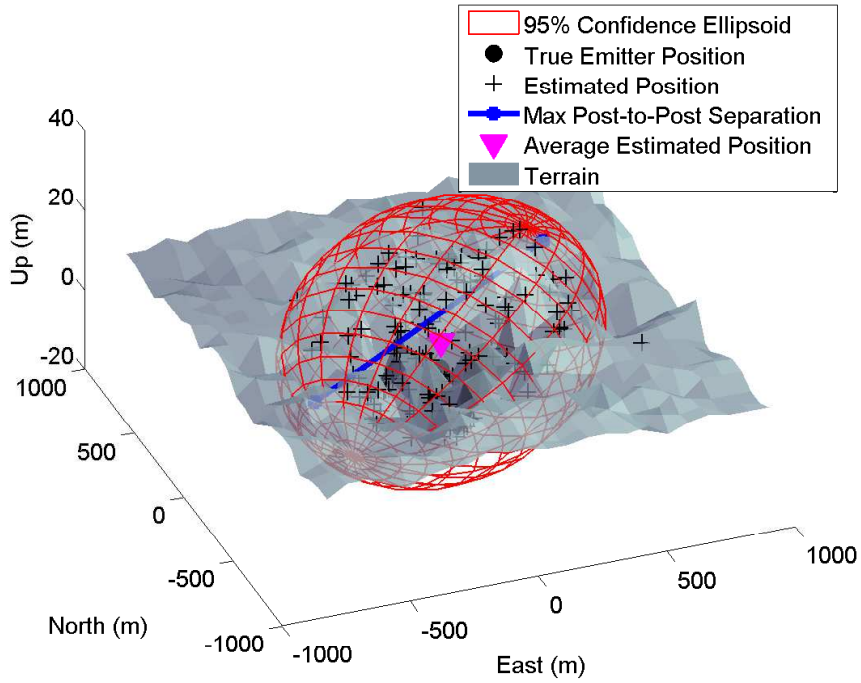

(b) Ground constrained

Figure 73. Three-ball TDOA satellite geometry 8 against Libya target

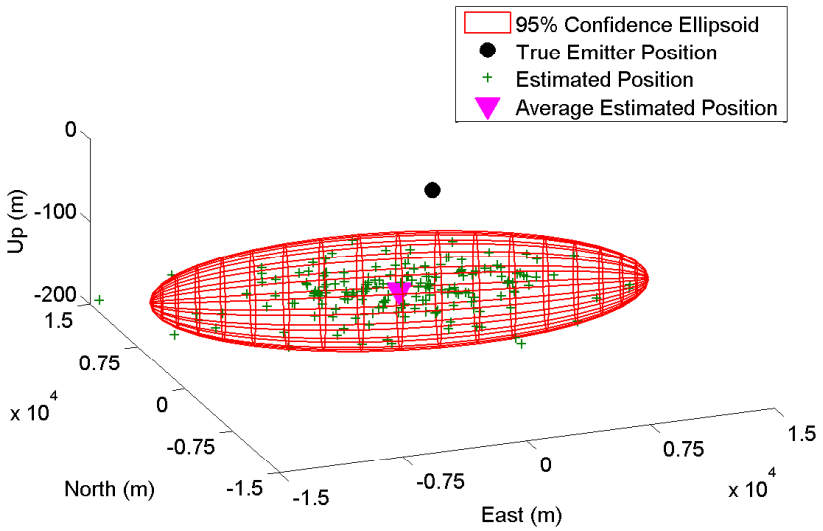

(a) No ground constraint

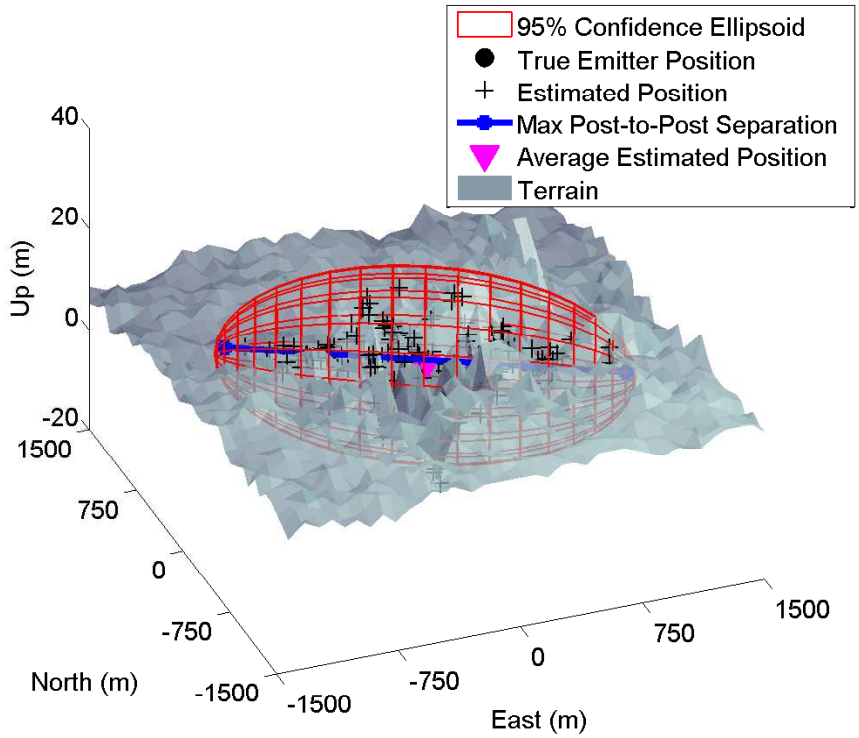

(b) Ground constrained

Figure 74. Three-ball TDOA satellite geometry 9 against Libya target

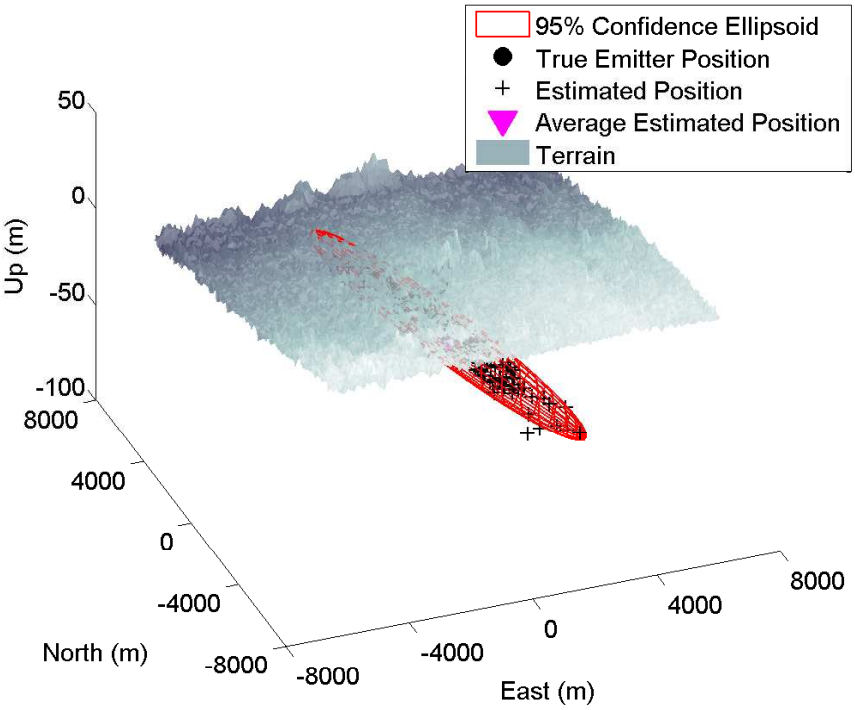

(a) No ground constraint

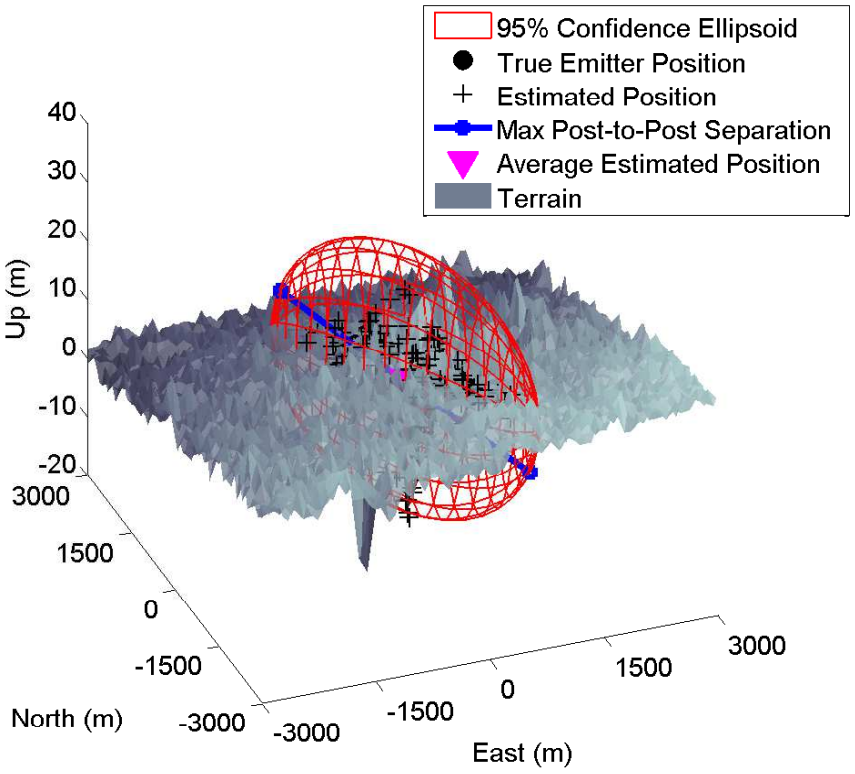

(b) Ground constrained

Figure 75. Three-ball TDOA satellite geometry 10 against Libya target

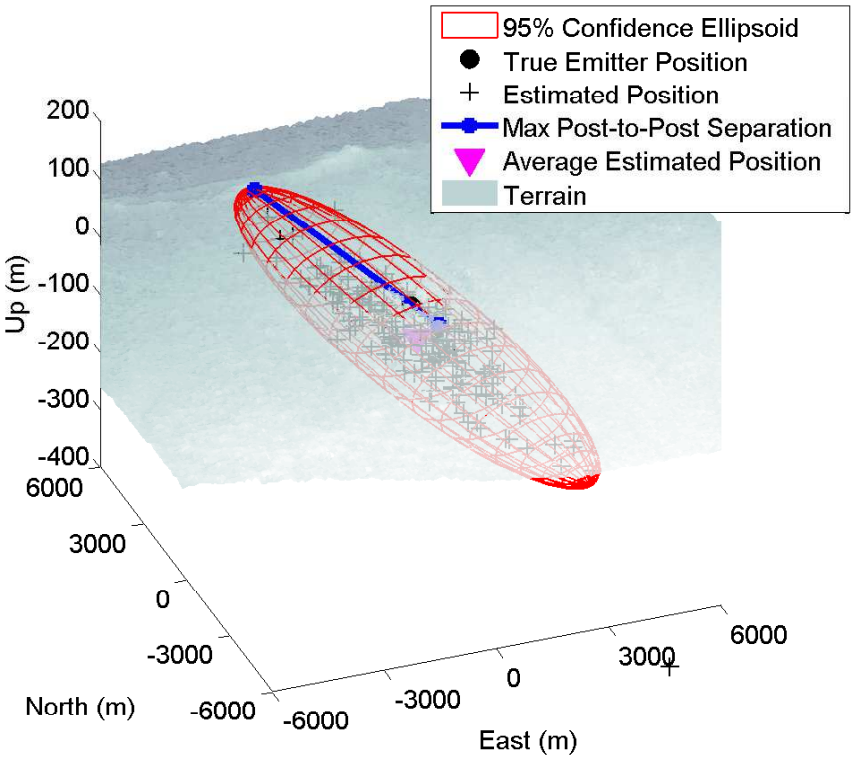

(a) No ground constraint

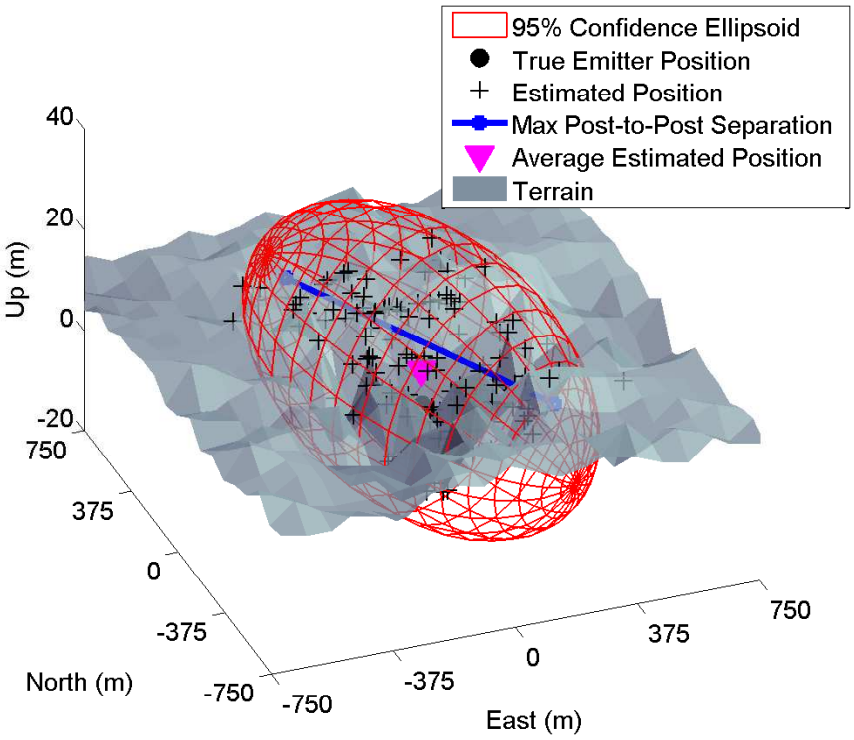

(b) Ground constrained

Figure 76. Three-ball TDOA satellite geometry 11 against Libya target

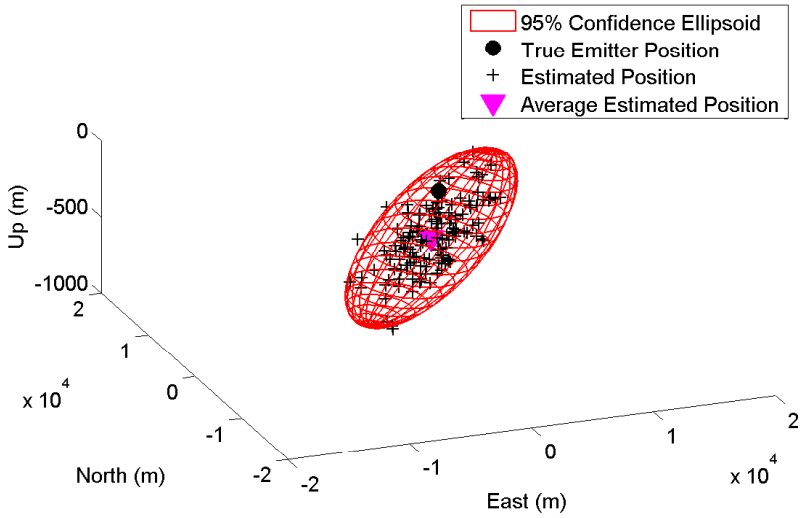

(a) No ground constraint

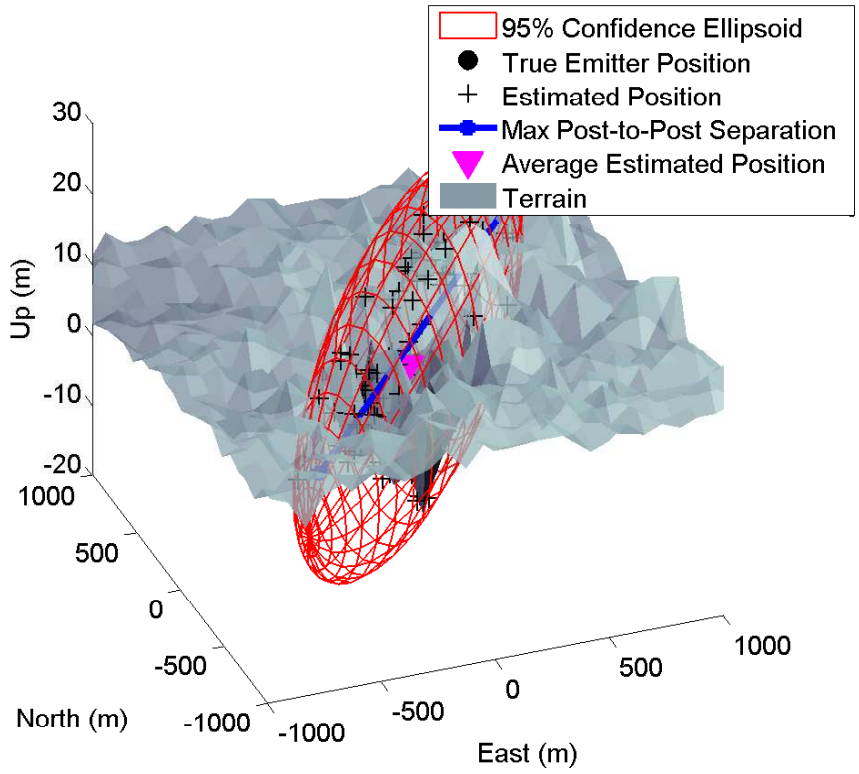

(b) Ground constrained

Figure 77. Three-ball TDOA satellite geometry 12 against Libya target

1.1.0.10 Four-ball TDOA Satellite Performance.

The following are the graphical depictions of the four-ball TDOA SV geolocation agents solutions for the Libya scenario.

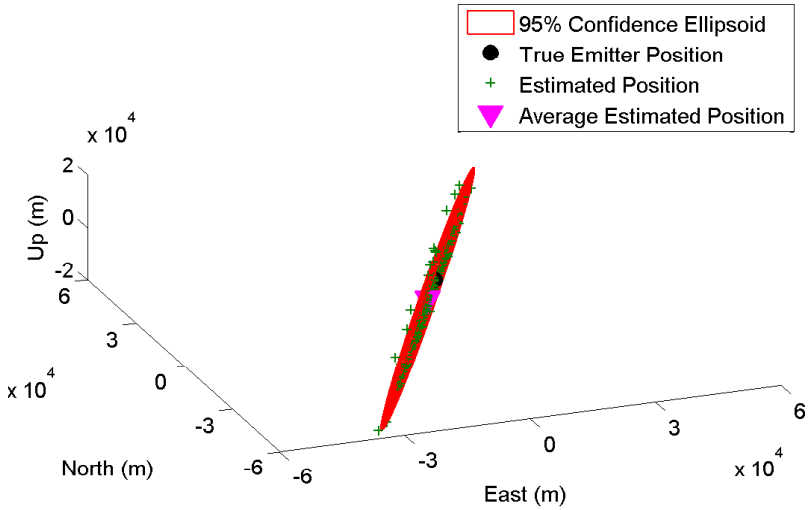

(a) No ground constraint

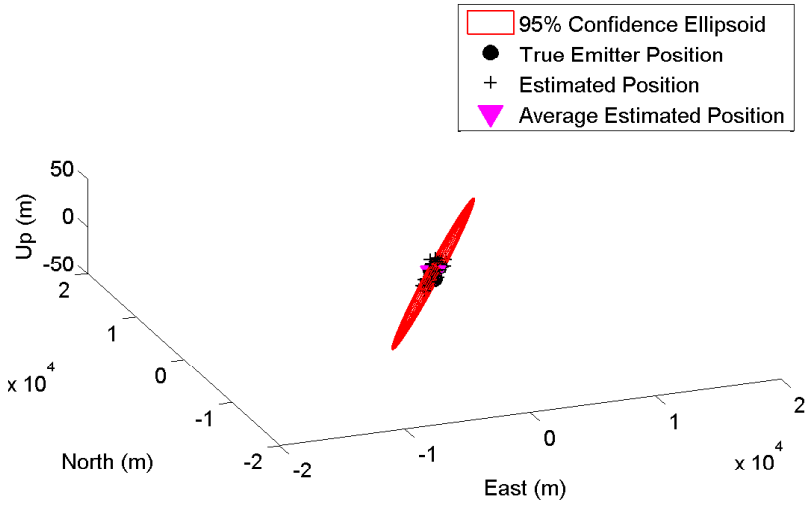

(b) Ground constrained

Figure 78. Four-ball TDOA satellite geometry 7 against Libya target

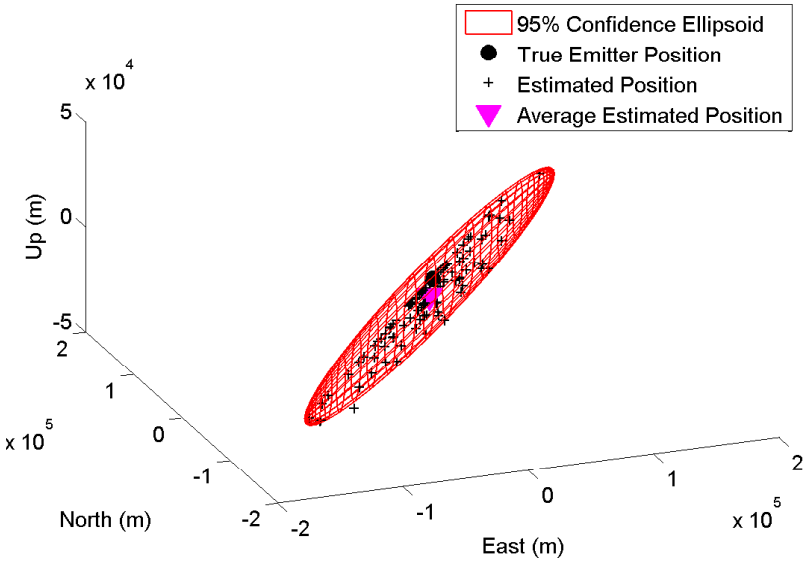

(a) No ground constraint

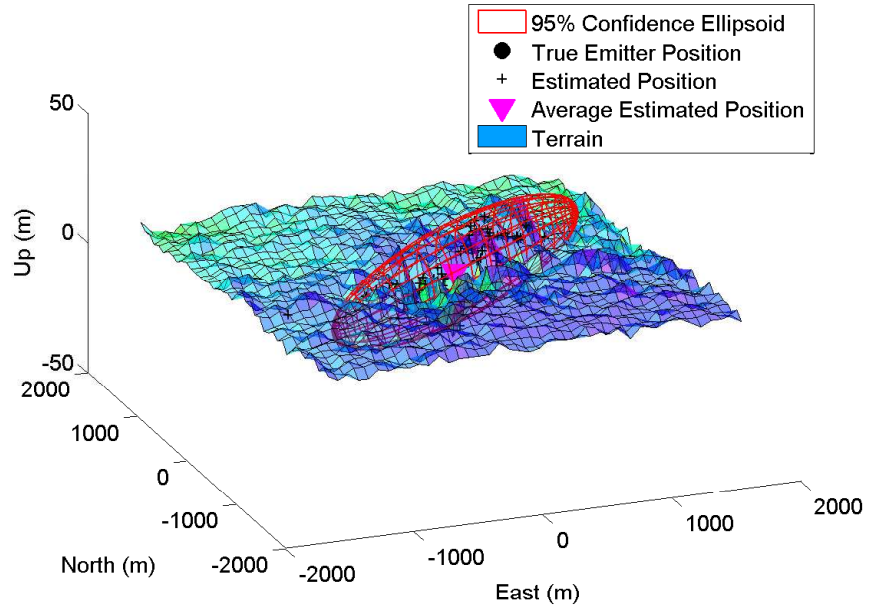

(b) Ground constrained

Figure 79. Four-ball TDOA satellite geometry 8 against Libya target

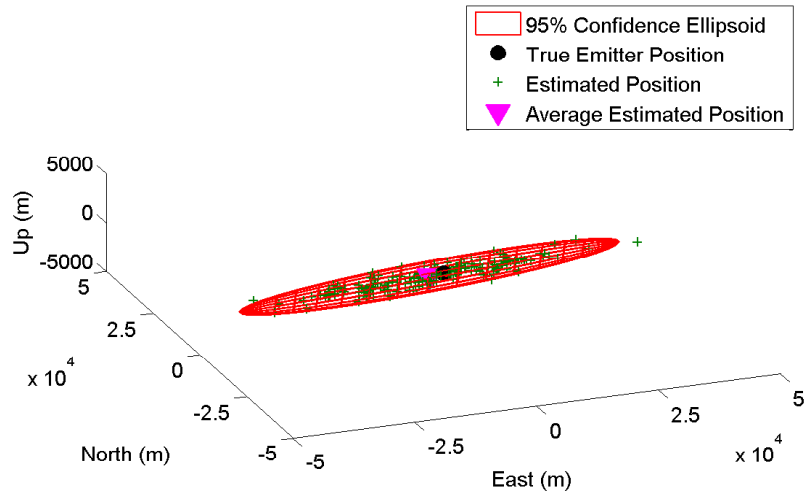

(a) No ground constraint

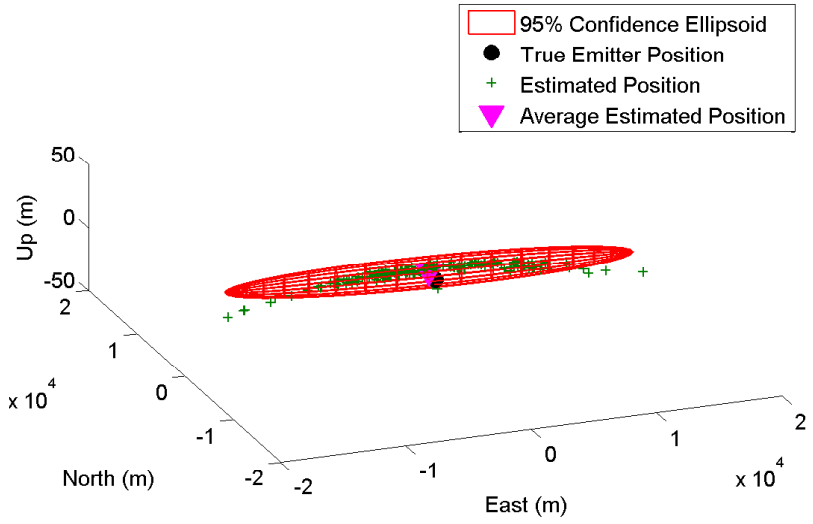

(b) Ground constrained

Figure 80. Four-ball TDOA satellite geometry 9 against Libya target

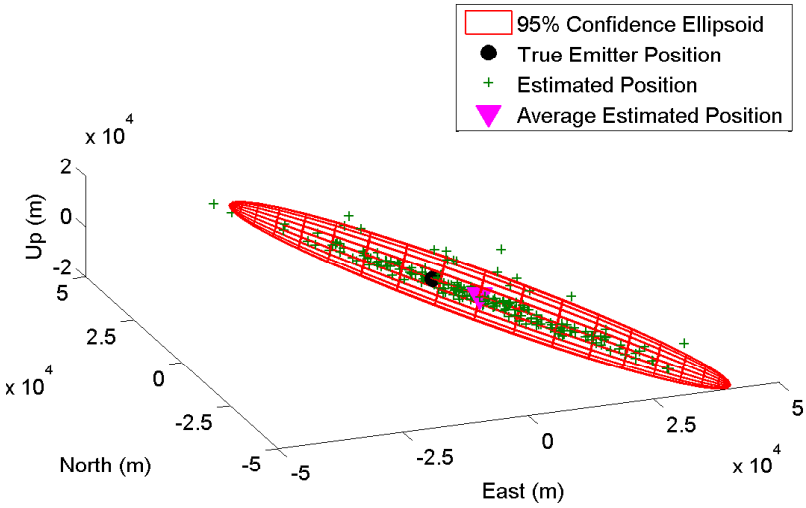

(a) No ground constraint

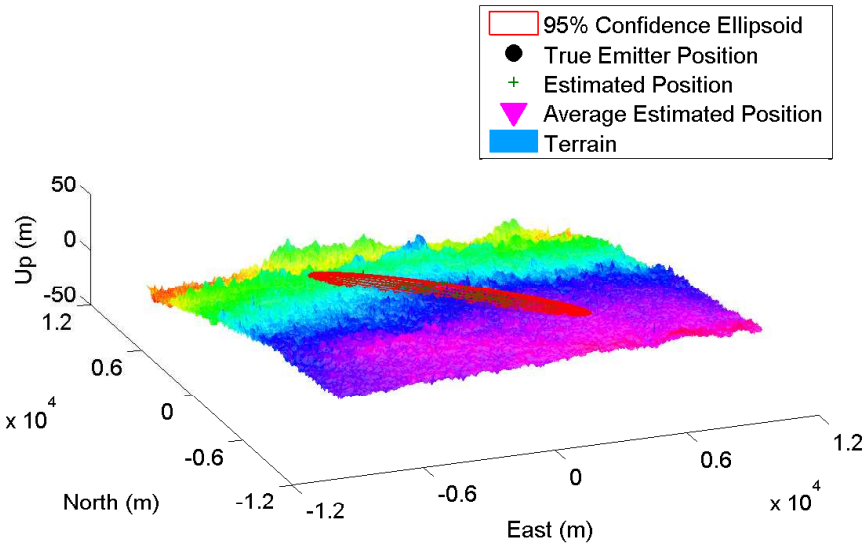

(b) Ground constrained

Figure 81. Four-ball satellite geometry 10 against Libya target

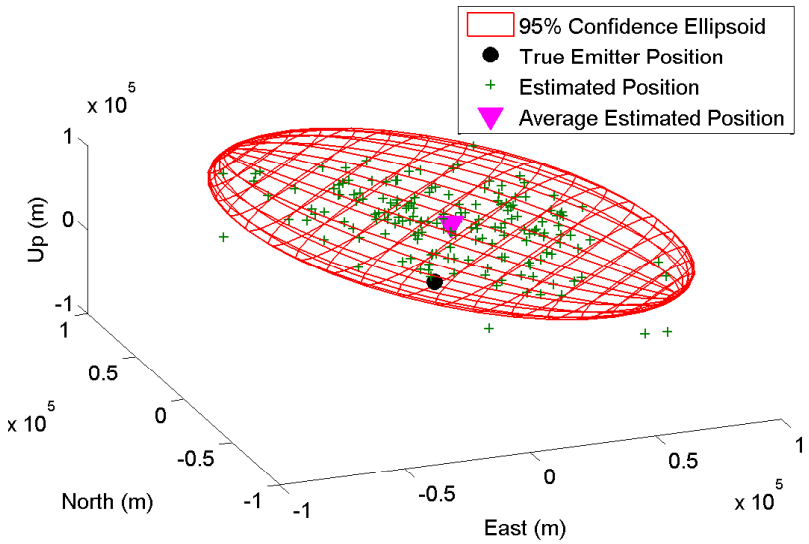

(a) No ground constraint

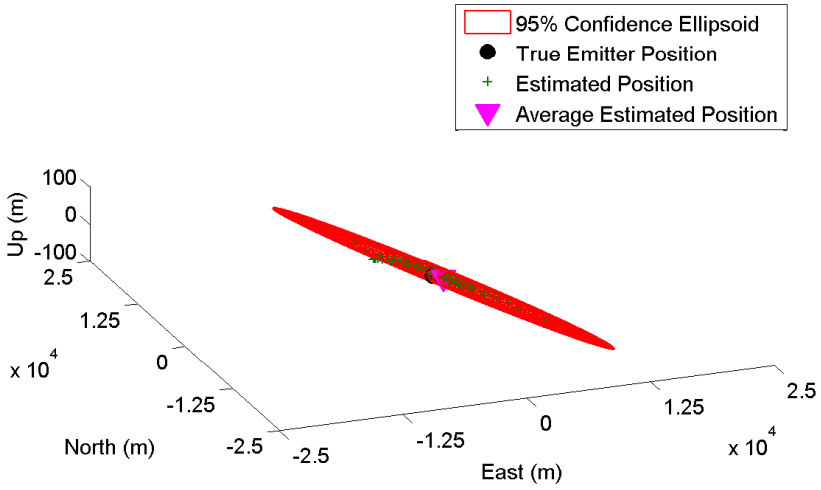

(b) Ground constrained

Figure 82. Four-ball TDOA satellite geometry 11 against Libya target

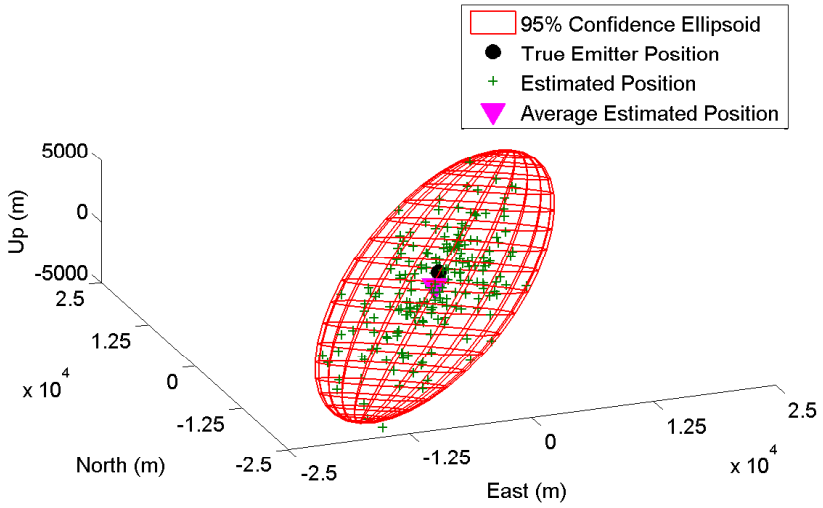

(a) No ground constraint

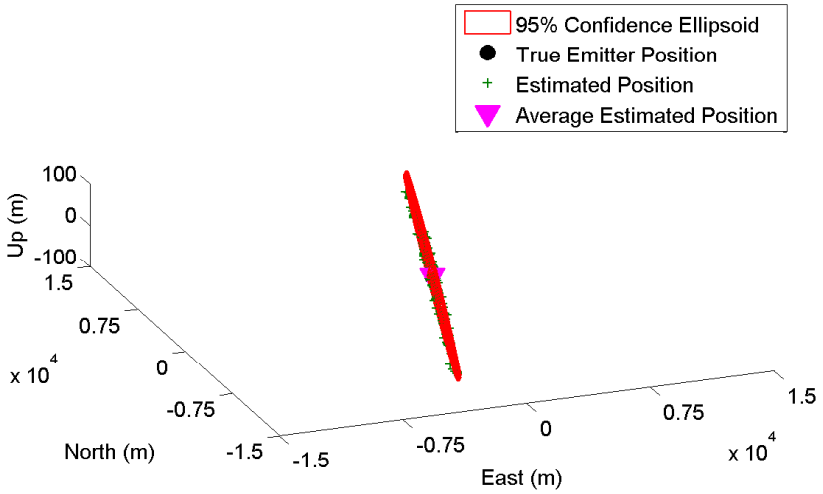

(b) Ground constrained

Figure 83. Four-ball TDOA satellite geometry 12 against Libya target

1.2 Afghanistan Single Geolocation Agent Figures

1.2.0.11 AOA Satellite Performance.

The following are the graphical depictions of the AOA SV geolocation agent solutions for the Afghanistan scenario.

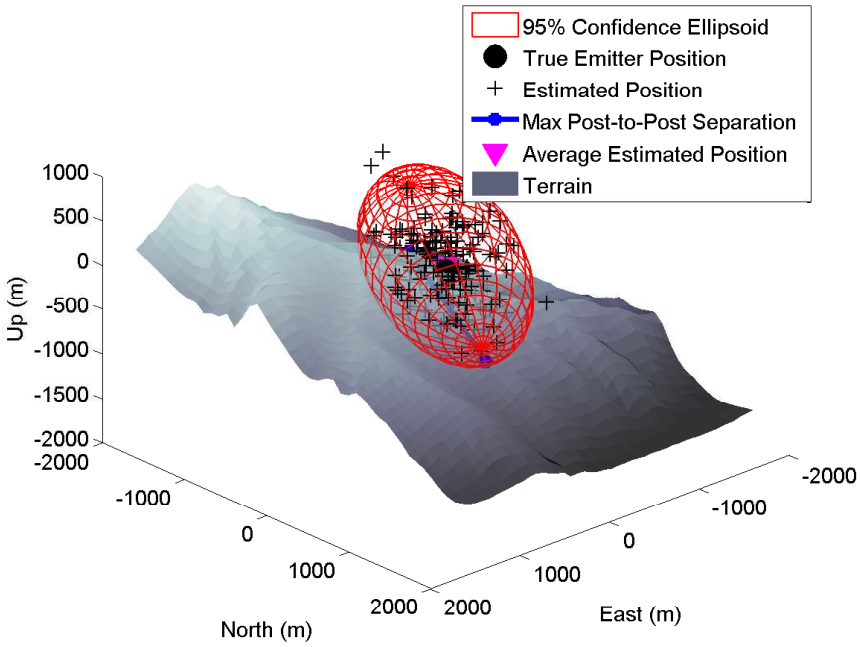

(a) No ground constraint

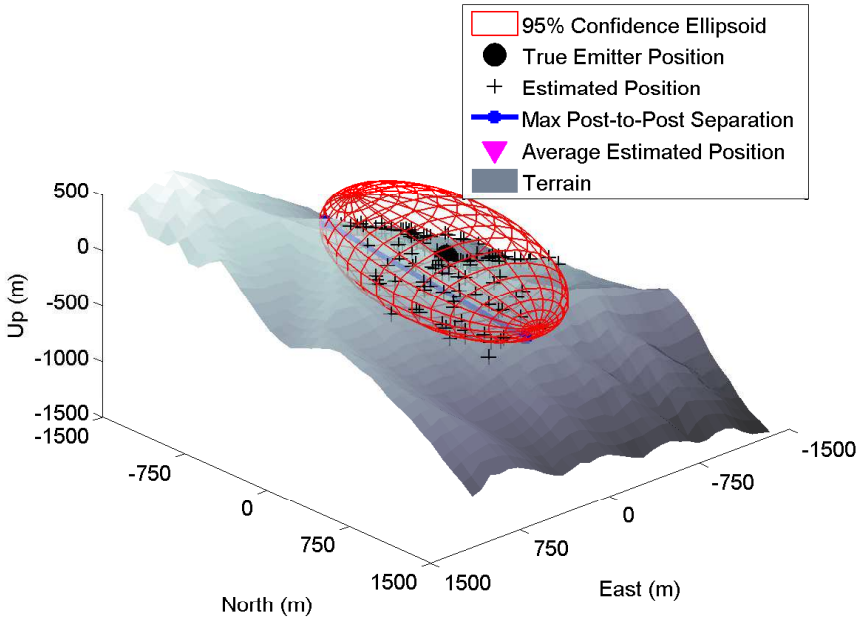

(b) Ground constrained

Figure 84. AOA satellite geometry 13 against Afghanistan target

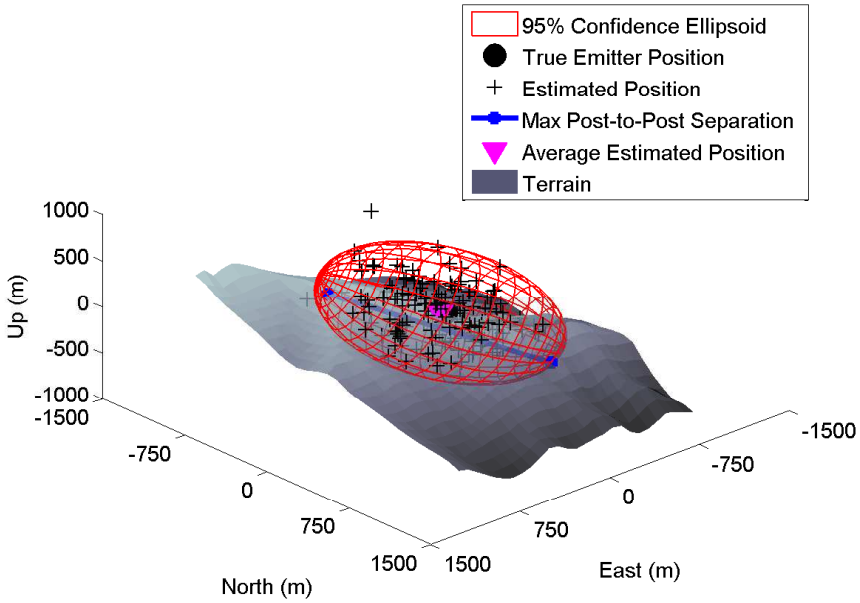

(a) No ground constraint

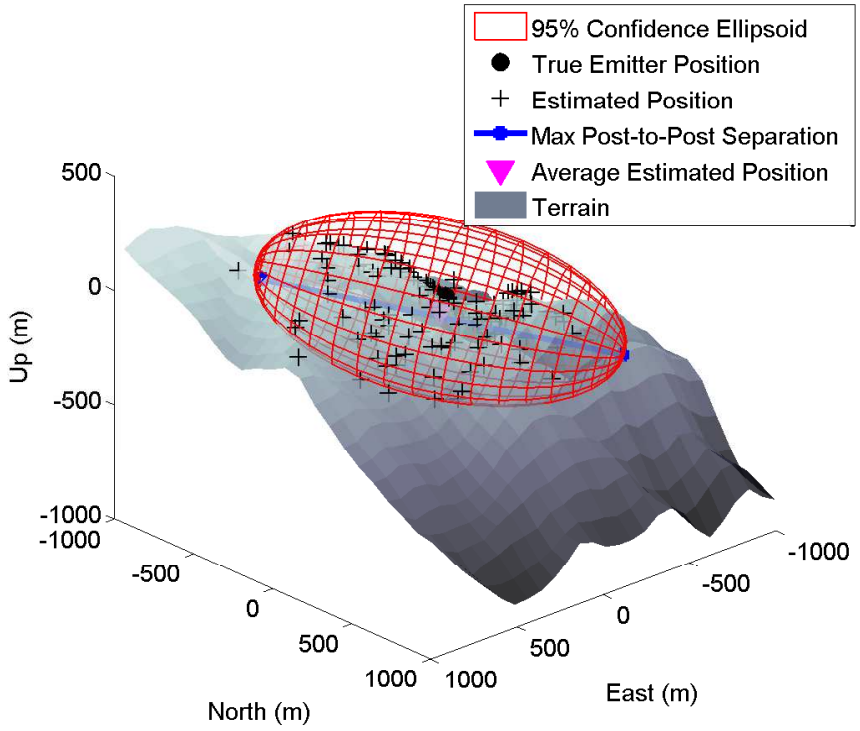

(b) Ground constrained

Figure 85. AOA satellite geometry 14 against Afghanistan target

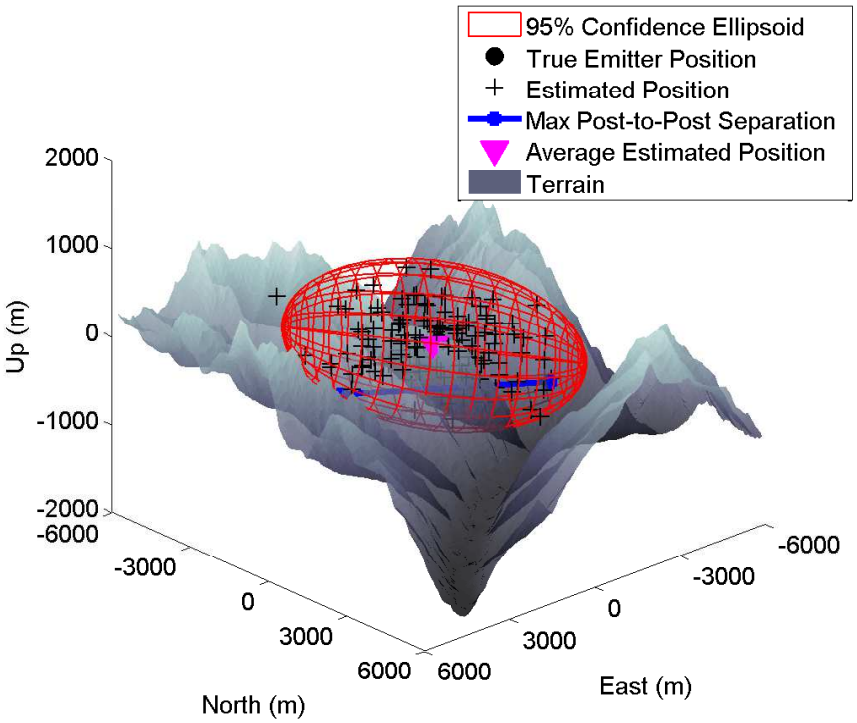

(a) No ground constraint

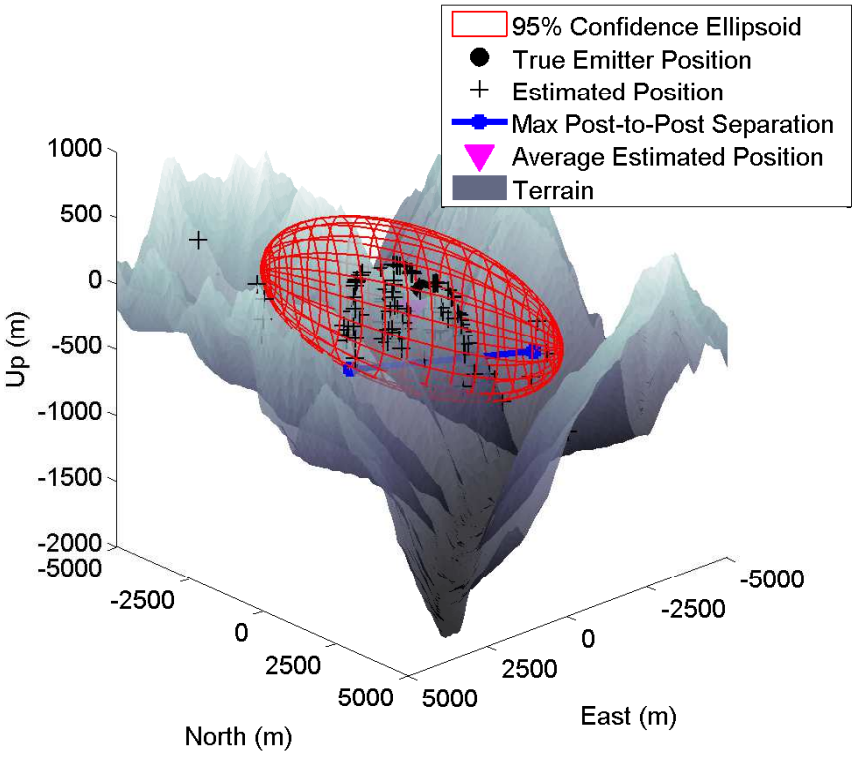

(b) Ground constrained

Figure 86. AOA satellite geometry 15 against Afghanistan target

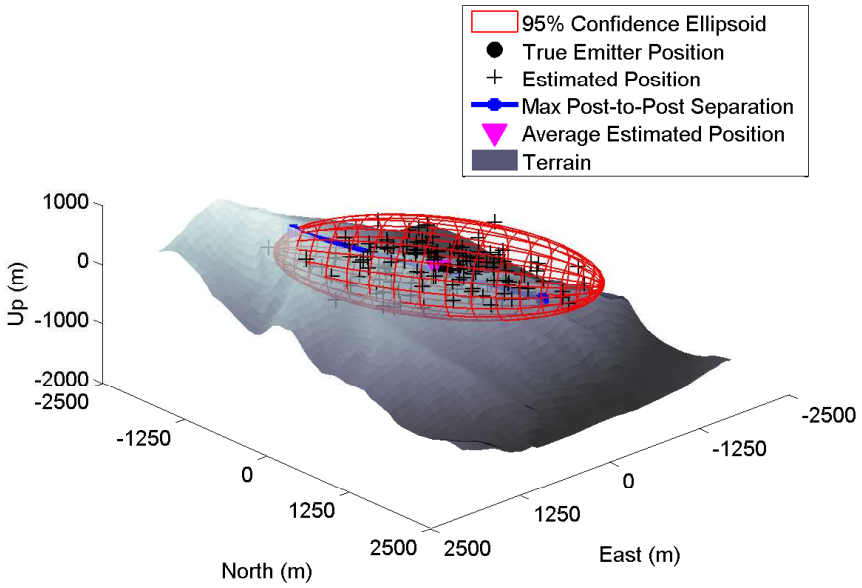

(a) No ground constraint

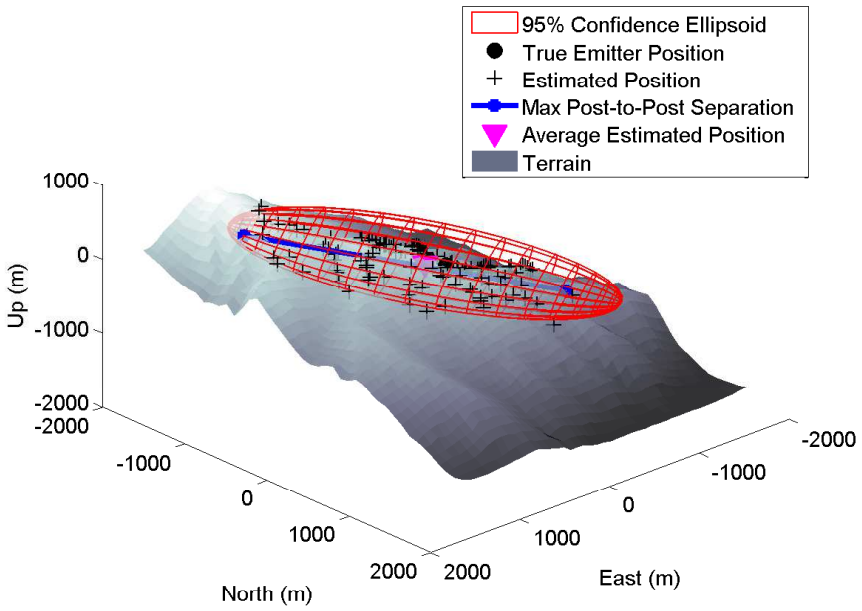

(b) Ground constrained

Figure 87. AOA satellite geometry 16 against Afghanistan target

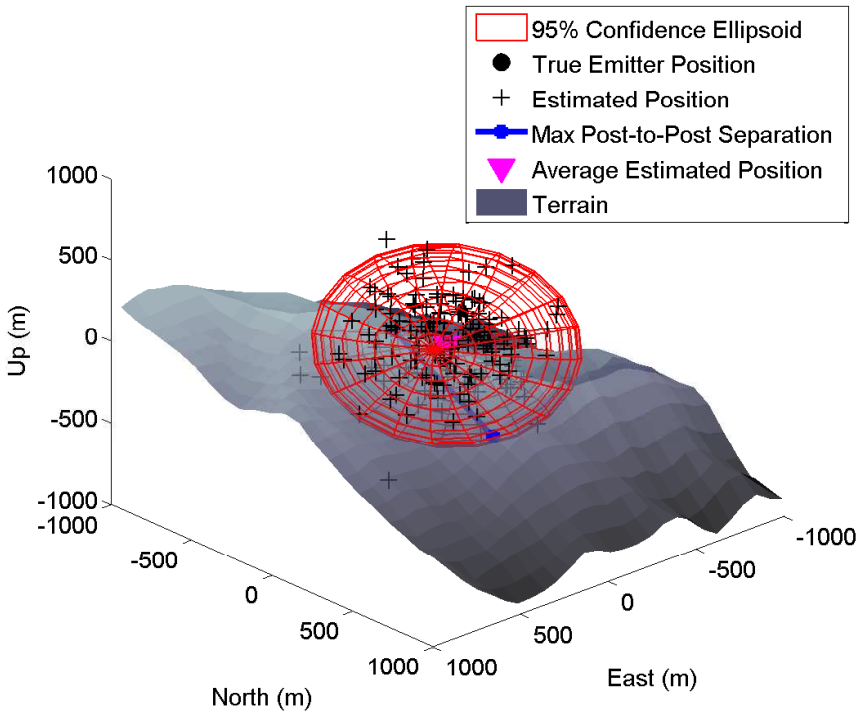

(a) No ground constraint

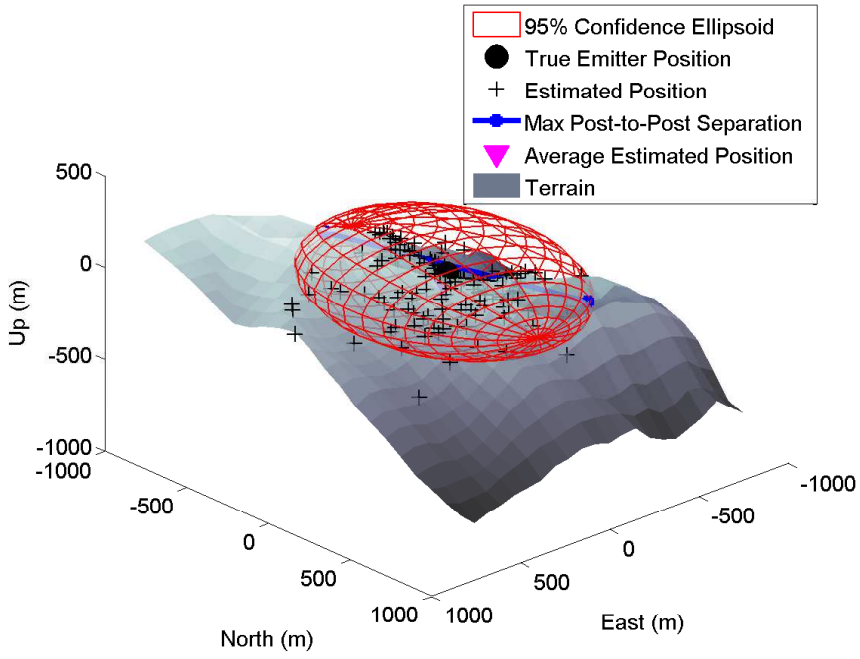

(b) Ground constrained

Figure 88. AOA satellite geometry 17 against Afghanistan target

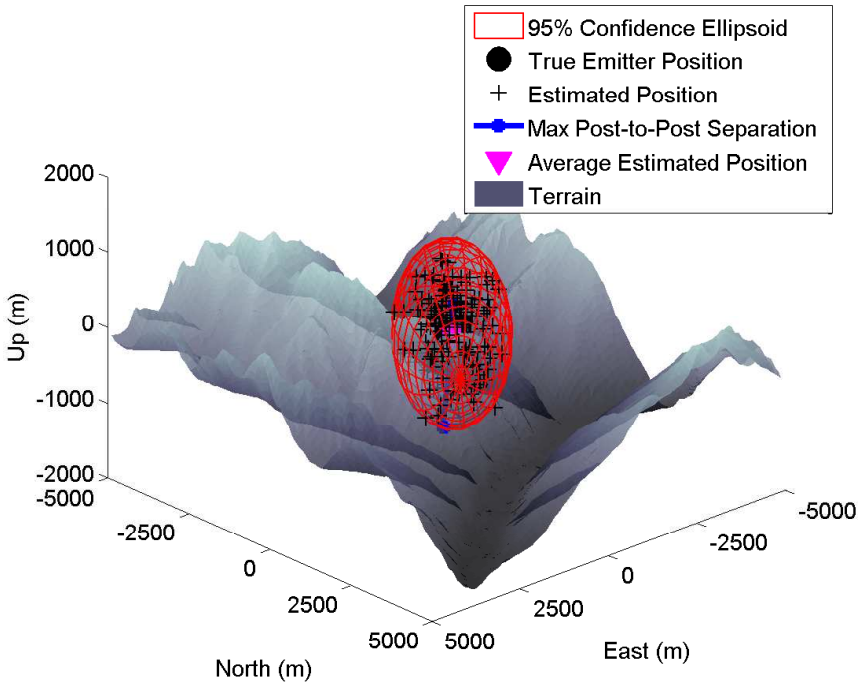

(a) No ground constraint

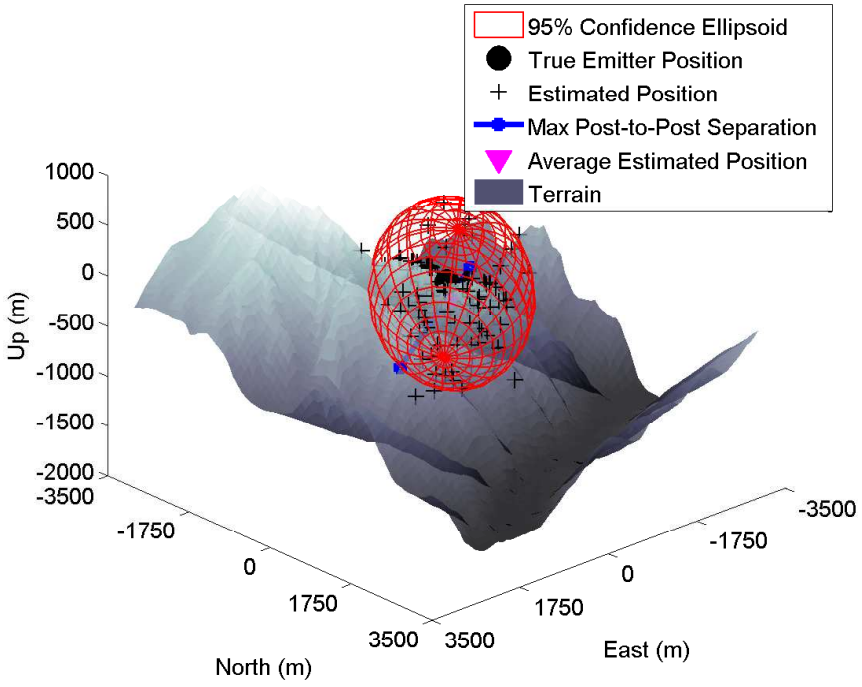

(b) Ground constrained

Figure 89. AOA satellite geometry 18 against Afghanistan target

1.2.0.12 AOA Aircraft Performance.

The follow are the graphical depictions of the AOA aircraft geolocation agent solutions for the Afghanistan scenario.

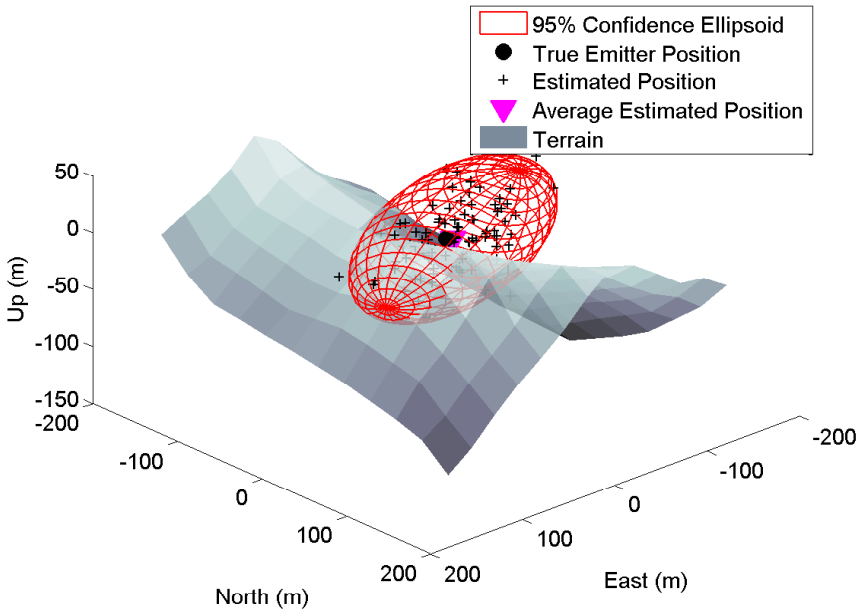

(a) No ground constraint

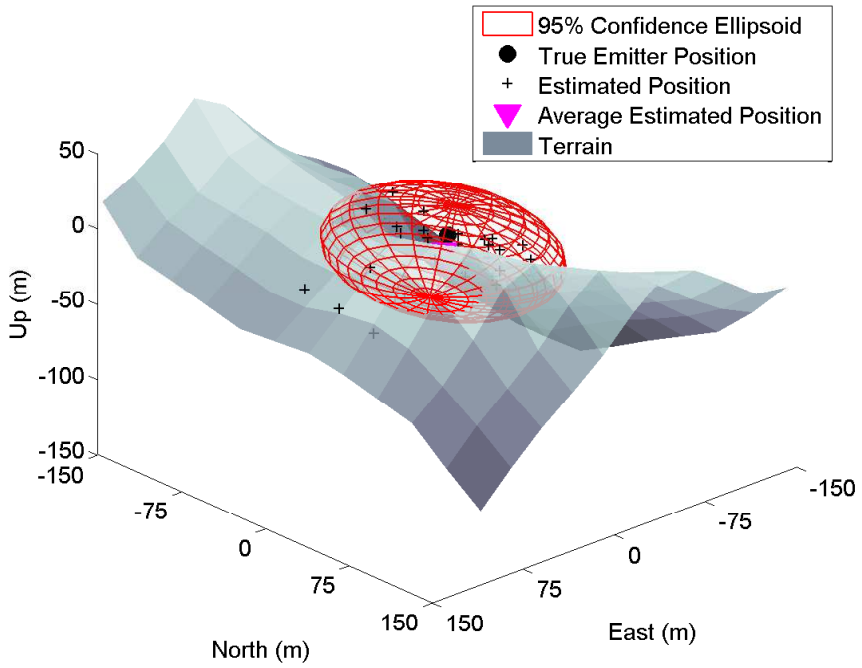

(b) Ground constrained

Figure 90. AOA aircraft geometry 9 against Afghanistan target

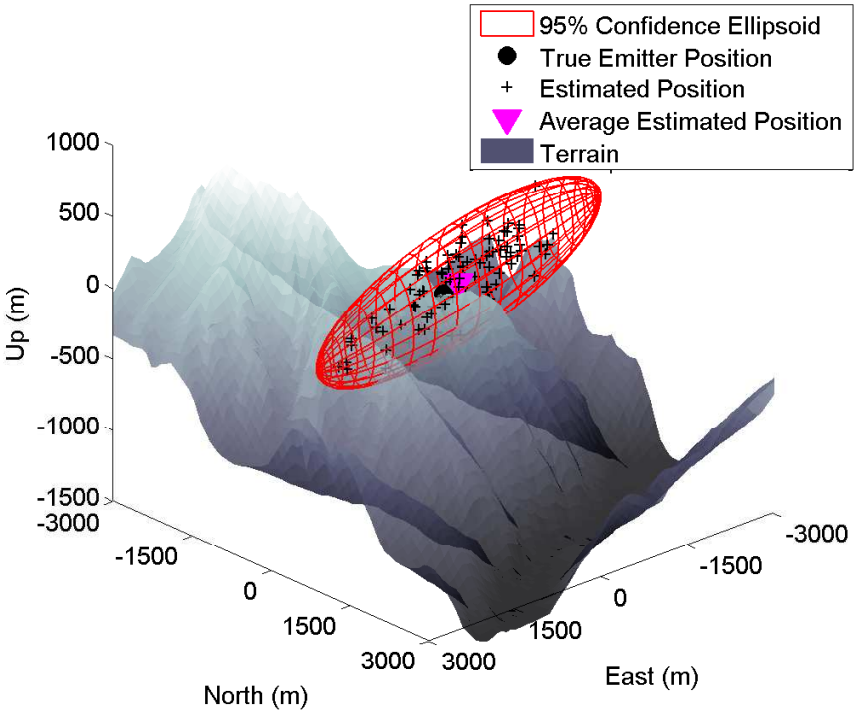

(a) No ground constraint

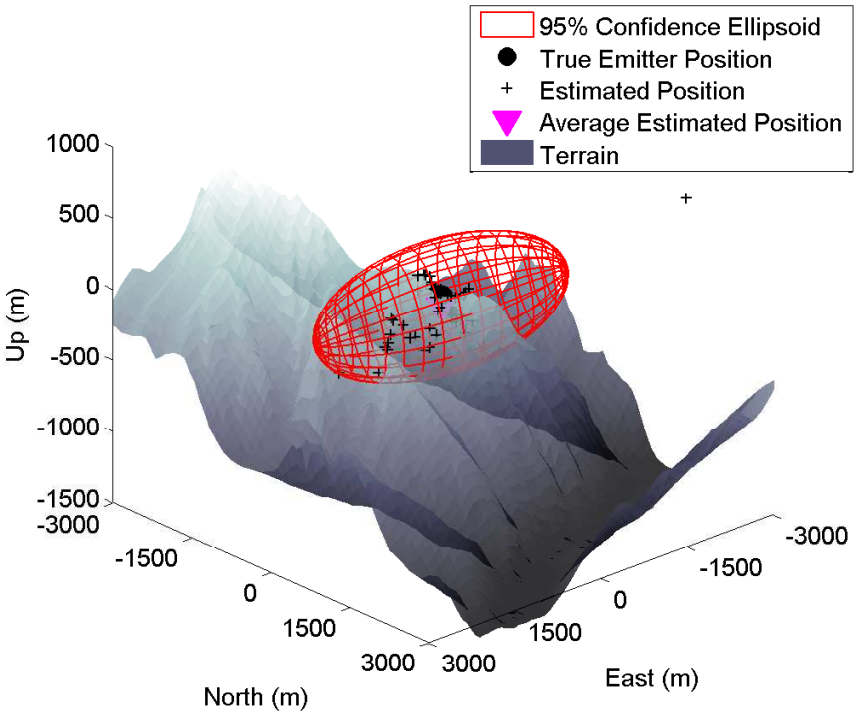

(b) Ground constrained

Figure 91. AOA aircraft geometry 10 against Afghanistan target

1.2.0.13 Three-ball TDOA Satellite Performance.

The following are the graphical depictions of the three-ball TDOA SV geolocation agent solutions for the Afghanistan scenario.

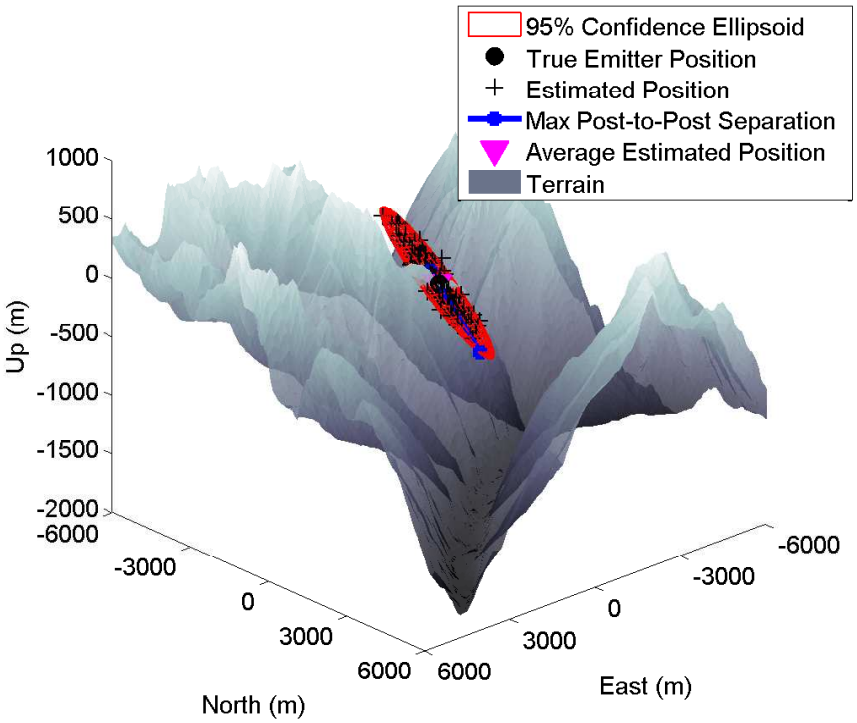

(a) No ground constraint

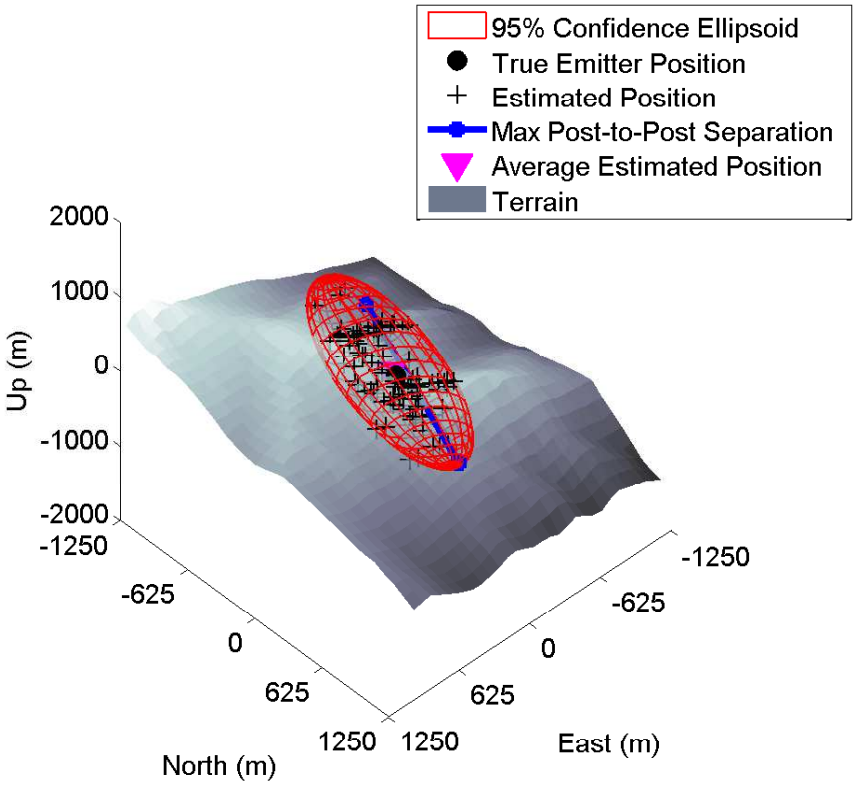

(b) Ground constrained

Figure 92. Three-ball TDOA satellite geometry 13 against Afghanistan target

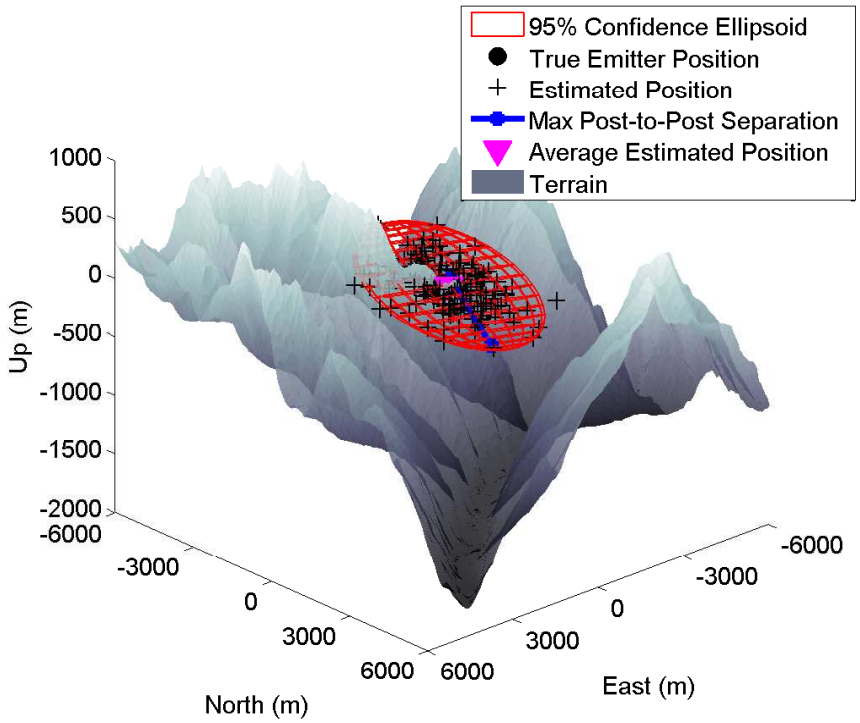

(a) No ground constraint

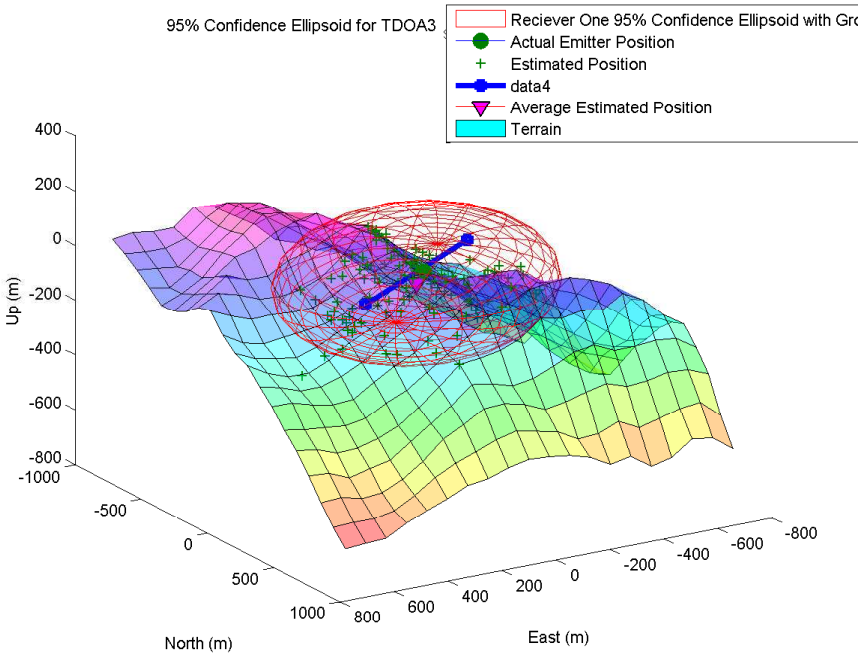

(b) Ground constrained

Figure 93. Three-ball TDOA satellite geometry 14 against Afghanistan target

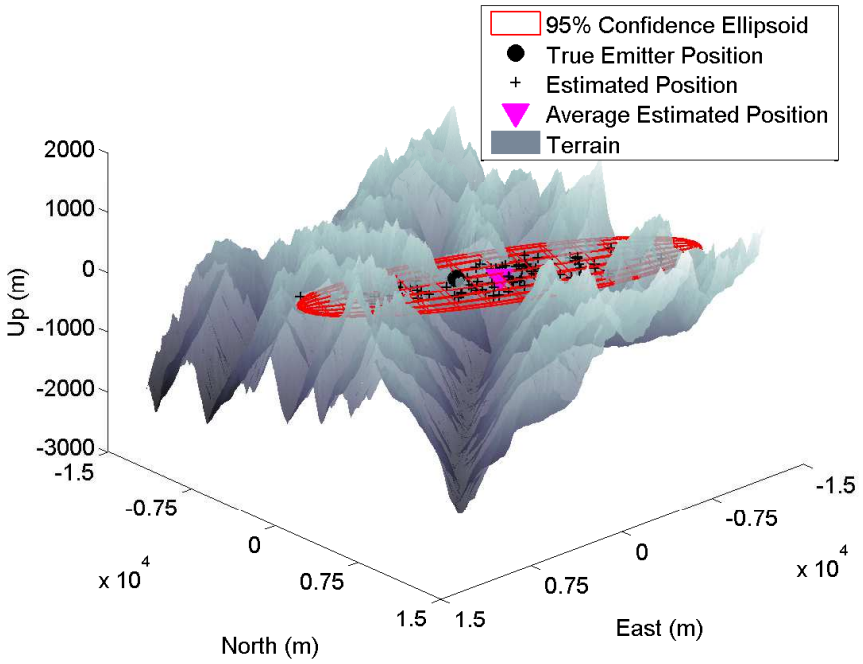

(a) No ground constraint

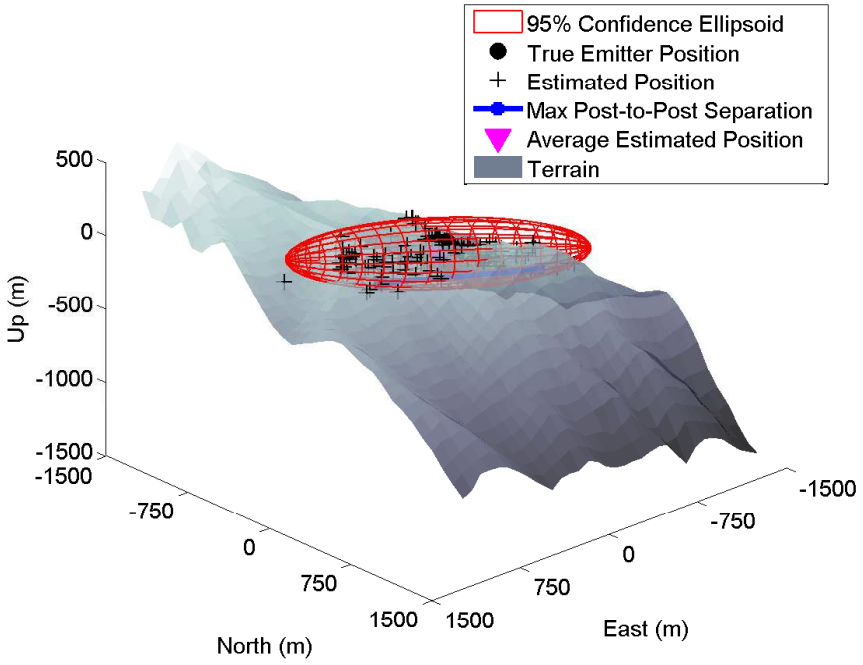

(b) Ground constrained

Figure 94. Three-ball TDOA satellite geometry 15 against Afghanistan target

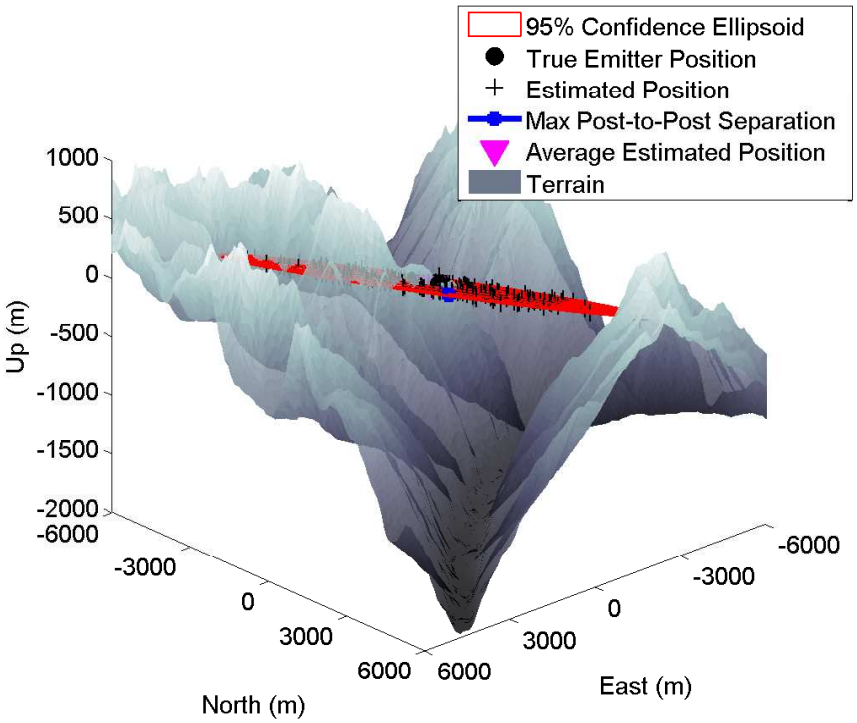

(a) No ground constraint

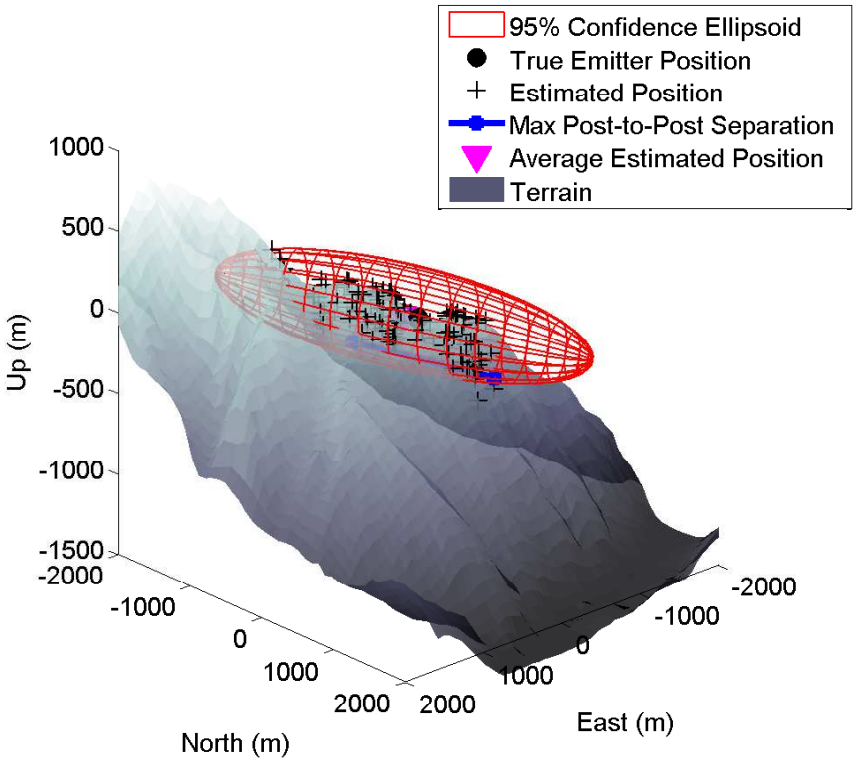

(b) Ground constrained

Figure 95. Three-ball TDOA satellite geometry 16 against Afghanistan target

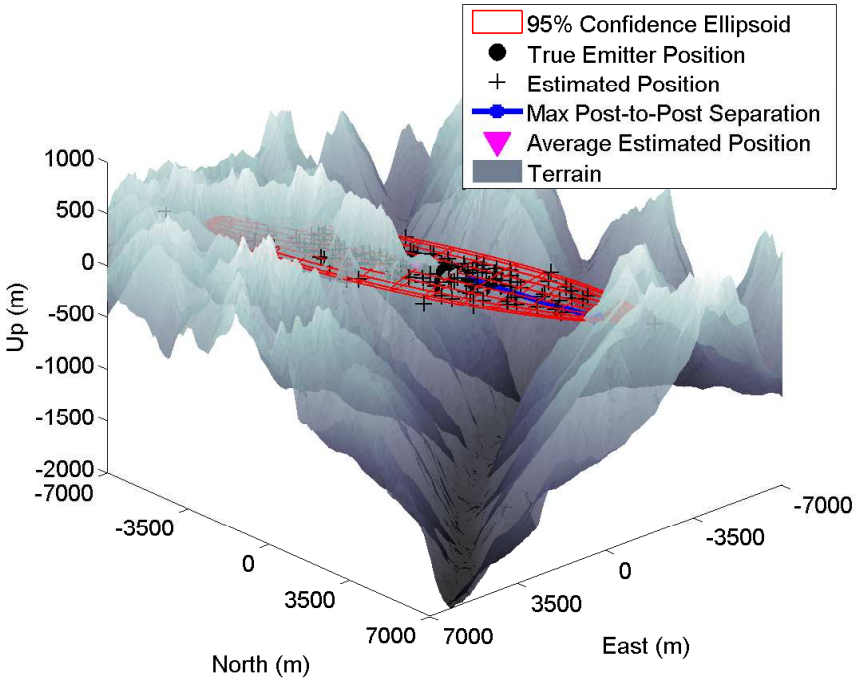

(a) No ground constraint

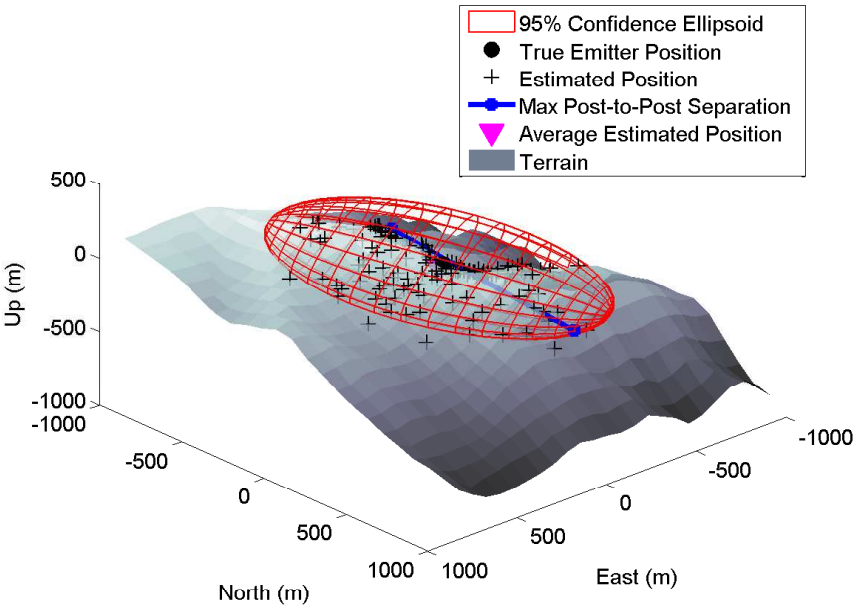

(b) Ground constrained

Figure 96. Three-ball TDOA satellite geometry 17 against Afghanistan target

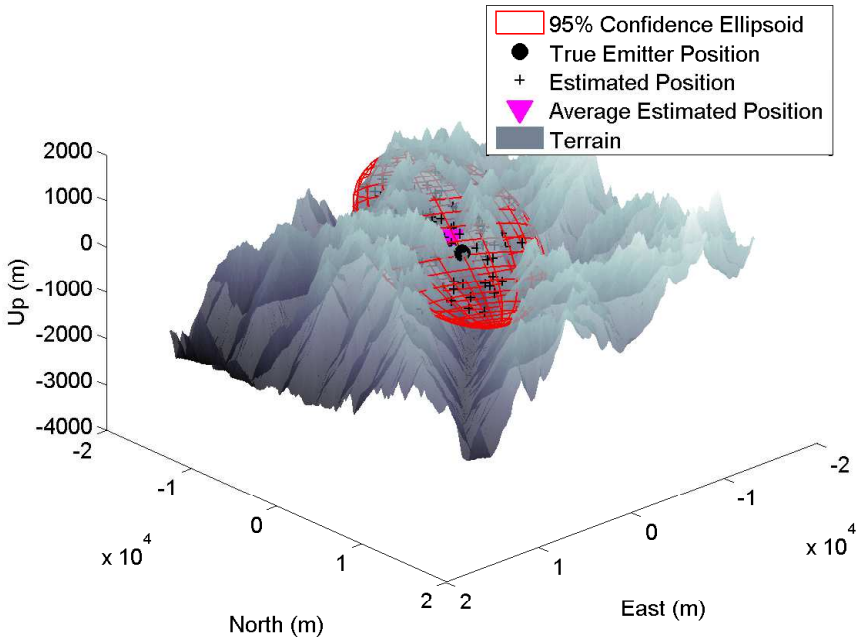

(a) No ground constraint

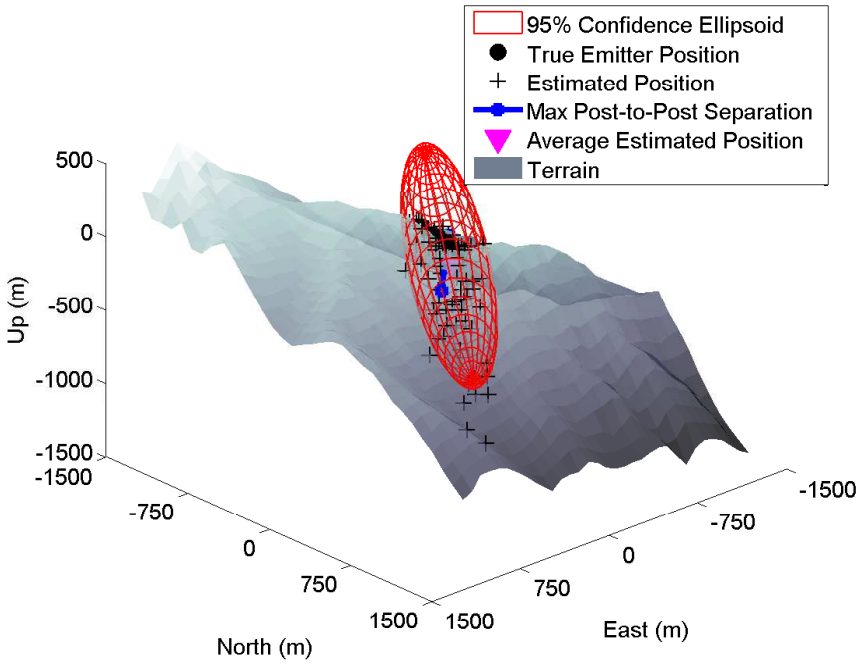

(b) Ground constrained

Figure 97. Three-ball TDOA satellite geometry 18 against Afghanistan target

1.2.0.14 Three-ball TDOA Aircraft Performance.

The following are the graphical depictions of the three-ball TDOA UAV geolocation agent solutions for the Afghanistan scenario.

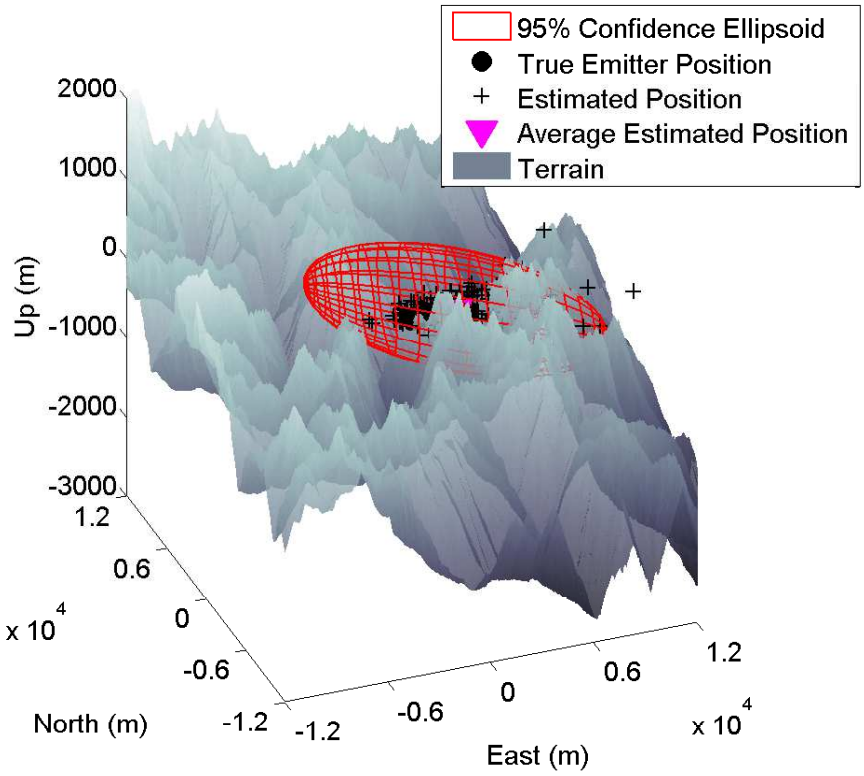

(a) No ground constraint

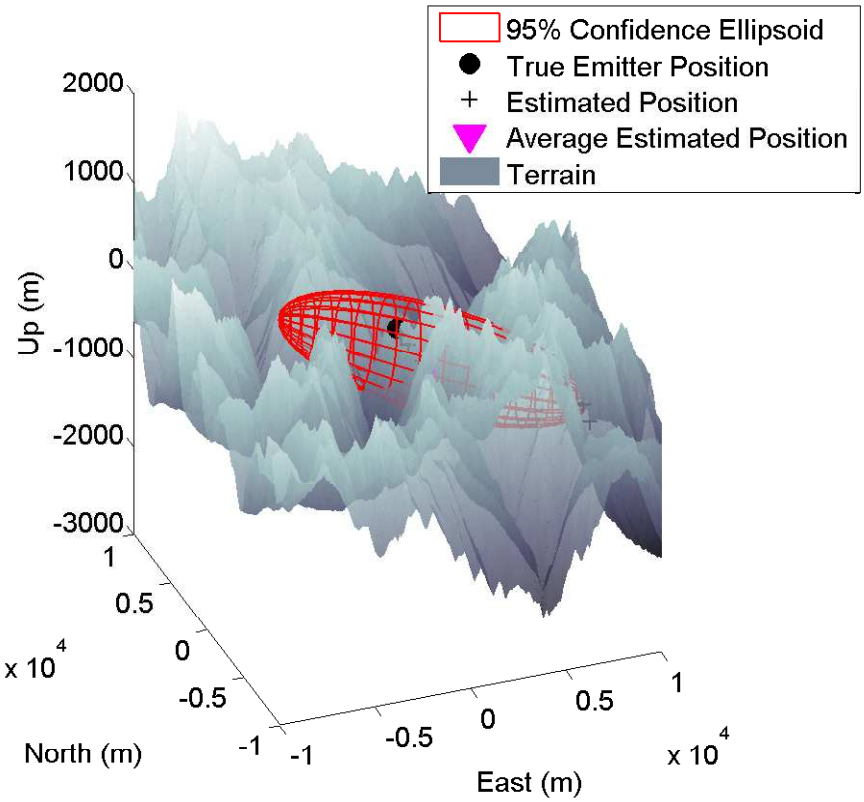

(b) Ground constrained

Figure 98. Three-ball TDOA UAV geometry 4 against Afghanistan target

1.2.0.15 Four-ball TDOA Satellite Performance.

The following are the graphical depictions of the four-ball TDOA SV geolocation agent solutions for the Afghanistan scenario.

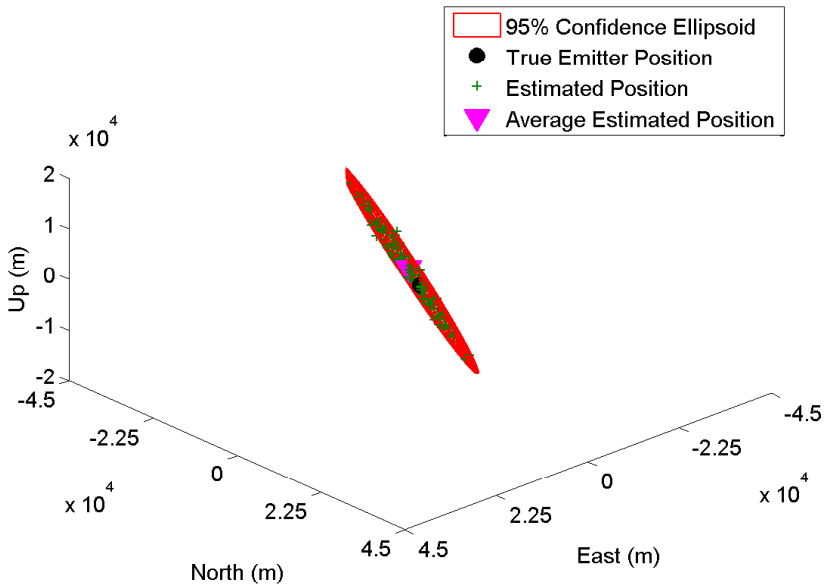

(a) No ground constraint

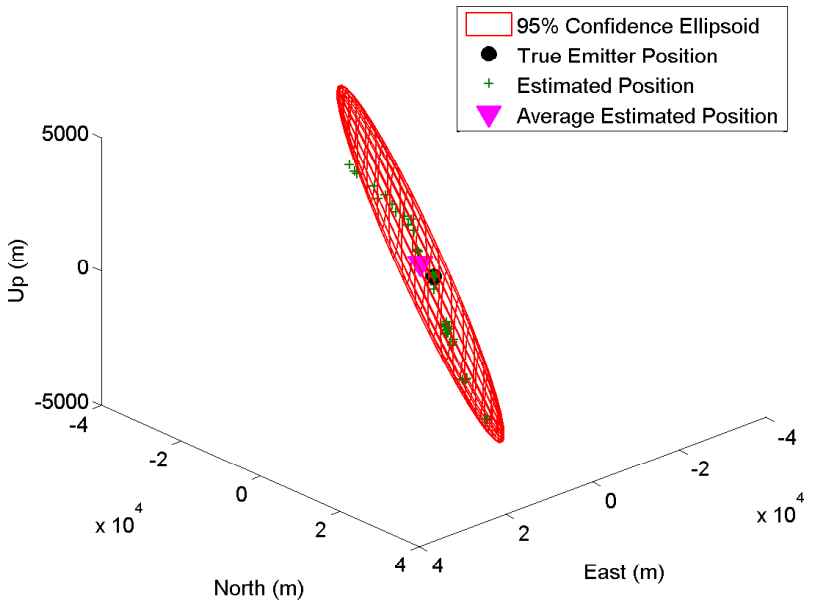

(b) Ground constrained

Figure 99. Four-ball TDOA satellite geometry 13 against Afghanistan target

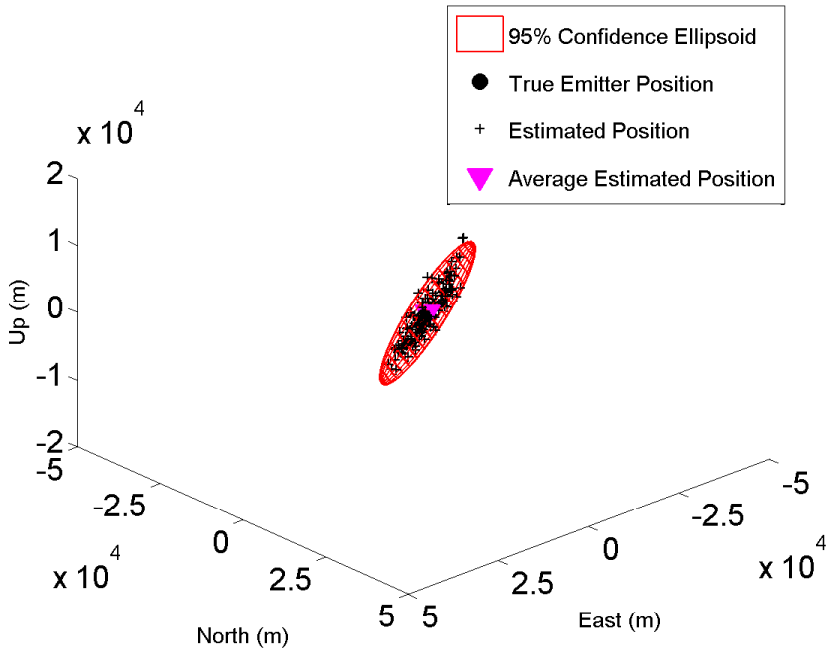

(a) No ground constraint

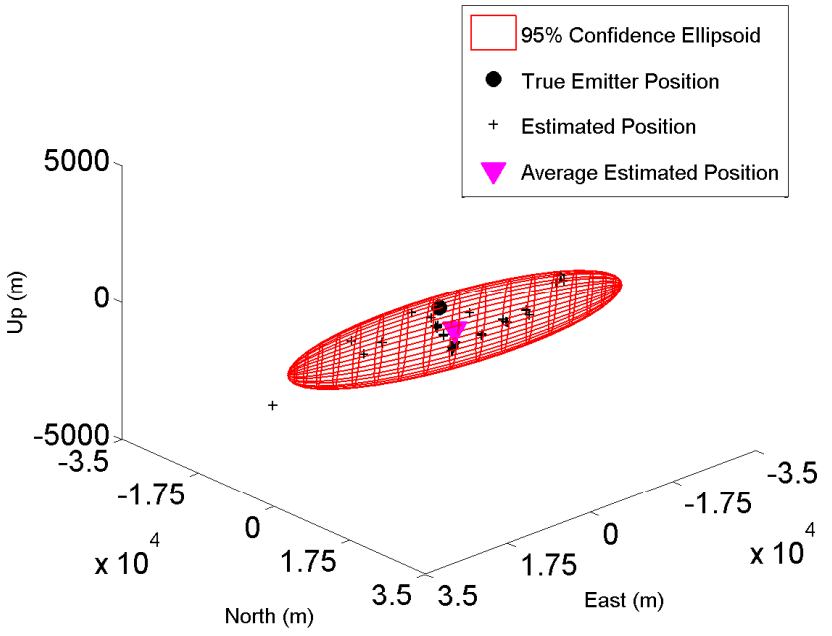

(b) Ground constrained

Figure 100. Four-ball TDOA satellite geometry 14 against Afghanistan target

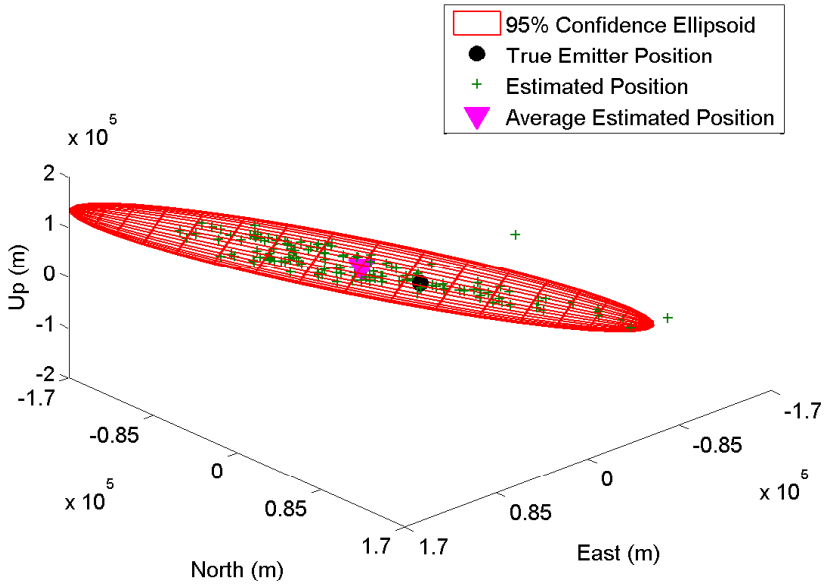

(a) No ground constraint

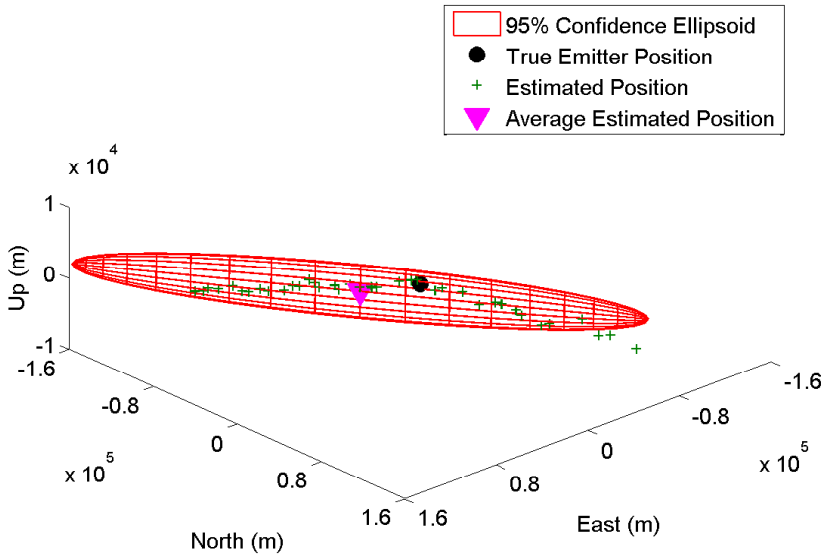

(b) Ground constrained

Figure 101. Four-ball TDOA satellite geometry 15 against Afghanistan target

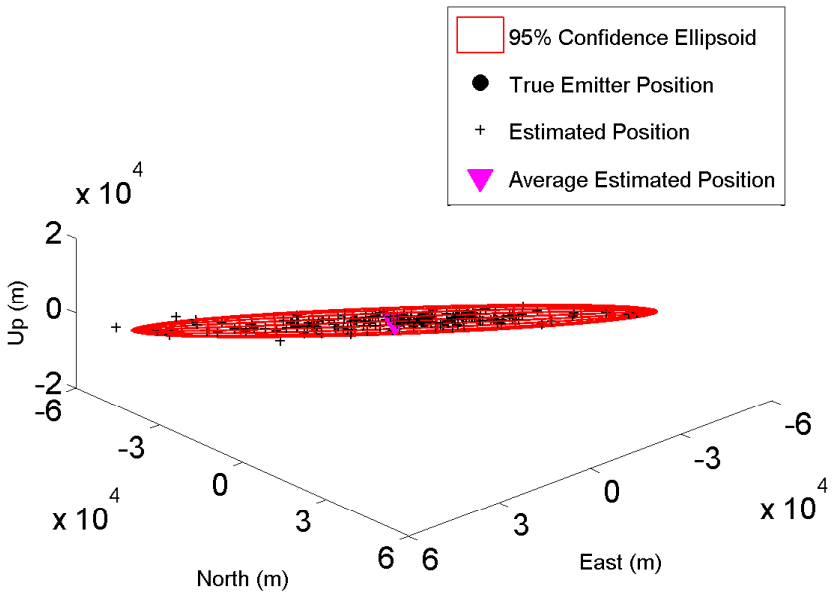

(a) No ground constraint

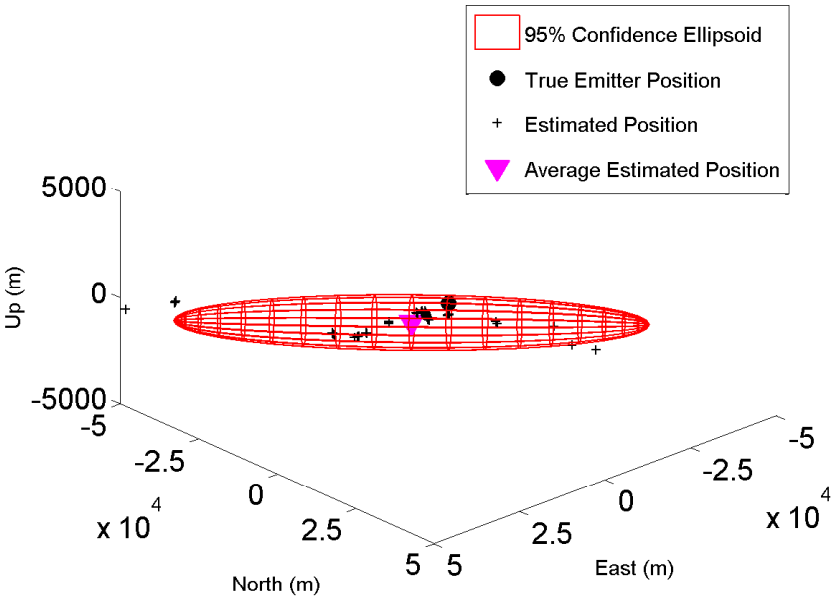

(b) Ground constrained

Figure 102. Four-ball satellite geometry 16 against Afghanistan target

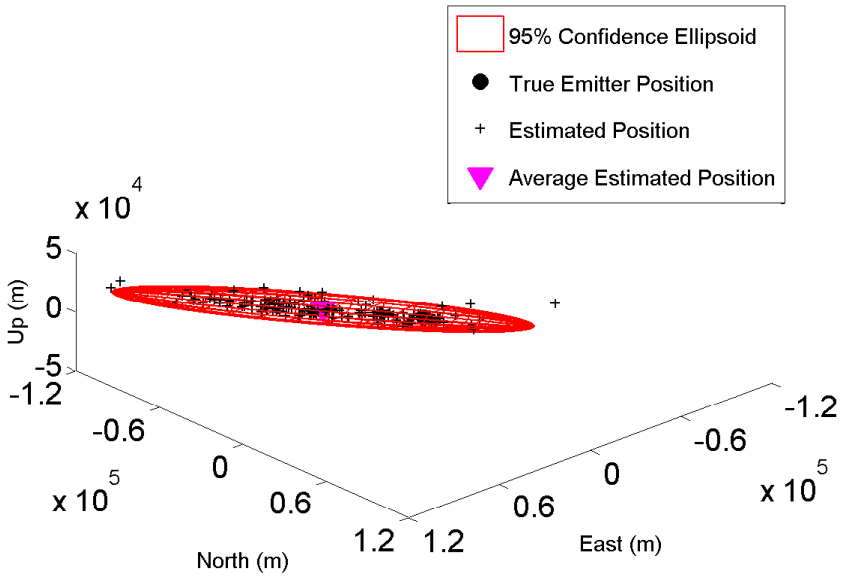

(a) No ground constraint

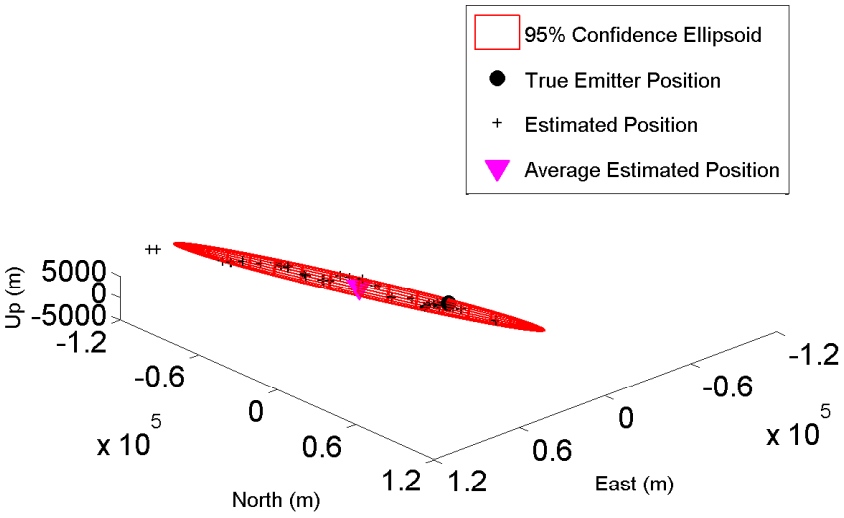

(b) Ground constrained

Figure 103. Four-ball TDOA satellite geometry 17 against Afghanistan target

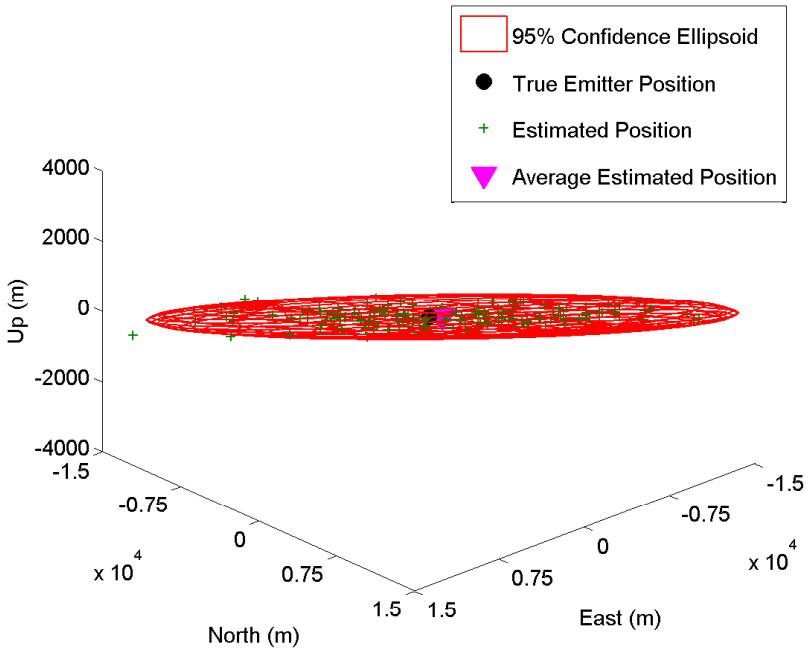

(a) No ground constraint

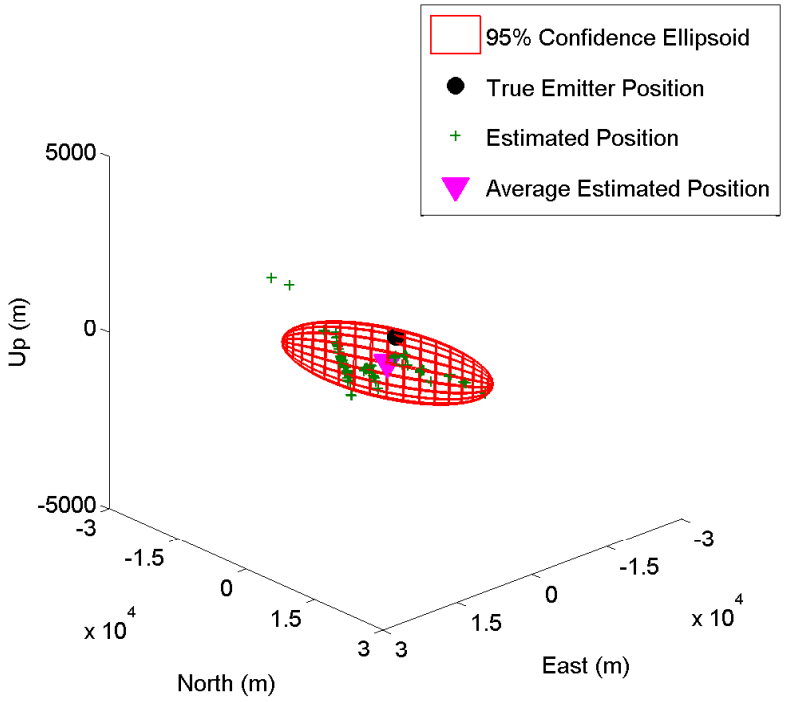

(b) Ground constrained

Figure 104. Four-ball TDOA satellite geometry 18 against Afghanistan target

B. Fusion Results

This chapter contains the full pass-by-pass fusion results and corresponding consistency values for the fused estimates from all of the fusion algorithms for each of the three scenarios.

2.1 AFIT Fusion Results

2.1.0.16 AOA Satellite Augmenting AOA Satellite Against AFIT Target.

The following are the full pass-by-pass fusion results and associated consistencies for each fusion algorithm for the augmentation of an AOA SV geolocation agent by an AOA SV geolocation agent against the AFIT target.

Table 64. Improvement from Largest Ellipsoid fusion based geolocation augmentation of AOA SV by AOA SV against AFIT target

	Ground Constrained						Non-Ground Constrained					
RMSE												
	AOA SV Pass						AOA SV Pass					
AOA SV Pass	1	2	3	4	5	6	1	2	3	4	5	6
1	-1%	25%	66%	47%	12%	77%	-1%	27%	67%	45%	14%	78%
2	60%	-2%	80%	53%	26%	87%	56%	-2%	78%	50%	26%	87%
3	11%	1%	0%	15%	5%	59%	11%	1%	0%	14%	6%	62%
4	46%	10%	67%	6%	20%	80%	45%	17%	68%	6%	23%	82%
5	58%	35%	83%	63%	0%	88%	55%	35%	82%	59%	1%	88%
6	11%	7%	41%	25%	1%	3%	5%	8%	41%	23%	5%	3%
Ave Miss												
	AOA SV Pass						AOA SV Pass					
AOA SV Pass	1	2	3	4	5	6	1	2	3	4	5	6
1	0%	27%	66%	46%	10%	77%	0%	28%	68%	44%	13%	76%
2	60%	-3%	79%	51%	27%	86%	55%	-2%	78%	49%	26%	85%
3	9%	0%	-2%	13%	4%	57%	10%	0%	-1%	13%	6%	58%
4	44%	9%	67%	3%	19%	78%	43%	17%	68%	4%	22%	80%
5	56%	36%	83%	62%	0%	87%	53%	36%	82%	59%	1%	87%
6	13%	7%	42%	22%	2%	3%	6%	7%	41%	21%	5%	3%
Ave SMA												
	AOA SV Pass						AOA SV Pass					
AOA SV Pass	1	2	3	4	5	6	1	2	3	4	5	6
1	58%	0%	60%	31%	0%	80%	59%	0%	58%	26%	2%	82%
2	54%	22%	81%	59%	0%	89%	51%	27%	79%	57%	0%	90%
3	0%	0%	8%	0%	0%	61%	0%	0%	40%	0%	0%	60%
4	27%	9%	58%	60%	0%	74%	29%	16%	58%	60%	0%	79%
5	59%	13%	84%	61%	21%	90%	58%	15%	82%	58%	27%	91%
6	16%	0%	11%	0%	0%	78%	12%	0%	32%	0%	0%	81%

Table 65. Largest Ellipsoid geolocation fusion consistency for augmentation of AOA SV by AOA SV against AFIT target

		Ground Constrained						Non-Ground Constrained					
		Ellipsoid Consistency AOA AV Pass						Ellipsoid Consistency AOA AV Pass					
		1	2	3	4	5	6	1	2	3	4	5	6
AOA SV Pass	1	70%	97%	80%	96%	98%	81%	68%	96%	78%	96%	100%	76%
	2	98%	92%	95%	96%	100%	97%	99%	86%	94%	96%	100%	94%
	3	94%	95%	84%	97%	98%	97%	98%	94%	79%	96%	95%	97%
	4	97%	97%	80%	65%	97%	87%	97%	98%	78%	67%	97%	87%
	5	96%	99%	94%	98%	90%	93%	98%	98%	94%	97%	89%	93%
	6	92%	95%	86%	98%	95%	44%	93%	95%	85%	97%	95%	38%
		Ellipse Consistency AOA AV Pass						Ellipse Consistency AOA AV Pass					
		1	2	3	4	5	6	1	2	3	4	5	6
AOA SV Pass	1	99%	98%	80%	98%	100%	80%	98%	98%	100%	100%	100%	100%
	2	100%	99%	97%	97%	100%	98%	98%	99%	99%	100%	100%	98%
	3	97%	98%	99%	99%	99%	100%	100%	99%	99%	99%	100%	100%
	4	99%	100%	81%	78%	99%	90%	98%	100%	82%	82%	100%	91%
	5	99%	99%	97%	98%	99%	96%	99%	99%	97%	100%	98%	98%
	6	99%	97%	100%	99%	99%	94%	100%	98%	89%	99%	99%	54%

Table 66. Improvement from Fast Determinant covariance intersection fusion based augmentation of AOA SV by AOA SV against AFIT target

	Ground Constrained						Non-Ground Constrained					
RMSE												
	AOA SV Pass						AOA SV Pass					
AOA SV Pass	1	2	3	4	5	6	1	2	3	4	5	6
1	0%	5%	36%	44%	1%	73%	0%	10%	38%	41%	2%	75%
2	48%	0%	65%	45%	25%	85%	46%	0%	63%	39%	22%	85%
3	0%	0%	-69%	0%	0%	58%	0%	0%	-65%	0%	0%	60%
4	46%	3%	38%	0%	4%	74%	45%	7%	43%	0%	4%	77%
5	54%	36%	70%	53%	0%	87%	50%	34%	68%	47%	0%	87%
6	0%	0%	0%	0%	0%	0%	0%	0%	0%	0%	0%	0%
Ave Miss												
	AOA SV Pass						AOA SV Pass					
AOA SV Pass	1	2	3	4	5	6	1	2	3	4	5	6
1	0%	5%	37%	44%	1%	72%	0%	10%	41%	42%	2%	74%
2	45%	0%	64%	45%	27%	84%	43%	0%	62%	39%	24%	84%
3	0%	0%	-74%	0%	0%	56%	0%	0%	-67%	0%	0%	56%
4	43%	3%	37%	0%	4%	72%	43%	7%	42%	0%	4%	75%
5	52%	38%	69%	53%	0%	86%	48%	36%	68%	47%	0%	86%
6	0%	0%	0%	0%	0%	0%	0%	0%	0%	0%	0%	0%
Ave SMA												
	AOA SV Pass						AOA SV Pass					
AOA SV Pass	1	2	3	4	5	6	1	2	3	4	5	6
1	0%	1%	46%	34%	-1%	75%	0%	3%	57%	35%	-2%	79%
2	54%	0%	75%	54%	4%	89%	52%	0%	79%	50%	4%	90%
3	0%	0%	-33%	0%	0%	54%	0%	0%	-3%	0%	0%	51%
4	32%	-3%	44%	0%	0%	74%	35%	-2%	57%	0%	0%	79%
5	59%	16%	78%	61%	0%	90%	57%	17%	82%	58%	0%	91%
6	0%	0%	0%	0%	0%	0%	0%	0%	0%	0%	0%	0%

Table 67. Fast Determinant covariance intersection geolocation fusion consistency for augmentation of AOA SV by AOA SV against AFIT target

		Ground Constrained						Non-Ground Constrained					
		Ellipsoid Consistency AOA SV Pass						Ellipsoid Consistency AOA SV Pass					
		1	2	3	4	5	6	1	2	3	4	5	6
AOA SV Pass	1	91%	96%	91%	99%	95%	91%	93%	95%	93%	100%	96%	94%
	2	96%	94%	94%	96%	99%	94%	95%	94%	94%	96%	99%	94%
	3	91%	94%	91%	98%	95%	97%	93%	94%	98%	95%	94%	100%
	4	99%	96%	98%	98%	95%	98%	100%	96%	95%	95%	96%	95%
	5	95%	99%	95%	95%	95%	95%	96%	99%	94%	96%	94%	94%
	6	91%	94%	97%	98%	95%	95%	94%	94%	100%	95%	94%	95%
		Ellipse Consistency AOA SV Pass						Ellipse Consistency AOA SV Pass					
		1	2	3	4	5	6	1	2	3	4	5	6
AOA SV Pass	1	98%	98%	99%	100%	99%	99%	100%	98%	100%	100%	100%	100%
	2	98%	98%	98%	98%	100%	98%	98%	98%	98%	99%	100%	98%
	3	99%	98%	99%	98%	99%	100%	100%	98%	99%	99%	99%	100%
	4	100%	98%	98%	98%	99%	98%	100%	99%	99%	99%	100%	99%
	5	99%	100%	99%	99%	99%	99%	100%	100%	99%	100%	99%	99%
	6	99%	98%	100%	98%	99%	100%	100%	98%	100%	99%	99%	100%

Table 68. Improvement from Fast Trace covariance intersection fusion based augmentation of AOA SV by AOA SV against AFIT target

	Ground Constrained						Non-Ground Constrained					
RMSE												
	AOA SV Pass						AOA SV Pass					
AOA SV Pass	1	2	3	4	5	6	1	2	3	4	5	6
1	-1%	16%	63%	47%	7%	74%	-1%	20%	64%	45%	9%	76%
2	54%	-2%	79%	50%	26%	86%	52%	-2%	77%	47%	26%	86%
3	3%	-2%	0%	8%	1%	59%	3%	-2%	0%	8%	2%	61%
4	46%	5%	64%	6%	11%	76%	45%	12%	66%	6%	15%	79%
5	56%	35%	82%	59%	0%	88%	53%	35%	81%	55%	1%	88%
6	1%	-2%	40%	11%	0%	3%	0%	-1%	39%	10%	1%	3%
Ave Miss												
	AOA SV Pass						AOA SV Pass					
AOA SV Pass	1	2	3	4	5	6	1	2	3	4	5	6
1	0%	16%	64%	46%	6%	73%	0%	20%	65%	44%	9%	75%
2	53%	-3%	79%	49%	28%	85%	50%	-2%	77%	46%	27%	84%
3	3%	-3%	-2%	6%	0%	57%	3%	-2%	-1%	6%	1%	57%
4	44%	4%	64%	3%	10%	74%	43%	11%	66%	4%	14%	76%
5	54%	37%	82%	58%	0%	87%	51%	36%	81%	54%	1%	86%
6	2%	-3%	41%	9%	0%	3%	1%	-2%	40%	8%	1%	3%
Ave SMA												
	AOA SV Pass						AOA SV Pass					
AOA SV Pass	1	2	3	4	5	6	1	2	3	4	5	6
1	0%	2%	58%	36%	-8%	75%	0%	6%	57%	35%	-8%	78%
2	55%	0%	81%	52%	5%	88%	54%	0%	79%	48%	5%	89%
3	-4%	-2%	0%	-6%	-1%	54%	-4%	-2%	0%	-5%	-2%	61%
4	33%	-8%	56%	0%	-1%	74%	35%	-7%	56%	0%	1%	79%
5	56%	16%	83%	61%	0%	90%	54%	18%	82%	58%	0%	91%
6	-3%	-1%	26%	1%	-1%	0%	-3%	-1%	24%	0%	-1%	0%

Table 69. Fast Trace covariance intersection geolocation fusion consistency for augmentation of AOA SV by AOA SV against AFIT target

		Ground Constrained						Non-Ground Constrained					
		Ellipsoid Consistency AOA AV Pass						Ellipsoid Consistency AOA AV Pass					
		1	2	3	4	5	6	1	2	3	4	5	6
AOA SV Pass	1	91%	97%	94%	100%	99%	93%	93%	96%	96%	100%	97%	96%
	2	97%	94%	95%	98%	99%	95%	96%	94%	94%	99%	99%	94%
	3	94%	95%	91%	98%	95%	97%	96%	94%	98%	97%	95%	99%
	4	100%	98%	98%	98%	99%	98%	100%	99%	97%	95%	97%	97%
	5	99%	99%	95%	99%	95%	95%	97%	99%	95%	97%	94%	94%
	6	93%	95%	97%	98%	95%	95%	96%	94%	99%	97%	94%	95%
		Ellipse Consistency AOA AV Pass						Ellipse Consistency AOA AV Pass					
		100%	200%	300%	400%	500%	600%	100%	200%	300%	400%	500%	600%
AOA SV Pass	1	98%	98%	100%	100%	100%	100%	100%	99%	100%	100%	100%	100%
	2	98%	98%	98%	98%	100%	98%	99%	98%	98%	100%	100%	98%
	3	100%	98%	99%	99%	99%	100%	100%	98%	99%	100%	100%	100%
	4	100%	98%	99%	98%	100%	99%	100%	100%	100%	99%	100%	99%
	5	100%	100%	99%	100%	99%	99%	100%	100%	100%	100%	99%	99%
	6	100%	98%	100%	99%	99%	100%	100%	98%	100%	99%	99%	100%

Table 70. Improvement from Ellipsoid Intersection fusion based augmentation of AOA SV by AOA SV against AFIT target

	Ground Constrained						Non-Ground Constrained					
RMSE												
	AOA SV Pass						AOA SV Pass					
AOA SV Pass	1	2	3	4	5	6	1	2	3	4	5	6
1	-	-	-	-	-	-	-1%	26%	67%	45%	13%	78%
2	-	-	-	-	-	-	56%	-2%	78%	50%	26%	87%
3	-	-	-	-	-	-	11%	1%	0%	14%	6%	62%
4	-	-	-	-	-	-	45%	17%	68%	6%	22%	82%
5	-	-	-	-	-	-	55%	35%	82%	60%	1%	88%
6	-	-	-	-	-	-	5%	8%	41%	23%	4%	3%
Ave Miss												
	AOA SV Pass						AOA SV Pass					
AOA SV Pass	1	2	3	4	5	6	1	2	3	4	5	6
1	-	-	-	-	-	-	0%	28%	68%	44%	13%	76%
2	-	-	-	-	-	-	55%	-2%	78%	49%	26%	85%
3	-	-	-	-	-	-	9%	0%	-1%	13%	6%	58%
4	-	-	-	-	-	-	43%	17%	68%	4%	22%	80%
5	-	-	-	-	-	-	53%	36%	82%	59%	1%	87%
6	-	-	-	-	-	-	6%	7%	41%	21%	4%	3%
	-	-	-	-	-	-						
Ave SMA												
	AOA SV Pass						AOA SV Pass					
AOA SV Pass	1	2	3	4	5	6	1	2	3	4	5	6
1	-	-	-	-	-	-	29%	32%	65%	54%	11%	79%
2	-	-	-	-	-	-	66%	29%	80%	59%	33%	91%
3	-	-	-	-	-	-	16%	3%	29%	8%	4%	69%
4	-	-	-	-	-	-	54%	16%	61%	29%	29%	85%
5	-	-	-	-	-	-	62%	42%	83%	70%	29%	91%
6	-	-	-	-	-	-	2%	14%	40%	31%	2%	29%

Table 71. Ellipsoid Intersection geolocation fusion consistency for augmentation of AOA SV by AOA SV against AFIT target

		Ground Constrained						Non-Ground Constrained					
		Ellipsoid Consistency AOA AV Pass						Ellipsoid Consistency AOA AV Pass					
		1	2	3	4	5	6	1	2	3	4	5	6
AOA SV Pass	1	-	-	-	-	-	-	0.74	0.93	0.95	0.96	0.96	0.94
	2	-	-	-	-	-	-	0.93	0.74	0.93	0.93	0.93	0.92
	3	-	-	-	-	-	-	0.94	0.94	0.67	0.95	0.95	0.94
	4	-	-	-	-	-	-	0.97	0.93	0.95	0.72	0.95	0.96
	5	-	-	-	-	-	-	0.98	0.93	0.94	0.95	0.75	0.94
	6	-	-	-	-	-	-	0.95	0.92	0.94	0.96	0.95	0.73
		Ellipse Consistency AOA AV Pass						Ellipse Consistency AOA AV Pass					
		1	2	3	4	5	6	1	2	3	4	5	6
AOA SV Pass	1	-	-	-	-	-	-	0.93	1.00	1.00	1.00	1.00	0.99
	2	-	-	-	-	-	-	1.00	0.93	0.98	0.99	1.00	0.98
	3	-	-	-	-	-	-	1.00	0.98	0.97	0.99	1.00	1.00
	4	-	-	-	-	-	-	1.00	0.99	0.99	0.93	0.98	0.99
	5	-	-	-	-	-	-	1.00	1.00	1.00	0.98	0.95	0.99
	6	-	-	-	-	-	-	0.99	0.98	1.00	0.99	0.99	0.91

Table 72. mprovement from Kalman filter fusion based augmentation of AOA SV by AOA SV against AFIT target

		Ground Constrained						Non-Ground Constrained					
Average RMSE													
		Augmented AOA SV Pass						Augmented AOA SV Pass					
		1	2	3	4	5	6	1	2	3	4	5	6
AOA SV Pass	1	-1%	25%	66%	47%	12%	77%	-1%	27%	67%	45%	14%	78%
	2	60%	-2%	80%	53%	26%	87%	56%	-2%	78%	50%	26%	87%
	3	11%	1%	0%	15%	5%	59%	11%	1%	0%	14%	6%	62%
	4	46%	10%	67%	6%	20%	80%	45%	17%	68%	6%	23%	82%
	5	58%	35%	83%	63%	0%	88%	55%	35%	82%	59%	1%	88%
	6	11%	7%	41%	25%	1%	3%	5%	8%	41%	23%	5%	3%
Average Miss													
		Augmented AOA SV Pass						Augmented AOA SV Pass					
		1	2	3	4	5	6	1	2	3	4	5	6
AOA SV Pass	1	0%	27%	66%	46%	10%	77%	0%	28%	68%	44%	13%	76%
	2	60%	-3%	79%	51%	27%	86%	55%	-2%	78%	49%	26%	85%
	3	9%	0%	-2%	13%	4%	57%	10%	0%	-1%	13%	6%	58%
	4	44%	9%	67%	3%	19%	78%	43%	17%	68%	4%	22%	80%
	5	56%	36%	83%	62%	0%	87%	53%	36%	82%	59%	1%	87%
	6	13%	7%	42%	22%	2%	3%	6%	7%	41%	21%	5%	3%
Average SMA													
		Augmented AOA SV Pass						Augmented AOA SV Pass					
		1	2	3	4	5	6	1	2	3	4	5	6
AOA SV Pass	1	29%	26%	66%	55%	9%	77%	29%	32%	65%	54%	11%	79%
	2	66%	29%	82%	60%	33%	90%	66%	29%	80%	59%	33%	91%
	3	16%	2%	29%	8%	4%	65%	16%	3%	29%	8%	4%	69%
	4	53%	11%	61%	29%	24%	82%	54%	16%	61%	29%	29%	85%
	5	63%	41%	84%	70%	29%	90%	62%	42%	83%	70%	29%	91%
	6	7%	12%	43%	31%	2%	29%	2%	14%	40%	31%	2%	29%

Table 73. Kalman filter geolocation fusion consistency for augmentation of AOA SV by AOA SV against AFIT target

		Ground Constrained						Non-Ground Constrained					
		Ellipsoid Consistency AOA AV Pass						Ellipsoid Consistency AOA AV Pass					
		1	2	3	4	5	6	1	2	3	4	5	6
AOA SV Pass	1	76%	91%	91%	95%	96%	91%	74%	93%	95%	97%	97%	94%
	2	91%	74%	93%	90%	94%	94%	93%	74%	93%	93%	93%	92%
	3	91%	93%	74%	96%	97%	92%	95%	93%	67%	95%	95%	94%
	4	95%	90%	96%	75%	95%	98%	97%	93%	95%	72%	95%	96%
	5	96%	94%	97%	95%	75%	92%	97%	93%	95%	95%	75%	95%
	6	91%	94%	92%	98%	92%	76%	94%	92%	94%	96%	95%	73%
		Ellipse Consistency AOA AV Pass						Ellipse Consistency AOA AV Pass					
		1	2	3	4	5	6	1	2	3	4	5	6
AOA SV Pass	1	84%	97%	96%	100%	99%	98%	93%	100%	100%	100%	100%	99%
	2	97%	92%	98%	98%	99%	97%	100%	93%	98%	99%	100%	98%
	3	96%	98%	94%	98%	99%	100%	100%	98%	97%	99%	100%	100%
	4	100%	98%	98%	92%	99%	99%	100%	99%	99%	93%	98%	99%
	5	99%	99%	99%	99%	95%	99%	100%	100%	100%	98%	95%	99%
	6	98%	97%	100%	99%	99%	93%	99%	98%	100%	99%	99%	91%

2.1.0.17 AOA Satellite Augmenting AOA Aircraft Against AFIT Target.

The following are the full pass-by-pass fusion results and associated consistencies for each fusion algorithm for the augmentation of an AOA AV geolocation agent by an AOA SV geolocation agent against the AFIT target.

Table 74. Improvement from Largest Ellipsoid fusion based augmentation of AOA AV by AOA SV against AFIT target

	Ground Constrained						Non-Ground Constrained					
RMSE												
	AOA Aircraft Pass						AOA Aircraft Pass					
AOA SV Pass	1	2	3	4	5	6	1	2	3	4	5	6
1	4%	7%	5%	13%	1%	-4%	1%	-1%	2%	12%	-2%	-1%
2	7%	7%	5%	10%	1%	-9%	4%	-3%	1%	10%	1%	-6%
3	2%	3%	4%	9%	1%	-7%	1%	-3%	3%	9%	-2%	-4%
4	4%	3%	4%	11%	4%	-6%	2%	-3%	2%	9%	2%	-3%
5	3%	6%	2%	9%	4%	-4%	1%	-1%	3%	8%	2%	-1%
6	2%	2%	3%	8%	-1%	-8%	1%	-2%	3%	8%	-2%	-4%
Ave Miss												
	AOA Aircraft Pass						AOA Aircraft Pass					
AOA SV Pass	1	2	3	4	5	6	1	2	3	4	5	6
1	0%	4%	4%	14%	-1%	-2%	-1%	-1%	0%	11%	-3%	2%
2	4%	4%	7%	14%	1%	-2%	2%	-2%	0%	9%	0%	-1%
3	-2%	2%	5%	11%	-1%	-6%	-1%	-2%	1%	9%	-3%	0%
4	0%	1%	5%	14%	2%	-3%	0%	-2%	0%	10%	1%	0%
5	-1%	5%	6%	13%	4%	-2%	-1%	0%	2%	8%	1%	0%
6	-2%	0%	4%	10%	-3%	-6%	-1%	-1%	1%	8%	-4%	-1%
Ave SMA												
	AOA Aircraft Pass						AOA Aircraft Pass					
AOA SV Pass	1	2	3	4	5	6	1	2	3	4	5	6
1	0%	0%	0%	0%	0%	0%	0%	0%	0%	0%	0%	0%
2	0%	0%	0%	0%	0%	0%	0%	0%	0%	0%	0%	0%
3	0%	0%	0%	0%	0%	0%	0%	0%	0%	0%	0%	0%
4	0%	0%	0%	0%	0%	0%	0%	0%	0%	0%	0%	0%
5	0%	0%	0%	0%	0%	0%	0%	0%	0%	0%	0%	0%
6	0%	0%	0%	0%	0%	0%	0%	0%	0%	0%	0%	0%

Table 75. Largest Ellipsoid geolocation fusion consistency for augmentation of AOA AV by AOA SV against AFIT target

		Ground Constrained						Non-Ground Constrained					
		Ellipsoid Consistency AOA Aircraft Pass						Ellipsoid Consistency AOA Aircraft Pass					
		1	2	3	4	5	6	1	2	3	4	5	6
AOA SV Pass	1	89%	91%	91%	94%	95%	90%	95%	96%	93%	97%	96%	94%
	2	94%	91%	91%	97%	97%	90%	96%	95%	94%	98%	96%	92%
	3	89%	91%	90%	95%	93%	89%	95%	95%	94%	96%	96%	93%
	4	93%	91%	90%	95%	93%	88%	95%	95%	95%	94%	96%	93%
	5	92%	91%	92%	97%	99%	90%	95%	96%	95%	97%	97%	94%
	6	84%	91%	90%	97%	92%	88%	94%	95%	94%	95%	97%	93%
		Ellipse Consistency AOA Aircraft Pass						Ellipse Consistency AOA Aircraft Pass					
		1	2	3	4	5	6	1	2	3	4	5	6
AOA SV Pass	1	100%	97%	99%	100%	100%	97%	100%	99%	100%	100%	100%	100%
	2	100%	98%	99%	100%	100%	98%	100%	99%	100%	100%	100%	99%
	3	100%	94%	99%	100%	99%	98%	100%	99%	100%	99%	100%	100%
	4	100%	95%	99%	99%	100%	98%	100%	99%	100%	99%	100%	100%
	5	100%	97%	99%	100%	100%	98%	100%	99%	100%	100%	100%	99%
	6	100%	95%	99%	100%	100%	98%	100%	99%	100%	99%	100%	100%

Table 76. Improvement from Fast Determinant CI fusion based augmentation of AOA AV by AOA SV against AFIT target

	Ground Constrained						Non-Ground Constrained					
RMSE												
	AOA Aircraft Pass							AOA Aircraft Pass				
AOA SV Pass	1	2	3	4	5	6	AOA SV Pass	1	2	3	4	5	6
1	2%	1%	4%	8%	0%	-7%	1	1%	-3%	3%	8%	-2%	-4%
2	2%	1%	4%	8%	0%	-7%	2	1%	-3%	3%	8%	-2%	-4%
3	2%	1%	4%	8%	0%	-7%	3	1%	-3%	3%	8%	-2%	-4%
4	2%	1%	4%	8%	0%	-7%	4	1%	-3%	3%	8%	-2%	-4%
5	2%	1%	4%	8%	0%	-7%	5	1%	-3%	3%	8%	-2%	-4%
6	2%	1%	4%	8%	0%	-7%	6	1%	-3%	3%	8%	-2%	-4%
Ave Miss												
	AOA Aircraft Pass							AOA Aircraft Pass				
AOA SV Pass	1	2	3	4	5	6	AOA SV Pass	1	2	3	4	5	6
1	-2%	0%	4%	10%	-2%	-6%	1	-1%	-2%	1%	8%	-3%	0%
2	-2%	0%	4%	10%	-2%	-6%	2	-1%	-2%	1%	8%	-3%	0%
3	-2%	0%	4%	10%	-2%	-6%	3	-1%	-2%	1%	8%	-3%	0%
4	-2%	0%	4%	10%	-2%	-6%	4	-1%	-2%	1%	8%	-3%	0%
5	-2%	0%	4%	10%	-2%	-6%	5	-1%	-2%	1%	8%	-3%	0%
6	-2%	0%	4%	10%	-2%	-6%	6	-1%	-2%	1%	8%	-3%	0%
Ave SMA												
	AOA Aircraft Pass							AOA Aircraft Pass				
AOA SV Pass	1	2	3	4	5	6	AOA SV Pass	1	2	3	4	5	6
1	0%	0%	0%	0%	0%	0%	1	0%	0%	0%	0%	0%	0%
2	0%	0%	0%	0%	0%	0%	2	0%	0%	0%	0%	0%	0%
3	0%	0%	0%	0%	0%	0%	3	0%	0%	0%	0%	0%	0%
4	0%	0%	0%	0%	0%	0%	4	0%	0%	0%	0%	0%	0%
5	0%	0%	0%	0%	0%	0%	5	0%	0%	0%	0%	0%	0%
6	0%	0%	0%	0%	0%	0%	6	0%	0%	0%	0%	0%	0%

Table 77. Fast Determinant CI geolocation fusion consistency for augmentation of AOA AV by AOA SV against AFIT target

		Ground Constrained						Non-Ground Constrained					
		Ellipsoid Consistency AOA Aircraft Pass						Ellipsoid Consistency AOA Aircraft Pass					
		1	2	3	4	5	6	1	2	3	4	5	6
AOA SV Pass	1	86%	91%	91%	97%	93%	88%	94%	95%	94%	94%	96%	93%
	2	86%	91%	91%	97%	93%	88%	94%	95%	94%	94%	96%	93%
	3	86%	91%	91%	97%	93%	88%	94%	95%	94%	94%	96%	93%
	4	86%	91%	91%	97%	93%	88%	94%	95%	94%	94%	96%	93%
	5	86%	91%	91%	97%	93%	88%	94%	95%	94%	94%	96%	93%
	6	86%	91%	91%	97%	93%	88%	94%	95%	94%	94%	96%	93%
		Ellipse Consistency AOA Aircraft Pass						Ellipse Consistency AOA Aircraft Pass					
		1	2	3	4	5	6	1	2	3	4	5	6
AOA SV Pass	1	100%	95%	99%	100%	100%	97%	100%	99%	100%	99%	100%	100%
	2	100%	95%	99%	100%	100%	97%	100%	99%	100%	99%	100%	100%
	3	100%	95%	99%	100%	100%	97%	100%	99%	100%	99%	100%	100%
	4	100%	95%	99%	100%	100%	97%	100%	99%	100%	99%	100%	100%
	5	100%	95%	99%	100%	100%	97%	100%	99%	100%	99%	100%	100%
	6	100%	95%	99%	100%	100%	97%	100%	99%	100%	99%	100%	100%

Table 78. Improvement from Fast Trace CI fusion based augmentation of AOA AV by AOA SV against AFIT target

	Ground Constrained						Non-Ground Constrained					
RMSE												
	AOA Aircraft Pass						AOA Aircraft Pass					
AOA SV Pass	1	2	3	4	5	6	1	2	3	4	5	6
1	2%	1%	4%	8%	0%	-7%	1%	-3%	3%	8%	-2%	-4%
2	2%	1%	4%	8%	0%	-7%	1%	-3%	3%	8%	-2%	-4%
3	2%	1%	4%	8%	0%	-7%	1%	-3%	3%	8%	-2%	-4%
4	2%	1%	4%	8%	0%	-7%	1%	-3%	3%	8%	-2%	-4%
5	2%	1%	4%	8%	0%	-7%	1%	-3%	3%	8%	-2%	-4%
6	2%	1%	4%	8%	0%	-7%	1%	-3%	3%	8%	-2%	-4%
Ave Miss												
	AOA Aircraft Pass						AOA Aircraft Pass					
AOA SV Pass	1	2	3	4	5	6	1	2	3	4	5	6
1	-2%	0%	4%	10%	-2%	-6%	-1%	-2%	1%	9%	-3%	0%
2	-2%	0%	4%	10%	-2%	-5%	-1%	-2%	1%	9%	-3%	0%
3	-2%	0%	4%	10%	-2%	-6%	-1%	-2%	1%	8%	-3%	0%
4	-2%	0%	4%	10%	-2%	-6%	-1%	-2%	1%	9%	-3%	0%
5	-2%	0%	4%	10%	-2%	-5%	-1%	-2%	1%	9%	-3%	0%
6	-2%	0%	4%	10%	-2%	-6%	-1%	-2%	1%	8%	-3%	0%
Ave SMA												
	AOA Aircraft Pass						AOA Aircraft Pass					
AOA SV Pass	1	2	3	4	5	6	1	2	3	4	5	6
1	0%	0%	0%	0%	0%	0%	0%	0%	0%	0%	0%	0%
2	-1%	0%	-1%	-1%	-1%	-1%	0%	0%	0%	-1%	-1%	-1%
3	0%	0%	0%	0%	0%	0%	0%	0%	0%	0%	0%	0%
4	0%	0%	0%	0%	0%	0%	0%	0%	0%	0%	0%	0%
5	-1%	-1%	-1%	-2%	-2%	-2%	-1%	0%	0%	-1%	-2%	-2%
6	0%	0%	0%	0%	0%	0%	0%	0%	0%	0%	0%	0%

Table 79. Fast Trace CI geolocation fusion consistency for augmentation of AOA AV by AOA SV against AFIT target

		Ground Constrained						Non-Ground Constrained					
		Ellipsoid Consistency AOA Aircraft Pass						Ellipsoid Consistency AOA Aircraft Pass					
		1	2	3	4	5	6	1	2	3	4	5	6
AOA SV Pass	1	86%	91%	91%	97%	94%	88%	94%	95%	94%	94%	96%	93%
	2	86%	91%	91%	97%	94%	89%	95%	95%	94%	97%	96%	93%
	3	86%	91%	91%	97%	93%	88%	94%	95%	94%	94%	96%	93%
	4	86%	91%	91%	97%	94%	88%	94%	95%	94%	94%	96%	93%
	5	86%	91%	91%	97%	94%	90%	95%	95%	94%	97%	98%	93%
	6	86%	91%	91%	97%	93%	88%	94%	95%	94%	94%	96%	93%
		Ellipse Consistency AOA Aircraft Pass						Ellipse Consistency AOA Aircraft Pass					
		1	2	3	4	5	6	1	2	3	4	5	6
AOA SV Pass	1	100%	95%	99%	100%	100%	97%	100%	99%	100%	99%	100%	100%
	2	100%	95%	99%	100%	100%	98%	100%	99%	100%	100%	100%	100%
	3	100%	95%	99%	100%	100%	97%	100%	99%	100%	99%	100%	100%
	4	100%	95%	99%	100%	100%	97%	100%	99%	100%	99%	100%	100%
	5	100%	95%	99%	100%	100%	98%	100%	99%	100%	100%	100%	100%
	6	100%	95%	99%	100%	100%	97%	100%	99%	100%	99%	100%	100%

Table 80. Improvement from Ellipsoid Intersection fusion based augmentation of AOA AV by AOA SV against AFIT target

Ground Constrained

RMSE

AOA SV Pass \ AOA Aircraft Pass	1	2	3	4	5	6
1	-	-	-	-	-	-
2	-	-	-	-	-	-
3	-	-	-	-	-	-
4	-	-	-	-	-	-
5	-	-	-	-	-	-
6	-	-	-	-	-	-

Ave Miss

AOA SV Pass \ AOA Aircraft Pass	1	2	3	4	5	6
1	-	-	-	-	-	-
2	-	-	-	-	-	-
3	-	-	-	-	-	-
4	-	-	-	-	-	-
5	-	-	-	-	-	-
6	-	-	-	-	-	-

Ave SMA

AOA SV Pass \ AOA Aircraft Pass	1	2	3	4	5	6
1	-	-	-	-	-	-
2	-	-	-	-	-	-
3	-	-	-	-	-	-
4	-	-	-	-	-	-
5	-	-	-	-	-	-
6	-	-	-	-	-	-

Non-Ground Constrained

RMSE

AOA SV Pass \ AOA Aircraft Pass	1	2	3	4	5	6
1	-207%	-186%	-271%	-57%	-376%	-59%
2	-385%	-280%	-339%	-134%	-789%	-330%
3	-4%	-10%	-5%	6%	1%	-8%
4	-578%	-104%	-407%	-71%	-200%	-17%
5	-441%	-319%	-1274%	-348%	-718%	-366%
6	-42%	-23%	-56%	-21%	-27%	-29%

Ave Miss

AOA SV Pass \ AOA Aircraft Pass	1	2	3	4	5	6
1	-247%	-209%	-318%	-62%	-437%	-62%
2	-451%	-316%	-396%	-152%	-917%	-379%
3	-6%	-10%	-8%	5%	-1%	-4%
4	-667%	-123%	-471%	-80%	-231%	-15%
5	-514%	-361%	-1455%	-401%	-836%	-421%
6	-50%	-22%	-62%	-20%	-29%	-26%

Ave SMA

AOA SV Pass \ AOA Aircraft Pass	1	2	3	4	5	6
1	0%	1%	0%	2%	1%	2%
2	1%	1%	1%	2%	3%	3%
3	0%	0%	0%	0%	0%	0%
4	1%	0%	0%	2%	3%	2%
5	1%	1%	1%	4%	3%	3%
6	0%	0%	0%	1%	0%	0%

Table 81. Ellipsoid Intersection geolocation fusion consistency for augmentation of AOA AV by AOA SV against AFIT target

	Ground Constrained						Non-Ground Constrained					
	Ellipsoid Consistency AOA Aircraft Pass						Ellipsoid Consistency AOA Aircraft Pass					
AOA SV Pass	1	2	3	4	5	6	1	2	3	4	5	6
1	-	-	-	-	-	-	0%	2%	0%	77%	0%	77%
2	-	-	-	-	-	-	0%	1%	0%	38%	0%	0%
3	-	-	-	-	-	-	89%	91%	89%	95%	96%	92%
4	-	-	-	-	-	-	0%	0%	0%	56%	8%	80%
5	-	-	-	-	-	-	0%	0%	0%	0%	0%	0%
6	-	-	-	-	-	-	52%	86%	53%	90%	81%	83%
	Ellipse Consistency AOA Aircraft Pass						Ellipse Consistency AOA Aircraft Pass					
AOA SV Pass	1	2	3	4	5	6	1	2	3	4	5	6
1	-	-	-	-	-	-	100%	99%	100%	100%	100%	100%
2	-	-	-	-	-	-	100%	99%	100%	100%	100%	99%
3	-	-	-	-	-	-	100%	99%	100%	99%	100%	100%
4	-	-	-	-	-	-	100%	99%	100%	99%	100%	100%
5	-	-	-	-	-	-	100%	99%	100%	100%	100%	99%
6	-	-	-	-	-	-	100%	99%	100%	99%	100%	100%

Table 82. Improvement from Kalman filter fusion based augmentation of AOA AV by AOA SV against AFIT target

	Ground Constrained						Non-Ground Constrained					
RMSE												
	AOA Aircraft Pass						AOA Aircraft Pass					
AOA SV Pass	1	2	3	4	5	6	1	2	3	4	5	6
1	4%	7%	5%	13%	1%	-4%	1%	-1%	2%	12%	-2%	-1%
2	7%	7%	5%	10%	1%	-9%	4%	-3%	1%	10%	1%	-6%
3	2%	3%	4%	9%	1%	-7%	1%	-3%	3%	9%	-2%	-4%
4	4%	3%	4%	11%	4%	-6%	2%	-3%	2%	9%	2%	-3%
5	3%	6%	2%	9%	4%	-4%	1%	-1%	3%	8%	2%	-1%
6	2%	2%	3%	8%	-1%	-8%	1%	-2%	3%	8%	-2%	-4%
Ave Miss												
	AOA Aircraft Pass						AOA Aircraft Pass					
AOA SV Pass	1	2	3	4	5	6	1	2	3	4	5	6
1	0%	4%	4%	14%	-1%	-2%	-1%	-1%	0%	11%	-3%	2%
2	4%	4%	7%	14%	1%	-2%	2%	-2%	0%	9%	0%	-1%
3	-2%	2%	5%	11%	-1%	-6%	-1%	-2%	1%	9%	-3%	0%
4	0%	1%	5%	14%	2%	-3%	0%	-2%	0%	10%	1%	0%
5	-1%	5%	6%	13%	4%	-2%	-1%	0%	2%	8%	1%	0%
6	-2%	0%	4%	10%	-3%	-6%	-1%	-1%	1%	8%	-4%	-1%
Ave SMA												
	AOA Aircraft Pass						AOA Aircraft Pass					
AOA SV Pass	1	2	3	4	5	6	1	2	3	4	5	6
1	0%	4%	2%	3%	1%	2%	0%	1%	0%	2%	1%	2%
2	2%	9%	3%	5%	3%	3%	1%	1%	1%	2%	3%	3%
3	0%	1%	0%	1%	0%	0%	0%	0%	0%	0%	0%	0%
4	1%	7%	2%	4%	3%	3%	1%	0%	0%	2%	3%	2%
5	2%	9%	4%	6%	3%	4%	1%	1%	1%	4%	3%	3%
6	0%	1%	0%	1%	0%	1%	0%	0%	0%	1%	0%	0%

Table 83. Kalman filter geolocation fusion consistency for augmentation of AOA AV by AOA SV against AFIT target

		Ground Constrained						Non-Ground Constrained					
		Ellipsoid Consistency AOA Aircraft Pass						Ellipsoid Consistency AOA Aircraft Pass					
		1	2	3	4	5	6	1	2	3	4	5	6
AOA SV Pass	1	86%	91%	91%	97%	94%	88%	94%	95%	94%	94%	96%	93%
	2	86%	91%	91%	97%	94%	89%	95%	95%	94%	97%	96%	93%
	3	86%	91%	91%	97%	93%	88%	94%	95%	94%	94%	96%	93%
	4	86%	91%	91%	97%	94%	88%	94%	95%	94%	94%	96%	93%
	5	86%	91%	91%	97%	94%	90%	95%	95%	94%	97%	98%	93%
	6	86%	91%	91%	97%	93%	88%	94%	95%	94%	94%	96%	93%
		Ellipse Consistency AOA Aircraft Pass						Ellipse Consistency AOA Aircraft Pass					
		1	2	3	4	5	6	1	2	3	4	5	6
AOA SV Pass	1	100%	95%	99%	100%	100%	97%	100%	99%	100%	99%	100%	100%
	2	100%	95%	99%	100%	100%	98%	100%	99%	100%	100%	100%	100%
	3	100%	95%	99%	100%	100%	97%	100%	99%	100%	99%	100%	100%
	4	100%	95%	99%	100%	100%	97%	100%	99%	100%	99%	100%	100%
	5	100%	95%	99%	100%	100%	98%	100%	99%	100%	100%	100%	100%
	6	100%	95%	99%	100%	100%	97%	100%	99%	100%	99%	100%	100%

2.1.0.18 AOA Satellite Augmenting Three-ball TDOA Satellites Against AFIT Target.

The following are the full pass-by-pass fusion results and associated consistencies for each fusion algorithm for the augmentation of a three-ball TDOA SV geolocation agent by an AOA SV geolocation agent against the AFIT target.

Table 84. Improvement from Largest Ellipsoid fusion based augmentation of three-ball TDOA SV by AOA SV against AFIT target

	Ground Constrained						Non-Ground Constrained					
RMSE												
	Three-ball TDOA Satellite Pass						Three-ball TDOA Satellite Pass					
	1	2	3	4	5	6		1	2	3	4	5	6
AOA SV Pass 1	30%	15%	67%	46%	19%	35%	AOA SV Pass 1	70%	69%	93%	82%	79%	95%
AOA SV Pass 2	57%	25%	66%	53%	28%	65%	AOA SV Pass 2	85%	82%	95%	84%	86%	97%
AOA SV Pass 3	10%	7%	25%	6%	4%	24%	AOA SV Pass 3	55%	42%	85%	42%	47%	91%
AOA SV Pass 4	45%	20%	57%	19%	7%	56%	AOA SV Pass 4	81%	73%	93%	68%	74%	96%
AOA SV Pass 5	60%	31%	73%	63%	33%	64%	AOA SV Pass 5	86%	85%	96%	87%	88%	97%
AOA SV Pass 6	3%	6%	41%	20%	4%	14%	AOA SV Pass 6	26%	22%	86%	67%	60%	84%
Ave Miss													
	Three-ball TDOA Satellite Pass						Three-ball TDOA Satellite Pass					
	1	2	3	4	5	6		1	2	3	4	5	6
AOA SV Pass 1	28%	17%	65%	46%	20%	32%	AOA SV Pass 1	68%	70%	93%	81%	78%	95%
AOA SV Pass 2	57%	26%	63%	50%	27%	62%	AOA SV Pass 2	84%	82%	95%	82%	85%	97%
AOA SV Pass 3	9%	9%	25%	6%	2%	20%	AOA SV Pass 3	53%	41%	83%	38%	46%	90%
AOA SV Pass 4	42%	20%	56%	19%	4%	54%	AOA SV Pass 4	79%	72%	92%	64%	73%	96%
AOA SV Pass 5	58%	31%	72%	59%	32%	60%	AOA SV Pass 5	85%	84%	95%	85%	87%	97%
AOA SV Pass 6	1%	8%	38%	19%	3%	12%	AOA SV Pass 6	25%	22%	85%	65%	60%	84%
Ave SMA													
	Three-ball TDOA Satellite Pass						Three-ball TDOA Satellite Pass					
	1	2	3	4	5	6		1	2	3	4	5	6
AOA SV Pass 1	56%	0%	34%	36%	0%	62%	AOA SV Pass 1	87%	65%	93%	76%	74%	96%
AOA SV Pass 2	54%	0%	73%	59%	8%	58%	AOA SV Pass 2	85%	84%	97%	87%	88%	98%
AOA SV Pass 3	0%	0%	0%	0%	0%	0%	AOA SV Pass 3	44%	38%	88%	52%	61%	92%
AOA SV Pass 4	37%	0%	61%	54%	0%	35%	AOA SV Pass 4	76%	65%	93%	86%	74%	96%
AOA SV Pass 5	65%	22%	73%	58%	1%	70%	AOA SV Pass 5	89%	85%	97%	86%	89%	98%
AOA SV Pass 6	11%	0%	0%	0%	0%	25%	AOA SV Pass 6	71%	52%	91%	62%	66%	94%

Table 85. Largest Ellipsoid geolocation fusion consistency for augmentation of three-ball TDOA SV by AOA SV against AFIT target

		Ground Constrained						Non-Ground Constrained					
		Ellipsoid Consistency						Ellipsoid Consistency					
		Three-ball TDOA Satellite Pass						Three-ball TDOA Satellite Pass					
		1	2	3	4	5	6	1	2	3	4	5	6
AOA SV Pass	1	89%	91%	91%	94%	95%	90%	95%	96%	93%	97%	96%	94%
	2	94%	91%	91%	97%	97%	90%	96%	95%	94%	98%	96%	92%
	3	89%	91%	90%	95%	93%	89%	95%	95%	94%	96%	96%	93%
	4	93%	91%	90%	95%	93%	88%	95%	95%	95%	94%	96%	93%
	5	92%	91%	92%	97%	99%	90%	95%	96%	95%	97%	97%	94%
	6	84%	91%	90%	97%	92%	88%	94%	95%	94%	95%	97%	93%
		Ellipse Consistency						Ellipse Consistency					
		Three-ball TDOA Satellite Pass						Three-ball TDOA Satellite Pass					
		1	2	3	4	5	6	1	2	3	4	5	6
AOA SV Pass	1	100%	97%	99%	100%	100%	97%	100%	99%	100%	100%	100%	100%
	2	100%	98%	99%	100%	100%	98%	100%	99%	100%	100%	100%	99%
	3	100%	94%	99%	100%	99%	98%	100%	99%	100%	99%	100%	100%
	4	100%	95%	99%	99%	100%	98%	100%	99%	100%	99%	100%	100%
	5	100%	97%	99%	100%	100%	98%	100%	99%	100%	100%	100%	99%
	6	100%	95%	99%	100%	100%	98%	100%	99%	100%	99%	100%	100%

Table 86. Improvement from Fast Determinant covariance intersection fusion based augmentation of three-ball TDOA SV by AOA SV against AFIT target

	Ground Constrained						Non-Ground Constrained					
RMSE												
	Three-ball TDOA Satellite Pass						Three-ball TDOA Satellite Pass					
AOA SV Pass	1	2	3	4	5	6	1	2	3	4	5	6
1	15%	5%	67%	19%	4%	27%	5%	30%	93%	14%	75%	96%
2	54%	25%	61%	52%	24%	61%	62%	81%	96%	42%	86%	98%
3	-5%	4%	-1%	-4%	3%	8%	2%	-4%	83%	8%	4%	91%
4	41%	7%	57%	5%	4%	54%	14%	49%	93%	10%	69%	97%
5	54%	31%	67%	61%	32%	59%	74%	85%	96%	72%	88%	98%
6	-5%	4%	-1%	-4%	3%	8%	2%	-4%	86%	8%	5%	85%
Ave Miss												
	Three-ball TDOA Satellite Pass						Three-ball TDOA Satellite Pass					
AOA SV Pass	1	2	3	4	5	6	1	2	3	4	5	6
1	15%	6%	65%	18%	4%	25%	7%	30%	92%	11%	73%	96%
2	52%	25%	57%	49%	23%	58%	61%	81%	95%	40%	85%	98%
3	-5%	5%	0%	-3%	2%	10%	4%	-5%	81%	6%	4%	90%
4	39%	8%	56%	6%	3%	52%	16%	48%	92%	7%	68%	96%
5	52%	31%	64%	58%	31%	56%	73%	84%	96%	69%	87%	98%
6	-5%	5%	0%	-3%	2%	9%	4%	-5%	85%	6%	4%	86%
Ave SMA												
	Three-ball TDOA Satellite Pass						Three-ball TDOA Satellite Pass					
AOA SV Pass	1	2	3	4	5	6	1	2	3	4	5	6
1	1%	-1%	52%	10%	0%	3%	1%	15%	93%	3%	64%	96%
2	58%	4%	66%	45%	-3%	64%	39%	74%	97%	21%	85%	98%
3	0%	0%	0%	0%	0%	0%	0%	0%	74%	0%	0%	90%
4	25%	0%	42%	-1%	-2%	36%	6%	38%	93%	1%	49%	96%
5	57%	1%	72%	60%	9%	62%	51%	80%	97%	46%	88%	98%
6	0%	0%	0%	0%	0%	0%	0%	0%	82%	0%	0%	80%

Table 87. Fast Determinant covariance intersection geolocation fusion consistency for augmentation of three-ball TDOA SV by AOA SV against AFIT target

		Ground Constrained						Non-Ground Constrained					
		Ellipsoid Consistency Three-ball TDOA Satellite Pass						Ellipsoid Consistency Three-ball TDOA Satellite Pass					
		1	2	3	4	5	6	1	2	3	4	5	6
AOA SV Pass	1	98%	97%	99%	96%	95%	98%	0%	7%	94%	1%	28%	93%
	2	98%	99%	96%	99%	100%	99%	0%	19%	94%	1%	79%	94%
	3	90%	97%	92%	94%	95%	92%	0%	5%	5%	1%	14%	99%
	4	98%	97%	99%	95%	96%	100%	0%	10%	95%	1%	28%	95%
	5	99%	100%	97%	100%	100%	99%	1%	37%	94%	1%	92%	94%
	6	90%	97%	92%	94%	95%	92%	0%	5%	13%	1%	14%	95%
		Ellipse Consistency Three-ball TDOA Satellite Pass						Ellipse Consistency Three-ball TDOA Satellite Pass					
		1	2	3	4	5	6	1	2	3	4	5	6
AOA SV Pass	1	100%	100%	100%	100%	99%	100%	96%	99%	100%	98%	100%	100%
	2	100%	100%	99%	100%	100%	100%	99%	100%	98%	100%	99%	98%
	3	99%	100%	94%	100%	99%	99%	96%	98%	100%	95%	100%	99%
	4	100%	100%	100%	100%	99%	100%	99%	99%	99%	96%	100%	99%
	5	100%	100%	99%	100%	100%	100%	99%	100%	99%	100%	100%	99%
	6	99%	100%	94%	100%	99%	99%	96%	98%	100%	95%	100%	100%

Table 88. Improvement from Fast Trace CI fusion based augmentation of three-ball TDOA SV by AOA SV against AFIT target

	Ground Constrained						Non-Ground Constrained					
RMSE												
	Three-ball TDOA Satellite Pass						Three-ball TDOA Satellite Pass					
AOA SV Pass	1	2	3	4	5	6	1	2	3	4	5	6
1	29%	10%	67%	45%	11%	35%	67%	68%	93%	79%	75%	96%
2	56%	26%	62%	51%	27%	63%	82%	82%	96%	81%	85%	98%
3	-1%	4%	13%	-2%	3%	15%	55%	43%	82%	43%	45%	91%
4	45%	13%	56%	18%	5%	56%	78%	70%	93%	67%	74%	97%
5	56%	31%	69%	60%	33%	61%	84%	85%	96%	84%	87%	98%
6	-4%	4%	19%	0%	3%	10%	21%	17%	81%	66%	60%	86%
Ave Miss												
	Three-ball TDOA Satellite Pass						Three-ball TDOA Satellite Pass					
AOA SV Pass	1	2	3	4	5	6	1	2	3	4	5	6
1	28%	11%	65%	45%	11%	33%	66%	69%	92%	77%	74%	96%
2	55%	26%	59%	47%	26%	60%	80%	82%	95%	79%	84%	98%
3	-1%	5%	14%	-2%	2%	15%	53%	41%	80%	38%	44%	90%
4	42%	14%	56%	18%	4%	54%	75%	69%	92%	63%	73%	96%
5	54%	31%	66%	57%	32%	58%	82%	84%	96%	82%	87%	98%
6	-4%	5%	17%	0%	2%	10%	21%	17%	80%	62%	60%	86%
Ave SMA												
	Three-ball TDOA Satellite Pass						Three-ball TDOA Satellite Pass					
AOA SV Pass	1	2	3	4	5	6	1	2	3	4	5	6
1	1%	-6%	62%	30%	-2%	6%	67%	65%	93%	77%	74%	96%
2	57%	4%	65%	47%	-4%	63%	86%	84%	97%	85%	88%	98%
3	-4%	-1%	-3%	-5%	-1%	-3%	36%	28%	83%	11%	29%	90%
4	31%	0%	46%	-2%	-7%	45%	76%	63%	93%	64%	72%	96%
5	56%	1%	72%	61%	11%	61%	87%	86%	97%	87%	89%	98%
6	-2%	-1%	8%	-1%	-1%	-3%	-4%	-8%	75%	46%	50%	81%

Table 89. Fast Trace CI geolocation fusion consistency for augmentation of three-ball TDOA SV by AOA SV against AFIT target

		Ground Constrained						Non-Ground Constrained					
		Ellipsoid Consistency						Ellipsoid Consistency					
		Three-ball TDOA Satellite Pass						Three-ball TDOA Satellite Pass					
		1	2	3	4	5	6	1	2	3	4	5	6
AOA SV Pass	1	100%	97%	100%	100%	97%	98%	94%	95%	94%	95%	98%	93%
	2	99%	99%	97%	99%	100%	99%	96%	97%	94%	94%	97%	94%
	3	92%	97%	95%	95%	95%	97%	25%	37%	99%	18%	73%	99%
	4	99%	98%	99%	100%	97%	99%	96%	95%	95%	98%	99%	95%
	5	99%	100%	99%	100%	100%	100%	97%	97%	94%	97%	96%	94%
	6	91%	97%	93%	94%	95%	93%	6%	20%	95%	5%	44%	96%
		Ellipse Consistency						Ellipse Consistency					
		Three-ball TDOA Satellite Pass						Three-ball TDOA Satellite Pass					
		1	2	3	4	5	6	1	2	3	4	5	6
AOA SV Pass	1	100%	100%	100%	100%	99%	100%	100%	100%	100%	100%	100%	100%
	2	100%	100%	99%	100%	100%	100%	98%	98%	98%	98%	98%	98%
	3	99%	100%	98%	100%	99%	100%	100%	100%	99%	100%	100%	99%
	4	100%	100%	100%	100%	100%	100%	100%	100%	99%	100%	99%	99%
	5	100%	100%	100%	100%	100%	100%	100%	100%	99%	100%	99%	99%
	6	99%	100%	98%	100%	99%	99%	100%	100%	100%	100%	100%	100%

Table 90. Improvement from Ellipsoid Intersection fusion based augmentation of three-ball TDOA SV by AOA SV against AFIT target

	Ground Constrained						Non-Ground Constrained					
RMSE												
	Three-ball TDOA Satellite Pass						Three-ball TDOA Satellite Pass					
	1	2	3	4	5	6		1	2	3	4	5	6
AOA SV Pass 1	-	-	-	-	-	-	AOA SV Pass 1	-	-	-	-	-	-
AOA SV Pass 2	-	-	-	-	-	-	AOA SV Pass 2	-	-	-	-	-	-
AOA SV Pass 3	-	-	-	-	-	-	AOA SV Pass 3	-	-	-	-	-	-
AOA SV Pass 4	-	-	-	-	-	-	AOA SV Pass 4	-	-	-	-	-	-
AOA SV Pass 5	-	-	-	-	-	-	AOA SV Pass 5	-	-	-	-	-	-
AOA SV Pass 6	-	-	-	-	-	-	AOA SV Pass 6	-	-	-	-	-	-
Ave Miss													
	Three-ball TDOA Satellite Pass						Three-ball TDOA Satellite Pass					
	1	2	3	4	5	6		1	2	3	4	5	6
AOA SV Pass 1	-	-	-	-	-	-	AOA SV Pass 1	-	-	-	-	-	-
AOA SV Pass 2	-	-	-	-	-	-	AOA SV Pass 2	-	-	-	-	-	-
AOA SV Pass 3	-	-	-	-	-	-	AOA SV Pass 3	-	-	-	-	-	-
AOA SV Pass 4	-	-	-	-	-	-	AOA SV Pass 4	-	-	-	-	-	-
AOA SV Pass 5	-	-	-	-	-	-	AOA SV Pass 5	-	-	-	-	-	-
AOA SV Pass 6	-	-	-	-	-	-	AOA SV Pass 6	-	-	-	-	-	-
Ave SMA													
	Three-ball TDOA Satellite Pass						Three-ball TDOA Satellite Pass					
	1	2	3	4	5	6		1	2	3	4	5	6
AOA SV Pass 1	-	-	-	-	-	-	AOA SV Pass 1	-	-	-	-	-	-
AOA SV Pass 2	-	-	-	-	-	-	AOA SV Pass 2	-	-	-	-	-	-
AOA SV Pass 3	-	-	-	-	-	-	AOA SV Pass 3	-	-	-	-	-	-
AOA SV Pass 4	-	-	-	-	-	-	AOA SV Pass 4	-	-	-	-	-	-
AOA SV Pass 5	-	-	-	-	-	-	AOA SV Pass 5	-	-	-	-	-	-
AOA SV Pass 6	-	-	-	-	-	-	AOA SV Pass 6	-	-	-	-	-	-

Table 91. Ellipsoid Intersection geolocation fusion consistency for augmentation of three-ball TDOA SV by AOA SV against AFIT target

		Ground Constrained						Non-Ground Constrained					
		Ellipsoid Consistency						Ellipsoid Consistency					
		Three-ball TDOA Satellite Pass						Three-ball TDOA Satellite Pass					
		1	2	3	4	5	6	1	2	3	4	5	6
AOA SV Pass	1	-	-	-	-	-	-	-	-	-	-	-	-
	2	-	-	-	-	-	-	-	-	-	-	-	-
	3	-	-	-	-	-	-	-	-	-	-	-	-
	4	-	-	-	-	-	-	-	-	-	-	-	-
	5	-	-	-	-	-	-	-	-	-	-	-	-
	6	-	-	-	-	-	-	-	-	-	-	-	-
		Ellipse Consistency						Ellipse Consistency					
		Three-ball TDOA Satellite Pass						Three-ball TDOA Satellite Pass					
		1	2	3	4	5	6	1	2	3	4	5	6
AOA SV Pass	1	-	-	-	-	-	-	-	-	-	-	-	-
	2	-	-	-	-	-	-	-	-	-	-	-	-
	3	-	-	-	-	-	-	-	-	-	-	-	-
	4	-	-	-	-	-	-	-	-	-	-	-	-
	5	-	-	-	-	-	-	-	-	-	-	-	-
	6	-	-	-	-	-	-	-	-	-	-	-	-

Table 92. Improvement from Kalman filter fusion based augmentation of three-ball TDOA SV by AOA SV against AFIT target

		Ground Constrained						Non-Ground Constrained					
RMSE													
		Three-ball TDOA Satellite Pass						Three-ball TDOA Satellite Pass					
		1	2	3	4	5	6	1	2	3	4	5	6
AOA SV Pass	1	30%	15%	67%	46%	19%	35%	70%	69%	93%	82%	79%	95%
	2	57%	25%	66%	53%	28%	65%	85%	82%	95%	84%	86%	97%
	3	10%	7%	25%	6%	4%	24%	55%	42%	85%	42%	47%	91%
	4	45%	20%	57%	19%	7%	56%	81%	73%	93%	68%	74%	96%
	5	60%	31%	73%	63%	33%	64%	86%	85%	96%	87%	88%	97%
	6	3%	6%	41%	20%	4%	14%	26%	22%	86%	67%	60%	84%
Ave Miss													
		Three-ball TDOA Satellite Pass						Three-ball TDOA Satellite Pass					
		1	2	3	4	5	6	1	2	3	4	5	6
AOA SV Pass	1	28%	17%	65%	46%	20%	32%	68%	70%	93%	81%	78%	95%
	2	57%	26%	63%	50%	27%	62%	84%	82%	95%	82%	85%	97%
	3	9%	9%	25%	6%	2%	20%	53%	41%	83%	38%	46%	90%
	4	42%	20%	56%	19%	4%	54%	79%	72%	92%	64%	73%	96%
	5	58%	31%	72%	59%	32%	60%	85%	84%	95%	85%	87%	97%
	6	1%	8%	38%	19%	3%	12%	25%	22%	85%	65%	60%	84%
Ave SMA													
		Three-ball TDOA Satellite Pass						Three-ball TDOA Satellite Pass					
		1	2	3	4	5	6	1	2	3	4	5	6
AOA SV Pass	1	30%	13%	70%	52%	21%	33%	71%	69%	94%	84%	80%	96%
	2	65%	32%	69%	58%	25%	69%	88%	85%	97%	86%	88%	98%
	3	14%	4%	23%	7%	1%	20%	55%	49%	86%	38%	47%	91%
	4	53%	29%	60%	27%	7%	61%	84%	70%	93%	68%	75%	96%
	5	64%	30%	76%	67%	37%	67%	88%	86%	97%	90%	90%	98%
	6	8%	3%	47%	25%	7%	10%	24%	19%	87%	69%	65%	83%

Table 93. Kalman filter geolocation fusion consistency for augmentation of three-ball TDOA SV by AOA SV against AFIT target

		Ground Constrained						Non-Ground Constrained					
		Ellipsoid Consistency						Ellipsoid Consistency					
		Three-ball TDOA Satellite Pass						Three-ball TDOA Satellite Pass					
		1	2	3	4	5	6	1	2	3	4	5	6
AOA SV Pass	1	93%	93%	97%	90%	94%	92%	1%	4%	3%	0%	16%	37%
	2	92%	95%	92%	91%	96%	94%	0%	5%	1%	2%	13%	50%
	3	90%	96%	94%	91%	94%	95%	0%	5%	0%	1%	11%	12%
	4	95%	95%	97%	94%	93%	94%	0%	2%	3%	1%	12%	33%
	5	93%	94%	96%	93%	97%	93%	0%	6%	0%	0%	14%	47%
	6	93%	97%	94%	91%	95%	95%	0%	4%	0%	1%	10%	18%
		Ellipse Consistency						Ellipse Consistency					
		Three-ball TDOA Satellite Pass						Three-ball TDOA Satellite Pass					
		1	2	3	4	5	6	1	2	3	4	5	6
AOA SV Pass	1	99%	100%	100%	99%	98%	99%	99%	99%	100%	100%	99%	100%
	2	99%	100%	100%	99%	99%	99%	98%	98%	99%	99%	98%	99%
	3	99%	100%	97%	100%	99%	100%	99%	100%	100%	100%	100%	99%
	4	100%	100%	100%	100%	99%	99%	99%	99%	99%	100%	98%	99%
	5	99%	100%	100%	99%	99%	99%	99%	99%	100%	100%	100%	99%
	6	100%	100%	100%	100%	100%	99%	100%	97%	100%	100%	99%	100%

2.1.0.19 AOA Satellite Augmenting Three-ball TDOA UAVs Against AFIT Target.

The following are the full pass-by-pass fusion results and associated consistencies for each fusion algorithm for the augmentation of an three-ball TDOA AV geolocation agent by an AOA SV geolocation agent against the Libya target.

Table 94. Improvement from Largest Ellipsoid fusion based augmentation of three-ball TDOA AV by AOA SV against Libya target

Ground Constrained				
RMSE				
		Three-ball TDOA Satellite Pass		
		1	2	3
AOA SV Pass	1	92%	62%	95%
	2	96%	78%	97%
	3	79%	33%	87%
	4	92%	65%	95%
	5	96%	80%	98%
	6	75%	23%	84%
Ave Miss				
		Three-ball TDOA Satellite Pass		
		1	2	3
AOA SV Pass	1	87%	58%	86%
	2	92%	74%	92%
	3	63%	28%	63%
	4	86%	61%	87%
	5	93%	78%	94%
	6	63%	26%	60%
Ave SMA				
		Three-ball TDOA Satellite Pass		
		1	2	3
AOA SV Pass	1	91%	72%	94%
	2	96%	81%	97%
	3	77%	31%	86%
	4	90%	61%	94%
	5	96%	83%	98%
	6	63%	62%	77%

Table 95. Largest Ellipsoid fusion consistency for augmentation of three-ball TDOA AV by AOA SV against Libya target

		Ground Constrained		
		Ellipsoid Consistency		
		Three-ball TDOA Satellite Pass		
		1	2	3
AOA SV Pass	1	77%	80%	75%
	2	93%	92%	93%
	3	95%	95%	94%
	4	67%	84%	71%
	5	93%	93%	96%
	6	62%	81%	57%
		Ellipse Consistency		
		Three-ball TDOA Satellite Pass		
		1	2	3
AOA SV Pass	1	75%	82%	73%
	2	98%	95%	97%
	3	100%	96%	98%
	4	75%	88%	76%
	5	97%	96%	97%
	6	100%	96%	100%

Table 96. Improvement from Fast Determinant CI fusion based augmentation of three-ball TDOA AV by AOA SV against Libya target

		Ground Constrained		
		RMSE		
		Three-ball TDOA Satellite Pass		
		1	2	3
AOA SV Pass	1	92%	58%	95%
	2	96%	77%	97%
	3	79%	14%	87%
	4	92%	60%	95%
	5	96%	80%	98%
	6	70%	3%	81%
		Ave Miss		
		Three-ball TDOA Satellite Pass		
		1	2	3
AOA SV Pass	1	86%	53%	87%
	2	92%	73%	92%
	3	62%	14%	63%
	4	86%	53%	86%
	5	93%	77%	93%
	6	51%	5%	51%
		Ave SMA		
		Three-ball TDOA Satellite Pass		
		1	2	3
AOA SV Pass	1	91%	59%	94%
	2	96%	81%	97%
	3	77%	6%	86%
	4	90%	58%	94%
	5	96%	83%	98%
	6	63%	0%	77%

Table 97. Fast Determinant CI fusion consistency for augmentation of three-ball TDOA AV by AOA SV against Libya target

		Ground Constrained		
		Ellipsoid Consistency		
		Three-ball TDOA Satellite Pass		
		1	2	3
AOA SV Pass	1	77%	80%	75%
	2	93%	92%	93%
	3	95%	95%	94%
	4	67%	84%	71%
	5	93%	93%	96%
	6	62%	81%	57%
		Ellipse Consistency		
		Three-ball TDOA Satellite Pass		
		1	2	3
AOA SV Pass	1	75%	82%	73%
	2	98%	95%	97%
	3	100%	96%	98%
	4	75%	88%	76%
	5	97%	96%	97%
	6	100%	96%	100%

Table 98. Improvement from Fast Trace CI fusion based augmentation of three-ball TDOA AV by AOA SV against Libya target

		Ground Constrained		
		RMSE		
		Three-ball TDOA Satellite Pass		
		1	2	3
AOA SV Pass	1	92%	59%	95%
	2	96%	77%	97%
	3	79%	33%	87%
	4	92%	64%	95%
	5	96%	80%	98%
	6	72%	17%	81%
		Ave Miss		
		Three-ball TDOA Satellite Pass		
		1	2	3
AOA SV Pass	1	86%	54%	87%
	2	92%	73%	92%
	3	62%	28%	63%
	4	86%	58%	86%
	5	93%	77%	93%
	6	54%	20%	52%
		Ave SMA		
		Three-ball TDOA Satellite Pass		
		1	2	3
AOA SV Pass	1	91%	57%	94%
	2	96%	81%	97%
	3	77%	17%	86%
	4	90%	59%	94%
	5	96%	83%	98%
	6	63%	0%	77%

Table 99. Fast Trace CI fusion consistency for augmentation of three-ball TDOA AV by AOA SV against Libya target

		Ground Constrained		
		Ellipsoid Consistency		
		Three-ball TDOA Satellite Pass		
		1	2	3
AOA SV Pass	1	91%	95%	91%
	2	94%	95%	94%
	3	93%	96%	92%
	4	98%	98%	98%
	5	95%	95%	95%
	6	95%	91%	95%
		Ellipse Consistency		
		Three-ball TDOA Satellite Pass		
		1	2	3
AOA SV Pass	1	99%	100%	99%
	2	98%	98%	98%
	3	99%	98%	99%
	4	98%	100%	98%
	5	99%	99%	99%
	6	100%	96%	100%

2.1.0.20 AOA Satellite Augmenting Four-ball TDOA Satellites Against AFIT Target.

The following are the full pass-by-pass fusion results and associated consistencies for each fusion algorithm for the augmentation of a four-ball TDOA SV geolocation agent by an AOA SV geolocation agent against the AFIT target.

Table 100. Improvement from Largest Ellipsoid fusion based augmentation of four-ball TDOA SV by AOA SV against AFIT target

	Ground Constrained						Non-Ground Constrained					
RMSE												
	Four-ball TDOA Satellite Pass						Four-ball TDOA Satellite Pass					
AOA SV Pass	1	2	3	4	5	6	1	2	3	4	5	6
1	38%	26%	100%	89%	93%	98%	95%	99%	99%	98%	93%	99%
2	65%	37%	99%	90%	94%	99%	98%	99%	100%	98%	95%	100%
3	19%	2%	98%	58%	70%	96%	92%	97%	98%	91%	81%	99%
4	58%	32%	99%	81%	88%	99%	97%	99%	99%	96%	93%	100%
5	65%	37%	100%	92%	95%	99%	98%	99%	100%	98%	96%	100%
6	9%	10%	99%	79%	85%	96%	79%	95%	98%	96%	81%	98%
Ave Miss												
	Four-ball TDOA Satellite Pass						Four-ball TDOA Satellite Pass					
AOA SV Pass	1	2	3	4	5	6	1	2	3	4	5	6
1	1%	-38%	99%	91%	92%	97%	95%	99%	99%	98%	93%	99%
2	45%	20%	99%	89%	93%	97%	98%	99%	100%	98%	95%	100%
3	-168%	-70%	99%	59%	71%	88%	92%	96%	98%	91%	80%	99%
4	-3%	4%	99%	85%	86%	95%	97%	99%	99%	96%	92%	99%
5	52%	21%	99%	92%	94%	98%	98%	99%	100%	98%	96%	100%
6	-265%	-96%	99%	81%	86%	94%	79%	95%	98%	96%	81%	98%
Ave SMA												
	Four-ball TDOA Satellite Pass						Four-ball TDOA Satellite Pass					
AOA SV Pass	1	2	3	4	5	6	1	2	3	4	5	6
1	63%	0%	99%	85%	92%	98%	98%	99%	99%	97%	92%	99%
2	60%	22%	100%	93%	95%	98%	98%	99%	100%	99%	96%	100%
3	0%	0%	98%	51%	68%	94%	91%	97%	98%	95%	82%	98%
4	41%	0%	99%	92%	94%	98%	97%	99%	99%	98%	93%	99%
5	71%	32%	100%	92%	95%	99%	99%	99%	100%	98%	97%	100%
6	25%	0%	96%	61%	81%	97%	96%	94%	97%	94%	90%	96%

Table 101. Largest Ellipsoid geolocation fusion consistency for augmentation of four-ball TDOA SV by AOA SV against AFIT target

		Ground Constrained						Non-Ground Constrained					
		Ellipsoid Consistency						Ellipsoid Consistency					
		Four-ball TDOA Satellite Pass						Four-ball TDOA Satellite Pass					
		1	2	3	4	5	6	1	2	3	4	5	6
AOA SV Pass	1	89%	91%	91%	94%	95%	90%	95%	96%	93%	97%	96%	94%
	2	94%	91%	91%	97%	97%	90%	96%	95%	94%	98%	96%	92%
	3	89%	91%	90%	95%	93%	89%	95%	95%	94%	96%	96%	93%
	4	93%	91%	90%	95%	93%	88%	95%	95%	95%	94%	96%	93%
	5	92%	91%	92%	97%	99%	90%	95%	96%	95%	97%	97%	94%
	6	84%	91%	90%	97%	92%	88%	94%	95%	94%	95%	97%	93%
		Ellipse Consistency						Ellipse Consistency					
		Four-ball TDOA Satellite Pass						Four-ball TDOA Satellite Pass					
		1	2	3	4	5	6	1	2	3	4	5	6
AOA SV Pass	1	100%	97%	99%	100%	100%	97%	100%	99%	100%	100%	100%	100%
	2	100%	98%	99%	100%	100%	98%	100%	99%	100%	100%	100%	99%
	3	100%	94%	99%	100%	99%	98%	100%	99%	100%	99%	100%	100%
	4	100%	95%	99%	99%	100%	98%	100%	99%	100%	99%	100%	100%
	5	100%	97%	99%	100%	100%	98%	100%	99%	100%	100%	100%	99%
	6	100%	95%	99%	100%	100%	98%	100%	99%	100%	99%	100%	100%

Table 102. Improvement from Fast Determinant CI fusion based augmentation of four-ball TDOA SV by AOA SV against AFIT target

		Ground Constrained						Non-Ground Constrained					
RMSE													
		Four-ball TDOA Satellite Pass						Four-ball TDOA Satellite Pass					
		1	2	3	4	5	6	1	2	3	4	5	6
AOA SV Pass	1	35%	-5%	99%	80%	86%	98%	95%	99%	99%	97%	92%	99%
	2	59%	10%	99%	88%	92%	99%	97%	99%	100%	97%	95%	100%
	3	5%	-5%	97%	51%	69%	95%	88%	97%	98%	91%	79%	99%
	4	58%	-4%	99%	79%	86%	98%	97%	99%	99%	96%	92%	100%
	5	59%	15%	99%	90%	93%	99%	97%	99%	100%	98%	96%	100%
	6	5%	-5%	96%	75%	84%	93%	61%	95%	97%	96%	69%	98%
Ave Miss													
		Four-ball TDOA Satellite Pass						Four-ball TDOA Satellite Pass					
		1	2	3	4	5	6	1	2	3	4	5	6
AOA SV Pass	1	34%	-5%	98%	78%	86%	94%	95%	99%	99%	97%	92%	99%
	2	56%	9%	99%	87%	91%	97%	97%	99%	100%	97%	95%	100%
	3	5%	-5%	95%	49%	69%	84%	88%	96%	98%	90%	77%	98%
	4	56%	-4%	98%	77%	84%	94%	97%	99%	99%	96%	92%	99%
	5	56%	15%	99%	89%	92%	97%	97%	99%	100%	98%	96%	100%
	6	5%	-5%	93%	73%	84%	80%	61%	95%	97%	95%	70%	98%
Ave SMA													
		Four-ball TDOA Satellite Pass						Four-ball TDOA Satellite Pass					
		1	2	3	4	5	6	1	2	3	4	5	6
AOA SV Pass	1	5%	0%	99%	81%	87%	96%	95%	99%	99%	97%	92%	99%
	2	65%	3%	99%	91%	94%	98%	98%	99%	100%	98%	96%	100%
	3	0%	0%	97%	29%	54%	91%	69%	97%	98%	77%	81%	98%
	4	41%	0%	99%	79%	86%	96%	98%	99%	99%	96%	92%	99%
	5	64%	6%	100%	92%	95%	99%	98%	99%	100%	98%	97%	100%
	6	0%	0%	96%	56%	72%	86%	38%	93%	97%	93%	64%	96%

Table 103. Fast Determinant CI geolocation fusion consistency for augmentation of four-ball TDOA SV by AOA SV against AFIT target

		Ground Constrained						Non-Ground Constrained					
		Ellipsoid Consistency						Ellipsoid Consistency					
		Four-ball TDOA Satellite Pass						Four-ball TDOA Satellite Pass					
		1	2	3	4	5	6	1	2	3	4	5	6
AOA SV Pass	1	89%	91%	91%	94%	95%	90%	95%	96%	93%	97%	96%	94%
	2	94%	91%	91%	97%	97%	90%	96%	95%	94%	98%	96%	92%
	3	89%	91%	90%	95%	93%	89%	95%	95%	94%	96%	96%	93%
	4	93%	91%	90%	95%	93%	88%	95%	95%	95%	94%	96%	93%
	5	92%	91%	92%	97%	99%	90%	95%	96%	95%	97%	97%	94%
	6	84%	91%	90%	97%	92%	88%	94%	95%	94%	95%	97%	93%
		Ellipse Consistency						Ellipse Consistency					
		Four-ball TDOA Satellite Pass						Four-ball TDOA Satellite Pass					
		1	2	3	4	5	6	1	2	3	4	5	6
AOA SV Pass	1	100%	97%	99%	100%	100%	97%	100%	99%	100%	100%	100%	100%
	2	100%	98%	99%	100%	100%	98%	100%	99%	100%	100%	100%	99%
	3	100%	94%	99%	100%	99%	98%	100%	99%	100%	99%	100%	100%
	4	100%	95%	99%	99%	100%	98%	100%	99%	100%	99%	100%	100%
	5	100%	97%	99%	100%	100%	98%	100%	99%	100%	100%	100%	99%
	6	100%	95%	99%	100%	100%	98%	100%	99%	100%	99%	100%	100%

Table 104. Improvement from Fast Traced CI fusion based augmentation of four-ball TDOA SV by AOA SV against AFIT target

	Ground Constrained						Non-Ground Constrained					
RMSE												
	Four-ball TDOA Satellite Pass						Four-ball TDOA Satellite Pass					
AOA SV Pass	1	2	3	4	5	6	1	2	3	4	5	6
1	37%	13%	99%	83%	88%	98%	95%	99%	99%	96%	92%	99%
2	62%	36%	99%	88%	92%	99%	97%	99%	100%	97%	95%	100%
3	11%	-5%	97%	56%	68%	96%	91%	97%	98%	90%	79%	99%
4	58%	16%	99%	80%	86%	98%	96%	99%	99%	96%	92%	100%
5	62%	37%	99%	90%	93%	99%	97%	99%	100%	98%	96%	100%
6	6%	-5%	98%	80%	85%	95%	79%	95%	97%	95%	78%	98%
Ave Miss												
	Four-ball TDOA Satellite Pass						Four-ball TDOA Satellite Pass					
AOA SV Pass	1	2	3	4	5	6	1	2	3	4	5	6
1	36%	12%	98%	81%	87%	94%	94%	99%	99%	96%	92%	99%
2	60%	37%	99%	87%	91%	97%	96%	99%	100%	97%	95%	100%
3	12%	-5%	95%	54%	67%	89%	90%	96%	98%	89%	78%	98%
4	56%	16%	98%	77%	85%	94%	96%	99%	99%	96%	92%	99%
5	60%	36%	99%	89%	93%	97%	97%	99%	100%	98%	96%	100%
6	6%	-5%	96%	78%	85%	87%	79%	95%	97%	95%	79%	98%
Ave SMA												
	Four-ball TDOA Satellite Pass						Four-ball TDOA Satellite Pass					
AOA SV Pass	1	2	3	4	5	6	1	2	3	4	5	6
1	7%	1%	99%	83%	88%	96%	95%	99%	99%	97%	92%	99%
2	64%	11%	99%	91%	94%	98%	98%	99%	100%	98%	96%	100%
3	-3%	-1%	97%	47%	66%	93%	93%	97%	98%	91%	81%	98%
4	44%	2%	99%	79%	86%	96%	96%	99%	99%	96%	92%	99%
5	62%	17%	100%	92%	95%	99%	98%	99%	100%	98%	97%	100%
6	-3%	-1%	97%	76%	83%	90%	78%	93%	97%	96%	72%	96%

Table 105. Fast Trace CI geolocation fusion consistency for augmentation of four-ball TDOA SV by AOA SV against AFIT target

		Ground Constrained						Non-Ground Constrained					
		Ellipsoid Consistency Four-ball TDOA Satellite Pass						Ellipsoid Consistency Four-ball TDOA Satellite Pass					
		1	2	3	4	5	6	1	2	3	4	5	6
AOA SV Pass	1	89%	91%	91%	94%	95%	90%	95%	96%	93%	97%	96%	94%
	2	94%	91%	91%	97%	97%	90%	96%	95%	94%	98%	96%	92%
	3	89%	91%	90%	95%	93%	89%	95%	95%	94%	96%	96%	93%
	4	93%	91%	90%	95%	93%	88%	95%	95%	95%	94%	96%	93%
	5	92%	91%	92%	97%	99%	90%	95%	96%	95%	97%	97%	94%
	6	84%	91%	90%	97%	92%	88%	94%	95%	94%	95%	97%	93%
		Ellipse Consistency Four-ball TDOA Satellite Pass						Ellipse Consistency Four-ball TDOA Satellite Pass					
		1	2	3	4	5	6	1	2	3	4	5	6
AOA SV Pass	1	100%	97%	99%	100%	100%	97%	100%	99%	100%	100%	100%	100%
	2	100%	98%	99%	100%	100%	98%	100%	99%	100%	100%	100%	99%
	3	100%	94%	99%	100%	99%	98%	100%	99%	100%	99%	100%	100%
	4	100%	95%	99%	99%	100%	98%	100%	99%	100%	99%	100%	100%
	5	100%	97%	99%	100%	100%	98%	100%	99%	100%	100%	100%	99%
	6	100%	95%	99%	100%	100%	98%	100%	99%	100%	99%	100%	100%

Table 106. Improvement from Ellipsoid Intersection fusion based augmentation of four-ball TDOA SV by AOA SV against AFIT target

	Ground Constrained						Non-Ground Constrained					
RMSE												
	Four-ball TDOA Satellite Pass						Four-ball TDOA Satellite Pass					
	1	2	3	4	5	6		1	2	3	4	5	6
AOA SV Pass 1	-	-	-	-	-	-	AOA SV Pass 1	85%	99%	99%	95%	93%	99%
AOA SV Pass 2	-	-	-	-	-	-	AOA SV Pass 2	86%	99%	100%	97%	95%	100%
AOA SV Pass 3	-	-	-	-	-	-	AOA SV Pass 3	89%	97%	98%	91%	81%	99%
AOA SV Pass 4	-	-	-	-	-	-	AOA SV Pass 4	88%	99%	99%	93%	93%	100%
AOA SV Pass 5	-	-	-	-	-	-	AOA SV Pass 5	84%	99%	100%	95%	96%	100%
AOA SV Pass 6	-	-	-	-	-	-	AOA SV Pass 6	75%	95%	98%	96%	81%	98%
Ave Miss													
	Four-ball TDOA Satellite Pass						Four-ball TDOA Satellite Pass					
	1	2	3	4	5	6		1	2	3	4	5	6
AOA SV Pass 1	-	-	-	-	-	-	AOA SV Pass 1	82%	99%	99%	94%	93%	99%
AOA SV Pass 2	-	-	-	-	-	-	AOA SV Pass 2	83%	99%	100%	97%	95%	100%
AOA SV Pass 3	-	-	-	-	-	-	AOA SV Pass 3	89%	96%	98%	90%	80%	99%
AOA SV Pass 4	-	-	-	-	-	-	AOA SV Pass 4	85%	99%	99%	92%	92%	99%
AOA SV Pass 5	-	-	-	-	-	-	AOA SV Pass 5	80%	99%	100%	94%	96%	100%
AOA SV Pass 6	-	-	-	-	-	-	AOA SV Pass 6	73%	95%	98%	96%	81%	98%
Ave SMA													
	Four-ball TDOA Satellite Pass						Four-ball TDOA Satellite Pass						
	1	2	3	4	5	6		1	2	3	4	5	6
AOA SV Pass 1	-	-	-	-	-	-	AOA SV Pass 1	95%	99%	99%	98%	93%	99%
AOA SV Pass 2	-	-	-	-	-	-	AOA SV Pass 2	98%	99%	100%	98%	96%	100%
AOA SV Pass 3	-	-	-	-	-	-	AOA SV Pass 3	93%	97%	98%	91%	82%	98%
AOA SV Pass 4	-	-	-	-	-	-	AOA SV Pass 4	98%	99%	99%	96%	92%	99%
AOA SV Pass 5	-	-	-	-	-	-	AOA SV Pass 5	98%	99%	100%	99%	97%	100%
AOA SV Pass 6	-	-	-	-	-	-	AOA SV Pass 6	79%	94%	97%	97%	81%	96%

Table 107. Ellipsoid Intersection geolocation fusion consistency for augmentation of four-ball TDOA SV by AOA SV against AFIT target

		Ground Constrained						Non-Ground Constrained					
		Ellipsoid Consistency						Ellipsoid Consistency					
		Four-ball TDOA Satellite Pass						Four-ball TDOA Satellite Pass					
		1	2	3	4	5	6	1	2	3	4	5	6
AOA SV Pass	1	-	-	-	-	-	-	95%	96%	93%	97%	96%	94%
	2	-	-	-	-	-	-	96%	95%	94%	98%	96%	92%
	3	-	-	-	-	-	-	95%	95%	94%	96%	96%	93%
	4	-	-	-	-	-	-	95%	95%	95%	94%	96%	93%
	5	-	-	-	-	-	-	95%	96%	95%	97%	97%	94%
	6	-	-	-	-	-	-	94%	95%	94%	95%	97%	93%
		Ellipse Consistency						Ellipse Consistency					
		Four-ball TDOA Satellite Pass						Four-ball TDOA Satellite Pass					
		1	2	3	4	5	6	1	2	3	4	5	6
AOA SV Pass	1	-	-	-	-	-	-	100%	99%	100%	100%	100%	100%
	2	-	-	-	-	-	-	100%	99%	100%	100%	100%	99%
	3	-	-	-	-	-	-	100%	99%	100%	99%	100%	100%
	4	-	-	-	-	-	-	100%	99%	100%	99%	100%	100%
	5	-	-	-	-	-	-	100%	99%	100%	100%	100%	99%
	6	-	-	-	-	-	-	100%	99%	100%	99%	100%	100%

Table 108. Improvement from Kalman filter fusion based augmentation of four-ball TDOA SV by AOA SV against AFIT target

	Ground Constrained						Non-Ground Constrained					
RMSE												
	Four-ball TDOA Satellite Pass						Four-ball TDOA Satellite Pass					
AOA SV Pass	1	2	3	4	5	6	1	2	3	4	5	6
1	38%	26%	100%	89%	93%	98%	95%	99%	99%	98%	93%	99%
2	65%	37%	99%	90%	94%	99%	98%	99%	100%	98%	95%	100%
3	19%	2%	98%	58%	70%	96%	92%	97%	98%	91%	81%	99%
4	58%	32%	99%	81%	88%	99%	97%	99%	99%	96%	93%	100%
5	65%	37%	100%	92%	95%	99%	98%	99%	100%	98%	96%	100%
6	9%	10%	99%	79%	85%	96%	79%	95%	98%	96%	81%	98%
Ave Miss												
	Four-ball TDOA Satellite Pass						Four-ball TDOA Satellite Pass					
AOA SV Pass	1	2	3	4	5	6	1	2	3	4	5	6
1	37%	25%	99%	88%	92%	95%	95%	99%	99%	98%	93%	99%
2	63%	38%	99%	89%	93%	98%	98%	99%	100%	98%	95%	100%
3	22%	2%	97%	56%	69%	90%	92%	96%	98%	91%	80%	99%
4	56%	32%	99%	80%	87%	97%	97%	99%	99%	96%	92%	99%
5	64%	36%	99%	91%	95%	98%	98%	99%	100%	98%	96%	100%
6	10%	12%	98%	78%	85%	89%	79%	95%	98%	96%	81%	98%
Ave SMA												
	Four-ball TDOA Satellite Pass						Four-ball TDOA Satellite Pass					
AOA SV Pass	1	2	3	4	5	6	1	2	3	4	5	6
1	34%	31%	100%	91%	93%	97%	95%	99%	99%	98%	93%	99%
2	69%	38%	99%	91%	94%	99%	98%	99%	100%	98%	96%	100%
3	19%	5%	98%	58%	71%	94%	93%	97%	98%	91%	82%	98%
4	60%	33%	99%	80%	88%	98%	98%	99%	99%	96%	92%	99%
5	68%	41%	100%	94%	96%	99%	98%	99%	100%	99%	97%	100%
6	9%	11%	99%	81%	86%	92%	79%	94%	97%	97%	81%	96%

Table 109. Improvement from Kalman filter fusion based augmentation of four-ball TDOA SV by AOA SV against AFIT target

		Ground Constrained						Non-Ground Constrained					
		Ellipsoid Consistency Four-ball TDOA Satellite Pass						Ellipsoid Consistency Four-ball TDOA Satellite Pass					
		1	2	3	4	5	6	1	2	3	4	5	6
AOA SV Pass	1	89%	91%	91%	94%	95%	90%	95%	96%	93%	97%	96%	94%
	2	94%	91%	91%	97%	97%	90%	96%	95%	94%	98%	96%	92%
	3	89%	91%	90%	95%	93%	89%	95%	95%	94%	96%	96%	93%
	4	93%	91%	90%	95%	93%	88%	95%	95%	95%	94%	96%	93%
	5	92%	91%	92%	97%	99%	90%	95%	96%	95%	97%	97%	94%
	6	84%	91%	90%	97%	92%	88%	94%	95%	94%	95%	97%	93%
		Ellipse Consistency Three-ball TDOA Satellite Pass						Ellipse Consistency Three-ball TDOA Satellite Pass					
		1	2	3	4	5	6	1	2	3	4	5	6
AOA SV Pass	1	100%	97%	99%	100%	100%	97%	100%	99%	100%	100%	100%	100%
	2	100%	98%	99%	100%	100%	98%	100%	99%	100%	100%	100%	99%
	3	100%	94%	99%	100%	99%	98%	100%	99%	100%	99%	100%	100%
	4	100%	95%	99%	99%	100%	98%	100%	99%	100%	99%	100%	100%
	5	100%	97%	99%	100%	100%	98%	100%	99%	100%	100%	100%	99%
	6	100%	95%	99%	100%	100%	98%	100%	99%	100%	99%	100%	100%

2.2 Libya Fusion Results

2.2.0.21 AOA Satellite Augmenting AOA Satellite Against Libya Target.

The following are the full pass-by-pass fusion results and associated consistency measurements for each fusion algorithm of an AOA SV geolocation agent by an AOA SV geolocation agent against the Libya target.

Table 110. Improvement from Largest Ellipsoid fusion based augmentation of AOA SV by AOA SV against Libya target

Ground Constrained

RMSE

AOA SV Pass	AOA SV Pass 1	2	3	4	5	6
1	1%	22%	78%	52%	14%	60%
2	56%	-2%	83%	53%	26%	77%
3	30%	4%	-6%	25%	4%	56%
4	54%	20%	78%	4%	21%	74%
5	57%	34%	85%	59%	-3%	79%
6	11%	8%	70%	39%	4%	8%

Ave Miss

AOA SV Pass	AOA SV Pass 1	2	3	4	5	6
1	2%	22%	77%	50%	17%	60%
2	54%	-1%	82%	53%	27%	77%
3	30%	5%	-9%	21%	6%	56%
4	53%	24%	76%	3%	24%	73%
5	57%	36%	84%	58%	-2%	78%
6	11%	12%	68%	36%	7%	9%

Ave SMA

AOA SV Pass	AOA SV Pass 1	2	3	4	5	6
1	38%	15%	77%	50%	1%	57%
2	51%	25%	86%	55%	7%	80%
3	23%	0%	0%	0%	2%	59%
4	30%	11%	73%	63%	0%	61%
5	57%	15%	87%	55%	26%	81%
6	27%	0%	55%	0%	6%	70%

Non-Ground Constrained

RMSE

AOA SV Pass	AOA SV Pass 1	2	3	4	5	6
1	2%	26%	78%	46%	17%	60%
2	55%	0%	83%	51%	31%	76%
3	28%	7%	-3%	23%	8%	54%
4	49%	23%	78%	2%	25%	71%
5	53%	35%	84%	55%	0%	76%
6	13%	12%	69%	33%	6%	6%

Ave Miss

AOA SV Pass	AOA SV Pass 1	2	3	4	5	6
1	3%	26%	77%	45%	18%	59%
2	53%	-1%	81%	50%	31%	74%
3	27%	6%	-5%	20%	9%	53%
4	48%	25%	76%	0%	26%	70%
5	52%	36%	83%	54%	1%	74%
6	12%	13%	68%	32%	7%	6%

Ave SMA

AOA SV Pass	AOA SV Pass 1	2	3	4	5	6
1	55%	20%	82%	53%	9%	74%
2	48%	30%	86%	58%	27%	78%
3	5%	0%	79%	8%	0%	50%
4	52%	7%	74%	1%	25%	71%
5	49%	24%	86%	60%	-5%	79%
6	0%	0%	74%	28%	0%	-2%

Table 111. Largest Ellipsoid fusion consistency for augmentation of AOA SV by AOA SV against Libya target

		Ground Constrained						Non-Ground Constrained					
		Ellipsoid Consistency AOA AV Pass						Ellipsoid Consistency AOA AV Pass					
		1	2	3	4	5	6	1	2	3	4	5	6
AOA SV Pass	1	47%	97%	92%	98%	96%	83%	69%	98%	91%	98%	97%	82%
	2	98%	79%	85%	97%	98%	78%	100%	91%	94%	97%	98%	95%
	3	92%	93%	85%	92%	88%	73%	99%	98%	32%	97%	97%	97%
	4	96%	94%	74%	56%	98%	72%	98%	100%	97%	94%	98%	96%
	5	93%	96%	87%	98%	79%	78%	98%	98%	97%	98%	95%	97%
	6	75%	78%	74%	85%	76%	40%	98%	99%	97%	96%	97%	94%
		Ellipse Consistency AOA AV Pass						Ellipse Consistency AOA AV Pass					
		1	2	3	4	5	6	1	2	3	4	5	6
AOA SV Pass	1	81%	100%	90%	99%	99%	79%	100%	100%	92%	100%	98%	83%
	2	99%	99%	96%	99%	99%	97%	100%	96%	96%	97%	99%	99%
	3	100%	100%	47%	100%	98%	98%	100%	100%	95%	100%	97%	100%
	4	99%	100%	80%	73%	99%	95%	100%	100%	89%	77%	99%	97%
	5	99%	99%	98%	99%	97%	99%	98%	99%	97%	99%	89%	99%
	6	99%	100%	93%	100%	99%	62%	100%	100%	100%	100%	99%	100%

Table 112. Improvement from Fast Determinant CI fusion based augmentation of AOA SV by AOA SV against Libya target

		Ground Constrained						Non-Ground Constrained					
RMSE													
		AOA SV Pass						AOA SV Pass					
		1	2	3	4	5	6	1	2	3	4	5	6
AOA SV Pass	1	1%	10%	71%	52%	2%	58%	2%	9%	71%	45%	4%	56%
	2	49%	-2%	82%	48%	24%	75%	44%	0%	81%	43%	29%	72%
	3	6%	-2%	-6%	6%	-3%	51%	4%	0%	-3%	2%	0%	50%
	4	54%	10%	72%	4%	7%	65%	48%	10%	72%	2%	8%	59%
	5	51%	32%	84%	51%	-3%	77%	45%	33%	83%	45%	0%	74%
	6	5%	-1%	67%	19%	-2%	8%	3%	0%	66%	5%	0%	6%
Ave Miss													
		AOA SV Pass						AOA SV Pass					
		1	2	3	4	5	6	1	2	3	4	5	6
AOA SV Pass	1	2%	11%	70%	50%	4%	58%	3%	7%	69%	44%	4%	56%
	2	48%	-1%	81%	45%	26%	74%	41%	-1%	80%	39%	30%	70%
	3	6%	-1%	-9%	5%	-2%	51%	4%	-1%	-5%	1%	1%	49%
	4	53%	12%	71%	3%	8%	65%	47%	10%	70%	0%	9%	58%
	5	50%	34%	83%	49%	-2%	76%	43%	34%	81%	43%	1%	73%
	6	7%	0%	64%	18%	-1%	9%	4%	-1%	65%	3%	1%	6%
Ave SMA													
		AOA SV Pass						AOA SV Pass					
		1	2	3	4	5	6	1	2	3	4	5	6
AOA SV Pass	1	0%	3%	71%	35%	-3%	55%	0%	3%	73%	34%	-1%	58%
	2	53%	0%	86%	49%	2%	79%	49%	0%	86%	45%	9%	78%
	3	1%	0%	0%	0%	0%	33%	0%	0%	0%	0%	0%	37%
	4	36%	-2%	71%	0%	3%	60%	36%	-1%	74%	0%	3%	60%
	5	55%	13%	87%	56%	0%	81%	49%	12%	86%	49%	0%	79%
	6	-4%	-1%	55%	5%	0%	0%	-1%	0%	59%	1%	0%	0%

Table 113. Fast Determinant CI fusion consistency for augmentation of AOA SV by AOA SV against Libya target

		Ground Constrained						Non-Ground Constrained					
		Ellipsoid Consistency AOA AV Pass						Ellipsoid Consistency AOA AV Pass					
		1	2	3	4	5	6	1	2	3	4	5	6
AOA SV Pass	1	92%	96%	94%	100%	94%	96%	96%	100%	96%	99%	96%	96%
	2	96%	92%	92%	98%	98%	91%	100%	97%	97%	99%	99%	97%
	3	94%	92%	85%	96%	91%	88%	96%	97%	98%	94%	96%	99%
	4	100%	98%	96%	96%	95%	97%	99%	99%	94%	94%	97%	94%
	5	94%	98%	91%	95%	91%	92%	96%	99%	96%	97%	96%	96%
	6	96%	91%	88%	98%	92%	79%	96%	97%	99%	94%	96%	95%
		Ellipse Consistency AOA AV Pass						Ellipse Consistency AOA AV Pass					
		1	2	3	4	5	6	1	2	3	4	5	6
AOA SV Pass	1	100%	100%	100%	100%	99%	100%	100%	100%	100%	100%	98%	100%
	2	100%	100%	100%	100%	99%	100%	100%	100%	100%	100%	99%	100%
	3	100%	100%	99%	100%	99%	100%	100%	100%	99%	100%	97%	100%
	4	100%	100%	100%	100%	99%	100%	100%	100%	100%	100%	98%	100%
	5	99%	99%	99%	99%	99%	99%	98%	99%	97%	98%	97%	97%
	6	100%	100%	100%	100%	99%	100%	100%	100%	100%	100%	97%	100%

Table 114. Improvement from Fast Trace CI fusion based augmentation of AOA SV by AOA SV against Libya target

	Ground Constrained						Non-Ground Constrained					
RMSE												
	AOA SV Pass						AOA SV Pass					
AOA SV Pass	1	2	3	4	5	6	1	2	3	4	5	6
1	1%	15%	73%	52%	7%	58%	2%	20%	73%	46%	12%	58%
2	52%	-2%	82%	50%	25%	75%	51%	0%	82%	48%	31%	73%
3	11%	-2%	-6%	9%	-2%	55%	12%	0%	-3%	7%	1%	52%
4	54%	14%	73%	4%	13%	67%	49%	19%	73%	2%	20%	65%
5	53%	33%	84%	55%	-3%	77%	50%	35%	83%	52%	0%	74%
6	6%	0%	69%	23%	-2%	8%	7%	2%	68%	19%	1%	6%
Ave Miss												
	AOA SV Pass						AOA SV Pass					
AOA SV Pass	1	2	3	4	5	6	1	2	3	4	5	6
1	2%	17%	71%	50%	9%	59%	3%	19%	72%	45%	13%	57%
2	51%	-1%	81%	48%	27%	74%	49%	-1%	80%	46%	31%	71%
3	12%	0%	-9%	8%	-1%	55%	12%	-1%	-5%	6%	2%	51%
4	53%	17%	72%	3%	14%	67%	48%	19%	72%	0%	20%	64%
5	53%	35%	83%	53%	-2%	77%	49%	36%	81%	50%	1%	73%
6	7%	1%	67%	22%	0%	9%	8%	1%	66%	18%	2%	6%
Ave SMA												
	AOA SV Pass						AOA SV Pass					
AOA SV Pass	1	2	3	4	5	6	1	2	3	4	5	6
1	0%	4%	72%	35%	-6%	54%	0%	8%	74%	35%	-5%	56%
2	53%	0%	86%	48%	2%	78%	52%	0%	86%	44%	9%	78%
3	3%	-1%	0%	-1%	-1%	40%	3%	-2%	0%	-1%	-1%	41%
4	37%	-4%	71%	0%	5%	60%	38%	-3%	74%	0%	9%	63%
5	54%	12%	87%	57%	0%	81%	47%	12%	86%	52%	0%	78%
6	-5%	-2%	60%	6%	-2%	0%	-6%	-2%	62%	7%	-3%	0%

Table 115. Fast Trace fusion consistency for augmentation of AOA SV by AOA SV against Libya target

		Ground Constrained						Non-Ground Constrained					
		Ellipsoid Consistency AOA AV Pass						Ellipsoid Consistency AOA AV Pass					
		1	2	3	4	5	6	1	2	3	4	5	6
AOA SV Pass	1	92%	99%	96%	100%	96%	97%	96%	100%	98%	100%	97%	98%
	2	99%	92%	92%	99%	98%	91%	100%	97%	98%	100%	99%	98%
	3	96%	92%	85%	98%	92%	94%	98%	98%	98%	95%	96%	100%
	4	100%	99%	98%	96%	96%	98%	100%	100%	95%	94%	99%	95%
	5	96%	98%	92%	96%	91%	92%	97%	99%	96%	99%	96%	96%
	6	97%	91%	94%	98%	92%	79%	98%	98%	100%	95%	96%	95%
		Ellipse Consistency AOA AV Pass						Ellipse Consistency AOA AV Pass					
		1	2	3	4	5	6	1	2	3	4	5	6
AOA SV Pass	1	100%	100%	100%	100%	99%	100%	100%	100%	100%	100%	99%	100%
	2	100%	100%	100%	100%	99%	100%	100%	100%	100%	100%	99%	100%
	3	100%	100%	99%	100%	99%	100%	100%	100%	99%	100%	97%	100%
	4	100%	100%	100%	100%	99%	100%	100%	100%	100%	100%	99%	100%
	5	99%	99%	99%	99%	99%	99%	99%	99%	97%	99%	97%	97%
	6	100%	100%	100%	100%	99%	100%	100%	100%	100%	100%	97%	100%

Table 116. Improvement from Ellipsoid Intersection fusion based augmentation of AOA SV by AOA SV against Libya target

	Ground Constrained						Non-Ground Constrained					
RMSE												
	AOA SV Pass						AOA SV Pass					
AOA SV Pass	1	2	3	4	5	6	1	2	3	4	5	6
1	-	-	-	-	-	-	2%	25%	78%	46%	17%	60%
2	-	-	-	-	-	-	55%	0%	83%	51%	30%	76%
3	-	-	-	-	-	-	28%	7%	-3%	23%	8%	54%
4	-	-	-	-	-	-	49%	23%	78%	2%	25%	71%
5	-	-	-	-	-	-	53%	35%	84%	55%	0%	76%
6	-	-	-	-	-	-	12%	12%	69%	33%	6%	6%
Ave Miss												
	AOA SV Pass						AOA SV Pass					
AOA SV Pass	1	2	3	4	5	6	1	2	3	4	5	6
1	-	-	-	-	-	-	3%	26%	77%	45%	18%	59%
2	-	-	-	-	-	-	53%	-1%	81%	49%	31%	74%
3	-	-	-	-	-	-	27%	6%	-5%	20%	9%	53%
4	-	-	-	-	-	-	48%	25%	76%	0%	26%	70%
5	-	-	-	-	-	-	52%	36%	83%	53%	1%	74%
6	-	-	-	-	-	-	12%	13%	68%	32%	7%	6%
Ave SMA												
	AOA SV Pass						AOA SV Pass					
AOA SV Pass	1	2	3	4	5	6	1	2	3	4	5	6
1	-	-	-	-	-	-	29%	35%	84%	54%	19%	63%
2	-	-	-	-	-	-	66%	29%	86%	58%	36%	82%
3	-	-	-	-	-	-	39%	3%	29%	22%	10%	62%
4	-	-	-	-	-	-	56%	23%	80%	29%	39%	76%
5	-	-	-	-	-	-	59%	38%	88%	68%	29%	80%
6	-	-	-	-	-	-	12%	18%	75%	41%	7%	29%

Table 117. Ellipsoid Intersection fusion consistency for augmentation of AOA SV by AOA SV against Libya target

	Ground Constrained						Non-Ground Constrained					
	Ellipsoid Consistency AOA AV Pass						Ellipsoid Consistency AOA AV Pass					
AOA SV Pass	1	2	3	4	5	6	1	2	3	4	5	6
1	-	-	-	-	-	-	72%	96%	92%	95%	97%	95%
2	-	-	-	-	-	-	97%	70%	96%	93%	95%	93%
3	-	-	-	-	-	-	93%	98%	68%	95%	93%	92%
4	-	-	-	-	-	-	95%	96%	95%	73%	94%	94%
5	-	-	-	-	-	-	96%	95%	94%	95%	76%	94%
6	-	-	-	-	-	-	95%	94%	92%	94%	95%	75%
	Ellipse Consistency AOA AV Pass						Ellipse Consistency AOA AV Pass					
AOA SV Pass	1	2	3	4	5	6	1	2	3	4	5	6
1	-	-	-	-	-	-	95%	100%	100%	100%	99%	100%
2	-	-	-	-	-	-	100%	90%	100%	100%	99%	99%
3	-	-	-	-	-	-	100%	100%	91%	100%	97%	100%
4	-	-	-	-	-	-	100%	100%	100%	98%	99%	100%
5	-	-	-	-	-	-	99%	99%	97%	99%	94%	98%
6	-	-	-	-	-	-	100%	99%	100%	100%	98%	97%

Table 118. Improvement from Kalman filter fusion based augmentation of AOA SV by AOA SV against Libya target

	Ground Constrained						Non-Ground Constrained					
RMSE												
	AOA SV Pass						AOA SV Pass					
AOA SV Pass	1	2	3	4	5	6	1	2	3	4	5	6
1	1%	22%	78%	52%	14%	60%	2%	26%	78%	46%	17%	60%
2	56%	-2%	83%	53%	26%	77%	55%	0%	83%	51%	31%	76%
3	30%	4%	-6%	25%	4%	56%	28%	7%	-3%	23%	8%	54%
4	54%	20%	78%	4%	21%	74%	49%	23%	78%	2%	25%	71%
5	57%	34%	85%	59%	-3%	79%	53%	35%	84%	55%	0%	76%
6	11%	8%	70%	39%	4%	8%	13%	12%	69%	33%	6%	6%
Ave Miss												
	AOA SV Pass						AOA SV Pass					
AOA SV Pass	1	2	3	4	5	6	1	2	3	4	5	6
1	2%	22%	77%	50%	17%	60%	3%	26%	77%	45%	18%	59%
2	54%	-1%	82%	53%	27%	77%	53%	-1%	81%	50%	31%	74%
3	30%	5%	-9%	21%	6%	56%	27%	6%	-5%	20%	9%	53%
4	53%	24%	76%	3%	24%	73%	48%	25%	76%	0%	26%	70%
5	57%	36%	84%	58%	-2%	78%	52%	36%	83%	54%	1%	74%
6	11%	12%	68%	36%	7%	9%	12%	13%	68%	32%	7%	6%
Ave SMA												
	AOA SV Pass						AOA SV Pass					
AOA SV Pass	1	2	3	4	5	6	1	2	3	4	5	6
1	29%	28%	82%	54%	14%	63%	29%	35%	84%	54%	19%	63%
2	65%	29%	86%	59%	31%	82%	66%	29%	86%	58%	36%	82%
3	38%	1%	29%	22%	10%	60%	39%	3%	29%	22%	10%	62%
4	56%	19%	78%	29%	30%	75%	56%	23%	80%	29%	39%	76%
5	62%	38%	89%	69%	29%	82%	59%	38%	88%	68%	29%	80%
6	14%	13%	73%	41%	7%	29%	12%	18%	75%	41%	7%	29%

Table 119. Kalman filter fusion consistency for augmentation of AOA SV by AOA SV against Libya target

		Ground Constrained						Non-Ground Constrained					
		Ellipsoid Consistency AOA AV Pass						Ellipsoid Consistency AOA AV Pass					
		1	2	3	4	5	6	1	2	3	4	5	6
AOA SV Pass	1	57%	86%	73%	87%	84%	61%	72%	97%	92%	95%	96%	95%
	2	86%	59%	71%	81%	83%	63%	97%	70%	96%	94%	94%	93%
	3	73%	71%	39%	79%	75%	53%	92%	96%	68%	95%	94%	92%
	4	87%	81%	79%	57%	77%	62%	95%	94%	95%	73%	94%	94%
	5	84%	83%	75%	77%	61%	66%	96%	94%	94%	94%	76%	94%
	6	61%	63%	53%	62%	66%	27%	95%	93%	92%	94%	94%	75%
		Ellipse Consistency AOA AV Pass						Ellipse Consistency AOA AV Pass					
		1	2	3	4	5	6	1	2	3	4	5	6
AOA SV Pass	1	95%	100%	100%	100%	99%	100%	95%	100%	100%	100%	99%	100%
	2	100%	94%	100%	100%	99%	100%	100%	90%	100%	100%	99%	99%
	3	100%	100%	90%	100%	99%	100%	100%	100%	91%	100%	97%	100%
	4	100%	100%	100%	97%	100%	100%	100%	100%	100%	98%	99%	100%
	5	99%	99%	99%	100%	95%	99%	99%	99%	97%	99%	94%	98%
	6	100%	100%	100%	100%	99%	97%	100%	99%	100%	100%	98%	97%

2.2.0.22 AOA Satellite Augmenting AOA Aircraft Against Libya Target.

The following are the full pass-by-pass fusion results and associated consistencies for each fusion algorithm for the augmentation of an AOA AV geolocation agent by an AOA SV geolocation agent against the Libya target.

Table 120. Improvement from Largest Ellipsoid fusion based augmentation of AOA AV by AOA SV against Libya target

	Ground Constrained		Non-Ground Constrained	
	RMSE			
	AOA Aircraft Pass		AOA Aircraft Pass	
	1	2	1	2
AOA SV Pass 1	21%	44%	20%	51%
AOA SV Pass 2	52%	70%	57%	72%
AOA SV Pass 3	29%	49%	27%	55%
AOA SV Pass 4	46%	66%	49%	68%
AOA SV Pass 5	43%	71%	47%	72%
AOA SV Pass 6	15%	40%	10%	42%
	Ave Miss			
	AOA Aircraft Pass		AOA Aircraft Pass	
	1	2	1	2
AOA SV Pass 1	21%	44%	17%	48%
AOA SV Pass 2	51%	68%	54%	68%
AOA SV Pass 3	28%	47%	23%	51%
AOA SV Pass 4	45%	64%	48%	65%
AOA SV Pass 5	43%	69%	45%	68%
AOA SV Pass 6	14%	40%	5%	39%
	Ave SMA			
	AOA Aircraft Pass		AOA Aircraft Pass	
	1	2	1	2
AOA SV Pass 1	0%	32%	36%	70%
AOA SV Pass 2	23%	64%	43%	72%
AOA SV Pass 3	3%	43%	0%	20%
AOA SV Pass 4	11%	58%	41%	67%
AOA SV Pass 5	45%	73%	45%	73%
AOA SV Pass 6	8%	39%	0%	18%

Table 121. Largest Ellipsoid fusion consistency for augmentation of AOA AV by AOA SV against Libya target

		Ground Constrained		Non-Ground Constrained	
		Ellipsoid Consistency		Ellipsoid Consistency	
		AOA Aircraft Pass		AOA Aircraft Pass	
		1	2	1	2
AOA SV Pass	1	47%	97%	69%	98%
	2	98%	79%	100%	91%
	3	92%	93%	99%	98%
	4	96%	94%	98%	100%
	5	93%	96%	98%	98%
	6	75%	78%	98%	99%
		Ellipse Consistency		Ellipse Consistency	
		AOA Aircraft Pass		AOA Aircraft Pass	
		1	2	1	2
AOA SV Pass	1	81%	100%	100%	100%
	2	99%	99%	100%	96%
	3	100%	100%	100%	100%
	4	99%	100%	100%	100%
	5	99%	99%	98%	99%
	6	99%	100%	100%	100%

Table 122. Improvement from Fast Determinant CI fusion based augmentation of AOA AV by AOA SV against Libya target

	Ground Constrained		Non-Ground Constrained	
	RMSE			
	AOA Aircraft Pass		AOA Aircraft Pass	
	1	2	1	2
AOA SV Pass 1	6%	28%	-2%	36%
AOA SV Pass 2	25%	70%	2%	71%
AOA SV Pass 3	6%	2%	-2%	1%
AOA SV Pass 4	9%	61%	-1%	66%
AOA SV Pass 5	26%	70%	2%	68%
AOA SV Pass 6	6%	4%	-2%	1%
	Ave Miss			
	AOA Aircraft Pass		AOA Aircraft Pass	
	1	2	1	2
AOA SV Pass 1	7%	27%	-2%	35%
AOA SV Pass 2	26%	68%	2%	67%
AOA SV Pass 3	6%	3%	-2%	1%
AOA SV Pass 4	9%	60%	-1%	62%
AOA SV Pass 5	26%	68%	2%	64%
AOA SV Pass 6	6%	4%	-2%	1%
	Ave SMA			
	AOA Aircraft Pass		AOA Aircraft Pass	
	1	2	1	2
AOA SV Pass 1	0%	9%	0%	14%
AOA SV Pass 2	7%	65%	1%	73%
AOA SV Pass 3	0%	1%	0%	0%
AOA SV Pass 4	1%	37%	0%	47%
AOA SV Pass 5	9%	66%	2%	68%
AOA SV Pass 6	0%	0%	0%	0%

Table 123. Fast Determinant CI fusion consistency for augmentation of AOA AV by AOA SV against Libya target

		Ground Constrained		Non-Ground Constrained	
		Ellipsoid Consistency		Ellipsoid Consistency	
		AOA Aircraft Pass		AOA Aircraft Pass	
		1	2	1	2
AOA SV Pass	1	93%	65%	94%	99%
	2	97%	89%	94%	100%
	3	92%	46%	94%	95%
	4	93%	70%	94%	100%
	5	99%	93%	95%	98%
	6	93%	49%	94%	95%
		Ellipse Consistency		Ellipse Consistency	
		AOA Aircraft Pass		AOA Aircraft Pass	
		1	2	1	2
AOA SV Pass	1	99%	100%	99%	100%
	2	99%	100%	99%	100%
	3	99%	100%	99%	100%
	4	99%	100%	99%	100%
	5	100%	100%	99%	99%
	6	99%	100%	99%	100%

Table 124. Improvement from Fast Trace CI fusion based augmentation of AOA AV by AOA SV against Libya target

	Ground Constrained			Non-Ground Constrained		
			RMSE			
		AOA Aircraft Pass			AOA Aircraft Pass	
		1	2		1	2
AOA SV Pass	1	16%	44%	1	12%	50%
	2	52%	66%	2	57%	68%
	3	8%	28%	3	2%	36%
	4	39%	65%	4	43%	67%
	5	43%	67%	5	48%	67%
	6	8%	26%	6	0%	31%
			Ave Miss			
		AOA Aircraft Pass			AOA Aircraft Pass	
		1	2		1	2
AOA SV Pass	1	16%	45%	1	11%	47%
	2	51%	64%	2	54%	63%
	3	9%	27%	3	1%	36%
	4	36%	64%	4	39%	64%
	5	43%	64%	5	45%	63%
	6	9%	27%	6	-1%	30%
			Ave SMA			
		AOA Aircraft Pass			AOA Aircraft Pass	
		1	2		1	2
AOA SV Pass	1	-8%	22%	1	-7%	29%
	2	29%	68%	2	39%	71%
	3	0%	11%	3	0%	16%
	4	13%	51%	4	20%	57%
	5	27%	67%	5	33%	68%
	6	-2%	2%	6	-3%	5%

Table 125. Fast Trace CI fusion consistency for augmentation of AOA AV by AOA SV against Libya target

		Ground Constrained		Non-Ground Constrained	
		Ellipsoid Consistency AOA Aircraft Pass		Ellipsoid Consistency AOA Aircraft Pass	
		1	2	1	2
AOA SV Pass	1	99%	88%	100%	100%
	2	100%	94%	100%	100%
	3	93%	56%	95%	99%
	4	100%	94%	100%	100%
	5	99%	93%	99%	98%
	6	93%	63%	96%	99%
		Ellipse Consistency AOA Aircraft Pass		Ellipse Consistency AOA Aircraft Pass	
		1	2	1	2
AOA SV Pass	1	100%	100%	100%	100%
	2	100%	100%	100%	100%
	3	99%	100%	99%	100%
	4	100%	100%	100%	100%
	5	100%	99%	100%	99%
	6	99%	100%	100%	100%

Table 126. Improvement from Ellipsoid Intersection fusion based augmentation of AOA AV by AOA SV against Libya target

	Ground Constrained		Non-Ground Constrained	
	RMSE			
	AOA Aircraft Pass		AOA Aircraft Pass	
	1	2	1	2
AOA SV Pass 1	-	-	-7%	49%
AOA SV Pass 2	-	-	51%	71%
AOA SV Pass 3	-	-	27%	55%
AOA SV Pass 4	-	-	18%	67%
AOA SV Pass 5	-	-	-79%	72%
AOA SV Pass 6	-	-	11%	43%
	Ave Miss			
	AOA Aircraft Pass		AOA Aircraft Pass	
	1	2	1	2
AOA SV Pass 1	-	-	-14%	47%
AOA SV Pass 2	-	-	43%	68%
AOA SV Pass 3	-	-	23%	51%
AOA SV Pass 4	-	-	11%	65%
AOA SV Pass 5	-	-	-113%	68%
AOA SV Pass 6	-	-	8%	39%
	Ave SMA			
	AOA Aircraft Pass		AOA Aircraft Pass	
	1	2	1	2
AOA SV Pass 1	-	-	19%	48%
AOA SV Pass 2	-	-	56%	78%
AOA SV Pass 3	-	-	28%	56%
AOA SV Pass 4	-	-	49%	69%
AOA SV Pass 5	-	-	52%	74%
AOA SV Pass 6	-	-	11%	35%

Table 127. Ellipsoid Intersection fusion consistency for augmentation of AOA AV by AOA SV against Libya target

		Ground Constrained		Non-Ground Constrained	
		Ellipsoid Consistency AOA Aircraft Pass		Ellipsoid Consistency AOA Aircraft Pass	
		1	2	1	2
AOA SV Pass	1	-	-	82%	94%
	2	-	-	47%	94%
	3	-	-	92%	95%
	4	-	-	66%	95%
	5	-	-	7%	96%
	6	-	-	93%	98%
		Ellipse Consistency AOA Aircraft Pass		Ellipse Consistency AOA Aircraft Pass	
		1	2	1	2
AOA SV Pass	1	-	-	100%	100%
	2	-	-	99%	100%
	3	-	-	99%	100%
	4	-	-	100%	100%
	5	-	-	99%	99%
	6	-	-	99%	100%

Table 128. Improvement from Kalman filter fusion based augmentation of AOA AV by AOA SV against Libya target

	Ground Constrained		Non-Ground Constrained	
RMSE				
	AOA Aircraft Pass		AOA Aircraft Pass	
	1	2	1	2
AOA SV Pass 1	21%	44%	20%	51%
AOA SV Pass 2	52%	70%	57%	72%
AOA SV Pass 3	29%	49%	27%	55%
AOA SV Pass 4	46%	66%	49%	68%
AOA SV Pass 5	43%	71%	47%	72%
AOA SV Pass 6	15%	40%	10%	42%
Ave Miss				
	AOA Aircraft Pass		AOA Aircraft Pass	
	1	2	1	2
AOA SV Pass 1	21%	44%	17%	48%
AOA SV Pass 2	51%	68%	54%	68%
AOA SV Pass 3	28%	47%	23%	51%
AOA SV Pass 4	45%	64%	48%	65%
AOA SV Pass 5	43%	69%	45%	68%
AOA SV Pass 6	14%	40%	5%	39%
Ave SMA				
	AOA Aircraft Pass		AOA Aircraft Pass	
	1	2	1	2
AOA SV Pass 1	17%	43%	19%	48%
AOA SV Pass 2	49%	74%	56%	78%
AOA SV Pass 3	24%	50%	28%	56%
AOA SV Pass 4	43%	65%	49%	69%
AOA SV Pass 5	47%	73%	52%	74%
AOA SV Pass 6	13%	31%	11%	35%

Table 129. Kalman filter fusion consistency for augmentation of AOA AV by AOA SV against Libya target

		Ground Constrained		Non-Ground Constrained	
		Ellipsoid Consistency		Ellipsoid Consistency	
		AOA Aircraft Pass		AOA Aircraft Pass	
		1	2	1	2
AOA SV Pass	1	82%	43%	94%	95%
	2	84%	43%	97%	96%
	3	77%	31%	92%	97%
	4	87%	47%	97%	96%
	5	80%	38%	95%	97%
	6	57%	21%	94%	98%
		Ellipse Consistency		Ellipse Consistency	
		AOA Aircraft Pass		AOA Aircraft Pass	
		1	2	1	2
AOA SV Pass	1	100%	100%	100%	100%
	2	99%	100%	99%	100%
	3	99%	100%	99%	100%
	4	100%	100%	100%	100%
	5	100%	99%	99%	99%
	6	99%	100%	99%	100%

2.2.0.23 AOA Satellite Augmenting Three-ball TDOA Satellites Against Libya Target.

The following are the full pass-by-pass fusion results and associated consistencies for each fusion algorithm for the augmentation of a three-ball TDOA SV geolocation agent by an AOA SV geolocation agent against the Libya target.

Table 130. Improvement from Largest Ellipsoid fusion based augmentation of three-ball TDOA SV by AOA SV against Libya target

	Ground Constrained							Non-Ground Constrained						
RMSE														
		Three-ball TDOA Satellite Pass							Three-ball TDOA Satellite Pass					
		1	2	3	4	5	6		1	2	3	4	5	6
AOA SV Pass	1	45%	12%	12%	67%	14%	12%	AOA SV Pass	67%	90%	90%	85%	81%	90%
	2	70%	45%	45%	71%	19%	45%		86%	94%	94%	87%	87%	94%
	3	48%	20%	20%	38%	10%	20%		74%	80%	80%	70%	66%	80%
	4	66%	46%	46%	44%	12%	46%		83%	92%	92%	74%	80%	92%
	5	70%	43%	43%	74%	24%	43%		85%	94%	94%	89%	88%	94%
	6	21%	4%	4%	57%	10%	4%		51%	80%	80%	79%	72%	80%
Ave Miss														
		Three-ball TDOA Satellite Pass							Three-ball TDOA Satellite Pass					
		1	2	3	4	5	6		1	2	3	4	5	6
AOA SV Pass	1	44%	13%	13%	65%	14%	13%	AOA SV Pass	67%	90%	90%	84%	80%	90%
	2	68%	41%	41%	69%	18%	41%		85%	93%	93%	86%	86%	93%
	3	47%	17%	17%	38%	10%	17%		73%	79%	79%	69%	64%	79%
	4	64%	44%	44%	44%	13%	44%		83%	91%	91%	72%	79%	91%
	5	67%	40%	40%	73%	24%	40%		83%	94%	94%	88%	88%	94%
	6	22%	4%	4%	55%	12%	4%		49%	79%	79%	78%	71%	79%
Ave SMA														
		Three-ball TDOA Satellite Pass							Three-ball TDOA Satellite Pass					
		1	2	3	4	5	6		1	2	3	4	5	6
AOA SV Pass	1	26%	0%	0%	64%	2%	0%	AOA SV Pass	84%	96%	96%	88%	89%	96%
	2	63%	31%	31%	70%	4%	31%		85%	96%	96%	89%	90%	96%
	3	41%	2%	2%	32%	4%	2%		64%	90%	90%	72%	75%	90%
	4	55%	0%	0%	74%	9%	0%		85%	91%	91%	72%	78%	91%
	5	73%	51%	51%	70%	2%	51%		86%	96%	96%	90%	90%	96%
	6	41%	9%	9%	1%	6%	9%		48%	78%	78%	79%	70%	78%

Table 131. Largest Ellipsoid fusion consistency for augmentation of three-ball TDOA SV by AOA SV against Libya target

		Ground Constrained						Non-Ground Constrained					
		Ellipsoid Consistency						Ellipsoid Consistency					
		Three-ball TDOA Satellite Pass						Three-ball TDOA Satellite Pass					
		1	2	3	4	5	6	1	2	3	4	5	6
AOA SV Pass	1	99%	92%	92%	98%	96%	92%	0%	2%	2%	2%	63%	2%
	2	97%	93%	93%	98%	99%	93%	1%	5%	5%	3%	71%	5%
	3	91%	90%	90%	92%	91%	90%	0%	2%	2%	2%	61%	2%
	4	96%	93%	93%	71%	95%	93%	0%	10%	10%	2%	81%	10%
	5	92%	90%	90%	97%	99%	90%	0%	7%	7%	2%	81%	7%
	6	74%	80%	80%	88%	78%	80%	0%	6%	6%	2%	80%	6%
		Ellipse Consistency						Ellipse Consistency					
		Three-ball TDOA Satellite Pass						Three-ball TDOA Satellite Pass					
		1	2	3	4	5	6	1	2	3	4	5	6
AOA SV Pass	1	100%	100%	100%	100%	100%	100%	100%	100%	100%	100%	100%	100%
	2	100%	99%	99%	100%	100%	99%	100%	98%	98%	99%	98%	98%
	3	100%	99%	99%	100%	100%	99%	100%	100%	100%	100%	100%	100%
	4	100%	99%	99%	100%	99%	99%	100%	100%	100%	100%	100%	100%
	5	100%	99%	99%	100%	100%	99%	100%	99%	99%	100%	99%	99%
	6	100%	99%	99%	100%	100%	99%	100%	100%	100%	100%	100%	100%

Table 132. Improvement from Fast Determinant CI fusion based augmentation of three-ball TDOA SV by AOA SV against Libya target

		Ground Constrained						Non-Ground Constrained					
RMSE													
		Three-ball TDOA Satellite Pass						Three-ball TDOA Satellite Pass					
		1	2	3	4	5	6	1	2	3	4	5	6
AOA SV Pass	1	38%	-4%	-4%	66%	3%	-4%	-3%	90%	90%	11%	81%	90%
	2	69%	30%	30%	68%	11%	30%	40%	94%	94%	58%	87%	94%
	3	8%	-6%	-6%	0%	2%	-6%	-5%	78%	78%	2%	18%	78%
	4	64%	6%	6%	42%	3%	6%	4%	91%	91%	5%	80%	91%
	5	67%	35%	35%	71%	19%	35%	47%	94%	94%	76%	88%	94%
	6	7%	-6%	-6%	22%	2%	-6%	-5%	80%	80%	2%	43%	80%
Ave Miss													
		Three-ball TDOA Satellite Pass						Three-ball TDOA Satellite Pass					
		1	2	3	4	5	6	1	2	3	4	5	6
AOA SV Pass	1	36%	-3%	-3%	64%	2%	-3%	-4%	90%	90%	11%	80%	90%
	2	67%	27%	27%	66%	10%	27%	39%	93%	93%	57%	86%	93%
	3	6%	-5%	-5%	0%	0%	-5%	-5%	78%	78%	2%	18%	78%
	4	62%	6%	6%	41%	2%	6%	3%	90%	90%	6%	79%	90%
	5	64%	34%	34%	69%	18%	34%	46%	94%	94%	74%	87%	94%
	6	6%	-5%	-5%	19%	1%	-5%	-5%	80%	80%	2%	42%	80%
Ave SMA													
		Three-ball TDOA Satellite Pass						Three-ball TDOA Satellite Pass					
		1	2	3	4	5	6	1	2	3	4	5	6
AOA SV Pass	1	10%	-1%	-1%	47%	-1%	-1%	0%	90%	90%	4%	71%	90%
	2	67%	14%	14%	68%	-2%	14%	25%	95%	95%	34%	88%	95%
	3	1%	0%	0%	1%	0%	0%	0%	69%	69%	0%	8%	69%
	4	47%	5%	5%	22%	-2%	5%	4%	91%	91%	2%	71%	91%
	5	66%	15%	15%	74%	3%	15%	30%	95%	95%	51%	90%	95%
	6	0%	0%	0%	10%	0%	0%	0%	76%	76%	0%	25%	76%

Table 133. Fast Determinant CI fusion consistency for augmentation of three-ball TDOA SV by AOA SV against Libya target

		Ground Constrained						Non-Ground Constrained					
		Ellipsoid Consistency						Ellipsoid Consistency					
		Three-ball TDOA Satellite Pass						Three-ball TDOA Satellite Pass					
		1	2	3	4	5	6	1	2	3	4	5	6
AOA SV Pass	1	98%	89%	89%	100%	94%	89%	0%	96%	96%	2%	96%	96%
	2	99%	94%	94%	99%	96%	94%	0%	97%	97%	4%	98%	97%
	3	94%	88%	88%	96%	94%	88%	0%	72%	72%	1%	75%	72%
	4	98%	89%	89%	100%	94%	89%	0%	95%	95%	1%	98%	95%
	5	98%	94%	94%	97%	99%	94%	0%	96%	96%	4%	95%	96%
	6	94%	88%	88%	99%	94%	88%	0%	97%	97%	1%	81%	97%
		Ellipse Consistency						Ellipse Consistency					
		Three-ball TDOA Satellite Pass						Three-ball TDOA Satellite Pass					
		1	2	3	4	5	6	1	2	3	4	5	6
AOA SV Pass	1	100%	99%	99%	100%	100%	99%	99%	100%	100%	96%	100%	100%
	2	100%	99%	99%	100%	100%	99%	100%	100%	100%	100%	100%	100%
	3	100%	99%	99%	100%	100%	99%	99%	100%	100%	95%	97%	100%
	4	100%	99%	99%	100%	100%	99%	100%	100%	100%	96%	100%	100%
	5	99%	99%	99%	98%	100%	99%	100%	97%	97%	100%	99%	97%
	6	100%	99%	99%	100%	100%	99%	99%	100%	100%	95%	100%	100%

Table 134. Improvement from Fast Trace CI fusion based augmentation of three-ball TDOA SV by AOA SV against Libya target

		Ground Constrained						Non-Ground Constrained					
RMSE													
		Three-ball TDOA Satellite Pass						Three-ball TDOA Satellite Pass					
		1	2	3	4	5	6	1	2	3	4	5	6
AOA SV Pass	1	67%	45%	45%	66%	17%	45%	82%	94%	94%	84%	86%	94%
	2	30%	-3%	-3%	20%	2%	-3%	74%	72%	72%	70%	65%	72%
	3	66%	39%	39%	43%	6%	39%	81%	91%	91%	72%	78%	91%
	4	65%	42%	42%	69%	23%	42%	82%	94%	94%	85%	88%	94%
	5	16%	-3%	-3%	50%	3%	-3%	52%	80%	80%	80%	70%	80%
	6	0%	0%	0%	0%	0%	0%	0%	0%	0%	0%	0%	0%
Ave Miss													
		Three-ball TDOA Satellite Pass						Three-ball TDOA Satellite Pass					
		1	2	3	4	5	6	1	2	3	4	5	6
AOA SV Pass	1	59%	33%	33%	58%	5%	33%	80%	93%	93%	82%	85%	93%
	2	13%	-25%	-25%	2%	-11%	-25%	73%	72%	72%	69%	63%	72%
	3	58%	26%	26%	30%	-7%	26%	80%	91%	91%	71%	78%	91%
	4	56%	29%	29%	62%	12%	29%	81%	94%	94%	84%	87%	94%
	5	-6%	-26%	-26%	38%	-10%	-26%	49%	80%	80%	78%	69%	80%
	6	-25%	-22%	-22%	-23%	-14%	-22%	0%	0%	0%	0%	0%	0%
Ave SMA													
		Three-ball TDOA Satellite Pass						Three-ball TDOA Satellite Pass					
		1	2	3	4	5	6	1	2	3	4	5	6
AOA SV Pass	1	69%	31%	31%	68%	-4%	31%	84%	95%	95%	86%	89%	95%
	2	10%	-1%	-1%	8%	0%	-1%	59%	68%	68%	57%	56%	68%
	3	56%	22%	22%	29%	-6%	22%	77%	91%	91%	70%	77%	91%
	4	66%	27%	27%	74%	4%	27%	85%	95%	95%	88%	90%	95%
	5	-1%	-3%	-3%	24%	-1%	-3%	35%	77%	77%	74%	58%	77%
	6	0%	0%	0%	0%	0%	0%	0%	0%	0%	0%	0%	0%

Table 135. Improvement from Ellipsoid Intersectoin fusion based augmentation of three-ball TDOA SV by AOA SV against Libya target

	Ground Constrained							Non-Ground Constrained						
RMSE														
	Three-ball TDOA Satellite Pass							Three-ball TDOA Satellite Pass						
		1	2	3	4	5	6		1	2	3	4	5	6
AOA SV Pass	1	-	-	-	-	-	-	1	-3308%	86%	86%	-2358%	-69%	86%
	2	-	-	-	-	-	-	2	-3053%	90%	90%	-2266%	-45%	90%
	3	-	-	-	-	-	-	3	-2919%	75%	75%	-2088%	-66%	75%
	4	-	-	-	-	-	-	4	-1420%	87%	87%	-2306%	-50%	87%
	5	-	-	-	-	-	-	5	-716%	86%	86%	-1408%	-2%	86%
	6	-	-	-	-	-	-	6	-2881%	63%	63%	-3332%	-80%	63%
Ave Miss														
	Three-ball TDOA Satellite Pass							Three-ball TDOA Satellite Pass						
		1	2	3	4	5	6		1	2	3	4	5	6
AOA SV Pass	1	-	-	-	-	-	-	1	-4082%	84%	84%	-2961%	-104%	84%
	2	-	-	-	-	-	-	2	-3770%	89%	89%	-2846%	-75%	89%
	3	-	-	-	-	-	-	3	-3605%	74%	74%	-2625%	-100%	74%
	4	-	-	-	-	-	-	4	-1765%	86%	86%	-2896%	-81%	86%
	5	-	-	-	-	-	-	5	-901%	85%	85%	-1778%	-23%	85%
	6	-	-	-	-	-	-	6	-3558%	59%	59%	-4174%	-118%	59%
Ave SMA														
	Three-ball TDOA Satellite Pass							Three-ball TDOA Satellite Pass						
		1	2	3	4	5	6		1	2	3	4	5	6
AOA SV Pass	1	-	-	-	-	-	-	1	67%	90%	90%	85%	80%	90%
	2	-	-	-	-	-	-	2	88%	95%	95%	88%	90%	95%
	3	-	-	-	-	-	-	3	75%	79%	79%	71%	70%	79%
	4	-	-	-	-	-	-	4	85%	91%	91%	73%	79%	91%
	5	-	-	-	-	-	-	5	86%	96%	96%	91%	91%	96%
	6	-	-	-	-	-	-	6	53%	79%	79%	79%	74%	79%

Table 136. Ellipsoid Intersection fusion consistency for augmentation of three-ball TDOA SV by AOA SV against Libya target

		Ground Constrained						Non-Ground Constrained					
		Ellipsoid Consistency						Ellipsoid Consistency					
		Three-ball TDOA Satellite Pass						Three-ball TDOA Satellite Pass					
		1	2	3	4	5	6	1	2	3	4	5	6
AOA SV Pass	1	-	-	-	-	-	-	0%	3%	3%	0%	0%	3%
	2	-	-	-	-	-	-	0%	0%	0%	0%	0%	0%
	3	-	-	-	-	-	-	0%	2%	2%	0%	0%	2%
	4	-	-	-	-	-	-	0%	0%	0%	0%	0%	0%
	5	-	-	-	-	-	-	0%	0%	0%	0%	0%	0%
	6	-	-	-	-	-	-	0%	0%	0%	0%	0%	0%
		Ellipse Consistency						Ellipse Consistency					
		Three-ball TDOA Satellite Pass						Three-ball TDOA Satellite Pass					
		1	2	3	4	5	6	1	2	3	4	5	6
AOA SV Pass	1	-	-	-	-	-	-	100%	100%	100%	100%	100%	100%
	2	-	-	-	-	-	-	100%	100%	100%	99%	100%	100%
	3	-	-	-	-	-	-	100%	100%	100%	100%	100%	100%
	4	-	-	-	-	-	-	99%	100%	100%	100%	100%	100%
	5	-	-	-	-	-	-	100%	99%	99%	100%	99%	99%
	6	-	-	-	-	-	-	100%	100%	100%	100%	100%	100%

Table 137. Improvement from Kalman filter fusion based augmentation of three-ball TDOA SV by AOA SV against Libya target

	Ground Constrained						Non-Ground Constrained					
RMSE												
	Three-ball TDOA Satellite Pass						Three-ball TDOA Satellite Pass					
	1	2	3	4	5	6		1	2	3	4	5	6
AOA SV Pass 1	45%	12%	12%	67%	14%	12%	AOA SV Pass 1	67%	90%	90%	85%	81%	90%
AOA SV Pass 2	70%	45%	45%	71%	19%	45%	AOA SV Pass 2	86%	94%	94%	87%	87%	94%
AOA SV Pass 3	48%	20%	20%	38%	10%	20%	AOA SV Pass 3	74%	80%	80%	70%	66%	80%
AOA SV Pass 4	66%	46%	46%	44%	12%	46%	AOA SV Pass 4	83%	92%	92%	74%	80%	92%
AOA SV Pass 5	70%	43%	43%	74%	24%	43%	AOA SV Pass 5	85%	94%	94%	89%	88%	94%
AOA SV Pass 6	21%	4%	4%	57%	10%	4%	AOA SV Pass 6	51%	80%	80%	79%	72%	80%
Ave Miss													
	Three-ball TDOA Satellite Pass						Three-ball TDOA Satellite Pass					
	1	2	3	4	5	6		1	2	3	4	5	6
AOA SV Pass 1	44%	13%	13%	65%	14%	13%	AOA SV Pass 1	67%	90%	90%	84%	80%	90%
AOA SV Pass 2	68%	41%	41%	69%	18%	41%	AOA SV Pass 2	85%	93%	93%	86%	86%	93%
AOA SV Pass 3	47%	17%	17%	38%	10%	17%	AOA SV Pass 3	73%	79%	79%	69%	64%	79%
AOA SV Pass 4	64%	44%	44%	44%	13%	44%	AOA SV Pass 4	83%	91%	91%	72%	79%	91%
AOA SV Pass 5	67%	40%	40%	73%	24%	40%	AOA SV Pass 5	83%	94%	94%	88%	88%	94%
AOA SV Pass 6	22%	4%	4%	55%	12%	4%	AOA SV Pass 6	49%	79%	79%	78%	71%	79%
Ave SMA													
	Three-ball TDOA Satellite Pass						Three-ball TDOA Satellite Pass						
	1	2	3	4	5	6		1	2	3	4	5	6
AOA SV Pass 1	40%	20%	20%	66%	20%	20%	AOA SV Pass 1	67%	90%	90%	85%	80%	90%
AOA SV Pass 2	73%	50%	50%	73%	24%	50%	AOA SV Pass 2	88%	95%	95%	88%	90%	95%
AOA SV Pass 3	50%	22%	22%	44%	9%	22%	AOA SV Pass 3	75%	79%	79%	71%	70%	79%
AOA SV Pass 4	68%	51%	51%	47%	10%	51%	AOA SV Pass 4	85%	91%	91%	73%	79%	91%
AOA SV Pass 5	72%	46%	46%	78%	33%	46%	AOA SV Pass 5	86%	96%	96%	91%	91%	96%
AOA SV Pass 6	27%	8%	8%	54%	15%	8%	AOA SV Pass 6	53%	79%	79%	79%	74%	79%

Table 138. Kalman filter fusion consistency for augmentation of three-ball TDOA SV by AOA SV against Libya target

		Ground Constrained						Non-Ground Constrained					
		Ellipsoid Consistency						Ellipsoid Consistency					
		Three-ball TDOA Satellite Pass						Three-ball TDOA Satellite Pass					
		1	2	3	4	5	6	1	2	3	4	5	6
AOA SV Pass	1	79%	81%	81%	86%	80%	81%	0%	3%	3%	2%	77%	3%
	2	83%	82%	82%	84%	83%	82%	0%	5%	5%	3%	74%	5%
	3	72%	75%	75%	75%	78%	75%	0%	3%	3%	2%	73%	3%
	4	82%	83%	83%	82%	86%	83%	0%	10%	10%	2%	78%	10%
	5	84%	82%	82%	80%	85%	82%	0%	6%	6%	2%	78%	6%
	6	65%	64%	64%	62%	64%	64%	0%	4%	4%	2%	78%	4%
		Ellipse Consistency						Ellipse Consistency					
		Three-ball TDOA Satellite Pass						Three-ball TDOA Satellite Pass					
		1	2	3	4	5	6	1	2	3	4	5	6
AOA SV Pass	1	100%	99%	99%	100%	100%	99%	100%	100%	100%	100%	100%	100%
	2	100%	99%	99%	100%	100%	99%	100%	100%	100%	99%	100%	100%
	3	100%	99%	99%	100%	100%	99%	100%	100%	100%	100%	100%	100%
	4	100%	99%	99%	100%	99%	99%	99%	100%	100%	100%	100%	100%
	5	99%	99%	99%	100%	100%	99%	100%	99%	99%	100%	99%	99%
	6	100%	99%	99%	100%	100%	99%	100%	100%	100%	100%	100%	100%

2.2.0.24 AOA Satellite Augmenting Four-ball TDOA Satellites Against Libya Target.

The following are the full pass-by-pass fusion results and associated consistencies for each fusion algorithm for the augmentation of a four-ball TDOA SV geolocation agent by an AOA SV geolocation agent against the Libya target.

Table 139. Improvement from Largest Ellipsoid fusion based augmentation of four-ball TDOA SV by AOA SV against Libya target

	Ground Constrained						Non-Ground Constrained					
RMSE												
	Four-ball TDOA Satellite Pass						Four-ball TDOA Satellite Pass					
	1	2	3	4	5	6		1	2	3	4	5	6
AOA SV Pass 1	93%	98%	96%	87%	96%	94%	AOA SV Pass 1	98%	99%	95%	98%	99%	94%
AOA SV Pass 2	97%	98%	95%	89%	97%	97%	AOA SV Pass 2	99%	100%	97%	99%	99%	97%
AOA SV Pass 3	94%	98%	81%	74%	95%	94%	AOA SV Pass 3	98%	99%	83%	97%	96%	83%
AOA SV Pass 4	97%	99%	92%	80%	95%	97%	AOA SV Pass 4	99%	99%	96%	97%	99%	94%
AOA SV Pass 5	97%	99%	96%	90%	98%	97%	AOA SV Pass 5	99%	100%	97%	99%	99%	97%
AOA SV Pass 6	90%	98%	93%	83%	95%	92%	AOA SV Pass 6	96%	98%	91%	98%	98%	87%
Ave Miss													
	Four-ball TDOA Satellite Pass						Four-ball TDOA Satellite Pass					
	1	2	3	4	5	6		1	2	3	4	5	6
AOA SV Pass 1	83%	94%	95%	87%	94%	94%	AOA SV Pass 1	97%	99%	95%	98%	99%	94%
AOA SV Pass 2	91%	94%	95%	89%	96%	97%	AOA SV Pass 2	99%	99%	97%	98%	99%	96%
AOA SV Pass 3	85%	94%	80%	73%	92%	94%	AOA SV Pass 3	97%	99%	83%	97%	97%	83%
AOA SV Pass 4	91%	94%	92%	81%	93%	97%	AOA SV Pass 4	98%	99%	95%	97%	99%	94%
AOA SV Pass 5	92%	94%	96%	90%	96%	97%	AOA SV Pass 5	99%	99%	97%	99%	99%	96%
AOA SV Pass 6	73%	94%	93%	82%	93%	92%	AOA SV Pass 6	96%	98%	91%	98%	98%	87%
Ave SMA													
	Four-ball TDOA Satellite Pass						Four-ball TDOA Satellite Pass					
	1	2	3	4	5	6		1	2	3	4	5	6
AOA SV Pass 1	93%	0%	96%	88%	97%	94%	AOA SV Pass 1	98%	96%	98%	97%	98%	97%
AOA SV Pass 2	97%	0%	96%	91%	97%	97%	AOA SV Pass 2	99%	96%	98%	99%	99%	97%
AOA SV Pass 3	95%	0%	82%	77%	95%	95%	AOA SV Pass 3	94%	90%	95%	96%	94%	92%
AOA SV Pass 4	95%	0%	96%	90%	98%	96%	AOA SV Pass 4	99%	94%	96%	97%	98%	94%
AOA SV Pass 5	98%	0%	96%	91%	98%	98%	AOA SV Pass 5	99%	96%	98%	99%	99%	97%
AOA SV Pass 6	95%	0%	79%	64%	93%	94%	AOA SV Pass 6	96%	78%	89%	98%	96%	85%

Table 140. Largest Ellipsoid fusion consistency for augmentation of four-ball TDOA SV by AOA SV against Libya target

		Ground Constrained						Non-Ground Constrained					
		Ellipsoid Consistency Four-ball TDOA Satellite Pass						Ellipsoid Consistency Four-ball TDOA Satellite Pass					
		1	2	3	4	5	6	1	2	3	4	5	6
AOA SV Pass	1	49%	93%	89%	13%	97%	98%	74%	75%	74%	97%	75%	72%
	2	56%	95%	77%	9%	97%	99%	97%	92%	89%	92%	89%	91%
	3	39%	92%	79%	5%	90%	92%	97%	90%	36%	91%	39%	54%
	4	47%	94%	61%	10%	70%	95%	92%	93%	97%	93%	94%	96%
	5	50%	96%	91%	11%	97%	95%	96%	95%	96%	94%	96%	95%
	6	30%	90%	84%	11%	83%	75%	93%	98%	98%	96%	96%	99%
		Ellipse Consistency Four-ball TDOA Satellite Pass						Ellipse Consistency Four-ball TDOA Satellite Pass					
		1	2	3	4	5	6	1	2	3	4	5	6
AOA SV Pass	1	100%	98%	100%	97%	97%	100%	76%	40%	100%	96%	76%	100%
	2	100%	99%	100%	98%	100%	100%	100%	47%	97%	99%	97%	97%
	3	100%	98%	97%	95%	99%	100%	99%	23%	70%	99%	99%	98%
	4	98%	99%	99%	71%	94%	100%	98%	32%	100%	76%	76%	100%
	5	100%	99%	100%	99%	100%	99%	100%	55%	98%	99%	97%	98%
	6	100%	98%	98%	99%	100%	100%	99%	28%	100%	99%	100%	100%

Table 141. Improvement from Fast Determinate CI fusion based augmentation of four-ball TDOA SV by AOA SV against Libya target

		Ground Constrained						Non-Ground Constrained					
RMSE													
		Four-ball TDOA Satellite Pass						Four-ball TDOA Satellite Pass					
		1	2	3	4	5	6	1	2	3	4	5	6
AOA SV Pass	1	93%	98%	96%	86%	94%	93%	97%	99%	95%	97%	99%	94%
	2	96%	98%	94%	88%	97%	96%	98%	99%	97%	98%	99%	96%
	3	94%	98%	76%	65%	94%	94%	97%	99%	82%	95%	96%	78%
	4	95%	98%	92%	80%	94%	95%	98%	99%	95%	97%	99%	94%
	5	96%	98%	95%	89%	97%	96%	99%	99%	97%	98%	99%	96%
	6	89%	98%	93%	83%	94%	92%	95%	98%	89%	95%	98%	87%
Ave Miss													
		Four-ball TDOA Satellite Pass						Four-ball TDOA Satellite Pass					
		1	2	3	4	5	6	1	2	3	4	5	6
AOA SV Pass	1	82%	94%	95%	86%	91%	93%	97%	99%	95%	97%	99%	93%
	2	89%	94%	94%	87%	95%	95%	98%	99%	96%	98%	99%	96%
	3	85%	94%	77%	65%	92%	94%	97%	99%	82%	94%	97%	77%
	4	86%	94%	91%	81%	92%	94%	97%	99%	95%	97%	99%	93%
	5	90%	94%	94%	89%	95%	96%	98%	99%	97%	98%	99%	96%
	6	72%	94%	93%	82%	90%	91%	94%	98%	89%	95%	98%	86%
Ave SMA													
		Four-ball TDOA Satellite Pass						Four-ball TDOA Satellite Pass					
		1	2	3	4	5	6	1	2	3	4	5	6
AOA SV Pass	1	93%	0%	95%	83%	94%	93%	98%	91%	95%	97%	98%	94%
	2	97%	0%	95%	90%	97%	97%	99%	95%	98%	99%	99%	97%
	3	92%	0%	55%	46%	94%	93%	96%	78%	83%	93%	94%	77%
	4	94%	0%	90%	78%	94%	94%	98%	94%	96%	97%	98%	94%
	5	97%	0%	96%	91%	98%	97%	99%	95%	98%	99%	99%	97%
	6	86%	0%	88%	75%	91%	90%	94%	68%	89%	94%	96%	85%

Table 142. Fast Determinate CI fusion consistency for augmentation of four-ball TDOA SV by AOA SV against Libya target

		Ground Constrained						Non-Ground Constrained					
		Ellipsoid Consistency Four-ball TDOA Satellite Pass						Ellipsoid Consistency Four-ball TDOA Satellite Pass					
		1	2	3	4	5	6	1	2	3	4	5	6
AOA SV Pass	1	95%	94%	99%	81%	93%	95%	96%	98%	96%	96%	96%	96%
	2	92%	94%	93%	87%	92%	92%	97%	97%	97%	97%	97%	97%
	3	79%	94%	94%	9%	91%	98%	99%	99%	98%	99%	98%	98%
	4	98%	94%	100%	87%	96%	98%	94%	95%	94%	94%	94%	94%
	5	91%	94%	92%	89%	91%	91%	96%	96%	96%	96%	96%	96%
	6	82%	94%	95%	22%	85%	90%	95%	100%	95%	95%	95%	95%
		Ellipse Consistency Four-ball TDOA Satellite Pass						Ellipse Consistency Four-ball TDOA Satellite Pass					
		1	2	3	4	5	6	1	2	3	4	5	6
AOA SV Pass	1	100%	99%	100%	100%	100%	100%	100%	100%	100%	100%	100%	100%
	2	100%	99%	100%	100%	100%	100%	100%	100%	100%	100%	100%	100%
	3	100%	99%	100%	98%	100%	100%	99%	20%	99%	99%	99%	99%
	4	100%	99%	100%	100%	100%	100%	100%	98%	100%	100%	100%	100%
	5	99%	99%	99%	99%	99%	99%	97%	97%	97%	97%	97%	97%
	6	100%	99%	100%	100%	100%	100%	100%	35%	100%	100%	100%	100%

Table 143. Improvement from Fast Trace CI fusion based augmentation of four-ball TDOA SV by AOA SV against Libya target

		Ground Constrained						Non-Ground Constrained					
RMSE													
		Four-ball TDOA Satellite Pass						Four-ball TDOA Satellite Pass					
		1	2	3	4	5	6	1	2	3	4	5	6
AOA SV Pass	1	93%	98%	92%	81%	94%	93%	97%	99%	95%	97%	99%	94%
	2	96%	98%	94%	87%	97%	96%	98%	99%	97%	98%	99%	96%
	3	94%	98%	80%	74%	93%	94%	97%	99%	83%	96%	96%	78%
	4	93%	98%	90%	80%	94%	94%	98%	99%	95%	97%	99%	94%
	5	96%	98%	94%	89%	97%	96%	99%	99%	97%	98%	99%	96%
	6	87%	98%	93%	83%	92%	91%	95%	98%	89%	97%	98%	87%
Ave Miss													
		Four-ball TDOA Satellite Pass						Four-ball TDOA Satellite Pass					
		1	2	3	4	5	6	1	2	3	4	5	6
AOA SV Pass	1	81%	94%	92%	81%	91%	92%	97%	99%	95%	97%	99%	93%
	2	89%	94%	93%	87%	95%	95%	98%	99%	96%	98%	99%	96%
	3	83%	94%	80%	73%	89%	94%	97%	99%	82%	96%	97%	78%
	4	83%	94%	90%	80%	92%	93%	97%	99%	95%	97%	99%	93%
	5	90%	94%	94%	88%	95%	96%	98%	99%	97%	98%	99%	96%
	6	65%	94%	93%	82%	88%	90%	95%	98%	89%	96%	98%	86%
Ave SMA													
		Four-ball TDOA Satellite Pass						Four-ball TDOA Satellite Pass					
		1	2	3	4	5	6	1	2	3	4	5	6
AOA SV Pass	1	93%	-1%	92%	80%	94%	93%	98%	91%	95%	97%	98%	94%
	2	97%	-3%	95%	90%	97%	97%	99%	95%	98%	99%	99%	97%
	3	92%	0%	79%	69%	91%	95%	97%	87%	83%	95%	94%	77%
	4	93%	-1%	90%	79%	94%	94%	98%	93%	96%	97%	98%	94%
	5	97%	-4%	96%	91%	98%	97%	99%	95%	98%	99%	99%	97%
	6	85%	0%	92%	78%	90%	88%	94%	78%	89%	96%	96%	85%

Table 144. Fast Trace CI fusion consistency for augmentation of four-ball TDOA SV by AOA SV against Libya target

		Ground Constrained						Non-Ground Constrained					
		Ellipsoid Consistency Four-ball TDOA Satellite Pass						Ellipsoid Consistency Four-ball TDOA Satellite Pass					
		1	2	3	4	5	6	1	2	3	4	5	6
AOA SV Pass	1	93%	95%	96%	94%	92%	93%	96%	96%	96%	96%	96%	96%
	2	92%	96%	92%	89%	92%	92%	97%	97%	97%	97%	97%	97%
	3	91%	94%	92%	64%	89%	91%	99%	99%	98%	99%	98%	98%
	4	96%	95%	96%	95%	96%	96%	94%	95%	94%	94%	94%	94%
	5	91%	96%	92%	91%	91%	91%	96%	96%	96%	96%	96%	96%
	6	82%	94%	87%	74%	83%	84%	95%	99%	97%	97%	95%	98%
		Ellipse Consistency Four-ball TDOA Satellite Pass						Ellipse Consistency Four-ball TDOA Satellite Pass					
		1	2	3	4	5	6	1	2	3	4	5	6
AOA SV Pass	1	100%	99%	100%	100%	100%	100%	100%	100%	100%	100%	100%	100%
	2	100%	99%	100%	100%	100%	100%	100%	100%	100%	100%	100%	100%
	3	100%	99%	100%	100%	100%	100%	99%	53%	100%	100%	99%	100%
	4	100%	99%	100%	100%	100%	100%	100%	100%	100%	100%	100%	100%
	5	99%	99%	99%	99%	99%	99%	97%	97%	97%	97%	97%	97%
	6	100%	99%	100%	100%	100%	100%	100%	91%	100%	100%	100%	100%

Table 145. Improvement from Ellipsoid Intersection CI fusion based augmentation of four-ball TDOA SV by AOA SV against Libya target

	Ground Constrained						Non-Ground Constrained					
RMSE												
	Four-ball TDOA Satellite Pass						Four-ball TDOA Satellite Pass					
	1	2	3	4	5	6		1	2	3	4	5	6
AOA SV Pass 1	-	-	-	-	-	-	1	95%	93%	95%	97%	99%	94%
AOA SV Pass 2	-	-	-	-	-	-	2	98%	95%	97%	99%	99%	96%
AOA SV Pass 3	-	-	-	-	-	-	3	97%	98%	83%	97%	96%	82%
AOA SV Pass 4	-	-	-	-	-	-	4	97%	95%	95%	96%	99%	94%
AOA SV Pass 5	-	-	-	-	-	-	5	98%	95%	97%	99%	99%	97%
AOA SV Pass 6	-	-	-	-	-	-	6	95%	97%	90%	97%	98%	87%
Ave Miss													
	Four-ball TDOA Satellite Pass						Four-ball TDOA Satellite Pass					
	1	2	3	4	5	6		1	2	3	4	5	6
AOA SV Pass 1	-	-	-	-	-	-	1	94%	91%	95%	97%	99%	94%
AOA SV Pass 2	-	-	-	-	-	-	2	98%	94%	97%	98%	99%	96%
AOA SV Pass 3	-	-	-	-	-	-	3	96%	98%	82%	97%	97%	83%
AOA SV Pass 4	-	-	-	-	-	-	4	96%	94%	95%	96%	99%	94%
AOA SV Pass 5	-	-	-	-	-	-	5	98%	94%	97%	98%	99%	96%
AOA SV Pass 6	-	-	-	-	-	-	6	95%	97%	89%	96%	98%	86%
Ave SMA													
	Four-ball TDOA Satellite Pass						Four-ball TDOA Satellite Pass					
	1	2	3	4	5	6		1	2	3	4	5	6
AOA SV Pass 1	-	-	-	-	-	-	1	98%	92%	95%	99%	98%	94%
AOA SV Pass 2	-	-	-	-	-	-	2	99%	96%	98%	99%	99%	97%
AOA SV Pass 3	-	-	-	-	-	-	3	98%	89%	83%	97%	94%	81%
AOA SV Pass 4	-	-	-	-	-	-	4	99%	95%	96%	97%	98%	94%
AOA SV Pass 5	-	-	-	-	-	-	5	99%	96%	98%	99%	99%	97%
AOA SV Pass 6	-	-	-	-	-	-	6	96%	79%	90%	98%	96%	86%

Table 146. Ellipsoid Intersection fusion consistency for augmentation of four-ball TDOA SV by AOA SV against Libya target

		Ground Constrained						Non-Ground Constrained					
		Ellipsoid Consistency						Ellipsoid Consistency					
		Four-ball TDOA Satellite Pass						Four-ball TDOA Satellite Pass					
		1	2	3	4	5	6	1	2	3	4	5	6
AOA SV Pass	1	-	-	-	-	-	-	96%	96%	96%	96%	96%	96%
	2	-	-	-	-	-	-	97%	97%	97%	97%	97%	97%
	3	-	-	-	-	-	-	99%	99%	98%	99%	98%	98%
	4	-	-	-	-	-	-	94%	95%	94%	94%	94%	94%
	5	-	-	-	-	-	-	96%	96%	96%	96%	96%	96%
	6	-	-	-	-	-	-	95%	99%	97%	97%	95%	98%
		Ellipse Consistency						Ellipse Consistency					
		Four-ball TDOA Satellite Pass						Four-ball TDOA Satellite Pass					
		1	2	3	4	5	6	1	2	3	4	5	6
AOA SV Pass	1	-	-	-	-	-	-	98%	56%	100%	97%	100%	100%
	2	-	-	-	-	-	-	99%	44%	100%	98%	100%	100%
	3	-	-	-	-	-	-	99%	23%	69%	99%	99%	98%
	4	-	-	-	-	-	-	98%	33%	100%	99%	100%	100%
	5	-	-	-	-	-	-	100%	54%	98%	98%	97%	98%
	6	-	-	-	-	-	-	99%	28%	100%	99%	100%	100%

Table 147. Improvement from Kalman filter fusion based augmentation of four-ball TDOA SV by AOA SV against Libya target

		Ground Constrained						Non-Ground Constrained					
RMSE													
		Four-ball TDOA Satellite Pass						Four-ball TDOA Satellite Pass					
		1	2	3	4	5	6	1	2	3	4	5	6
AOA SV Pass	1	93%	98%	96%	87%	96%	94%	98%	99%	95%	98%	99%	94%
	2	97%	98%	95%	89%	97%	97%	99%	100%	97%	99%	99%	97%
	3	94%	98%	81%	74%	95%	94%	98%	99%	83%	97%	96%	83%
	4	97%	99%	92%	80%	95%	97%	99%	99%	96%	97%	99%	94%
	5	97%	99%	96%	90%	98%	97%	99%	100%	97%	99%	99%	97%
	6	90%	98%	93%	83%	95%	92%	96%	98%	91%	98%	98%	87%
Ave Miss													
		Four-ball TDOA Satellite Pass						Four-ball TDOA Satellite Pass					
		1	2	3	4	5	6	1	2	3	4	5	6
AOA SV Pass	1	83%	94%	95%	87%	94%	94%	97%	99%	95%	98%	99%	94%
	2	91%	94%	95%	89%	96%	97%	99%	99%	97%	98%	99%	96%
	3	85%	94%	80%	73%	92%	94%	97%	99%	83%	97%	97%	83%
	4	91%	94%	92%	81%	93%	97%	98%	99%	95%	97%	99%	94%
	5	92%	94%	96%	90%	96%	97%	99%	99%	97%	99%	99%	96%
	6	73%	94%	93%	82%	93%	92%	96%	98%	91%	98%	98%	87%
Ave SMA													
		Four-ball TDOA Satellite Pass						Four-ball TDOA Satellite Pass					
		1	2	3	4	5	6	1	2	3	4	5	6
AOA SV Pass	1	93%	5%	96%	88%	97%	94%	98%	92%	95%	99%	98%	94%
	2	98%	6%	95%	91%	98%	98%	99%	96%	98%	99%	99%	97%
	3	95%	2%	82%	77%	95%	95%	98%	89%	83%	97%	94%	81%
	4	97%	7%	92%	81%	95%	97%	99%	95%	96%	97%	98%	94%
	5	97%	6%	97%	93%	98%	97%	99%	96%	98%	99%	99%	97%
	6	89%	3%	93%	85%	95%	92%	96%	79%	90%	98%	96%	86%

Table 148. Kalman filter fusion consistency for augmentation of four-ball TDOA SV by AOA SV against Libya target

		Ground Constrained						Non-Ground Constrained					
		Ellipsoid Consistency Four-ball TDOA Satellite Pass						Ellipsoid Consistency Four-ball TDOA Satellite Pass					
		1	2	3	4	5	6	1	2	3	4	5	6
AOA SV Pass	1	41%	90%	73%	7%	87%	93%	97%	93%	94%	97%	96%	95%
	2	38%	92%	72%	9%	82%	90%	96%	95%	95%	93%	97%	94%
	3	28%	86%	61%	5%	79%	84%	94%	94%	94%	94%	97%	94%
	4	39%	93%	71%	9%	87%	97%	92%	93%	97%	92%	94%	96%
	5	39%	93%	70%	8%	84%	90%	96%	94%	95%	94%	96%	95%
	6	29%	80%	54%	7%	63%	72%	93%	96%	97%	96%	96%	98%
		Ellipse Consistency Four-ball TDOA Satellite Pass						Ellipse Consistency Four-ball TDOA Satellite Pass					
		1	2	3	4	5	6	1	2	3	4	5	6
AOA SV Pass	1	100%	98%	99%	100%	100%	100%	98%	56%	100%	97%	100%	100%
	2	99%	99%	100%	100%	98%	100%	99%	44%	100%	98%	100%	100%
	3	100%	98%	98%	98%	100%	100%	99%	23%	69%	99%	99%	98%
	4	100%	99%	99%	100%	100%	100%	98%	33%	100%	99%	100%	100%
	5	100%	98%	100%	96%	98%	99%	100%	54%	98%	98%	97%	98%
	6	100%	98%	98%	99%	100%	99%	99%	28%	100%	99%	100%	100%

2.3 Afghanistan Fusion Results

2.3.0.25 AOA Satellite Augmenting AOA Satellite Against Afghanistan Target.

The following are the full pass-by-pass fusion results and associated consistencies for each fusion algorithm for the augmentation on an AOA SV geolocation agent with another AOA SV geolocation agent against the Afghanistan target.

Table 149. Improvement from Largest Ellipsoid fusion based augmentation of AOA SV by AOA SV against Afghanistan target

	Ground Constrained						Non-Ground Constrained					
RMSE												
	AOA SV Pass						AOA SV Pass					
AOA SV Pass	1	2	3	4	5	6	1	2	3	4	5	6
1	-1%	24%	73%	54%	17%	68%	0%	23%	71%	50%	17%	65%
2	39%	1%	77%	54%	26%	76%	49%	2%	77%	53%	31%	78%
3	14%	8%	-4%	24%	3%	51%	27%	13%	-2%	24%	10%	60%
4	34%	17%	65%	0%	17%	67%	44%	20%	66%	-3%	25%	69%
5	40%	32%	78%	58%	-4%	75%	47%	34%	78%	57%	-3%	76%
6	9%	14%	56%	35%	4%	0%	8%	15%	59%	29%	4%	1%
Ave Miss												
	AOA SV Pass						AOA SV Pass					
AOA SV Pass	1	2	3	4	5	6	1	2	3	4	5	6
1	-1%	23%	69%	52%	15%	60%	-2%	24%	70%	48%	16%	63%
2	37%	2%	73%	53%	26%	69%	48%	3%	76%	51%	31%	77%
3	13%	9%	-4%	25%	1%	37%	26%	14%	-1%	24%	8%	56%
4	31%	17%	61%	-1%	15%	58%	41%	20%	65%	-3%	24%	68%
5	38%	34%	74%	57%	-4%	69%	45%	34%	76%	56%	-4%	75%
6	10%	14%	48%	33%	3%	1%	8%	14%	56%	28%	4%	-1%
Ave SMA												
	AOA SV Pass						AOA SV Pass					
AOA SV Pass	1	2	3	4	5	6	1	2	3	4	5	6
1	41%	9%	73%	51%	3%	68%	51%	0%	74%	54%	4%	74%
2	31%	30%	79%	64%	6%	75%	44%	19%	81%	60%	13%	81%
3	0%	0%	0%	3%	0%	54%	0%	0%	71%	9%	0%	33%
4	25%	25%	64%	64%	3%	49%	45%	9%	78%	59%	22%	74%
5	39%	22%	83%	62%	-1%	80%	51%	5%	80%	52%	32%	81%
6	0%	0%	38%	0%	0%	63%	16%	0%	37%	0%	0%	71%

Table 150. Largest Ellipsoid fusion consistency for augmentation of AOA SV by AOA SV against Afghanistan target

		Ground Constrained						Non-Ground Constrained					
		Ellipsoid Consistency AOA AV Pass						Ellipsoid Consistency AOA AV Pass					
		1	2	3	4	5	6	1	2	3	4	5	6
AOA SV Pass	1	75%	94%	86%	94%	95%	86%	74%	97%	89%	99%	98%	80%
	2	96%	83%	89%	94%	95%	94%	100%	92%	99%	99%	100%	99%
	3	94%	88%	85%	90%	90%	98%	99%	99%	50%	98%	99%	99%
	4	97%	94%	72%	59%	95%	86%	99%	100%	82%	61%	98%	87%
	5	95%	95%	90%	95%	45%	90%	96%	99%	95%	99%	85%	89%
	6	91%	92%	98%	95%	90%	80%	98%	97%	97%	99%	97%	50%
		Ellipse Consistency AOA AV Pass						Ellipse Consistency AOA AV Pass					
		1	2	3	4	5	6	1	2	3	4	5	6
AOA SV Pass	1	99%	100%	94%	99%	100%	93%	81%	99%	92%	100%	100%	81%
	2	100%	97%	97%	97%	100%	99%	100%	99%	100%	99%	100%	100%
	3	99%	99%	95%	100%	97%	100%	99%	100%	99%	100%	100%	100%
	4	99%	100%	82%	74%	99%	89%	100%	100%	84%	77%	100%	88%
	5	100%	100%	100%	100%	99%	100%	98%	99%	96%	100%	97%	94%
	6	100%	99%	100%	100%	98%	100%	100%	99%	100%	100%	100%	99%

Table 151. Improvement from Fast Determinant CI fusion based augmentation of AOA SV by AOA SV against Afghanistan target

	Ground Constrained						Non-Ground Constrained					
RMSE												
	AOA SV Pass						AOA SV Pass					
AOA SV Pass	1	2	3	4	5	6	1	2	3	4	5	6
1	-1%	14%	68%	53%	6%	64%	0%	12%	62%	50%	3%	62%
2	32%	1%	75%	49%	26%	72%	41%	2%	74%	46%	30%	75%
3	-1%	1%	-4%	1%	-3%	51%	2%	2%	-2%	-1%	-3%	59%
4	33%	7%	55%	0%	4%	50%	44%	8%	56%	-3%	6%	57%
5	32%	32%	76%	52%	-4%	74%	38%	33%	74%	47%	-3%	75%
6	-1%	1%	56%	1%	-3%	0%	0%	2%	58%	-1%	-3%	1%
Ave Miss												
	AOA SV Pass						AOA SV Pass					
AOA SV Pass	1	2	3	4	5	6	1	2	3	4	5	6
1	-1%	14%	64%	51%	5%	56%	-2%	12%	59%	48%	2%	59%
2	30%	2%	71%	48%	25%	65%	40%	3%	73%	45%	30%	73%
3	0%	2%	-4%	1%	-4%	37%	0%	3%	-1%	-1%	-4%	56%
4	30%	8%	48%	-1%	4%	38%	41%	9%	54%	-3%	5%	55%
5	31%	33%	72%	51%	-4%	67%	37%	33%	72%	45%	-4%	73%
6	0%	2%	48%	1%	-4%	1%	-2%	3%	55%	-1%	-4%	-1%
Ave SMA												
	AOA SV Pass						AOA SV Pass					
AOA SV Pass	1	2	3	4	5	6	1	2	3	4	5	6
1	0%	1%	73%	39%	-5%	68%	0%	2%	65%	39%	-2%	66%
2	24%	0%	79%	49%	-8%	75%	45%	0%	80%	51%	11%	81%
3	0%	0%	0%	0%	0%	39%	0%	0%	0%	0%	0%	52%
4	2%	-5%	56%	0%	-4%	49%	28%	-2%	59%	0%	3%	60%
5	36%	14%	83%	60%	0%	80%	43%	11%	80%	54%	0%	81%
6	0%	0%	48%	1%	0%	0%	-1%	0%	51%	1%	0%	0%

Table 152. Fast Determinant CI fusion consistency for augmentation of AOA SV by AOA SV against Afghanistan target

		Ground Constrained						Non-Ground Constrained					
		Ellipsoid Consistency AOA AV Pass						Ellipsoid Consistency AOA AV Pass					
		1	2	3	4	5	6	1	2	3	4	5	6
AOA SV Pass	1	89%	94%	90%	100%	93%	90%	97%	98%	97%	100%	97%	97%
	2	94%	89%	89%	93%	97%	89%	98%	96%	96%	97%	100%	96%
	3	90%	89%	85%	91%	89%	99%	97%	96%	96%	96%	91%	100%
	4	100%	93%	91%	91%	91%	91%	100%	97%	96%	95%	96%	96%
	5	93%	97%	89%	91%	89%	89%	97%	100%	91%	96%	91%	91%
	6	90%	89%	99%	91%	89%	87%	97%	96%	100%	96%	91%	98%
		Ellipse Consistency AOA AV Pass						Ellipse Consistency AOA AV Pass					
		1	2	3	4	5	6	1	2	3	4	5	6
AOA SV Pass	1	100%	100%	100%	100%	98%	100%	99%	100%	99%	100%	100%	99%
	2	100%	99%	99%	99%	100%	99%	100%	99%	99%	100%	100%	99%
	3	100%	99%	97%	99%	97%	100%	99%	99%	99%	100%	100%	100%
	4	100%	99%	99%	99%	98%	99%	100%	100%	100%	100%	100%	100%
	5	98%	100%	97%	98%	97%	97%	100%	100%	100%	100%	100%	100%
	6	100%	99%	100%	99%	97%	100%	99%	99%	100%	100%	100%	100%

Table 153. Improvement from Fast Trace CI fusion based augmentation of AOA SV by AOA SV against Afghanistan target

		Ground Constrained						Non-Ground Constrained						
RMSE														
		AOA SV Pass							AOA SV Pass					
		1	2	3	4	5	6		1	2	3	4	5	6
AOA SV Pass	1	-1%	23%	69%	52%	15%	65%	1	0%	20%	66%	50%	12%	63%
	2	38%	1%	75%	51%	26%	73%	2	47%	2%	75%	50%	31%	75%
	3	3%	2%	-4%	12%	-3%	51%	3	12%	4%	-2%	10%	-1%	60%
	4	30%	12%	60%	0%	10%	61%	4	44%	15%	60%	-3%	18%	63%
	5	38%	32%	76%	55%	-4%	74%	5	44%	33%	75%	53%	-3%	75%
	6	2%	4%	56%	23%	-2%	0%	6	3%	4%	59%	14%	-2%	1%
Ave Miss														
		AOA SV Pass							AOA SV Pass					
		1	2	3	4	5	6		1	2	3	4	5	6
AOA SV Pass	1	-1%	22%	65%	50%	13%	57%	1	-2%	20%	63%	48%	11%	61%
	2	37%	2%	71%	50%	25%	66%	2	46%	3%	73%	49%	31%	74%
	3	4%	3%	-4%	12%	-3%	37%	3	10%	4%	-1%	10%	-2%	56%
	4	28%	12%	54%	-1%	9%	51%	4	41%	16%	59%	-3%	17%	61%
	5	36%	33%	73%	54%	-4%	67%	5	42%	34%	73%	52%	-4%	73%
	6	2%	4%	48%	22%	-3%	1%	6	1%	4%	56%	13%	-3%	-1%
Ave SMA														
		AOA SV Pass							AOA SV Pass					
		1	2	3	4	5	6		1	2	3	4	5	6
AOA SV Pass	1	0%	0%	72%	40%	-13%	67%	1	0%	3%	66%	39%	-6%	64%
	2	23%	0%	78%	47%	-8%	75%	2	46%	0%	80%	50%	12%	81%
	3	-1%	-3%	0%	-1%	-2%	40%	3	3%	-3%	0%	0%	-2%	53%
	4	4%	-11%	56%	0%	-9%	53%	4	28%	-6%	59%	0%	6%	62%
	5	31%	14%	83%	58%	0%	80%	5	40%	11%	80%	55%	0%	80%
	6	-4%	-2%	48%	8%	-3%	0%	6	-6%	-2%	52%	6%	-3%	0%

Table 154. Fast Trace CI fusion consistency for augmentation of AOA SV by AOA SV against Afghanistan target

		Ground Constrained						Non-Ground Constrained					
		Ellipsoid Consistency AOA AV Pass						Ellipsoid Consistency AOA AV Pass					
		1	2	3	4	5	6	1	2	3	4	5	6
AOA SV Pass	1	89%	98%	93%	99%	95%	92%	97%	99%	99%	100%	100%	98%
	2	98%	89%	92%	96%	97%	93%	99%	96%	97%	99%	100%	97%
	3	93%	92%	85%	93%	90%	99%	99%	97%	96%	98%	95%	100%
	4	99%	96%	93%	91%	92%	96%	100%	99%	98%	95%	98%	98%
	5	95%	97%	90%	92%	89%	90%	100%	100%	95%	98%	91%	95%
	6	92%	93%	99%	96%	90%	87%	98%	97%	100%	98%	95%	98%
		Ellipse Consistency AOA AV Pass						Ellipse Consistency AOA AV Pass					
		1	2	3	4	5	6	1	2	3	4	5	6
AOA SV Pass	1	100%	100%	100%	100%	100%	100%	99%	100%	100%	100%	100%	100%
	2	100%	99%	99%	100%	100%	99%	100%	99%	99%	100%	100%	99%
	3	100%	99%	97%	100%	97%	100%	100%	99%	99%	100%	100%	100%
	4	100%	100%	100%	99%	99%	100%	100%	100%	100%	100%	100%	100%
	5	100%	100%	97%	99%	97%	97%	100%	100%	100%	100%	100%	100%
	6	100%	99%	100%	100%	97%	100%	100%	99%	100%	100%	100%	100%

Table 155. Improvement from Ellipsoid Intersection fusion based augmentation of AOA SV by AOA SV against Afghanistan target

	Ground Constrained						Non-Ground Constrained					
RMSE												
	AOA SV Pass						AOA SV Pass					
AOA SV Pass	1	2	3	4	5	6	1	2	3	4	5	6
1	-1%	22%	73%	52%	15%	68%	0%	23%	71%	50%	17%	65%
2	40%	1%	77%	54%	23%	76%	49%	2%	77%	53%	31%	78%
3	13%	6%	-4%	24%	0%	51%	27%	13%	-2%	24%	10%	60%
4	35%	15%	65%	0%	14%	67%	44%	20%	66%	-3%	25%	69%
5	41%	29%	78%	56%	-4%	75%	47%	34%	78%	57%	-3%	77%
6	9%	13%	56%	34%	2%	0%	8%	14%	59%	29%	4%	1%
Ave Miss												
	AOA SV Pass						AOA SV Pass					
AOA SV Pass	1	2	3	4	5	6	1	2	3	4	5	6
1	-1%	22%	69%	50%	12%	60%	-2%	24%	70%	48%	16%	63%
2	39%	2%	73%	53%	21%	70%	48%	3%	76%	51%	31%	77%
3	11%	6%	-4%	24%	-2%	37%	26%	13%	-1%	24%	8%	56%
4	32%	16%	61%	-1%	13%	58%	41%	20%	65%	-3%	24%	67%
5	39%	30%	74%	54%	-4%	69%	45%	34%	76%	56%	-4%	75%
6	9%	13%	48%	33%	1%	1%	8%	14%	56%	28%	4%	-1%
Ave SMA												
	AOA SV Pass						AOA SV Pass					
AOA SV Pass	1	2	3	4	5	6	1	2	3	4	5	6
1	29%	28%	80%	56%	15%	72%	29%	25%	77%	57%	19%	69%
2	45%	29%	80%	57%	22%	79%	58%	29%	82%	61%	38%	84%
3	26%	7%	29%	26%	5%	57%	35%	7%	29%	28%	14%	67%
4	29%	10%	68%	29%	8%	70%	49%	17%	70%	29%	33%	76%
5	48%	39%	84%	65%	29%	81%	55%	38%	83%	68%	29%	82%
6	12%	17%	63%	41%	3%	29%	8%	18%	66%	39%	5%	29%

Table 156. Ellipsoid Intersection fusion consistency for augmentation of AOA SV by AOA SV against Afghanistan target

		Ground Constrained						Non-Ground Constrained					
		Ellipsoid Consistency AOA AV Pass						Ellipsoid Consistency AOA AV Pass					
		1	2	3	4	5	6	1	2	3	4	5	6
AOA SV Pass	1	72%	85%	87%	88%	85%	87%	75%	97%	95%	96%	94%	96%
	2	93%	70%	86%	92%	88%	91%	95%	71%	97%	95%	92%	96%
	3	87%	80%	65%	85%	85%	91%	95%	97%	72%	93%	95%	98%
	4	90%	86%	86%	68%	86%	91%	96%	95%	93%	69%	95%	96%
	5	93%	85%	88%	87%	74%	90%	96%	92%	95%	96%	74%	95%
	6	84%	85%	90%	88%	83%	73%	97%	96%	98%	96%	94%	74%
		Ellipse Consistency AOA AV Pass						Ellipse Consistency AOA AV Pass					
		1	2	3	4	5	6	1	2	3	4	5	6
AOA SV Pass	1	96%	100%	100%	99%	99%	99%	97%	99%	99%	99%	100%	99%
	2	100%	91%	100%	99%	98%	99%	99%	90%	100%	99%	100%	99%
	3	100%	100%	88%	98%	99%	100%	99%	100%	94%	100%	100%	100%
	4	99%	99%	98%	88%	99%	100%	99%	99%	100%	92%	99%	100%
	5	99%	98%	99%	99%	94%	100%	100%	100%	100%	99%	92%	100%
	6	99%	99%	100%	100%	100%	95%	99%	99%	100%	100%	100%	93%

Table 157. Improvement from Kalman filter fusion based augmentation of AOA SV by AOA SV against Afghanistan target

	Ground Constrained						Non-Ground Constrained					
RMSE												
	AOA SV Pass						AOA SV Pass					
AOA SV Pass	1	2	3	4	5	6	1	2	3	4	5	6
1	-1%	24%	73%	54%	17%	68%	0%	23%	71%	50%	17%	65%
2	39%	1%	77%	54%	26%	76%	49%	2%	77%	53%	31%	78%
3	14%	8%	-4%	24%	3%	51%	27%	13%	-2%	24%	10%	60%
4	34%	17%	65%	0%	17%	67%	44%	20%	66%	-3%	25%	69%
5	40%	32%	78%	58%	-4%	75%	47%	34%	78%	57%	-3%	76%
6	9%	14%	56%	35%	4%	0%	8%	15%	59%	29%	4%	1%
Ave Miss												
	AOA SV Pass						AOA SV Pass					
AOA SV Pass	1	2	3	4	5	6	1	2	3	4	5	6
1	-1%	23%	69%	52%	15%	60%	-2%	24%	70%	48%	16%	63%
2	37%	2%	73%	53%	26%	69%	48%	3%	76%	51%	31%	77%
3	13%	9%	-4%	25%	1%	37%	26%	14%	-1%	24%	8%	56%
4	31%	17%	61%	-1%	15%	58%	41%	20%	65%	-3%	24%	68%
5	38%	34%	74%	57%	-4%	69%	45%	34%	76%	56%	-4%	75%
6	10%	14%	48%	33%	3%	1%	8%	14%	56%	28%	4%	-1%
Ave SMA												
	AOA SV Pass						AOA SV Pass					
AOA SV Pass	1	2	3	4	5	6	1	2	3	4	5	6
1	29%	28%	80%	56%	15%	72%	29%	25%	77%	57%	19%	69%
2	45%	29%	80%	57%	22%	79%	58%	29%	82%	61%	38%	84%
3	26%	7%	29%	26%	5%	57%	35%	7%	29%	28%	14%	67%
4	29%	10%	68%	29%	8%	70%	49%	17%	70%	29%	33%	76%
5	48%	39%	84%	65%	29%	81%	55%	38%	83%	68%	29%	82%
6	12%	17%	63%	41%	3%	29%	8%	18%	66%	39%	5%	29%

Table 158. Kalman filter fusion consistency for augmentation of AOA SV by AOA SV against Afghanistan target

		Ground Constrained						Non-Ground Constrained					
		Ellipsoid Consistency AOA AV Pass						Ellipsoid Consistency AOA AV Pass					
		1	2	3	4	5	6	1	2	3	4	5	6
AOA SV Pass	1	0.72	0.90	0.87	0.88	0.89	0.86	0.75	0.95	0.95	0.96	0.94	0.97
	2	0.90	0.70	0.83	0.89	0.90	0.86	0.95	0.71	0.96	0.95	0.92	0.96
	3	0.87	0.83	0.65	0.84	0.88	0.90	0.95	0.96	0.72	0.93	0.95	0.98
	4	0.88	0.89	0.84	0.68	0.90	0.89	0.96	0.95	0.93	0.69	0.95	0.96
	5	0.89	0.90	0.88	0.90	0.74	0.86	0.94	0.92	0.95	0.95	0.74	0.94
	6	0.86	0.86	0.90	0.89	0.86	0.73	0.97	0.96	0.98	0.96	0.94	0.74
		Ellipse Consistency AOA AV Pass						Ellipse Consistency AOA AV Pass					
		1	2	3	4	5	6	1	2	3	4	5	6
AOA SV Pass	1	0.96	1.00	1.00	0.99	0.99	0.99	0.97	0.99	0.99	0.99	1.00	0.99
	2	1.00	0.91	1.00	0.99	0.98	0.99	0.99	0.90	1.00	0.99	1.00	0.99
	3	1.00	1.00	0.88	0.98	0.99	1.00	0.99	1.00	0.94	1.00	1.00	1.00
	4	0.99	0.99	0.98	0.88	0.99	1.00	0.99	0.99	1.00	0.92	0.99	1.00
	5	0.99	0.98	0.99	0.99	0.94	1.00	1.00	1.00	1.00	0.99	0.92	1.00
	6	0.99	0.99	1.00	1.00	1.00	0.95	0.99	0.99	1.00	1.00	1.00	0.93

2.3.0.26 AOA Satellite Augmenting AOA Aircraft Against Afghanistan Target.

The following are the full pass-by-pass fusion results and associated consistencies for each fusion algorithm for the augmentation on an AOA AV geolocation agent with an AOA SV geolocation agent against the Afghanistan target.

Table 159. Improvement from Largest Ellipsoid fusion based augmentation of AOA AV by AOA SV against Afghanistan target

	Ground Constrained			Non-Ground Constrained		
RMSE						
	AOA Aircraft Pass			AOA Aircraft Pass		
		1	2		1	2
AOA SV Pass	1	1%	66%	1	0%	66%
	2	1%	68%	2	2%	72%
	3	-1%	29%	3	-1%	35%
	4	4%	61%	4	5%	67%
	5	-1%	67%	5	-2%	71%
	6	0%	40%	6	0%	41%
Ave Miss						
	AOA Aircraft Pass			AOA Aircraft Pass		
		1	2		1	2
AOA SV Pass	1	0%	45%	1	0%	64%
	2	0%	50%	2	1%	70%
	3	-2%	3%	3	-1%	32%
	4	3%	40%	4	3%	65%
	5	-1%	49%	5	-1%	69%
	6	0%	10%	6	0%	39%
Ave SMA						
	AOA Aircraft Pass			AOA Aircraft Pass		
		1	2		1	2
AOA SV Pass	1	0%	51%	1	0%	72%
	2	0%	67%	2	0%	72%
	3	0%	0%	3	0%	50%
	4	0%	50%	4	0%	72%
	5	0%	71%	5	0%	77%
	6	0%	27%	6	0%	31%

Table 160. Largest Ellipsoid fusion consistency for augmentation of AOA AV by AOA SV against Afghanistan target

		Ground Constrained		Non-Ground Constrained	
		Ellipsoid Consistency		Ellipsoid Consistency	
		AOA Aircraft Pass		AOA Aircraft Pass	
		1	2	1	2
AOA SV Pass	1	92%	98%	92%	93%
	2	91%	94%	94%	100%
	3	90%	97%	92%	93%
	4	93%	97%	95%	94%
	5	90%	95%	95%	96%
	6	90%	96%	94%	96%
		0%	0%	91%	91%
		Ellipse Consistency		Ellipse Consistency	
		AOA Aircraft Pass		AOA Aircraft Pass	
		1	2	1	2
AOA SV Pass	1	97%	99%	99%	99%
	2	97%	100%	99%	100%
	3	97%	99%	99%	99%
	4	97%	98%	99%	99%
	5	97%	100%	100%	99%
	6	97%	100%	99%	99%

Table 161. Improvement from Fast Determinant CI fusion based augmentation of AOA AV by AOA SV against Afghanistan target

	Ground Constrained		Non-Ground Constrained	
	RMSE			
	AOA Aircraft Pass		AOA Aircraft Pass	
	1	2	1	2
AOA SV Pass 1	0%	65%	0%	62%
AOA SV Pass 2	0%	61%	0%	71%
AOA SV Pass 3	0%	21%	0%	-1%
AOA SV Pass 4	0%	61%	0%	62%
AOA SV Pass 5	0%	60%	0%	70%
AOA SV Pass 6	0%	22%	0%	-1%
	Ave Miss			
	AOA Aircraft Pass		AOA Aircraft Pass	
	1	2	1	2
AOA SV Pass 1	0%	44%	0%	60%
AOA SV Pass 2	0%	37%	0%	69%
AOA SV Pass 3	0%	18%	0%	-3%
AOA SV Pass 4	0%	39%	0%	60%
AOA SV Pass 5	0%	37%	0%	67%
AOA SV Pass 6	0%	19%	0%	-2%
	Ave SMA			
	AOA Aircraft Pass		AOA Aircraft Pass	
	1	2	1	2
AOA SV Pass 1	0%	65%	0%	45%
AOA SV Pass 2	0%	64%	0%	67%
AOA SV Pass 3	0%	0%	0%	0%
AOA SV Pass 4	0%	54%	0%	45%
AOA SV Pass 5	0%	70%	0%	70%
AOA SV Pass 6	0%	1%	0%	0%

Table 162. Fast Determinant CI fusion consistency for augmentation of AOA AV by AOA SV against Afghanistan target

		Ground Constrained		Non-Ground Constrained	
		Ellipsoid Consistency		Ellipsoid Consistency	
		AOA Aircraft Pass		AOA Aircraft Pass	
		1	2	1	2
AOA SV Pass	1	91%	99%	91%	99%
	2	91%	94%	91%	100%
	3	91%	96%	91%	95%
	4	91%	99%	91%	99%
	5	91%	90%	91%	99%
	6	91%	97%	91%	95%
		0%	0%	91%	91%
		Ellipse Consistency		Ellipse Consistency	
		AOA Aircraft Pass		AOA Aircraft Pass	
		1	2	1	2
AOA SV Pass	1	97%	100%	99%	99%
	2	97%	100%	99%	100%
	3	97%	99%	99%	99%
	4	97%	100%	99%	99%
	5	97%	100%	99%	100%
	6	97%	99%	99%	99%

Table 163. Improvement from Fast Trace CI fusion based augmentation of AOA AV by AOA SV against Afghanistan target

	Ground Constrained		Non-Ground Constrained	
	RMSE			
	AOA Aircraft Pass		AOA Aircraft Pass	
	1	2	1	2
AOA SV Pass 1	0%	63%	0%	66%
AOA SV Pass 2	0%	63%	0%	68%
AOA SV Pass 3	0%	30%	0%	25%
AOA SV Pass 4	0%	60%	0%	67%
AOA SV Pass 5	0%	62%	0%	66%
AOA SV Pass 6	0%	40%	0%	32%
	Ave Miss			
	AOA Aircraft Pass		AOA Aircraft Pass	
	1	2	1	2
AOA SV Pass 1	0%	41%	0%	63%
AOA SV Pass 2	0%	42%	0%	65%
AOA SV Pass 3	0%	15%	0%	21%
AOA SV Pass 4	0%	38%	0%	64%
AOA SV Pass 5	0%	41%	0%	64%
AOA SV Pass 6	0%	19%	0%	29%
	Ave SMA			
	AOA Aircraft Pass		AOA Aircraft Pass	
	1	2	1	2
AOA SV Pass 1	-1%	66%	0%	62%
AOA SV Pass 2	-1%	64%	-1%	69%
AOA SV Pass 3	0%	-4%	0%	2%
AOA SV Pass 4	0%	54%	0%	64%
AOA SV Pass 5	-1%	69%	-1%	70%
AOA SV Pass 6	0%	11%	0%	14%

Table 164. Fast Trace CI fusion consistency for augmentation of AOA AV by AOA SV against Afghanistan target

		Ground Constrained		Non-Ground Constrained	
		Ellipsoid Consistency AOA Aircraft Pass		Ellipsoid Consistency AOA Aircraft Pass	
		1	2	1	2
AOA SV Pass	1	91%	98%	91%	100%
	2	91%	95%	92%	100%
	3	91%	97%	91%	99%
	4	91%	99%	91%	100%
	5	91%	92%	92%	98%
	6	91%	97%	91%	99%
		Ellipse Consistency AOA Aircraft Pass		Ellipse Consistency AOA Aircraft Pass	
		1	2	1	2
AOA SV Pass	1	97%	100%	99%	100%
	2	97%	100%	99%	100%
	3	97%	99%	99%	99%
	4	97%	100%	99%	100%
	5	97%	100%	99%	100%
	6	97%	100%	99%	99%

Table 165. Improvement from Ellipsoid Intersection fusion based augmentation of AOA AV by AOA SV against Afghanistan target

	Ground Constrained			Non-Ground Constrained		
RMSE						
	AOA Aircraft Pass			AOA Aircraft Pass		
		1	2		1	2
AOA SV Pass	1	-455%	66%	1	-139%	63%
	2	-1161%	67%	2	-220%	68%
	3	-170%	30%	3	-9%	32%
	4	-518%	61%	4	-173%	67%
	5	-2924%	66%	5	-114%	69%
	6	-93%	39%	6	-2%	38%
Ave Miss						
	AOA Aircraft Pass			AOA Aircraft Pass		
		1	2		1	2
AOA SV Pass	1	-521%	45%	1	-158%	61%
	2	-1316%	48%	2	-250%	66%
	3	-196%	4%	3	-9%	29%
	4	-593%	40%	4	-199%	65%
	5	-3298%	46%	5	-134%	67%
	6	-109%	9%	6	-4%	35%
Ave SMA						
	AOA Aircraft Pass			AOA Aircraft Pass		
		1	2		1	2
AOA SV Pass	1	1%	72%	1	1%	70%
	2	2%	71%	2	2%	74%
	3	0%	21%	3	0%	32%
	4	2%	67%	4	2%	73%
	5	2%	73%	5	2%	76%
	6	0%	41%	6	0%	46%

Table 166. Ellipsoid Intersection fusion consistency for augmentation of AOA AV by AOA SV against Afghanistan target

		Ground Constrained		Non-Ground Constrained	
		Ellipsoid Consistency		Ellipsoid Consistency	
		AOA Aircraft Pass		AOA Aircraft Pass	
		1	2	1	2
AOA SV Pass	1	0%	92%	1%	93%
	2	0%	90%	2%	95%
	3	0%	91%	89%	98%
	4	0%	90%	0%	94%
	5	0%	89%	6%	92%
	6	0%	93%	92%	92%
		Ellipse Consistency		Ellipse Consistency	
		AOA Aircraft Pass		AOA Aircraft Pass	
		1	2	1	2
AOA SV Pass	1	97%	99%	99%	99%
	2	97%	100%	99%	99%
	3	97%	99%	99%	99%
	4	97%	99%	99%	99%
	5	97%	100%	100%	100%
	6	97%	100%	99%	99%

Table 167. Improvement from Kalman filter fusion based augmentation of AOA AV by AOA SV against Afghanistan target

	Ground Constrained		Non-Ground Constrained	
RMSE				
	AOA Aircraft Pass		AOA Aircraft Pass	
	1	2	1	2
AOA SV Pass 1	1%	66%	0%	66%
AOA SV Pass 2	1%	68%	2%	72%
AOA SV Pass 3	-1%	29%	-1%	35%
AOA SV Pass 4	4%	61%	5%	67%
AOA SV Pass 5	-1%	67%	-2%	71%
AOA SV Pass 6	0%	40%	0%	41%
Ave Miss				
	AOA Aircraft Pass		AOA Aircraft Pass	
	1	2	1	2
AOA SV Pass 1	0%	45%	0%	64%
AOA SV Pass 2	0%	50%	1%	70%
AOA SV Pass 3	-2%	3%	-1%	32%
AOA SV Pass 4	3%	40%	3%	65%
AOA SV Pass 5	-1%	49%	-1%	69%
AOA SV Pass 6	0%	10%	0%	39%
Ave SMA				
	AOA Aircraft Pass		AOA Aircraft Pass	
	1	2	1	2
AOA SV Pass 1	1%	72%	1%	70%
AOA SV Pass 2	2%	71%	2%	74%
AOA SV Pass 3	0%	21%	0%	32%
AOA SV Pass 4	2%	67%	2%	73%
AOA SV Pass 5	2%	73%	2%	76%
AOA SV Pass 6	0%	41%	0%	46%

Table 168. Kalman filter fusion consistency for augmentation of AOA AV by AOA SV against Afghanistan target

		Ground Constrained		Non-Ground Constrained	
		Ellipsoid Consistency		Ellipsoid Consistency	
		AOA Aircraft Pass		AOA Aircraft Pass	
		1	2	1	2
AOA SV Pass	1	92%	91%	92%	93%
	2	91%	89%	94%	96%
	3	90%	92%	91%	95%
	4	93%	90%	95%	90%
	5	90%	91%	92%	95%
	6	90%	93%	94%	93%
		Ellipse Consistency		Ellipse Consistency	
		AOA Aircraft Pass		AOA Aircraft Pass	
		1	2	1	2
AOA SV Pass	1	97%	99%	99%	99%
	2	97%	100%	99%	99%
	3	97%	99%	99%	99%
	4	97%	99%	99%	99%
	5	97%	100%	100%	100%
	6	97%	100%	99%	99%

2.3.0.27 AOA Satellite Augmenting Three-ball TDOA Satellites Against Afghanistan Target.

The following are the full pass-by-pass fusion results and associated consistencies for each fusion algorithm for the augmentation of a three-ball TDOA SV geolocation agent by an AOA SV geolocation agent against the Afghanistan target.

Table 169. Improvement from Largest Ellipsoid fusion based augmentation of three-ball TDOA SV by AOA SV against Afghanistan target

	Ground Constrained						Non-Ground Constrained					
RMSE												
	Three-ball TDOA SV Pass						Three-ball TDOA SV Pass					
AOA SV Pass	1	2	3	4	5	6	1	2	3	4	5	6
1	22%	18%	37%	57%	24%	33%	72%	67%	90%	84%	81%	93%
2	44%	25%	36%	61%	23%	46%	85%	81%	94%	87%	88%	95%
3	19%	6%	-1%	40%	4%	19%	74%	55%	77%	69%	71%	86%
4	36%	22%	23%	36%	10%	45%	83%	67%	89%	68%	76%	92%
5	39%	29%	37%	64%	29%	47%	84%	81%	94%	88%	88%	95%
6	4%	1%	16%	46%	11%	18%	49%	40%	80%	76%	72%	84%
Ave Miss												
	Three-ball TDOA SV Pass						Three-ball TDOA SV Pass					
AOA SV Pass	1	2	3	4	5	6	1	2	3	4	5	6
1	20%	17%	32%	48%	22%	29%	72%	67%	89%	83%	81%	93%
2	40%	21%	32%	51%	23%	42%	84%	80%	93%	86%	87%	95%
3	16%	4%	-2%	28%	4%	11%	73%	54%	76%	67%	69%	86%
4	33%	18%	19%	25%	10%	37%	82%	67%	88%	67%	75%	92%
5	36%	28%	33%	56%	26%	40%	83%	80%	93%	87%	87%	95%
6	6%	3%	11%	34%	9%	11%	49%	40%	79%	74%	69%	84%
Ave SMA												
	Three-ball TDOA SV Pass						Three-ball TDOA SV Pass					
AOA SV Pass	1	2	3	4	5	6	1	2	3	4	5	6
1	37%	5%	3%	65%	9%	44%	86%	83%	94%	88%	90%	96%
2	32%	10%	40%	70%	25%	32%	84%	81%	94%	89%	88%	96%
3	0%	0%	0%	29%	0%	2%	37%	18%	72%	70%	58%	81%
4	24%	5%	30%	69%	20%	5%	87%	84%	95%	88%	90%	96%
5	36%	7%	39%	68%	17%	44%	88%	82%	94%	87%	89%	96%
6	0%	0%	0%	0%	0%	2%	75%	51%	71%	57%	59%	80%

Table 170. Largest Ellipsoid fusion consistency for augmentation of three-ball TDOA SV by AOA SV against Afghanistan target

		Ground Constrained						Non-Ground Constrained					
		Ellipsoid Consistency Three-ball TDOA SV Pass						Ellipsoid Consistency Three-ball TDOA SV Pass					
		1	2	3	4	5	6	1	2	3	4	5	6
AOA SV Pass	1	94%	97%	91%	96%	97%	91%	0%	5%	0%	0%	26%	16%
	2	98%	96%	90%	97%	96%	91%	0%	9%	0%	0%	37%	31%
	3	94%	91%	84%	98%	94%	89%	0%	9%	0%	0%	33%	16%
	4	98%	97%	90%	78%	91%	98%	0%	8%	0%	0%	22%	15%
	5	97%	97%	93%	98%	98%	95%	0%	7%	0%	0%	38%	28%
	6	92%	89%	85%	99%	93%	87%	0%	4%	0%	0%	28%	4%
		Ellipse Consistency Three-ball TDOA SV Pass						Ellipse Consistency Three-ball TDOA SV Pass					
		1	2	3	4	5	6	1	2	3	4	5	6
AOA SV Pass	1	100%	100%	100%	99%	100%	100%	100%	98%	95%	100%	97%	95%
	2	100%	100%	99%	100%	100%	99%	100%	99%	100%	100%	100%	99%
	3	100%	100%	99%	100%	99%	99%	100%	100%	100%	100%	100%	99%
	4	100%	100%	99%	99%	100%	99%	100%	100%	100%	100%	100%	100%
	5	100%	100%	100%	100%	100%	99%	98%	97%	95%	100%	98%	94%
	6	100%	100%	99%	100%	100%	99%	100%	100%	99%	100%	100%	100%

Table 171. Improvement from Fast Determinant CI fusion based augmentation of three-ball TDOA SV by AOA SV against Afghanistan target

		Ground Constrained						Non-Ground Constrained					
RMSE													
		Three-ball TDOA SV Pass						Three-ball TDOA SV Pass					
		1	2	3	4	5	6	1	2	3	4	5	6
AOA SV Pass	1	12%	4%	11%	57%	6%	18%	4%	17%	90%	15%	81%	93%
	2	44%	21%	26%	59%	16%	45%	46%	74%	93%	59%	88%	96%
	3	1%	0%	1%	17%	1%	1%	1%	-1%	75%	-2%	19%	84%
	4	18%	5%	4%	35%	2%	22%	9%	27%	88%	0%	74%	92%
	5	39%	26%	30%	61%	24%	47%	49%	79%	93%	72%	88%	96%
	6	1%	0%	1%	17%	1%	1%	1%	-2%	78%	-2%	15%	84%
Ave Miss													
		Three-ball TDOA SV Pass						Three-ball TDOA SV Pass					
		1	2	3	4	5	6	1	2	3	4	5	6
AOA SV Pass	1	11%	4%	9%	48%	6%	16%	3%	18%	89%	15%	80%	93%
	2	40%	17%	22%	48%	16%	41%	45%	74%	93%	59%	87%	95%
	3	2%	0%	-1%	5%	2%	2%	1%	0%	74%	-4%	17%	84%
	4	18%	5%	3%	25%	3%	20%	8%	26%	87%	-1%	74%	92%
	5	36%	26%	26%	52%	22%	40%	48%	78%	93%	72%	87%	95%
	6	1%	0%	-1%	5%	2%	2%	1%	-1%	77%	-4%	13%	84%
Ave SMA													
		Three-ball TDOA SV Pass						Three-ball TDOA SV Pass					
		1	2	3	4	5	6	1	2	3	4	5	6
AOA SV Pass	1	0%	-2%	4%	39%	0%	6%	1%	9%	88%	9%	73%	92%
	2	26%	7%	9%	56%	-1%	33%	26%	61%	94%	37%	89%	96%
	3	0%	0%	0%	0%	0%	0%	0%	0%	51%	0%	12%	79%
	4	7%	1%	0%	15%	-2%	9%	4%	19%	86%	1%	61%	91%
	5	24%	2%	16%	64%	6%	34%	29%	63%	94%	49%	89%	96%
	6	0%	0%	0%	0%	0%	0%	0%	0%	67%	0%	9%	78%

Table 172. Fast Determinant CI fusion consistency for augmentation of three-ball TDOA SV by AOA SV against Afghanistan target

		Ground Constrained						Non-Ground Constrained					
		Ellipsoid Consistency Three-ball TDOA SV Pass						Ellipsoid Consistency Three-ball TDOA SV Pass					
		1	2	3	4	5	6	1	2	3	4	5	6
AOA SV Pass	1	93%	94%	90%	100%	94%	86%	0%	11%	95%	0%	76%	97%
	2	100%	97%	93%	99%	97%	96%	0%	18%	97%	0%	94%	96%
	3	90%	92%	86%	99%	93%	85%	0%	7%	0%	0%	37%	98%
	4	95%	94%	89%	100%	94%	87%	0%	11%	98%	0%	72%	95%
	5	100%	97%	93%	96%	98%	98%	0%	20%	95%	0%	93%	91%
	6	90%	92%	86%	99%	93%	85%	0%	7%	0%	0%	36%	98%
		Ellipse Consistency Three-ball TDOA SV Pass						Ellipse Consistency Three-ball TDOA SV Pass					
		1	2	3	4	5	6	1	2	3	4	5	6
AOA SV Pass	1	100%	100%	99%	100%	100%	100%	99%	99%	99%	99%	100%	99%
	2	100%	100%	100%	100%	100%	100%	100%	100%	99%	100%	100%	99%
	3	100%	100%	99%	100%	100%	98%	99%	98%	100%	98%	100%	99%
	4	100%	100%	99%	100%	100%	100%	100%	99%	100%	99%	100%	100%
	5	100%	100%	100%	100%	100%	100%	100%	100%	100%	100%	100%	100%
	6	100%	100%	99%	100%	100%	98%	99%	98%	100%	98%	100%	100%

Table 173. Improvement from Fast Trace CI fusion based augmentation of three-ball TDOA SV by AOA SV against Afghanistan target

		Ground Constrained						Non-Ground Constrained					
RMSE													
		Three-ball TDOA SV Pass						Three-ball TDOA SV Pass					
		1	2	3	4	5	6	1	2	3	4	5	6
AOA SV Pass	1	22%	14%	36%	54%	20%	33%	70%	66%	89%	79%	79%	93%
	2	43%	24%	36%	58%	23%	47%	82%	80%	93%	84%	88%	96%
	3	5%	1%	1%	35%	2%	7%	74%	55%	76%	69%	68%	85%
	4	31%	14%	18%	36%	6%	41%	80%	63%	88%	68%	75%	92%
	5	38%	29%	37%	61%	29%	46%	82%	80%	93%	84%	87%	96%
	6	2%	0%	5%	41%	3%	5%	50%	40%	77%	76%	69%	84%
Ave Miss													
		Three-ball TDOA SV Pass						Three-ball TDOA SV Pass					
		1	2	3	4	5	6	1	2	3	4	5	6
AOA SV Pass	1	19%	13%	32%	44%	19%	29%	68%	66%	89%	77%	78%	93%
	2	40%	20%	33%	47%	22%	42%	81%	80%	93%	83%	87%	95%
	3	5%	1%	-1%	25%	3%	6%	73%	54%	75%	68%	67%	84%
	4	28%	11%	15%	25%	7%	34%	78%	63%	87%	66%	74%	92%
	5	36%	28%	34%	51%	26%	39%	80%	79%	93%	82%	86%	95%
	6	3%	0%	3%	30%	3%	5%	50%	40%	76%	74%	66%	84%
Ave SMA													
		Three-ball TDOA SV Pass						Three-ball TDOA SV Pass					
		1	2	3	4	5	6	1	2	3	4	5	6
AOA SV Pass	1	0%	-8%	22%	48%	-3%	14%	70%	64%	89%	79%	79%	92%
	2	27%	8%	18%	56%	-2%	39%	87%	83%	94%	88%	90%	96%
	3	-1%	-1%	-3%	8%	-2%	0%	68%	41%	69%	62%	57%	79%
	4	12%	2%	1%	19%	-9%	22%	76%	58%	86%	68%	75%	91%
	5	26%	3%	28%	65%	9%	38%	86%	83%	94%	88%	90%	96%
	6	-4%	-3%	-2%	12%	-2%	-3%	25%	10%	69%	71%	57%	78%

Table 174. Fast Trace CI fusion consistency for augmentation of three-ball TDOA SV by AOA SV against Afghanistan target

		Ground Constrained						Non-Ground Constrained					
		Ellipsoid Consistency Three-ball TDOA SV Pass						Ellipsoid Consistency Three-ball TDOA SV Pass					
		1	2	3	4	5	6	1	2	3	4	5	6
AOA SV Pass	1	98%	97%	96%	99%	98%	95%	93%	94%	98%	98%	99%	97%
	2	100%	99%	97%	99%	99%	97%	99%	98%	97%	99%	99%	97%
	3	92%	94%	90%	100%	94%	85%	24%	52%	89%	38%	95%	98%
	4	96%	95%	93%	100%	97%	98%	97%	93%	98%	96%	96%	95%
	5	100%	97%	97%	94%	98%	97%	98%	97%	95%	97%	96%	91%
	6	92%	94%	90%	100%	94%	85%	23%	49%	92%	36%	96%	98%
		Ellipse Consistency Three-ball TDOA SV Pass						Ellipse Consistency Three-ball TDOA SV Pass					
		1	2	3	4	5	6	1	2	3	4	5	6
AOA SV Pass	1	100%	100%	100%	100%	100%	100%	100%	100%	99%	100%	99%	99%
	2	100%	100%	100%	100%	100%	100%	100%	99%	99%	100%	99%	99%
	3	100%	100%	99%	100%	100%	100%	100%	100%	100%	100%	100%	99%
	4	100%	100%	100%	100%	100%	100%	100%	100%	100%	100%	100%	100%
	5	100%	100%	100%	100%	100%	100%	100%	100%	100%	100%	100%	100%
	6	100%	100%	99%	100%	100%	100%	100%	100%	100%	100%	100%	100%

Table 175. Improvement from Ellipsoid Intersection fusion based augmentation of three-ball TDOA SV by AOA SV against Afghanistan target

	Ground Constrained						Non-Ground Constrained					
RMSE												
	Three-ball TDOA SV Pass						Three-ball TDOA SV Pass					
AOA SV Pass	1	2	3	4	5	6	1	2	3	4	5	6
1	17%	16%	21%	53%	18%	25%	-9962%	-15017%	-80%	-6067%	-635%	91%
2	36%	11%	28%	49%	21%	49%	-8460%	-12291%	-47%	-5843%	-518%	93%
3	16%	5%	-2%	41%	1%	16%	-4810%	-5799%	-10%	-3604%	-170%	85%
4	37%	18%	-9%	39%	7%	46%	-2295%	-14709%	-146%	-12359%	-925%	90%
5	38%	29%	21%	64%	17%	41%	-4265%	-5073%	42%	-756%	-88%	94%
6	3%	-1%	2%	44%	9%	14%	-7852%	-5799%	54%	13%	-41%	81%
Ave Miss												
	Three-ball TDOA SV Pass						Three-ball TDOA SV Pass					
AOA SV Pass	1	2	3	4	5	6	1	2	3	4	5	6
1	16%	14%	14%	44%	15%	17%	-12173%	-17585%	-115%	-7577%	-794%	90%
2	31%	6%	22%	38%	21%	44%	-10340%	-14395%	-76%	-7299%	-652%	92%
3	12%	2%	-5%	28%	-1%	4%	-5889%	-6801%	-30%	-4511%	-227%	85%
4	33%	13%	-17%	28%	5%	38%	-2821%	-17225%	-194%	-15410%	-1147%	90%
5	36%	27%	14%	56%	14%	33%	-5223%	-5951%	31%	-966%	-129%	94%
6	3%	1%	-5%	32%	6%	7%	-9598%	-6801%	47%	-4%	-70%	81%
Ave SMA												
	Three-ball TDOA SV Pass						Three-ball TDOA SV Pass					
AOA SV Pass	1	2	3	4	5	6	1	2	3	4	5	6
1	29%	18%	47%	60%	25%	40%	72%	68%	89%	86%	82%	92%
2	48%	35%	41%	64%	28%	55%	87%	85%	95%	88%	90%	96%
3	25%	13%	4%	41%	10%	29%	76%	59%	72%	71%	72%	83%
4	40%	27%	30%	43%	9%	50%	84%	67%	87%	71%	77%	91%
5	46%	31%	48%	69%	36%	54%	86%	83%	95%	90%	91%	96%
6	8%	3%	21%	44%	14%	14%	45%	36%	78%	77%	72%	80%

Table 176. Ellipsoid Intersection fusion consistency for augmentation of three-ball TDOA SV by AOA SV against Afghanistan target

		Ground Constrained						Non-Ground Constrained					
		Ellipsoid Consistency Three-ball TDOA SV Pass						Ellipsoid Consistency Three-ball TDOA SV Pass					
		1	2	3	4	5	6	1	2	3	4	5	6
AOA SV Pass	1	84%	83%	68%	91%	84%	71%	0%	0%	0%	0%	0%	2%
	2	91%	81%	66%	86%	84%	88%	0%	0%	0%	0%	0%	4%
	3	84%	81%	71%	87%	85%	69%	0%	0%	0%	0%	0%	16%
	4	94%	85%	53%	93%	85%	90%	0%	0%	0%	0%	0%	6%
	5	89%	86%	62%	93%	77%	88%	0%	0%	0%	0%	0%	22%
	6	85%	83%	73%	91%	90%	80%	0%	0%	0%	0%	0%	11%
		Ellipse Consistency Three-ball TDOA SV Pass						Ellipse Consistency Three-ball TDOA SV Pass					
		1	2	3	4	5	6	1	2	3	4	5	6
AOA SV Pass	1	99%	98%	99%	100%	100%	100%	100%	98%	99%	100%	100%	99%
	2	100%	100%	99%	100%	100%	99%	99%	100%	100%	100%	100%	99%
	3	100%	100%	99%	100%	99%	99%	100%	100%	100%	100%	100%	99%
	4	100%	100%	99%	100%	100%	99%	100%	100%	100%	100%	100%	100%
	5	99%	99%	100%	99%	100%	99%	100%	99%	100%	100%	100%	100%
	6	100%	100%	99%	100%	100%	99%	100%	100%	100%	100%	100%	100%

Table 177. Improvement from Kalman filter fusion based augmentation of three-ball TDOA SV by AOA SV against Afghanistan target

	Ground Constrained						Non-Ground Constrained					
RMSE												
	Three-ball TDOA SV Pass						Three-ball TDOA SV Pass					
AOA SV Pass	1	2	3	4	5	6	1	2	3	4	5	6
1	22%	18%	37%	57%	24%	33%	72%	67%	90%	84%	81%	93%
2	44%	25%	36%	61%	23%	46%	85%	81%	94%	87%	88%	95%
3	19%	6%	-1%	40%	4%	19%	74%	55%	77%	69%	71%	86%
4	36%	22%	23%	36%	10%	45%	83%	67%	89%	68%	76%	92%
5	39%	29%	37%	64%	29%	47%	84%	81%	94%	88%	88%	95%
6	4%	1%	16%	46%	11%	18%	49%	40%	80%	76%	72%	84%
Ave Miss												
	Three-ball TDOA SV Pass						Three-ball TDOA SV Pass					
AOA SV Pass	1	2	3	4	5	6	1	2	3	4	5	6
1	20%	17%	32%	48%	22%	29%	72%	67%	89%	83%	81%	93%
2	40%	21%	32%	51%	23%	42%	84%	80%	93%	86%	87%	95%
3	16%	4%	-2%	28%	4%	11%	73%	54%	76%	67%	69%	86%
4	33%	18%	19%	25%	10%	37%	82%	67%	88%	67%	75%	92%
5	36%	28%	33%	56%	26%	40%	83%	80%	93%	87%	87%	95%
6	6%	3%	11%	34%	9%	11%	49%	40%	79%	74%	69%	84%
Ave SMA												
	Three-ball TDOA SV Pass						Three-ball TDOA SV Pass					
AOA SV Pass	1	2	3	4	5	6	1	2	3	4	5	6
1	29%	18%	47%	60%	25%	40%	73%	68%	89%	86%	82%	92%
2	48%	35%	41%	64%	28%	55%	87%	85%	95%	88%	90%	96%
3	25%	13%	4%	41%	10%	29%	76%	59%	72%	71%	72%	83%
4	40%	27%	30%	43%	9%	50%	84%	67%	87%	71%	77%	91%
5	46%	31%	48%	69%	36%	54%	86%	84%	95%	90%	91%	96%
6	8%	3%	21%	44%	14%	14%	46%	37%	78%	77%	72%	80%

Table 178. Kalman filter fusion consistency for augmentation of three-ball TDOA SV by AOA SV against Afghanistan target

		Ground Constrained						Non-Ground Constrained					
		Ellipsoid Consistency Three-ball TDOA SV Pass						Ellipsoid Consistency Three-ball TDOA SV Pass					
		1	2	3	4	5	6	1	2	3	4	5	6
AOA SV Pass	1	89%	88%	84%	96%	93%	86%	0%	8%	0%	0%	35%	20%
	2	91%	90%	85%	93%	89%	84%	0%	7%	0%	0%	34%	26%
	3	87%	86%	80%	96%	91%	83%	0%	8%	0%	0%	33%	16%
	4	92%	93%	84%	92%	91%	85%	0%	9%	0%	0%	30%	22%
	5	89%	86%	77%	93%	92%	86%	0%	7%	0%	0%	36%	17%
	6	87%	89%	85%	98%	91%	80%	0%	4%	0%	0%	32%	11%
		Ellipse Consistency Three-ball TDOA SV Pass						Ellipse Consistency Three-ball TDOA SV Pass					
		1	2	3	4	5	6	1	2	3	4	5	6
AOA SV Pass	1	99%	98%	99%	100%	100%	100%	100%	98%	99%	100%	100%	99%
	2	100%	100%	99%	100%	100%	99%	99%	100%	100%	100%	100%	99%
	3	100%	100%	99%	100%	99%	99%	100%	100%	100%	100%	100%	99%
	4	100%	100%	99%	100%	100%	99%	100%	100%	100%	100%	100%	100%
	5	99%	99%	100%	99%	100%	99%	100%	99%	100%	100%	100%	100%
	6	100%	100%	99%	100%	100%	99%	100%	100%	100%	100%	100%	100%

2.3.0.28 AOA Satellite Augmenting Three-ball TDOA UAVs Against Afghanistan Target.

The following are the full pass-by-pass fusion results and associated consistencies for each fusion algorithm for the augmentation of a three-ball TDOA AV geolocation agent by an AOA SV geolocation agent against the Afghanistan target.

Table 179. Improvement from Largest Ellipsoid fusion based augmentation of three-ball TDOA AV by AOA SV against Afghanistan target

	Ground Constrained		Non-Ground Constrained	
	RMSE			
	Three-ball TDOA UAV Pass		Three-ball TDOA UAV Pass	
	7		1	
AOA SV Pass	1	87%	1	86%
	2	90%	2	91%
	3	68%	3	67%
	4	82%	4	84%
	5	91%	5	91%
	6	77%	6	68%
	Ave Miss			
	Three-ball TDOA UAV Pass		Three-ball TDOA UAV Pass	
	7		7	
AOA SV Pass	1	81%	1	83%
	2	84%	2	89%
	3	56%	3	61%
	4	73%	4	81%
	5	85%	5	89%
	6	66%	6	63%
	Ave SMA			
	Three-ball TDOA UAV Pass		Three-ball TDOA UAV Pass	
	7		7	
AOA SV Pass	1	86%	1	91%
	2	89%	2	90%
	3	61%	3	60%
	4	78%	4	91%
	5	92%	5	90%
	6	59%	6	50%

Table 180. Largest Ellipsoid fusion consistency for augmentation of three-ball TDOA AV by AOA SV against Afghanistan target

		Ground Constrained	Non-Ground Constrained
		Ellipsoid Consistency Three-ball TDOA UAV Pass 7	Ellipsoid Consistency Three-ball TDOA UAV Pass 7
AOA SV Pass	1	85%	97%
	2	83%	96%
	3	84%	96%
	4	62%	95%
	5	88%	91%
	6	85%	98%
		Ellipse Consistency Three-ball TDOA UAV Pass 7	Ellipse Consistency Three-ball TDOA UAV Pass 7
AOA SV Pass	1	92%	86%
	2	95%	99%
	3	99%	100%
	4	69%	77%
	5	100%	94%
	6	100%	100%

Table 181. Improvement from Fast Determinant CI fusion based augmentation of three-ball TDOA AV by AOA SV against Afghanistan target

	Ground Constrained	Non-Ground Constrained
	RMSE	
	Three-ball TDOA UAV Pass	Three-ball TDOA UAV Pass
	7	7
AOA SV Pass 1	87%	85%
AOA SV Pass 2	90%	90%
AOA SV Pass 3	59%	65%
AOA SV Pass 4	81%	82%
AOA SV Pass 5	90%	90%
AOA SV Pass 6	66%	67%
	Ave Miss	
	Three-ball TDOA UAV Pass	Three-ball TDOA UAV Pass
	7	7
AOA SV Pass 1	80%	81%
AOA SV Pass 2	84%	88%
AOA SV Pass 3	46%	60%
AOA SV Pass 4	72%	79%
AOA SV Pass 5	85%	88%
AOA SV Pass 6	58%	60%
	Ave SMA	
	Three-ball TDOA UAV Pass	Three-ball TDOA UAV Pass
	7	7
AOA SV Pass 1	86%	82%
AOA SV Pass 2	89%	90%
AOA SV Pass 3	50%	50%
AOA SV Pass 4	78%	79%
AOA SV Pass 5	92%	90%
AOA SV Pass 6	58%	50%

Table 182. Fast Determinant CI fusion consistency for augmentation of three-ball TDOA AV by AOA SV against Afghanistan target

		Ground Constrained	Non-Ground Constrained
		Ellipsoid Consistency Three-ball TDOA UAV Pass 7	Ellipsoid Consistency Three-ball TDOA UAV Pass 7
AOA SV Pass	1	89%	97%
	2	89%	96%
	3	86%	98%
	4	91%	95%
	5	89%	91%
	6	87%	100%
		Ellipse Consistency Three-ball TDOA UAV Pass 7	Ellipse Consistency Three-ball TDOA UAV Pass 7
AOA SV Pass	1	100%	99%
	2	99%	99%
	3	97%	99%
	4	99%	100%
	5	97%	100%
	6	100%	100%

Table 183. Improvement from Fast Trace CI fusion based augmentation of three-ball TDOA AV by AOA SV against Afghanistan target

	Ground Constrained	Non-Ground Constrained
	RMSE	
	Three-ball TDOA UAV Pass	Three-ball TDOA UAV Pass
	7	7
AOA SV Pass 1	87%	85%
AOA SV Pass 2	90%	90%
AOA SV Pass 3	66%	68%
AOA SV Pass 4	81%	83%
AOA SV Pass 5	90%	90%
AOA SV Pass 6	72%	69%
	Ave Miss	
	Three-ball TDOA UAV Pass	Three-ball TDOA UAV Pass
	7	7
AOA SV Pass 1	80%	82%
AOA SV Pass 2	84%	88%
AOA SV Pass 3	52%	62%
AOA SV Pass 4	72%	79%
AOA SV Pass 5	85%	88%
AOA SV Pass 6	63%	63%
	Ave SMA	
	Three-ball TDOA UAV Pass	Three-ball TDOA UAV Pass
	7	7
AOA SV Pass 1	86%	82%
AOA SV Pass 2	89%	90%
AOA SV Pass 3	52%	50%
AOA SV Pass 4	78%	78%
AOA SV Pass 5	92%	90%
AOA SV Pass 6	61%	51%

Table 184. Fast Trace CI fusion consistency for augmentation of three-ball TDOA AV by AOA SV against Afghanistan target

		Ground Constrained	Non-Ground Constrained
		Ellipsoid Consistency Three-ball TDOA UAV Pass 7	Ellipsoid Consistency Three-ball TDOA UAV Pass 7
AOA SV Pass	1	90%	98%
	2	89%	97%
	3	91%	98%
	4	92%	96%
	5	89%	91%
	6	94%	99%
		Ellipse Consistency Three-ball TDOA UAV Pass 7	Ellipse Consistency Three-ball TDOA UAV Pass 7
AOA SV Pass	1	100%	99%
	2	99%	99%
	3	99%	100%
	4	100%	100%
	5	97%	100%
	6	100%	100%

Table 185. Improvement from Ellipsoid Intersection fusion based augmentation of three-ball TDOA AV by AOA SV against Afghanistan target

	Ground Constrained	Non-Ground Constrained
	RMSE	
	Three-ball TDOA UAV Pass	Three-ball TDOA UAV Pass
	1	7
AOA SV Pass 1	87%	86%
AOA SV Pass 2	90%	91%
AOA SV Pass 3	68%	67%
AOA SV Pass 4	82%	84%
AOA SV Pass 5	91%	91%
AOA SV Pass 6	76%	68%
	Ave Miss	
	Three-ball TDOA UAV Pass	Three-ball TDOA UAV Pass
	7	7
AOA SV Pass 1	81%	83%
AOA SV Pass 2	84%	89%
AOA SV Pass 3	56%	62%
AOA SV Pass 4	72%	81%
AOA SV Pass 5	85%	89%
AOA SV Pass 6	65%	63%
	Ave SMA	
	Three-ball TDOA UAV Pass	Three-ball TDOA UAV Pass
	7	7
AOA SV Pass 1	87%	84%
AOA SV Pass 2	90%	91%
AOA SV Pass 3	65%	61%
AOA SV Pass 4	80%	81%
AOA SV Pass 5	92%	91%
AOA SV Pass 6	73%	67%

Table 186. Ellipsoid Intersection fusion consistency for augmentation of three-ball TDOA AV by AOA SV against Afghanistan target

		Ground Constrained	Non-Ground Constrained
		Ellipsoid Consistency Three-ball TDOA UAV Pass 7	Ellipsoid Consistency Three-ball TDOA UAV Pass 7
AOA SV Pass	1	81%	95%
	2	83%	96%
	3	77%	96%
	4	89%	96%
	5	85%	93%
	6	81%	94%
		Ellipse Consistency Three-ball TDOA UAV Pass 1	Ellipse Consistency Three-ball TDOA UAV Pass 1
AOA SV Pass	1	100%	99%
	2	99%	100%
	3	99%	99%
	4	99%	100%
	5	98%	100%
	6	100%	100%

Table 187. Improvement from Kalman filter fusion based augmentation of three-ball TDOA AV by AOA SV against Afghanistan target

	Ground Constrained		Non-Ground Constrained	
	RMSE			
	Three-ball TDOA UAV Pass		Three-ball TDOA UAV Pass	
	7		7	
AOA SV Pass 1	87%		86%	
AOA SV Pass 2	90%		91%	
AOA SV Pass 3	68%		67%	
AOA SV Pass 4	82%		84%	
AOA SV Pass 5	91%		91%	
AOA SV Pass 6	77%		68%	
	Ave Miss			
	Three-ball TDOA UAV Pass		Three-ball TDOA UAV Pass	
	7		7	
AOA SV Pass 1	81%		83%	
AOA SV Pass 2	84%		89%	
AOA SV Pass 3	56%		61%	
AOA SV Pass 4	73%		81%	
AOA SV Pass 5	85%		89%	
AOA SV Pass 6	66%		63%	
	Ave SMA			
	Three-ball TDOA UAV Pass		Three-ball TDOA UAV Pass	
	7		7	
AOA SV Pass 1	87%		84%	
AOA SV Pass 2	90%		91%	
AOA SV Pass 3	65%		61%	
AOA SV Pass 4	80%		81%	
AOA SV Pass 5	92%		91%	
AOA SV Pass 6	73%		67%	

Table 188. Kalman filter fusion consistency for augmentation of three-ball TDOA AV by AOA SV against Afghanistan target

		Ground Constrained	Non-Ground Constrained
		Ellipsoid Consistency Three-ball TDOA UAV Pass 7	Ellipsoid Consistency Three-ball TDOA UAV Pass 7
AOA SV Pass	1	81%	95%
	2	82%	95%
	3	79%	96%
	4	88%	95%
	5	85%	93%
	6	84%	94%
		Ellipse Consistency Three-ball TDOA UAV Pass 7	Ellipse Consistency Three-ball TDOA UAV Pass 7
AOA SV Pass	1	100%	99%
	2	99%	100%
	3	99%	99%
	4	99%	100%
	5	98%	100%
	6	100%	100%

2.3.0.29 AOA Satellite Augmenting Four-ball TDOA Satellites Against Afghanistan Target.

The following are the full pass-by-pass fusion results and associated consistencies for each fusion algorithm for the augmentation of a four-ball TDOA SV geolocation agent by an AOA SV geolocation agent against the Afghanistan target.

Table 189. Improvement from Largest Ellipsoid fusion based augmentation of four-ball TDOA SV by AOA SV against Afghanistan target

	Ground Constrained						Non-Ground Constrained					
RMSE												
	Four-ball TDOA SV Pass						Four-ball TDOA SV Pass					
AOA SV Pass	1	2	3	4	5	6	1	2	3	4	5	6
1	98%	99%	100%	98%	99%	96%	98%	99%	99%	98%	99%	95%
2	99%	99%	100%	98%	100%	97%	99%	99%	100%	98%	99%	97%
3	98%	98%	99%	96%	99%	95%	98%	98%	98%	97%	98%	87%
4	98%	99%	99%	97%	99%	97%	99%	99%	99%	97%	99%	94%
5	99%	99%	100%	98%	100%	97%	99%	99%	100%	99%	99%	97%
6	96%	97%	99%	97%	99%	94%	95%	97%	98%	97%	98%	85%
Ave Miss												
	Four-ball TDOA SV Pass						Four-ball TDOA SV Pass					
AOA SV Pass	1	2	3	4	5	6	1	2	3	4	5	6
1	98%	99%	100%	98%	99%	96%	98%	99%	99%	98%	99%	95%
2	99%	99%	100%	98%	100%	97%	99%	99%	100%	98%	99%	97%
3	97%	98%	99%	96%	99%	95%	98%	98%	98%	96%	98%	87%
4	98%	99%	99%	96%	99%	97%	98%	99%	99%	96%	99%	94%
5	99%	99%	100%	98%	100%	97%	98%	99%	100%	98%	99%	97%
6	96%	97%	99%	96%	99%	93%	95%	97%	98%	97%	98%	86%
Ave SMA												
	Four-ball TDOA SV Pass						Four-ball TDOA SV Pass					
AOA SV Pass	1	2	3	4	5	6	1	2	3	4	5	6
1	99%	99%	100%	98%	99%	98%	98%	99%	99%	98%	99%	97%
2	99%	99%	100%	99%	99%	98%	99%	99%	100%	99%	99%	97%
3	98%	98%	99%	97%	99%	96%	95%	97%	98%	97%	96%	83%
4	98%	98%	100%	98%	99%	97%	98%	99%	99%	98%	98%	97%
5	99%	99%	100%	99%	99%	98%	99%	99%	100%	99%	99%	97%
6	98%	99%	99%	95%	98%	95%	98%	98%	98%	95%	96%	85%

Table 190. Largest Ellipsoid fusion consistency for augmentation of four-ball TDOA SV by AOA SV against Afghanistan target

		Ground Constrained						Non-Ground Constrained					
		Ellipsoid Consistency Four-ball TDOA SV Pass						Ellipsoid Consistency Four-ball TDOA SV Pass					
		1	2	3	4	5	6	1	2	3	4	5	6
AOA SV Pass	1	77%	91%	86%	87%	77%	83%	79%	76%	81%	96%	79%	81%
	2	93%	92%	87%	90%	88%	89%	98%	96%	94%	94%	94%	95%
	3	88%	84%	88%	92%	76%	92%	97%	81%	57%	91%	58%	60%
	4	84%	91%	62%	69%	65%	91%	97%	76%	71%	66%	70%	70%
	5	88%	89%	92%	91%	89%	90%	89%	87%	86%	95%	87%	91%
	6	77%	75%	92%	94%	83%	93%	60%	52%	53%	97%	54%	51%
		Ellipse Consistency Four-ball TDOA SV Pass						Ellipse Consistency Four-ball TDOA SV Pass					
		1	2	3	4	5	6	1	2	3	4	5	6
AOA SV Pass	1	89%	95%	100%	95%	95%	99%	81%	80%	82%	97%	80%	87%
	2	98%	99%	100%	95%	99%	99%	100%	100%	99%	100%	99%	100%
	3	96%	99%	100%	97%	87%	96%	99%	99%	99%	100%	99%	98%
	4	88%	96%	100%	71%	82%	98%	97%	79%	71%	69%	71%	100%
	5	100%	100%	100%	100%	98%	97%	99%	93%	93%	100%	93%	95%
	6	97%	98%	98%	97%	93%	97%	100%	100%	100%	100%	100%	95%

Table 191. Improvement from Fast Determinant CI fusion based augmentation of four-ball TDOA SV by AOA SV against Afghanistan target

	Ground Constrained						Non-Ground Constrained					
RMSE												
	Four-ball TDOA SV Pass						Four-ball TDOA SV Pass					
AOA SV Pass	1	2	3	4	5	6	1	2	3	4	5	6
1	98%	99%	99%	98%	99%	96%	98%	99%	99%	97%	99%	94%
2	99%	99%	100%	98%	100%	97%	99%	99%	100%	98%	99%	96%
3	94%	97%	98%	93%	98%	95%	98%	97%	98%	96%	98%	85%
4	97%	98%	99%	97%	99%	94%	98%	99%	99%	97%	99%	93%
5	99%	99%	100%	98%	100%	97%	98%	99%	100%	98%	99%	96%
6	95%	97%	98%	94%	98%	94%	95%	97%	98%	97%	98%	85%
Ave Miss												
	Four-ball TDOA SV Pass						Four-ball TDOA SV Pass					
AOA SV Pass	1	2	3	4	5	6	1	2	3	4	5	6
1	98%	99%	99%	97%	99%	95%	97%	99%	99%	97%	99%	94%
2	98%	99%	100%	98%	100%	96%	98%	99%	100%	98%	99%	96%
3	94%	97%	98%	93%	98%	95%	98%	97%	98%	96%	98%	85%
4	97%	98%	99%	96%	99%	94%	97%	99%	99%	96%	99%	93%
5	98%	99%	100%	98%	100%	96%	98%	99%	100%	98%	99%	96%
6	95%	97%	99%	94%	99%	93%	95%	97%	98%	97%	98%	85%
Ave SMA												
	Four-ball TDOA SV Pass						Four-ball TDOA SV Pass					
AOA SV Pass	1	2	3	4	5	6	1	2	3	4	5	6
1	99%	99%	99%	98%	99%	96%	98%	99%	99%	98%	99%	94%
2	99%	99%	100%	99%	99%	97%	99%	99%	100%	99%	99%	97%
3	95%	96%	98%	93%	97%	95%	98%	97%	98%	96%	96%	83%
4	98%	98%	99%	97%	99%	95%	98%	99%	99%	97%	98%	93%
5	99%	99%	100%	99%	99%	98%	99%	99%	100%	99%	99%	97%
6	95%	97%	98%	94%	97%	93%	94%	97%	98%	98%	96%	82%

Table 192. Fast Determinant CI fusion consistency for augmentation of four-ball TDOA SV by AOA SV against Afghanistan target

		Ground Constrained						Non-Ground Constrained					
		Ellipsoid Consistency Four-ball TDOA SV Pass						Ellipsoid Consistency Four-ball TDOA SV Pass					
		1	2	3	4	5	6	1	2	3	4	5	6
AOA SV Pass	1	89%	89%	89%	89%	89%	90%	97%	97%	97%	97%	97%	97%
	2	89%	89%	89%	89%	89%	89%	96%	96%	96%	96%	96%	96%
	3	85%	85%	85%	85%	85%	97%	98%	96%	96%	97%	96%	96%
	4	91%	91%	91%	91%	91%	93%	95%	95%	95%	95%	95%	95%
	5	89%	89%	89%	89%	89%	89%	91%	91%	91%	91%	91%	91%
	6	87%	87%	87%	87%	87%	99%	99%	98%	98%	99%	98%	98%
		Ellipse Consistency Four-ball TDOA SV Pass						Ellipse Consistency Four-ball TDOA SV Pass					
		1	2	3	4	5	6	1	2	3	4	5	6
AOA SV Pass	1	100%	100%	100%	100%	100%	100%	99%	99%	99%	99%	99%	99%
	2	99%	99%	99%	99%	99%	99%	99%	99%	99%	99%	99%	99%
	3	97%	97%	97%	97%	97%	100%	100%	99%	99%	100%	99%	99%
	4	99%	99%	99%	99%	99%	100%	100%	100%	100%	100%	100%	100%
	5	97%	97%	97%	97%	97%	97%	100%	100%	100%	100%	100%	100%
	6	100%	100%	100%	100%	100%	100%	100%	100%	100%	100%	100%	100%

Table 193. Improvement from Fast Trace CI fusion based augmentation of four-ball TDOA SV by AOA SV against Afghanistan target

	Ground Constrained						Non-Ground Constrained					
RMSE												
	Four-ball TDOA SV Pass						Four-ball TDOA SV Pass					
AOA SV Pass	1	2	3	4	5	6	1	2	3	4	5	6
1	98%	99%	99%	98%	99%	96%	98%	99%	99%	97%	99%	94%
2	99%	99%	100%	98%	100%	97%	99%	99%	100%	98%	99%	96%
3	95%	97%	98%	93%	98%	95%	98%	97%	98%	96%	98%	85%
4	97%	98%	99%	97%	99%	94%	98%	99%	99%	97%	99%	93%
5	99%	99%	100%	98%	100%	97%	98%	99%	100%	98%	99%	96%
6	95%	97%	98%	94%	98%	93%	95%	97%	98%	97%	98%	85%
Ave Miss												
	Four-ball TDOA SV Pass						Four-ball TDOA SV Pass					
AOA SV Pass	1	2	3	4	5	6	1	2	3	4	5	6
1	98%	99%	99%	97%	99%	95%	97%	99%	99%	97%	99%	94%
2	98%	99%	100%	98%	100%	96%	98%	99%	100%	98%	99%	96%
3	94%	97%	98%	93%	98%	95%	97%	97%	98%	95%	98%	86%
4	97%	98%	99%	96%	99%	94%	97%	99%	99%	96%	99%	93%
5	98%	99%	100%	98%	100%	96%	98%	99%	100%	98%	99%	96%
6	95%	97%	99%	94%	99%	93%	94%	97%	98%	96%	98%	85%
Ave SMA												
	Four-ball TDOA SV Pass						Four-ball TDOA SV Pass					
AOA SV Pass	1	2	3	4	5	6	1	2	3	4	5	6
1	99%	99%	99%	98%	99%	96%	98%	99%	99%	98%	99%	94%
2	99%	99%	100%	99%	99%	97%	99%	99%	100%	99%	99%	97%
3	95%	96%	98%	93%	97%	96%	97%	97%	98%	95%	96%	83%
4	98%	98%	99%	97%	99%	95%	98%	99%	99%	97%	98%	93%
5	99%	99%	100%	99%	99%	98%	99%	99%	100%	99%	99%	97%
6	95%	97%	98%	94%	97%	93%	94%	97%	98%	96%	96%	82%

Table 194. Fast Trace CI fusion consistency for augmentation of four-ball TDOA SV by AOA SV against Afghanistan target

		Ground Constrained						Non-Ground Constrained					
		Ellipsoid Consistency Four-ball TDOA SV Pass						Ellipsoid Consistency Four-ball TDOA SV Pass					
		1	2	3	4	5	6	1	2	3	4	5	6
AOA SV Pass	1	89%	89%	89%	89%	89%	90%	97%	97%	97%	98%	97%	97%
	2	89%	89%	89%	89%	89%	89%	96%	96%	96%	96%	96%	96%
	3	86%	85%	85%	85%	85%	94%	98%	96%	96%	97%	96%	96%
	4	91%	91%	91%	91%	91%	93%	95%	95%	95%	95%	95%	95%
	5	89%	89%	89%	89%	89%	89%	91%	91%	91%	91%	91%	91%
	6	87%	87%	87%	87%	87%	93%	99%	98%	98%	99%	98%	98%
		Ellipse Consistency Four-ball TDOA SV Pass						Ellipse Consistency Four-ball TDOA SV Pass					
		1	2	3	4	5	6	1	2	3	4	5	6
AOA SV Pass	1	100%	100%	100%	100%	100%	100%	99%	99%	99%	99%	99%	99%
	2	99%	99%	99%	99%	99%	99%	99%	99%	99%	99%	99%	99%
	3	97%	97%	97%	97%	97%	100%	99%	99%	99%	100%	99%	99%
	4	99%	99%	99%	99%	99%	100%	100%	100%	100%	100%	100%	100%
	5	97%	97%	97%	97%	97%	97%	100%	100%	100%	100%	100%	100%
	6	100%	100%	100%	100%	100%	100%	100%	100%	100%	100%	100%	100%

Table 195. Improvement from Ellipsoid Intersection fusion based augmentation of four-ball TDOA SV by AOA SV against Afghanistan target

	Ground Constrained						Non-Ground Constrained					
RMSE												
	Four-ball TDOA SV Pass						Four-ball TDOA SV Pass					
AOA SV Pass	1	2	3	4	5	6	1	2	3	4	5	6
1	98%	99%	99%	98%	99%	94%	89%	99%	99%	97%	99%	95%
2	99%	99%	99%	98%	99%	84%	91%	99%	100%	95%	99%	97%
3	98%	98%	99%	96%	99%	89%	94%	98%	98%	95%	98%	87%
4	98%	99%	99%	97%	99%	81%	97%	99%	99%	96%	99%	94%
5	99%	99%	99%	98%	100%	90%	98%	99%	100%	94%	99%	97%
6	96%	97%	99%	97%	99%	93%	93%	97%	98%	95%	98%	85%
Ave Miss												
	Four-ball TDOA SV Pass						Four-ball TDOA SV Pass					
AOA SV Pass	1	2	3	4	5	6	1	2	3	4	5	6
1	98%	99%	99%	98%	99%	92%	86%	99%	99%	97%	99%	95%
2	98%	99%	99%	98%	99%	81%	89%	99%	100%	94%	99%	96%
3	97%	98%	99%	96%	99%	87%	92%	98%	98%	94%	98%	87%
4	98%	99%	98%	96%	99%	77%	96%	99%	99%	96%	99%	94%
5	99%	99%	99%	98%	100%	88%	98%	99%	100%	92%	99%	97%
6	96%	97%	99%	96%	99%	93%	91%	97%	98%	95%	98%	86%
Ave SMA												
	Four-ball TDOA SV Pass						Four-ball TDOA SV Pass					
AOA SV Pass	1	2	3	4	5	6	1	2	3	4	5	6
1	99%	99%	100%	98%	99%	96%	98%	99%	99%	99%	99%	94%
2	99%	99%	100%	99%	99%	98%	99%	99%	100%	99%	99%	97%
3	98%	98%	99%	97%	99%	96%	98%	98%	98%	97%	96%	84%
4	99%	99%	99%	97%	99%	97%	99%	99%	99%	97%	98%	93%
5	99%	99%	100%	99%	99%	98%	99%	99%	100%	99%	99%	97%
6	96%	98%	99%	98%	99%	94%	95%	97%	98%	98%	96%	83%

Table 196. Ellipsoid Intersection fusion consistency for augmentation of four-ball TDOA SV by AOA SV against Afghanistan target

		Ground Constrained						Non-Ground Constrained					
		Ellipsoid Consistency Four-ball TDOA SV Pass						Ellipsoid Consistency Four-ball TDOA SV Pass					
		1	2	3	4	5	6	1	2	3	4	5	6
AOA SV Pass	1	85%	87%	17%	91%	92%	7%	0%	97%	97%	60%	97%	96%
	2	91%	88%	0%	93%	82%	0%	0%	96%	96%	1%	96%	93%
	3	88%	80%	75%	92%	76%	25%	8%	96%	96%	42%	95%	97%
	4	88%	90%	16%	93%	91%	0%	36%	96%	95%	85%	95%	94%
	5	89%	88%	1%	91%	95%	0%	68%	92%	91%	0%	91%	95%
	6	87%	81%	96%	91%	84%	97%	15%	96%	97%	57%	98%	93%
		Ellipse Consistency Four-ball TDOA SV Pass						Ellipse Consistency Four-ball TDOA SV Pass					
		1	2	3	4	5	6	1	2	3	4	5	6
AOA SV Pass	1	98%	100%	99%	98%	98%	98%	99%	99%	99%	100%	99%	99%
	2	97%	100%	99%	97%	93%	99%	99%	99%	99%	100%	99%	99%
	3	95%	99%	100%	97%	87%	96%	99%	98%	99%	100%	99%	98%
	4	98%	100%	99%	100%	97%	99%	100%	100%	100%	99%	100%	100%
	5	98%	100%	100%	98%	96%	97%	99%	100%	100%	100%	100%	100%
	6	96%	96%	98%	97%	93%	96%	100%	99%	100%	100%	100%	94%

Table 197. Improvement from Kalman filter fusion based augmentation of four-ball TDOA SV by AOA SV against Afghanistan target

	Ground Constrained						Non-Ground Constrained					
RMSE												
	Four-ball TDOA SV Pass						Four-ball TDOA SV Pass					
AOA SV Pass	1	2	3	4	5	6	1	2	3	4	5	6
1	98%	99%	100%	98%	99%	96%	98%	99%	99%	98%	99%	95%
2	99%	99%	100%	98%	100%	97%	99%	99%	100%	98%	99%	97%
3	98%	98%	99%	96%	99%	95%	98%	98%	98%	97%	98%	87%
4	98%	99%	99%	97%	99%	97%	99%	99%	99%	97%	99%	94%
5	99%	99%	100%	98%	100%	97%	99%	99%	100%	99%	99%	97%
6	96%	97%	99%	97%	99%	94%	95%	97%	98%	97%	98%	85%
Ave Miss												
	Four-ball TDOA SV Pass						Four-ball TDOA SV Pass					
AOA SV Pass	1	2	3	4	5	6	1	2	3	4	5	6
1	98%	99%	100%	98%	99%	96%	98%	99%	99%	98%	99%	95%
2	99%	99%	100%	98%	100%	97%	99%	99%	100%	98%	99%	97%
3	97%	98%	99%	96%	99%	95%	98%	98%	98%	96%	98%	87%
4	98%	99%	99%	96%	99%	97%	98%	99%	99%	96%	99%	94%
5	99%	99%	100%	98%	100%	97%	98%	99%	100%	98%	99%	97%
6	96%	97%	99%	96%	99%	93%	95%	97%	98%	97%	98%	86%
Ave SMA												
	Four-ball TDOA SV Pass						Four-ball TDOA SV Pass					
AOA SV Pass	1	2	3	4	5	6	1	2	3	4	5	6
1	99%	99%	100%	98%	99%	96%	98%	99%	99%	99%	99%	94%
2	99%	99%	100%	99%	99%	98%	99%	99%	100%	99%	99%	97%
3	98%	98%	99%	97%	99%	96%	98%	98%	98%	97%	96%	84%
4	99%	99%	99%	97%	99%	97%	99%	99%	99%	97%	98%	93%
5	99%	99%	100%	99%	99%	98%	99%	99%	100%	99%	99%	97%
6	96%	98%	99%	98%	99%	94%	95%	97%	98%	98%	96%	83%

Table 198. Kalman filter fusion consistency for augmentation of four-ball TDOA SV by AOA SV against Afghanistan target

		Ground Constrained						Non-Ground Constrained					
		Ellipsoid Consistency Four-ball TDOA SV Pass						Ellipsoid Consistency Four-ball TDOA SV Pass					
		1	2	3	4	5	6	1	2	3	4	5	6
AOA SV Pass	1	85%	85%	90%	90%	83%	88%	94%	97%	97%	96%	97%	96%
	2	88%	88%	90%	91%	86%	87%	96%	96%	96%	95%	96%	95%
	3	86%	79%	88%	92%	71%	87%	93%	96%	96%	96%	95%	97%
	4	90%	89%	92%	92%	91%	90%	96%	96%	95%	95%	95%	95%
	5	86%	88%	92%	89%	88%	89%	94%	92%	91%	92%	91%	95%
	6	87%	81%	89%	91%	82%	89%	98%	96%	97%	92%	98%	94%
		Ellipse Consistency Four-ball TDOA SV Pass						Ellipse Consistency Four-ball TDOA SV Pass					
		1	2	3	4	5	6	1	2	3	4	5	6
AOA SV Pass	1	98%	100%	99%	98%	98%	98%	99%	99%	99%	100%	99%	99%
	2	97%	100%	99%	97%	93%	99%	99%	99%	99%	100%	99%	99%
	3	95%	99%	100%	97%	87%	96%	99%	98%	99%	100%	99%	98%
	4	98%	100%	99%	100%	97%	99%	100%	100%	100%	99%	100%	100%
	5	98%	100%	100%	98%	96%	97%	99%	100%	100%	100%	100%	100%
	6	96%	96%	98%	97%	93%	96%	100%	99%	100%	100%	100%	94%

Bibliography

1. Mathews, C. P. and Zoltowski, M. D., "Eigenstructure techniques for 2-D angle estimation with uniform circular arrays," *Signal Processing, IEEE Transactions on*, Vol. 42, No. 9, 1994, pp. 2395–2407.

2. Oispuu, M. and Schikora, M., "Multiple emitter localization using a realistic airborne array sensor," *Information Fusion (FUSION), 2011 Proceedings of the 14th International Conference on*, 2011, pp. 1–8.

3. Hartzell, S., "Non-Linear Optimization Applied to Angle-of-Arrival Satellite-Based Geolocation," MS thesis, AFIT-ENG-T-14-J-7, Air Force Institute of Technology, Wright-Patterson AFB OH, June 2014 (ADA602553).

4. National Geospatial-Intelligence Agency, Office of Geomatics, *NGA/-NASA EGM96, N=M=360 Earth Gravitational Model*, 2014, [`http://earth-info.nga.mil/GandG/wgs84/gravitymod/egm96/egm96.html`. Accessed:12/10/2014.].

5. Lemoin, F. G. and Pavlis, N., *EGM 96: The NASA and NIMA Joint Geopotential Model*, NASA, 2004, [`http://cddis.gsfc.nasa.gov/926/egm96/egm96.html`. Accessed:12/10/2014.].

6. Sijs, J. and Lazar, M., "State fusion with unknown correlation: Ellipsoidal intersection," *Automatica*, Vol. 48, No. 8, 8 2012, pp. 1874–1878.

7. Bailey, E., Burns, A., Dinh, D., Jewell, B., Kelly, S., LaSarge, J., Schmidt, N., and Dyne, D. V., "Anubis ASYS 631 Final Report," Tech. rep., Air Force Institute of Technology, 2014.

8. National Imagery and Mapping Agency, *PERFORMANCE SPECIFICATION DIGITAL TERRAIN ELEVATION DATA (DTED)*, MIL-PRF-89020B. Washington: GPO, 23 May 2000.

9. "MC-12W Liberty," [http://www.globalsecurity.org/intell/systems/mc-12-liberty-specs.htm. Accessed: 12/29/14].

10. *ScanEagle*, Product Brochure. Bingen WA: Insitu, 2012.

11. "MQ-1B Predator," U.S. Air Force Fact Sheet, 20 July 2010, [http://www.af.mil/AboutUs/FactSheets/Display/tabid/224/Article/104469/mq-1b-predator.aspx. Accessed: 12/29/14].

12. "MC-12," U.S. Air Force Fact Sheet, 5 August 2009, [http://www.af.mil/AboutUs/FactSheets/Display/tabid/224/Article/104497/mc-12.aspx. Accessed: 12/29/14].

13. Stansfield, R. G., "Statistical theory of d.f. fixing," *Electrical Engineers - Part IIIA: Radiocommunication, Journal of the Institution of*, Vol. 94, No. 15, 1947, pp. 762–770.

14. Musicki, D. and Koch, W., "Geolocation using TDOA and FDOA measurements," *Information Fusion, 2008 11th International Conference on*, 2008, pp. 1–8.

15. Adib, N. and Douglas, S. C., "Root-MSE geolocation performance using angle-of-arrival measurements," *Signals, Systems and Computers, 2013 Asilomar Conference on*, 2013, pp. 476–480.

16. Hale, K. N., *Expanding the Use of Time/Frequency Difference of Arrival Geolocaiton in the Department of Defense*, PhD dissertation. Pardee RAND Graduate School, 2012.

17. Isherwood, M., "Layering ISR Forces," Tech. rep., Mitchell Institute for Airpower Studies, 2011.

18. Isherwood, M., *Layered ISR: USAF Investment for the Joint Team*, Mitchell Institute for Airpower Studies, [`https://secure.afa.org/Mitchell/Presentations/011712_MP8_ISR_slides.pdf`. Accessed: 01/01/2015.].

19. Ho, K. C., Lu, X., and Kovavisaruch, L., "Source Localization Using TDOA and FDOA Measurements in the Presence of Receiver Location Errors: Analysis and Solution," *Signal Processing, IEEE Transactions on*, Vol. 55, No. 2, 2007, pp. 684–696.

20. Loomis, H. H., "Geolocation of Electromagnetic Emitters," MS thesis, Naval Postgraduate School, Monterey CA, September 1997 (ADA640492997).

21. Mikhalev, A. and Ormondroyd, R., "Passive emitter geolocation using agent-based data fusion of AOA, TDOA and FDOA measurements," *Information Fusion, 2007 10th International Conference on*, 2007, pp. 1–6.

22. Okello, N. and Musicki, D., "Emitter Geolocation with Two UAVs," *Information, Decision and Control, 2007. IDC '07*, 2007, pp. 254–259.

23. Marsh, L., Gossink, D., Drake, S. P., and Calbert, G., "UAV Team Formation for Emitter Geolocation," *Information, Decision and Control, 2007. IDC '07*, 2007, pp. 176–181.

24. National Reconnaissance Office, *The National Reconnaissance Office Innovation Campaign: The CubeSat Program*, 2014, [`http://www.nro.gov/about/innovation/2013-05.pdf`. Accessed:12/19/2014.].

25. "SAMSON Summary," [`http://samson.technion.ac.il`. Accessed:12/19/2014.].

26. Bailey, E., Burns, A., Dinh, D., Jewll, B., Kelly, S., LaSarge, J., Schmidt, N., and Dyne, D. V., "Anubis ASYS 632 Final Report," Tech. rep., Air Force Institute of Technology, 2014.

27. Basel, J., Basel, J., BuPane, E., DiGiacomo, W. J., Kester, B., Schaffer, M., Thompson, J., and Small, A., "Geoloco ASYS 631 Final Report," Tech. rep., Air Force Institute of Technology, 2013.

28. Baston, L., Birge, C., Claybrook, J., Le, K., Moore, B., Montgomery, J., Nastasi, K., and Shepherd, J., "Team BLKJ3CK ASYS 631 Final Report," Tech. rep., Air Force Institute of Technology, 2013.

29. Buckle, L., Bull, K., Couch, C., Jenson, D., Lesko, J., Moomey, D., Penn, D., Salvador, V., and Udell, H., "LOTIS CubeSat Satellite Design," Tech. rep., Air Force Institute of Technology, 2014.

30. Dalton, K., Eken, M., McAnally, T., O'Sullivan, D., Pena, A., Red, J., Rosander, T., Sutherlin, K., and Thomas, M., "G-Cubed ASYS 631: Spacecraft Systems Engineering," Tech. rep., Air Force Institute of Technology, 2014.

31. DiGiacomo, W. J., "Feasibility Assessment of Repurposing an Aerial Radio Frequency Geolocation Sensor to the Space Environment," 2014, MS thesis, AFIT-ENY-14-M-16, Air Force Institute of Technology, Wright-Patterson AFB OH, March 2014 (AD).

32. Basel, J. P., "Analysis of Geolocation Approaches Using Satellites," MS thesis, AFIT-ENY-14-M-07, Air Force Institute of Technology, Wright-Patterson AFB OH, March 2014 (ADA598324).

33. Small, A., "Radio Frequency Emitter Geolocation Using Cubesats," MS thesis,

AFIT-ENG-14-M-68, Air Force Institute of Technology, Wright-Patterson AFB OH, March 2014 (ADA610719).

34. Benaskeur, A. R., "Consistent fusion of correlated data sources," *IECON 02 [Industrial Electronics Society, IEEE 2002 28th Annual Conference of the]*, Vol. 4, 2002, pp. 2652–2656 vol.4.

35. Chen, L., Arambel, P. O., and Mehra, R. K., "Estimation under unknown correlation: covariance intersection revisited," *Automatic Control, IEEE Transactions on*, Vol. 47, No. 11, 2002, pp. 1879–1882.

36. Heidt, H., Puig-Suari, J., Moore, A. S., Nakasuka, S., and Twiggs, R. J., "CubeSat: A new Generation of Picosatellite for Education and Industry Low-Cost Space Experimentation," *14th Annual/USU Conference on Small Satellites*, Vol. 5, p. 1.

37. Black, J., "Tactical Electronic Support 2," Tech. rep., Air Force Institute of Technology, 2013.

38. Gurfil, P. and Herscovitz, J., "The SAMSON Project - Cluster Flight and Geolocation with Three Autonomous Nano-satellites," *Proceedings of the AIAA/USU Conference on Small Satelllites*, Growing the Community, SSC-12-VII-2. [`http://digitalcommons.usu.edu/smallsat/2012/all2012/1`.].

39. Watt, R. A. W. and Herd, J. F., "An instantaneous direct-reading radiogoniometer," *Electrical Engineers, Journal of the Institution of*, Vol. 64, No. 353, 1926, pp. 611–617.

40. Alfke, P. and Padovani, R., "Radiation Tolerance of High-Density FPGAs," Tech. rep., Xilinx Inc, [`http://www.xilinx.com/esp/mil_aero/collateral/RadiationEffects/radiation_tolerance.pdf`. Accessed:12/23/2014].

41. Habinc, S., "Suitability of Reprogrammable FPGAs in Space Applications," Tech. Rep. FPGA-002-01, Gaisler Research, 2002.

42. "SWIFT Radios for CubeSats," 2014, Tethers Unlimited Inc., [http://www.tethers.com/SWIFT.html. Accessed: 12/22/14.].

43. "What is the difference between FPGA and ASIC?" 2008, ASIC-SOC Blog, [http://asic-soc.blogspot.com/2007/11/what-is-difference-between-fpga-and_06.html. Accessed:12/23/2014].

44. Fernandez-Leon, A., Pouponnot, A., and Habinc, S., *The Use of Reprogrammable FPGAs in Space*, European Space Agency, 2014, [http://www.esa.int/Our_Activities/Space_Engineering_Technology/Microelectronics/The_use_of_reprogrammable_FPGAs_in_space. Accessed:12/23/2014].

45. Sklar, B., *Digital Communications Fundamentals and Applications*, Prentice-Hall Inc, 2006.

46. Reisert, J. H., *Antenna Polarization*, Astron Wireless Technologies Inc., 2014, [http://www.astronwireless.com/topic-archives-antennas-polarization.asp. Accessed: 12/01/2014].

47. Waltz, E. and Llinas, J., *Multisensor Data Fusion*, Artech House Inc, 1990.

48. Stein, S., "Algorithms for ambiguity function processing," *Acoustics, Speech and Signal Processing, IEEE Transactions on*, Vol. 29, No. 3, 1981, pp. 588–599.

49. Stone, J., "Methods of determining the direction of space-telegraph signals," U.S. Patent 716134A, December 16, 1902.

50. Schmidt, R. O., "Multiple emitter location and signal parameter estimation," *Antennas and Propagation, IEEE Transactions on*, Vol. 34, No. 3, 1986, pp. 276–280.

51. Stoica, P. and Nehorai, A., "MUSIC, maximum likelihood and Cramer-Rao bound," *Acoustics, Speech, and Signal Processing, 1988. ICASSP-88., 1988 International Conference on*, 1988, pp. 2296–2299 vol.4.

52. Yau, S. F. and Bresler, Y., "A compact Cramer-Rao bound expression for parametric estimation of superimposed signals," *Signal Processing, IEEE Transactions on*, Vol. 40, No. 5, 1992, pp. 1226–1230.

53. Fowler, M. L. and Hu, X., "Signal models for TDOA/FDOA estimation," *Aerospace and Electronic Systems, IEEE Transactions on*, Vol. 44, No. 4, 2008, pp. 1543–1550.

54. Stewart, A., *Comparing Time-Based and Hybrid Time-Based/Frequency Based Multi-Platform Geo-Location Systems*, MS thesis. Naval Postgraduate School, Monterey CA, 1997.

55. Ho, K. C. and Chan, Y. T., "Solution and performance analysis of geolocation by TDOA," *Aerospace and Electronic Systems, IEEE Transactions on*, Vol. 29, No. 4, 1993, pp. 1311–1322.

56. Ho, K. C. and Chan, Y. T., "Geolocation of a known altitude object from TDOA and FDOA measurements," *Aerospace and Electronic Systems, IEEE Transactions on*, Vol. 33, No. 3, 1997, pp. 770–783.

57. Boas, M., *Lines and Planes*, Mathematical Methods in the Physcial Sciences, John Wiley and Sons Inc, 2006, pp. 106–110.

58. StackExchange, *Point closest to a set of four lines in 3D*, 2011, [http://math.stackexchange.com/questions/36398/point-closest-to-a-set-four-of-lines-in-3d. Accessed: 12/9/2014].

59. Durland, N. H., "Defining Mean Sea Level in Military Simulations with DTED," Tech. rep., Northrop Grumman Corporation.

60. Farr, T. G., Rosen, P. A., Caro, E., Crippen, R., Duren, R., Hensley, S., Kobrick, M., Paller, M., Rodriguez, E., Roth, L., Seal, D., Shaffer, S., Shimada, J., Umland, J., Werner, M., Oskin, M., Burbank, D., and Alsdorf, D., "The Shuttle Radar Topography Mission," *Reviews of Geophysics*, , No. 45, 2007.

61. "Guidelines for Digital Elevation Data," Tech. rep., National Digital Elevation Program, 2004, [http://www.ndep.gov/NDEP_Elevation_Guidelines_Ver1_10May2004.pdf. Accessed:12/11/2014].

62. Sermeno, M., *DTED questions*, NGA Office of International Affairs, Electronic Message. 0528Z, 7 October 2014.

63. Kershner, C. M., *DTED Questions*, National Geospatial-Intelligence Agency, Electronic Message. 0200Z, 6 October 2014.

64. MathWorks, *Sources of Terrain Data*, 2014, [http://www.mathworks.com/help/map/sources-of-terrain-data.html. Accessed:10/10/14.].

65. NASA Jet Propulsion Laboratory, *US Releases Enhanced Shuttle Land Elevation Data*, 2014, [http://www2.jpl.nasa.gov/srtm. Accessed: 11/1/14].

66. Franken, D. and Hupper, A., "Improved fast covariance intersection for distributed data fusion," *Information Fusion, 2005 8th International Conference on*, Vol. 1, 2005, p. 7 pp.

67. Fowler, M. L., "Analysis of single-platform passive emitter location with terrain data," *Aerospace and Electronic Systems, IEEE Transactions on*, Vol. 37, No. 2, 2001, pp. 495–507.

68. Julier, S. J. and Uhlmann, J. K., "A Non-divergent Estimation Algorithm in the Presence of Unknown Correlations," *Proceedings of the American Control Conference*, AACC, Albuquerque, New Mexico, 1997, pp. 2369–2373.

69. Niehsen, W., "Information fusion based on fast covariance intersection filtering," *Information Fusion, 2002. Proceedings of the Fifth International Conference on*, Vol. 2, 2002, pp. 901–904 vol.2.

70. Qiao, L., Rizos, C., and Dempster, A. G., "Analysis and Comparison of CubeSat Lifetime," Tech. rep., Australian Centre for Space Engineering Research.

71. Everett, D. F., Pushell, J. J., and Wertz, J. R., *Space Mission Engineering: The New SMAD*, Microcasm Press, 2011.

72. Romero, L. A. and Mason, J., "Evaluation of Direct and Iterative Methods for Overdetermined Systems of TOA Geolocation Equations," *Aerospace and Electronic Systems, IEEE Transactions on*, Vol. 47, No. 2, 2011, pp. 1213–1229.

73. Yang, K., Jiang, L., and Luo, Z.-Q., "Efficient semidefinite relaxation for robust geolocation of unknown emitter by a satellite cluster using TDOA and FDOA measurements," *Acoustics, Speech and Signal Processing (ICASSP), 2011 IEEE International Conference on*, 2011, pp. 2584–2587.

74. Luo, C. and McClellan, J. H., "Robust geolocation estimation using adaptive RANSAC algorithm," *Acoustics Speech and Signal Processing (ICASSP), 2010 IEEE International Conference on*, 2010, pp. 3862–3865.

75. Mikhalev, A. and Ormondroyd, R., "Passive emitter geolocation using agent-based data fusion of AOA, TDOA and FDOA measurements," *Information Fusion, 2007 10th International Conference on*, 2007, pp. 1–6.

76. Wang, S., Jackson, B. R., and Inkol, R., "Hybrid RSS/AOA emitter location estimation based on least squares and maximum likelihood criteria," *Communications (QBSC), 2012 26th Biennial Symposium on*, 2012, pp. 24–29.

77. Wang, S., Jackson, B. R., and Inkol, R., "Performance Characterization of AOA Geolocation Systems Using the Von Mises Distribution," *Vehicular Technology Conference (VTC Fall), 2012 IEEE*, 2012, pp. 1–5.

78. Rohatgi, V. K., *Statistical Inference*, Dover Publications Inc, 2003.

79. Gemayel, N. E., Jakel, H., and Jondral, F. K., "A Hybrid TDOA/RSSD Geolocation System Using the Unscented Kalman Filter," *Vehicular Technology Conference (VTC Fall), 2013 IEEE 78th*, 2013, pp. 1–5.

80. Savage, C. O., Cramer, R. L., and Schmitt, H. A., "TDOA Geolocation with the Unscented Kalman Filter," *Networking, Sensing and Control, 2006. ICNSC '06. Proceedings of the 2006 IEEE International Conference on*, 2006, pp. 602–606.

81. Mikhalev, A., Hughes, E. J., and Ormondroyd, R. F., "Comparison of Hough Transform and particle filter methods of passive emitter geolocation using fusion of TDOA and AOA data," *Information Fusion (FUSION), 2010 13th Conference on*, 2010, pp. 1–8.

REPORT DOCUMENTATION PAGE

Form Approved
OMB No. 0704–0188

1. REPORT DATE *(DD–MM–YYYY)*	2. REPORT TYPE	3. DATES COVERED *(From — To)*
26–03–2015	Master's Thesis	Sept 2013 — March 2015

4. TITLE AND SUBTITLE

Evaluation of the Military Utility of Employing an Angle of Arrival Payload Hosted on a CubeSat as an Augmentation to Existing Geolocation Systems

5a. CONTRACT NUMBER

5b. GRANT NUMBER

5c. PROGRAM ELEMENT NUMBER

6. AUTHOR(S)

Schmidt, Nicholas, S, Capt

5d. PROJECT NUMBER

5e. TASK NUMBER

5f. WORK UNIT NUMBER

7. PERFORMING ORGANIZATION NAME(S) AND ADDRESS(ES)

Air Force Institute of Technology
Graduate School of Engineering and Management (AFIT/EN)
2950 Hobson Way
WPAFB OH 45433-7765

8. PERFORMING ORGANIZATION REPORT NUMBER

AFIT-ENY-MS-15-M-213

9. SPONSORING / MONITORING AGENCY NAME(S) AND ADDRESS(ES)

Intentionally Left Blank

10. SPONSOR/MONITOR'S ACRONYM(S)

11. SPONSOR/MONITOR'S REPORT NUMBER(S)

12. DISTRIBUTION / AVAILABILITY STATEMENT

DISTRIBUTION STATEMENT A:
Approved for Public Release; Distribution Unlimited

13. SUPPLEMENTARY NOTES

14. ABSTRACT

This research models the performance of the proposed augmentation system as well as three and four-ball TDOA satellite systems and AOA and three-ball TDOA airborne systems individually, and performs geolocation estimate fusion via a variety of techniques to determine the increase in performance due to geolocation estimate fusion in operationally representative scenarios. It also introduces a high fidelity surface of the earth constraint based upon a digital elevation model across all geolocation algorithms.
The results from this research show that the proposed augmentation system does have military utility when combined with other geolocation systems of similar or worse individual performance. Additionally, it demonstrates the performance improvement due to correct application of a surface of the earth constraint, and the most appropriate estimate fusion technique.

15. SUBJECT TERMS

Geolocation, CubeSat, Cross-platform, fusion, surface of the earth constraint, digital elevation model

16. SECURITY CLASSIFICATION OF:			17. LIMITATION OF ABSTRACT	18. NUMBER OF PAGES	19a. NAME OF RESPONSIBLE PERSON
a. REPORT	b. ABSTRACT	c. THIS PAGE			Dr. Richard. G. Cobb, AFIT/ENY
U	U	U	UU	426	19b. TELEPHONE NUMBER *(include area code)* (937) 255-3636, x4559; richard.cobb@afit.edu